A COMPUTATIONAL INVESTIGATION OF HYDROCARBON CRACKING: GAS PHASE AND HETEROGENEOUS CATALYTIC REACTIONS ON ZEOLITES

by Xiaobo Zheng

_____

A Dissertation Submitted to the Faculty of the

DEPARTMENT OF CHEMICAL AND ENVIRONMENTAL ENGINEERING

In Partial Fulfillment of the Requirements for the Degree of

DOCTOR OF PHILOSOPHY WITH A MAJOR IN CHEMICAL ENGINEERING

In the Graduate College

THE UNIVERSITY OF ARIZONA

STATEMENT BY AUTHOR

This dissertation has been submitted in partial fulfillment of requirements for an advanced degree at The University of Arizona and is deposited in the University Library to be made available to borrowers under rules of the Library.

Brief quotations from this dissertation are allowable without special permission, provided that accurate acknowledgment of source is made. Requests for permission for extended quotation from or reproduction of this manuscript in whole or in part may be granted by the head of the major department or the Dean of the Graduate College when in his or her judgment the proposed use of the material is in the interests of scholarship. In all other instances, however, permission must be obtained from the author.

SIGNED: _____

TABLE OF CONTENTS

LIST OF TABLES v

LIST OF FIGURES viii

ABSTRACT 1

CHAPTER 1. INTRODUCTION 3

References *13*

CHAPTER 2. BACKGROUND 15

2.1 Introduction to Computational Methods *15*
2.1.1 Molecular Mechanics 15
2.1.2 Quantum Mechanics 16
2.1.3 Density Functional Methods 24
2.1.4 Basis Sets 29

2.2 Computational Approaches in the Investigation of Hydrocarbon Heterogeneous Catalytic Reactions *31*
2.2.1 Zeolite Catalyst Basics 31
2.2.2 The Cluster Approach and the Choice of a Zeolite Cluster Model 34
2.2.3 Computational Methods in Catalytic Reactions 37

2.3 Transition State *38*
2.3.1 General Approach for Locating Transition States 39
2.3.2 A Hierarchical Approach for Narrowing Down Difficult Transition States 40
2.3.3 Verification of Transition States 43

2.4 Partition Functions *44*

2.5 Reaction Rate Constant Estimation Theory *46*
2.5.1 Rice-Ramsperger-Kassel-Marcus (RRKM) Theory 46
2.5.2 Canonical Transition State Theory (CTST) 48
2.5.3 General Steps for Obtaining Reaction Rate Constants 49

References *50*

CHAPTER 3. THE CHOICE AND DEVELOPMENT OF A NEW COMPOSITE ENERGY METHOD 56

3.1 Introduction to Composite Energy Methods *56*
3.1.1 Gaussian-2 (G2) Composite Energy Method 57
3.1.2 Gaussian-3 (G3) Composite Energy Method 65
3.1.3 Complete Basis Set (CBS) Composite Energy Method 70

3.2 The Development and Evaluation of a New Composite Energy Method *76*
3.2.1 The Development of a new Composite Method 76
3.2.2 Computational Methods 77
3.2.3 Results and Discussion 79

3.3 Conclusions *93*

References *95*

CHAPTER 4. HYDROCARBON RADICAL THERMAL CRACKING REACTIONS: CARBON-CARBON BOND SCISSION 102

4.1 $*CH_2CH_2CH_3 \rightarrow CH_2CH_2 + *CH_3$ *104*
4.1.1 Reaction Pathway and Energetics 105
4.1.2 Reaction Kinetic Modeling 110

4.2 $*CH_2CH_2CH_2CH_3 \rightarrow CH_2CH_2 + *CH_2CH_3$ *117*
4.2.1 Reaction Pathway and Energetics 117
4.2.2 Reaction Kinetic Modeling 123

4.3 $CH_3*CHCH_2CH_3 \rightarrow CH_2CHCH_3 + *CH_3$ *127*
4.3.1 Reaction Pathway and Energetics 127
4.3.2 Reaction Kinetic Modeling 131

4.4 $*CH_2C(CH_3)_3 \rightarrow CH_2C(CH_3)_2 + *CH_3$ *136*
4.4.1 Reaction Pathway and Energetics 137
4.4.2 Reaction Kinetic Modeling 142

4.5 Conclusions *146*

References *148*

CHAPTER 5. HYDROCARBON RADICAL THERMAL CRACKING REACTIONS: CARBON-HYDROGEN BOND SCISSION 151

5.1 $*CHClCH_3 \rightarrow CHClCH_2 + *H$ *152*
5.1.1 Reaction Pathway and Energetics 153
5.1.2 Reaction Kinetic Modeling 157

5.2 $CH_3*C(CH_3)_2 \rightarrow CH_2C(CH_3)_2 + *H$ *162*
5.1.1 Reaction Pathway and Energetics 163
5.1.2 Reaction Kinetic Modeling 168

5.3 Conclusions *172*

References *174*

CHAPTER 6. HYDROCARBON HETEROGENEOUS REACTIONS ON ZEOLITE CATALYSTS 176

6.1 Methane Reactions *178*
6.1.1 Computational Methods 180
6.1.2 $CH_4 + H_3SiOAlH_2(OH)SiH_3 \rightarrow CH_4 + H_3Si(OH)AlH_2OSiH_3$ 182
6.1.3 $CH_4 + H_3SiOAlH_2(OH)SiH_3 \rightarrow H_2 + H_3Si(OCH_3)AlH_2OSiH_3$ 186
6.1.4 Acidity Effects 188
6.1.5 Reaction Rate Constant Estimations 197

6.2 Ethane Reactions *201*
6.2.1 Computational Methods 202
6.2.2 $CH_3CH_3 + H_3SiOAlH_2(OH)SiH_3 \rightarrow CH_4 + H_3Si(OCH_3)AlH_2OSiH_3$ 203
6.2.3 $CH_3CH_3 + H_3SiOAlH_2(OH)SiH_3 \rightarrow CH_3CH_3 + H_3Si(OH)AlH_2OSiH_3$ 208
6.2.4 $CH_3CH_3 + H_3SiOAlH_2(OH)SiH_3 \rightarrow H_2 + H_3Si(OC_2H_5)AlH_2OSiH_3$ 209
6.2.5 The Effects of Geometry Optimization Methods 211
6.2.6 Cluster Size Effects 212
6.2.7 Acidity Effects 215

6.3 Propane Reactions *222*
6.3.1 Computational Methods 222
6.3.2 $CH_3CH_2CH_3 + H_3SiOAlH_2(OH)SiH_3 \rightarrow CH_4 + H_3Si(OC_2H_5)AlH_2OSiH_3$ .. 222
6.3.3 $CH_3CH_2CH_3 + H_3SiOAlH_2(OH)SiH_3 \rightarrow CH_3CH_2CH_3 + H_3Si(OH)AlH_2OSiH_3$ 228
6.3.4 $CH_3CH_2CH_3 + H_3SiOAlH_2(OH)SiH_3 \rightarrow H_2 + H_3Si(OC_3H_7)AlH_2OSiH_3$ 231
6.3.5 Basis Set Effects 233
6.3.6 Acidity Effects 236

6.4 Iso-butane Reactions *245*
6.4.1 Computational Methods 245
6.4.2 $CH_3CH(CH_3)_2 + H_3SiOAlH_2(OH)SiH_3 \rightarrow CH_4 + H_3Si(OC_3H_7)AlH_2OSiH_3$ 245
6.4.3 $CH_3CH(CH_3)_2 + H_3SiOAlH_2(OH)SiH_3 \rightarrow CH_2H_3CH(CH_3)_2 + H_3Si(OH)AlH_2OSiH_3$ 250
6.4.4 CH3CH(CH3)2 + H3SiOAlH2(OH)SiH3 → H2 + H3Si(OC4H9)AlH2OSiH3 253
6.4.5 Acidity Effects 255

6.5 Conclusions *264*

References *267*

CHAPTER 7. HYDROGEN EXCHANGE REACTIONS OF LIGHT ALKANES ON ZEOLITES 278

7.1 Computational Methods *279*

7.2 $CH_4 + H_3SiOAlH_2(OH)SiH_3 \rightarrow CH_4 + H_3Si(OH)AlH_2OSiH_3$ *280*

7.3 $CH_3CH_3 + H_3SiOAlH_2(OH)SiH_3 \rightarrow CH_3CH_3 + H_3Si(OH)AlH_2OSiH_3$ 283

7.4 $CH_3CH_2CH_3 + H_3SiOAlH_2(OH)SiH_3 \rightarrow CH_3CH_2CH_3 + H_3Si(OH)AlH_2OSiH_3$. 285

7.5 $CH_3CH_2CH_2CH_3 + H_3SiOAlH_2(OH)SiH_3 \rightarrow CH_3CH_2CH_2CH_3 + H_3Si(OH)AlH_2OSiH_3$ 290

7.6 Deprotonation Energy and Activation Energy Relationship 295

7.7 Conclusions 297

References 298

CHAPTER 8. CONCLUSIONS 301

References 307

CHAPTER 9. FUTURE WORK 309

9.1 Hydrocarbon Thermal Cracking Research 309

9.2 Hydrocarbon Catalytic Cracking Research 311

References 315

LIST OF TABLES

Table 1-1. Thermal Cracking vs. Catalytic Cracking..... 7

Table 1-2. Reactions investigated in this project 11

Table 3-1. Optimized coefficients for G2 composite method..... 65

Table 3-2. Summary of error measurements for composite energy methods 75

Table 3-3. Brief description of the composite energy methods used in this chapter 78

Table 3-4. Geometry and frequency calculation results obtained by MP2(full)/6-31g* and QCISD(fc)/6-31g* methods for the propyl radical ($CH_2CH_2CH_3$)..... 81

Table 3-5. Geometry and frequency calculation results obtained by MP2(full)/6-31g* and QCISD(fc)/6-31g* methods for the neo-pentyl radical ($CH_2C(CH_3)_3$) 83

Table 3-6. Geometry and frequency calculation results obtained by MP2(full)/6-31g* and QCISD(fc)/6-31g* methods for the transition state of the propyl radical β-scission reaction ($CH_2CH_2CH_3 \rightarrow CH_2CH_2 + CH_3$) 84

Table 3-7. Comparison of computed composite heats of reaction..... 86

Table 3-8. Comparison of computed composite activation energy..... 88

Table 3-9. Carbon-carbon bond cracking reaction calculation results compared with Saeys, et al.'s work..... 91

Table 4-1. Comparison of calculated geometries of propane, propyl and the propyl β-scission transition state structure 106

Table 4-2. Calculated energies for the propyl β-scission reaction 108

Table 4-3. Comparison of calculated geometry of butane, butyl and the butyl β-scission transition state structure 119

Table 4-4. Calculated energies of the butyl β-scission reaction..... 121

Table 4-5. Comparison of calculated geometry of butane, *sec*-butyl and the *sec*-butyl

β-scission transition state structure 128

Table 4-6. Calculated energies of the *sec*-butyl β-scission reaction 130

Table 4-7. Comparison of the calculated geometry of neopentyl and the neopentyl β-scission transition state structure 138

Table 4-8. Calculated energies of the neopentyl β-scission reaction 139

Table 4-9. Computational cost comparison of the single point calculations using the G3 and CBS composite energy methods 141

Table 5-1. Comparison of the calculated geometry of 1-choroethane, 1-chloroethyl, and the 1-chloroethyl decomposition transition state structure 154

Table 5-2. Calculated energies of 1-chloroethyl decomposition reaction..... 156

Table 5-3. Comparison of the calculated geometries of *tert*-butane, *tert*-butyl, and the *tert*-butyl decomposition transition state structures 164

Table 5-4. Calculated energies of *tert*-butyl decomposition 166

Table 6-1. Activation barrier calculation results for methane reactions on zeolites 184

Table 6-2. Effects of Si-H distances on methane reaction activation barriers 195

Table 6-3. Rate constants of methane conversion reactions 199

Table 6-4. Calculated results using MP2/6-31g* and experimental data..... 203

Table 6-5. Activation energy calculation results for ethane conversion reactions on zeolites using the CBS method 206

Table 6-6. Calculated activation energies for the ethane cracking reaction with different cluster sizes and the average zeolite catalyst 213

Table 6-7. Effects of Si-H distances on activation energies..... 220

Table 6-8. Activation barrier calculation results for propane conversion reactions on zeolites using the CBS method 225

Table 6-9. Calculated activation barriers for the propane protolytic cracking reaction with different basis sets 235

Table 6-10. Effects of Si-H distances on activation barriers..... 243

Table 6-11. Activation barrier calculation results for *iso*-butane conversion reactions on zeolites compared with previous computational and experimental studies 248

Table 6-12. Effects of Si-H distances on activation barriers..... 262

Table 6-13. Summary of activation barrier calculation results for hydrocarbon conversion reactions on zeolites 266

Table 7-1. Selected bond lengths and angles of the methane hydrogen exchange reaction transition state structure 282

Table 7-2. Selected bond lengths and angles of the ethane hydrogen exchange reaction transition state structure 285

Table 7-3. Selected bond lengths and angles of the propane primary carbon hydrogen exchange reaction transition state structure 287

Table 7-4. Selected bond lengths and angles of the propane secondary carbon hydrogen exchange reaction transition state structure 289

Table 7-5. Selected bond lengths and angles of the butane primary and secondary carbon hydrogen exchange reaction transition state structures 292

Table 8-1. Summary of kinetic models of the hydrocarbon radical cracking reactions studied in this work 304

Table 8-2. Summary of analytical expressions for acidity effects of hydrocarbon conversion reactions on zeolites studied in this work..... 306

LIST OF FIGURES

Figure 2-1. Comparison of computational methods 20

Figure 2-2. The ZSM-5 zeolite structure 33

Figure 2-3. Three methods to model catalysts 34

Figure 2-4. Commonly used zeolite cluster models..... 36

Figure 2-5. Transition state structure of ethane cracking reaction on the zeolite cluster.. 41

Figure 3-1. Computational cost of *tert*-butyl radical calculations using G2, G3, CBS-Q and CBS-RAD(MP2) methods 93

Figure 4-1. Calculated reaction coordinate of the propyl radical β-scission reaction using the CBS compound model 109

Figure 4-2. Propyl radical β-scission reaction rate constant calculated results as a function of pressure at T = 680 K..... 110

Figure 4-3a. – 4-3c. RRKM theory rate constants for the propyl β-scission reaction with different bath gases compared with experimental data from Bencsura, et al. 112

Figure 4-4. High pressure canonical transition state theory rate constant calculation results for the propyl β-scission reaction compared with experimental data from Warnatz, et al..... 114

Figure 4-5. Propyl radical β-scission reaction kinetic model at T = 800 K 115

Figure 4-6. Error analysis of the propyl radical β-scission reaction kinetic model compared to full computational chemistry predictions..... 116

Figure 4-7. Calculated reaction coordinate of the butyl radical β-scission reaction using the CBS compound model 122

Figure 4-8a. – 4-8b. RRKM theory rate constants for the butyl β- scission reaction under different bath gases compared with experimental data from Knyazev, et al. 124

Figure 4-9. High pressure canonical transition state theory rate constant calculation

results for the butyl β-scission reaction compared with experimental data from Gierczak, et al. 125

Figure 4-10. Butyl radical β-scission reaction kinetic model at T = 600 K 126

Figure 4-11. Calculated reaction coordinate of the *sec*-butyl radical β-scission reaction using the CBS compound model 131

Figure 4-12a. – 4-12c. RRKM theory rate constants for the *sec*-butyl β-scission reaction using different bath gases compared with experimental data from Knyazev, et al. 133

Figure 4-13. High pressure canonical transition state theory rate constant calculation results for the *sec*-butyl β-scission reaction compared with experimental data from Marshall, et al. and Tsang 134

Figure 4-14. *Sec*-butyl radical β-scission reaction kinetic model at T =640 K 136

Figure 4-15. The calculated reaction coordinate of the neopentyl radical β-scission reaction using the CBS compound model 140

Figure 4-16a. – 4-16c. RRKM theory reaction rates for the neopentyl β-scission reaction using different bath gases compared with experimental data from Slagel, et al. 143

Figure 4-17. High pressure canonical transition state theory rate constant results for the neopentyl β-scission reaction compared with experimental data from Baldwin and Tsang 144

Figure 4-18. Neopentyl radical β-scission reaction kinetic models at T = 610 K 146

Figure 5-1. The calculated reaction coordinate of the 1-chloroethyl radical decomposition reaction using the CBS compound model 157

Figure 5-2a. – 5-2c. RRKM theory reaction rates for the 1-chloroethyl decomposition reaction using different bath gases compared with experimental data from Knyazev, et al. 159

Figure 5-3. High pressure canonical transition state theory rate constant results for the 1-chloroethyl decomposition reaction compared with experimental data from Manion 160

Figure 5-4. 1-chloroethyl radical decomposition reaction kinetic models at T = 950 K 162

Figure 5-5. The calculated reaction coordinate of the *tert*-butyl radical decomposition reaction using the CBS compound model 167

Figure 5-6a. – 5-6b. RRKM theory reaction rates for the *tert*-butyl decomposition reaction using different bath gases compared with experimental data from Knyazev, et al.

..... 169

Figure 5-7. High pressure canonical transition state theory rate constant results for the *tert*-butyl decomposition reaction compared with experimental data from Tsang 170

Figure 5-8. *tert*-butyl radical decomposition reaction kinetic models at T = 750 K..... 172

Figure 6-1(a). Transition state structures for methane hydrogen exchange reaction on a T3 zeolite cluster 183

Figure 6-1(b). Transition state structure for methane dehydrogenation reaction on a T3 zeolite cluster 187

Figure 6-2. $H_3Si\text{-}O\text{-}AlH_2\text{-}(OH)\text{-}SiH_3$ cluster structures with changing terminal Si-H bond distances..... 190

Figure 6-3. Transition state structures of methane hydrogen exchange reaction with changing terminal Si-H bond distances 192

Figure 6-4. Transition state structures for the methane dehydrogenation reaction with changing terminal Si-H bond distances 193

Figure 6-5. Corrections to the calculated methane reactions activation energies for the acidity effect..... 196

Figure 6-6. Reaction rate constant predictions of methane reactions on zeolite catalyst using the B3LYP/6-31G* geometry optimization and CBS-QB3 energy calculations with canonical transition state theory..... 200

Figure 6-7(a). Transition state structures for ethane protolytic cracking reaction on a T3 zeolite cluster 204

Figure 6-7(b). Transition state structures for ethane hydrogen exchange reaction on zeolite cluster 209

Figure 6-7(c). Transition state structures for ethane dehydrogenation reaction on a T3 zeolite cluster 210

Figure 6-8. Corrections to the calculated ethane cracking reaction activation energies for the cluster size effect..... 214

Figure 6-9. H3Si-O-AlH2-(OH)-SiH3 cluster structures with changing terminal Si-H bond distances..... 216

Figure 6-10. Transition state structures of the ethane cracking reaction with changing terminal Si-H bond distances..... 218

Figure 6-11. Corrections to the calculated ethane conversion reactions activation energies for the acidity effect 221

Figure 6-12(a). Transition state structure (TS1) for propane protolytic cracking reactions on a T3 zeolite cluster 224

Figure 6-12(b). Transition state structure (TS2) for propane protolytic cracking reactions on a T3 zeolite cluster 227

Figure 6-12(c). Transition state structure for the propane primary hydrogen exchange reaction on a T3 zeolite cluster 229

Figure 6-12(d). Transition state structure for the propane secondary hydrogen exchange reaction on a T3 zeolite cluster 230

Figure 6-12(e). Transition state structure for propane dehydrogenation reaction on a T3 zeolite cluster 232

Figure 6-13. Transition state structures of propane cracking reaction with changing terminal Si-H bond distances 237

Figure 6-14. Transition state structures of propane primary hydrogen exchange reaction with changing terminal Si-H bond distances 239

Figure 6-15. Transition state structures of propane secondary hydrogen exchange reaction with changing terminal Si-H bond distances 240

Figure 6-16. Transition state structures of propane dehydrogenation reaction with changing terminal Si-H bond distances 241

Figure 6-17. Corrections to the calculated propane conversion reactions activation barriers for the acidity effect 244

Figure 6-18(a). Transition state structures for *iso*-butane protolytic cracking reaction on a T3 zeolite cluster 246

Figure 6-18(b). Transition state structure for the *iso*-butane primary hydrogen exchange reaction on a T3 zeolite cluster 251

Figure 6-18(c). Transition state structure for the *iso*-butane tertiary hydrogen exchange reaction on a T3 zeolite cluster 252

Figure 6-18(d). Transition state structures for *iso*-butane dehydrogenation reaction on a T3 zeolite cluster 254

Figure 6-19. Transition state structures of *iso*-butane cracking reaction with changing

terminal Si-H bond distances 256

Figure 6-20. Transition state structures of iso-butane primary hydrogen exchange reaction with changing terminal Si-H bond distances 258

Figure 6-21. Transition state structures of iso-butane tertiary hydrogen exchange reaction with changing terminal Si-H bond distances 259

Figure 6-22. Transition state structures of *iso*-butane dehydrogenation reaction with changing terminal Si-H bond distances 260

Figure 6-23. Corrections to the calculated *iso*-butane conversion reactions activation barriers for the acidity effects represented by deprotonation energies 263

Figure 7-1. Calculated transition state structure for the methane hydrogen exchange reaction on a T3 zeolite cluster 281

Figure 7-2. Calculated transition state structure for the ethane hydrogen exchange reaction on a T3 zeolite cluster 284

Figure 7-3. Calculated transition state structure for the propane primary carbon hydrogen exchange reaction on a T3 zeolite cluster 286

Figure 7-4. Calculated transition state structure for the propane secondary carbon hydrogen exchange reaction on a T3 zeolite cluster 288

Figure 7-5. Calculated transition state structure for the butane primary carbon hydrogen exchange reaction on a T3 zeolite cluster 291

Figure 7-6. Calculated transition state structure for the butane secondary carbon hydrogen exchange reaction on a T3 zeolite cluster 293

Figure 7-7. Hydrogen exchange reaction activation energy and deprotonation energy relationship for light alkanes 296

Figure 9-1. Hierarchical approach to catalytic systems modeling 313

ABSTRACT

For many years, researchers have been developing theoretical methods of estimating reaction rates and energetics when experimental measurements are not available. Recent advances have led to composite energy methods with near chemical accuracy. The performance of these new methods for predicting activation energies and rate constants have not been evaluated for large hydrocarbon cracking reactions.

In this work, we investigate the suitability of using composite energy methods for estimating activation energies for the cracking reactions of many hydrocarbon species including ethyl, n-propyl, iso-propyl, n-butyl, sec-butyl, iso-butyl, neo-pentyl radicals in the gas phase. Further work using Canonical Transition State Theory (CTST) and Rice-Ramsperger-Marcus (RRKM) theory is done to estimate the rate constants for these reactions. A comparison of our theoretical methods shows that activation energies normally are predicted within 4 kcal/mol of experimental values for G3 and Complete Basis Set (CBS) composite energy methods, and reaction rate constants can be accurately.

Also, in this work, quantum chemical methods have been used to predict catalytic conversion reactions of light alkanes including methane, ethane, propane, and iso-butane on zeolite surface. A silicon free cluster model and an aluminosilicate cluster model containing three tetrahedral (Si, Al) atoms (T3 cluster) was applied to investigation reaction pathways and energetics. The activation energies were obtained and compared with available experimental data. We find that the activation energy is a strong function of zeolite acidity and the relationships of the activation energy as a function of acid strength were also investigated by changing the terminal hydrogen bond length.

This work not only allows for a more thorough understanding of the hydrocarbon reactions which is of high importance of petroleum and combustion industry, but also offers a reliable tools to guide the engineering reactor design which sometime cannot be achieved through direct experimental studies.

CHAPTER 1
INTRODUCTION

Hydrocarbons, as their name states, are compounds of carbon and hydrogen. As such, they represent one of the most significant classes of organic compounds.(Grayson and Eckroth, 1984) Methane (CH_4), the simplest saturated alkane, has a single carbon atom. It is bonded to four hydrogen atoms. In the higher saturated alkanes, generally in the form of C_nH_{2n+2}, all carbon atoms are bound to each other by single σ-bonds. Also, carbon atoms can form multiple bonds with other carbon atoms resulting in unsaturated hydrocarbons such as alkenes (C_nH_{2n}) which contain a carbon-carbon double bond, or acetylenes (C_nH_{2n-2}) which contain a carbon-carbon triple bond. Dienes and polyenes contain two or more unsaturated bonds.

Low-molecular weight olefins, such as ethylene and propylene, are very rare or absent in hydrocarbon sources like crude oil.(Magee and Dolbear, 1998). Demand for these olefins requires their preparation from readily available petroleum sources. As a result, hydrocarbon cracking, the process by which higher-molecular-weight

hydrocarbons are converted to more useful lower-molecular-weight hydrocarbons (Olah and Molnar, 1995) like ethylene and propylene through carbon-carbon bond scission, is broadly applied in petroleum industry. The cracking of hydrocarbons is of primary importance in the production of gasoline. Indeed, the widespread use of automobiles was made possible by the ready availability of gasoline from petroleum sources.(Olah and Molnar, 2003)

There are three mechanisms for hydrocarbon cracking reactions: thermal cracking, catalytic cracking, and hydrocracking.(Xiao, 2001) Each process has its own characteristics concerning operating conditions and product compositions. In thermal cracking, high temperatures (typically in the range of 450°C to 750°C) and pressures (up to about 70 atmospheres) are used to break large hydrocarbons into smaller ones; in catalytic cracking, catalysts, usually zeolites, are used to break the large hydrocarbons into smaller fragments; while in hydrocracking, the large hydrocarbons are broken into smaller ones by the addition of hydrogen in the presence of a catalyst.

Thermal cracking is the simplest and oldest method for petroleum refinery processes and is also considered the dominant reaction mechanism during kerogen maturation and oil or gas generation in the geological environment.(Olah and Molnar, 2003)

The thermal cracking process alone, however, cannot meet the high demand for quality gasoline. During World War I, a new industrial process, catalytic cracking,

was introduced. Catalytic cracking gets its name from the fact that the principal catalyzed reaction involves the cleavage of large molecules into two or more smaller pieces.(Magee and Dolbear, 1998) Since its introduction, hydrocarbon catalytic cracking has become one of the most important aspects of the petroleum refining processes. The reasons for the application of these reactions and the most significant characteristics of the cracking processes are their flexibility in treating the variety of feedstocks available from whatever crudes are available for refining. This flexibility becomes increasingly important as refineries are obliged to resort to heavier crudes because of crude shortages and the high price of the more desirable feedstocks.(Wojciechowski and Corma, 1986)

Hydrocracking is the process where cracking takes place in the presence of added hydrogen under high pressure, possibly in the presence of special catalysts. The essential feature of such catalysts is their bi-functional nature, where the catalyst contains an acidic component as well as a hydrogenation-dehydrogenation component. Hydrocracking process produces no olefins whatsoever as the added hydrogen used and the high operating pressure condition saturates the carbon backbone with hydrogen atoms. However, feedstocks which are not suitable for catalytic cracking may be processed by hydrocracking.(Olah and Molnar, 2003)

Since hydrocracking process will not produce any unsaturated hydrocarbons which are in high demand in petroleum industry, in this project, only two types of

hydrocarbon cracking reactions, namely, thermal cracking and catalytic cracking are investigated because of their broad application in industrial petroleum refining.

Thermal cracking occurs at high temperatures without the benefit of a catalyst. The intermediates are uncharged, but highly reactive radicals. The products of thermal cracking are substantially different from those formed during catalytic cracking. High yields of ethylene and small amounts of methane and alpha olefins (a double bond between carbon 1 and 2) are typical from thermal cracking. Catalytic cracking, on the other hand, requires catalysts, and the reaction intermediates are charged species generated by hydrocarbon interaction with the strong acid sites on the catalyst.(Magee and Dolbear, 1998) Depending on different feedstocks, the products are quite different between thermal cracking and catalytic cracking and a summary is listed in Table 1-1.

Table 1-1. Thermal cracking vs. catalytic cracking

Hydrocarbon Cracked	Thermal Cracking Products	Catalytic Cracking Products
n-Hexadecane	C_2 is the major product C_1 is produced in large amounts C_4 to C_{15} olefins are in products No branched-chain products	C_3 to C_6 are the major products No olefins larger than C_4 Branched-chain paraffins present in products
Aliphatics	Little aromatization at 500℃	Significant aromatization at 500℃
Alkyl aromatics	Cracking occurs within the side chain	Dealkylation is the dominant cracking reaction
n-Olefins	Slow double-bond isomerization Little skeletal isomerization	Rapid isomerization of double bonds Rapid skeletal isomerization
Naphthenes	Cracking is slower than that of paraffins	Cracking rates comparable to those of paraffins

Source: Adapted from B. W. Wojciechowski, A. Corma, *Catalytic Cracking Catalysts, Chemistry and Kinetics*, M. Dekker, New York, New York, 1986. and J. Magee, G. Dolbear, *Petroleum Catalysis in Nontechnical Language*, PenWell, Tulsa, OK, 1998

The knowledge of kinetics of hydrocarbon cracking reactions is essential for accurate modeling of the physical and chemical behavior of combustion systems and the oil refining industrial processes.(Tsang, 1987; Tsang and Hampson, 1986) However, due to the complexity of the reaction schemes, all types of reactions, like cracking, dehydrogenation, dehydrocyclization, isomerization, alkylation, metathesis, oxidation, oligomerization, and polymerization, etc., may take place simultaneously, making the experimental measurement of the cracking reaction kinetics very difficult. On the other hand, the dramatic increase of computer speed has greatly increased the ability to apply computational tools for investigating different chemical systems in the last decade, which makes quantum chemical approaches a good alternative to experiment.(Curtiss and Gordon, 2004; Frash and van Santen, 1999)

The mechanisms for hydrocarbon thermal cracking are generally accepted to involve free-radical chain reactions. Among the elementary steps involved in the thermal cracking reactions, the most important ones are:

(1) Chain initiation reactions where a hydrocarbon molecule is decomposed into two radicals, $HR \rightarrow *R + *H$;

(2) Hydrogen transfer reactions where radicals reacts with the hydrocarbon molecules to form a new radical and hydrocarbon species, $*R_1 + HR_2 \rightarrow HR_1 + *R_2$;

(3) Radical decomposition reactions where a hydrocarbon radical decomposes into an olefin and a smaller radical, $*R \rightarrow *R_1 + R_2$

The corresponding reverse reactions are radical termination, hydrogen transfer, and radical addition, respectively.(Xiao, 2001)

Hydrocarbon catalytic cracking is generally considered to be a chain reaction, but the mechanisms are quite different from that of thermal cracking. Hydrocarbon catalytic reactions include chain initiation, chain propagation and chain annihilation steps.(Frash and van Santen, 1999)

Initial elementary reaction includes:

chemisorption of olefins, $R^{=} + H^{+}_{ads} \rightarrow R^{+}_{ads}$;

protolytic cracking of paraffins, $R_1\text{-}R_2 + H^{+}_{ads} \rightarrow R_1{}^{+}_{ads} + R_2\text{-}H$;

and, protolytic dehydrogenation of paraffins, $R_1\text{-}H + H^{+}_{ads} \rightarrow R_1{}^{+}_{ads} + H_2$

Then adsorbed carbenium ions R^{+}_{ads} go through further propagation reactions that include:

skeletal isomerization, $R_1R_2CH\text{-}R_3CH^{+}_{ads} \rightarrow R_2R_3CH\text{-}R_1CH^{+}_{ads}$;

β-scission, $R\text{-}CH_2\text{-}(CH_3)CH^{+}_{ads} \rightarrow R^{+}_{ads} + H_2C{=}CH\text{-}CH_3$;

and alkylation reactions, $R^{+}_{ads} + H_2C{=}CH\text{-}CH_3 \rightarrow R\text{-}CH_2\text{-}(CH_3)CH^{+}_{ads}$.

Finally, the chain reaction is terminated by the annihilation of carbenium ions R^{+}_{ads} .

In this project, computational methods are applied to the investigation of hydrocarbon cracking reaction energetics and kinetics. The reactions investigated are listed in Table 1-2. This project includes the study of both the hydrocarbon gas-phase reactions (thermal cracking) and heterogeneous catalytic reactions, which

also involve the reactions of C-C bond or C-H bond breaking. The reactants greatly vary from methane, which has only one carbon molecule, to neo-pentyl radical which has five carbon molecules.

Table 1-2. Reactions investigated in this project

		Reactions Investigated
Gas Phase Reactions	C-C Bond Breaking	$*CH_2CH_2CH_3 \rightarrow CH_2CH_2 + *CH_3$
		$*CH_2CH_2CH_2CH_3 \rightarrow CH_2CH_2 + *CH_2CH_3$
		$CH_3*CHCH_2CH_3 \rightarrow CH_2CHCH_3 + *CH_3$
		$*CH_2C(CH_3)_3 \rightarrow CH_2C(CH_3)_2 + *CH_3$
	C-H Breaking	$*CHClCH_3 \rightarrow CHClCH_2 + *H$
		$CH_3*C(CH_3)_2 \rightarrow CH_2C(CH_3)_2 + *H$
Catalytic Reactions	Methane (CH_4)	$CH_4 + H_3SiOAlH_2(OH')SiH_3 \rightarrow CH_3H' + H_3Si(OH)AlH_2OSiH_3$
		$CH_4 + H_3SiOAlH_2(OH)SiH_3 \rightarrow H_2 + H_3Si(OCH_3)AlH_2OSiH_3$
	Ethane (C_2H_6)	$CH_3CH_3 + H_3SiOAlH_2(OH)SiH_3 \rightarrow CH_4 + H_3Si(OCH_3)AlH_2OSiH_3$
		$CH_3CH_3 + H_3SiOAlH_2(OH')SiH_3 \rightarrow CH_3CH_2H' + H_3Si(OH)AlH_2OSiH_3$
		$CH_3CH_3 + H_3SiOAlH_2(OH)SiH_3 \rightarrow H_2 + H_3Si(OC_2H_5)AlH_2OSiH_3$
	Propane (C_3H_8)	$CH_3CH_2CH_3 + H_3SiOAlH_2(OH)SiH_3 \rightarrow CH_4 + H_3Si(OC_2H_5)AlH_2OSiH_3$
		$CH_3CH_2\underline{\mathbf{C}}H_3 + H_3SiOAlH_2(OH')SiH_3 \rightarrow CH_3CH_2\underline{\mathbf{C}}H_2H' + H_3Si(OH)AlH_2OSiH_3$
		$CH_3\underline{\mathbf{C}}H_2CH_3 + H_3SiOAlH_2(OH')SiH_3 \rightarrow CH_3\underline{\mathbf{C}}HH'CH_3 + H_3Si(OH)AlH_2OSiH_3$
		$CH_3CH_2CH_3 + H_3SiOAlH_2(OH)SiH_3 \rightarrow H_2 + H_3Si(OC_3H_7)AlH_2OSiH_3$

	Iso- butane (C_4H_{10})	$CH_3CH(CH_3)_2 + H_3SiOAlH_2(OH)SiH_3 \rightarrow CH_4 + H_3Si(OC_3H_7)AlH_2OSiH_3$
		$\underline{C}H_3CH(CH_3)_2 + H_3SiOAlH_2(OH')SiH_3 \rightarrow \underline{C}H_2H'CH(CH_3)_2 + H_3Si(OH)AlH_2OSiH_3$
		$CH_3\underline{C}H(CH_3)_2 + H_3SiOAlH_2(OH')SiH_3 \rightarrow CH_3\underline{C}H'(CH_3)_2 + H_3Si(OH)AlH_2OSiH_3$
		$CH_3CH(CH_3)_2 + H_3SiOAlH_2(OH)SiH_3 \rightarrow H_2 + H_3Si(OC_4H_9)AlH_2OSiH_3$

The results of this project offer a highly accurate hydrocarbon radical thermal cracking reaction kinetic database. Also, this project reveals the mechanisms and reaction pathways of hydrocarbon catalytic cracking reactions on zeolitic surfaces as discussed in Chapter 5. Energetics and kinetics of the catalytic reactions and the catalyst influence of the reactions are investigated as well. The information obtained in this project will have broad applications in the petroleum industry, which will greatly facilitate the engineering design of real-life cracking reactors and the choice of zeolite catalysts.

References:

Curtiss, L.A. and Gordon, M.S., 2004. *Computational materials chemistry methods and applications*. Kluwer academic publishers, Boston.

Frash, M.V. and van Santen, R.A., 1999. Quantum-chemical modeling of the hydrocarbon transformations in acid zeolite catalysts. *Topics in Catalysis*, 9(3-4): 191-205.

Grayson, M. and Eckroth, D., 1984. *Kirk-Othmer Encyclopedia of Chemical Technology*. Wiley-Interscience, New York.

Magee, J. and Dolbear, G., 1998. *Petroleum catalysis in nontechnical language*. PennWell, Tulsa, OK.

Olah, G.A. and Molnar, A., 1995. *Hydrocarbon Chemistry*. John Wiley & Sons, Inc., New York.

Olah, G.A. and Molnar, A., 2003. *Hydrocarbon Chemistry*. John Wiley & Sons, Inc., New York.

Tsang, W., 1987. Chemical Kinetic Database for Combustion Chemistry .2. Methanol. *Journal of Physical and Chemical Reference Data*, 16(3): 471-508.

Tsang, W. and Hampson, R.F., 1986. Chemical Kinetic Database for Combustion Chemistry .1. Methane and Related-Compounds. *Journal of Physical and Chemical Reference Data*, 15(3): 1087-1279.

Wojciechowski, B.W. and Corma, A., 1986. *Catalytic cracking : catalysts, chemistry, and kinetics*. M. Dekker, New York.

Xiao, Y., 2001. Modeling the kinetics and mechanisms of petroleum and natural gas generation: A first principles approach. *Reviews in Mineralogy & Geochemistry*,

42(Molecular Modeling Theory): 383-436.

CHAPTER 2
BACKGROUND

2.1 Introduction to Computational Methods

There are three broad areas within computational chemistry devoted to the structure of molecules and their reactivity: molecular mechanics, electronic structure methods (also referred to as quantum mechanics), and density functional methods. The basic types of calculation they perform includes computing the energy or properties related to energy of a particular molecular structure; performing geometry optimizations; and, computing the vibrational frequencies of molecules resulting from interatomic motion within the molecule.(Foresman and Frisch, 1996) This chapter will explore these methods and their limitations to highlight the choices made for the methods employed in this research.

2.1.1 Molecular Mechanics

Molecular mechanics simulations apply the classical physics laws to predict the structures and properties of molecules. These methods are characterized by their

particular force fields representing the interactions between atomic species. Molecular mechanics calculations are performed based on nuclei interactions and do not treat the electrons in a molecular system explicitly. However, electron effects are included implicitly in force fields through parameterizations. The parameterizations have not been carried out for transition states, which is why molecular mechanics methods are not suitable for investigating reaction phenomena like those investigated extensively in this work.

The approximations in molecular mechanical calculations make the computations quite inexpensive, which allows the method to be used for very large systems containing thousands of atoms. However, there are still two major drawbacks. Firstly, each force field achieves good results only for a limited class of molecules for which the force field is parameterized. No force field can be used for all molecular systems. Secondly, molecular mechanics methods cannot treat chemical systems where electronic effects dominate because of the neglect of electrons. For example, they cannot describe processes involving bond formation or bond breaking, as just described.

2.1.2 Quantum Mechanics

Electronic structure methods apply the laws of quantum mechanics rather than classical physics as the basis for the calculations. The energies and structures of molecules are obtained through the solution of the Schrödinger equation, which can be written as:

$$\hat{H}\Psi = E\Psi \qquad (2.1)$$

E in the Schrödinger equation stands for the energy of the system, which also is the eigenvalue solution of the equation. Ψ is the wave function or state function. $\hat{H}$ in the Schrödinger equation is named the Hamiltonian, and it represents the sum of the total potential and kinetic energies of the system. (Levine, 2000) It can be written as:

$$\hat{H} = -\frac{\hbar^2}{2}\sum_i \frac{1}{m_i}\left(\frac{\partial^2}{\partial x_i^{\,2}} + \frac{\partial^2}{\partial y_i^{\,2}} + \frac{\partial^2}{\partial z_i^{\,2}}\right) + \sum_{i<j}\sum\left(\frac{e_i e_j}{r_{ij}}\right) \qquad (2.2)$$

The first term in the equation accounts for the kinetic energies and the second term accounts for the potential energies, including attractions or repulsions between particles.

Equation (2.1) is the time-independent Schrödinger equation because time-derivatives and time-dependent terms have been eliminated. The time-dependent form is usually used when one is concerned with transient phenomena such as rapidly oscillating electric fields or scattering.(Levine, 2000) This research will not be interested in these phenomena so Equation (2.1) is acceptable here.

For any but the smallest systems, however, exact solutions to the Schrödinger equation cannot be computed. Based upon the various mathematical approximations to its solution, electronic structure methods are divided into two classes: semi-empirical methods and *ab initio* methods.

Semi-empirical methods use parameters derived from experimental data to simplify the computations. They solve the Schrödinger equation approximately, and depend on the availability of appropriate parameters for the chemical system of interest. The semi-empirical methods are less demanding than *ab initio* methods, but may lead to large errors for some systems.(Foresman and Frisch, 1996; Frank, 1999; Leach, 1998; Levine, 2000)

Ab initio quantum chemistry has long been applied as a major tool for investigating the structure, stability, reaction kinetics and mechanisms of different molecular systems.(Jursic, 1997; Lynch and Truhlar, 2001; Saeys et al., 2003; Truong, 2000; Truong and Truong, 1999; Wong et al., 1994; Wong and Radom, 1995; Wong and Radom, 1998; Xiao et al., 1997; Zheng and Paul, 2005) *Ab initio* calculations are based on the laws of quantum mechanics only and on the values of a small number of physical constants like the speed of light, the masses and charges of electrons and nuclei, Planck's constant, etc. These methods compute solutions to the Schrödinger equation through a series of rigorous mathematical approximations.

The difference between semi-empirical and *ab initio* methods lies in the trade-off between computational cost and accuracy of results. With the availability of good parameters, semi-empirical calculations are relatively inexpensive and provide fairly accurate energies and structures. *Ab initio* methods, in contrast, provide highly accurate predictions for a broad range of systems.(Frank, 1999) However, the chemical systems of interest are restricted to up to a few hundred atoms because of

the high computational cost.(Foresman and Frisch, 1996) A comparison of different computational methods is summarized in Figure 2-1 below.

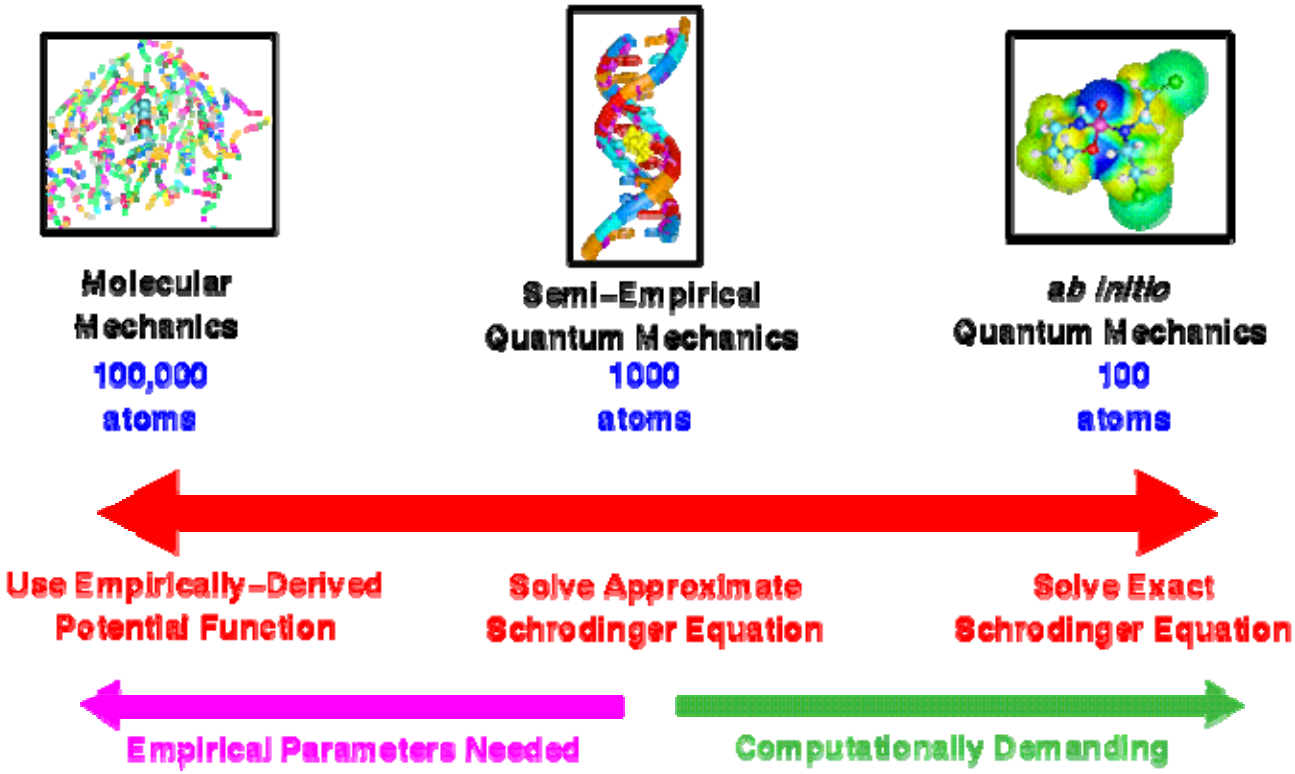

Figure 2-1. Comparison of computational methods

The Schrödinger equation is very difficult to solve despite its simple appearance. As a result, approximations have to be made in order to simplify the solution. One of the most important simplifications is the Born-Oppenheimer approximation. The electrons move much faster than the nuclei, which make the nuclei look stationary from the viewpoint of the electronic configuration. This means the assumption that all nuclear positions are fixed and only electronic motions will be considered is a good one. Under this approximation, the total energy is the sum of the energies of nuclei and electrons.

$$E_{total} = E_{unclei} + E_{electrons} \tag{2.3}$$

$$\hat{H}_{el}\,\Psi_{el} = E_{el}\Psi_{el} \tag{2.4}$$

$$\hat{H}_{el} = -\frac{\hbar^2}{2m_e}\sum_i \nabla^2 - \sum_\alpha \sum_i \frac{Z_\alpha e'^2}{r_{i\alpha}} + \sum_j \sum_{i>j} \frac{e'^2}{r_{ij}} \tag{2.5}$$

The first term in wave equation (2.5) is the operator for the kinetic energy of the electrons. The second term is the potential energy sum of the attractions between the electrons and the nuclei, where $r_{i\alpha}$ is the distance between electron i and the nucleus. The third term is the potential energy of the repulsion between electron i and j. Now that the basics regarding quantum mechanics has been covered, the discussion will turn to the different methods currently used in practice to solve the Schrödinger equation.

The simplest and least inexpensive ab initio method in common usage is the Hartree-Fock Self Consistent Field (HF-SCF) method.(Hehre et al., 1969) In this

method, the electronic Schrödinger equation (2.4) is simplified such that each electron interacts with the averaged field of the other electrons. These are the so-called Fock equations, and they are solved iteratively until self-consistency is obtained. HF-SCF has the advantage of being the best approximation that can be achieved without taking electron correlation into consideration, and is also reasonably inexpensive to execute. The expense of the calculational methods and their assumptions will become important as the discussion moves on since it is impossible to use the 'best' computational methods to study many systems of interest, just as those encountered in this work.

Because of the "averaged field" assumption in the scheme, HF-SCF theory provides an inadequate treatment of the correlation between the motions of the electrons within a molecular system, especially those arising between electrons of opposite spin.(Foresman and Frisch, 1996) Thus, electron correlation methods or post-SCF methods were developed in order to treat the electron correlations properly. Møller-Plesset (MP) perturbation theory is one approach to attack the electron correlation problem. Qualitatively, Moller-Plesset perturbation theory adds higher excitations to Hartree-Fock theory as a non-iterative correction applying the many-body perturbation theory.(Moller and Plesset, 1934)

Most commonly, one takes the perturbation expansion to second order (MP2). This can successfully model a wide variety of systems, and MP2 geometries are usually quite accurate.(Frank, 1999) Thus, MP2 remains a very useful tool in

computational chemistry. However, there are problems where MP2 theory fails.(Foresman and Frisch, 1996) In general, the more unusual the electronic structure a system has, the higher level of theory that will be needed to model it accurately. Higher-level MPn methods are available for cases where the MP2 method fails. However, since MP3 is usually not sufficient to handle cases where MP2 does poorly, MP4 sees wide use.(Foresman and Frisch, 1996) MP4 successfully addresses many problems which MP2 cannot handle with the additional cost of computation time. Moller-Plesset methods generally perform well at including the correlation energy which is defined as the difference between the "exact" HF energy and the energy from the exact solution.

However, it has been shown that the MPn series expansion yields poor results for many heavy element systems.(Reddy and Prasad, 1989) Thus an "infinite order" method such as Coupled Cluster (CC) or Quadratic Configuration Interaction (QCI) was proposed in the 1970s.(Cizek, 1966; Pople et al., 1977) These methods use summation techniques to add certain terms in the MP expansion to infinite order. These approaches are also size-consistent - meaning that the methods scale correctly with the number of particles in the system, which is a problem when MP or truncated Configuration-Interaction methods are applied to systems with a large number of electrons.

2.1.3 Density Functional Theory Methods

Density functional theory (DFT) calculations of the geometry optimization, single point energy and other properties of molecules are based on the fact that the properties of a molecule in a ground electronic state are determined by the ground state electron density. Density functional methods are similar to *ab initio* methods in many ways. DFT calculations have the same computational cost as Hartree-Fock theory, the least expensive *ab initio* method but include the effects of electron correlation, which is the fact that electrons react to each other's motion, in their methodology.

The electron density in this formalism is defined as:

$$\rho(\vec{r}_1) = N\int ...\int \left|\psi(\vec{x}_1, \vec{x}_2, \cdots, \vec{x}_N)\right|^2 d\vec{x}_1 d\vec{x}_2 \cdots d\vec{x}_N \qquad (2.6)$$

where the ψ is the wave function of a molecule. The electron density is a function of position only, that is, of just three variables, while the wave function of an n-electron molecule is a function of 4n variables. No matter how large the molecule is, the electron density is still a function of only three variables, while the complexity of the wave function for the *ab initio* methods just described in the previous section increases with the number of electrons. Therefore, DFT is less computationally expensive and more accessible than wave function computational methods with similar accuracy, especially for larger systems.

The DFT ground state energy of a molecule, which is a function of the ground state electron density, can be expressed as (Frank, 1999):

$$E_0 = -\sum_{nucleiA} Z_A \int \frac{\rho_0(\vec{r}_1)}{r_{1A}} d\vec{r}_1 - \frac{1}{2}\sum_{i=1}^{2n} \left\langle \psi_i^{KS} \left| \nabla_1^2 \right| \psi_i^{KS} \right\rangle + \frac{1}{2}\iint \frac{\rho_0(\vec{r}_1)\rho_0(\vec{r}_2)}{r_{12}} d\vec{r}_1 d\vec{r}_2 + E_{XC}[\rho_0] \quad (2.7)$$

The first term is the potential energy due to the nuclei-electron attraction; the second term is the non-interaction electronic kinetic energy; the third term is the classical repulsion energy term; the fourth term is defined as the remainder after subtraction of the non-interaction kinetic energy, attraction energy and repulsion energy from the real total energy that includes the terms needed for an exact energy. Unlike the Hartree-Fock approximate energy, Eq (2.7) is the exact energy of the system. Once we know the density function $\rho_0(\vec{r})$ and the exchange-correlation energy function $E_{XC}[\rho_0]$, we can get the exact energy. The density function $\rho(\vec{r})$ can be calculated using Eq. (2.8) where the wave function can be obtained by solving the Kohn-Sham equation:

$$[-\frac{1}{2}\nabla_i^2 - \sum_{nucleiA} \frac{Z_A}{r_{1A}} + \int \frac{\rho(\vec{r}_2)}{r_{12}} d\vec{r}_2 + v_{XC}]\psi_i^{KS} = \varepsilon_i^{KS}\psi_i^{KS} \quad (2.8)$$

where the ψ_i^{KS} is the KS spatial orbital function, ε_i^{KS} is the KS energy level and v_{XC} is the exchange correlation potential which is defined as the functional derivative of $E_{XC}[\rho(\vec{r})]$ with respect to $\rho(\vec{r})$:

$$v_{XC}(\vec{r}) = \frac{\delta E_{XC}[\rho(\vec{r})]}{\delta \rho(\vec{r})} \quad (2.9)$$

The exchange-correlation energy $E_{XC}[\rho(\vec{r})]$ is a function of $\rho(\vec{r})$. The various approximations of $E_{XC}[\rho(\vec{r})]$ separate the different DFT methods from each other.

2.1.3.1 Local density approximation (LDA)

The simplest approximation to $E_{XC}[\rho(\vec{r})]$ is the local density approximation, which assumes the system is a homogeneous electron gas and $E_{XC}[\rho(\vec{r})]$ depends only on the local value of the electron density. $E_{XC}[\rho(\vec{r})]$ can be written in a simple form:

$$E_{XC}^{LDA}[\rho] = \int \rho(\vec{r})\varepsilon_{XC}[\rho(\vec{r})]d\vec{r} \qquad (2.10)$$

where $\varepsilon_{XC}[\rho(\vec{r})]$ is the exchange-correlation energy per particle of a uniform electron gas of density $\rho(\vec{r})$. $\varepsilon_{XC}[\rho(\vec{r})]$ is composed of two parts:

$$\varepsilon_{XC}[\rho(\vec{r})] = \varepsilon_X[\rho(\vec{r})] + \varepsilon_C[\rho(\vec{r})] \qquad (2.11)$$

The exchange part represents the exchange energy of an electron in a uniform electron gas, and was approximated by Bloch and Dirac (Bloch, 1927):

$$\varepsilon_X = -\frac{3}{4}\sqrt[3]{\frac{3\rho(\vec{r})}{\pi}} \qquad (2.12)$$

The correlation part was studied by various authors based on sophisticated interpolation schemes. The most popular $\varepsilon_{XC}[\rho(\vec{r})]$ functional was developed by Vosko, Wilk and Nusair (Vosko et al., 1980), and the more recent and probably the most accurate expression of $\varepsilon_{XC}[\rho(\vec{r})]$ was the one given by Perdew and Wang (PWC) (Perdew and Wang, 1992).

Because of the inclusion of the exchange-correlation term, LDA approximations are more accurate than HF approximations with similar computational cost. Experience has shown that LDA can successfully determine the optimized geometries (Andzelm and Wimmer, 1992; Dickson and Becke, 1993) and harmonic frequencies

(Johnson et al., 1993; Zhou et al., 1996) for investigated systems. However, the energies calculated by the LDA functional are rather poor due to the assumption of a homogenous electron gas in the system. Due to some of these limitations, the LDA methods were not explored further here.

2.1.3.2 Generalized gradient approximation (GGA)

The electron density in a real molecule varies greatly from place to place. To get a more accurate approximation of the exchange-correlation energy, functionals which include not only the electron density but also the gradient of the electron density were developed. Usually, E_{XC}^{GGA} is calculated by the sum of the exchange and correlation parts:

$$E_{XC}^{GGA} = E_{X}^{GGA} + E_{C}^{GGA} \qquad (2.13)$$

The most widely used exchange functional was developed by Becke (Becke, 1993), which was designed to recover the exchange energy density asymptotically far from a finite system. Other exchange energy functionals include FT97 (Filatov and Thiel, 1997) and PW91 (Perdew, 1991). One of the most popular correlation functionals is the LYP functional (Lee et al., 1988). The other most used choice is the P86 functional (Perdew, 1986).

Previous studies demonstrated that, for the main group element systems, the GGA calculations generally provide better approximations for energetic properties than the LDA functional, but do not lead to improvement for molecular geometries (Koch and Holthausen, 2001). However, for transition metal systems which are limited to

carbonyl complexes, GGA usually gives more accurate answers than LDA methods for both geometries and energies. Since it is not possible to use the HF and MP methods to accurately model transition metal systems, and DFT methods usually give better results than HF and MP methods for investigated systems; GGA methods are applied more for transition metal systems than the other methods.

2.1.3.3 Hybrid functionals

Recently, Becke has formulated functionals which include a mixture of Hartree-Fock and DFT exchange along with DFT correlation. The exchange-correlation energy function E_{XC} is defined as:

$$E_{XC,hybrid} = c_{HF} E_{X,HF} + c_{DFT} E_{XC,DFT} \qquad (2.14)$$

where the c's are constants.(Foresman and Frisch, 1996)

For example, a Becke-style three-parameter functional may be defined as:

$$E_{XC,B3LYP} = E_{X,LDA} + c_0 (E_{X,HF} - E_{X,LDA}) + c_X \Delta E_{X,B88} + E_{C,VWN3} + c_C (E_{C,LYP} - E_{C,VWN3}) \qquad (2.15)$$

where VWN is the Vosko, Wilk, Nusair functional (Vosko et al., 1980), and LYP is the Lee, Yang, Parr functional (Lee et al., 1988). Here, the parameter c_0 allows any admixture of Hartree-Fock and LDA local exchange to be used. In addition, Becke's gradient correction to LDA exchange is also included, scaled by the parameter c_X. Similarly, the VWN3 local correlation functional is used, and it may be optionally

corrected by the LYP correlation correction via the parameter c_C. In the B3LYP hybrid functional method, the parameters are determined by fitting data from calculation to experimental for the atomization energies, ionization potentials, proton affinities and first-row atomic energies in the G1 molecule set (Pople et al., 1989) with c_0=0.20, c_X=0.72, and c_C=0.81.(Becke, 1993; Lee et al., 1988)

Different functionals can be constructed in the same way by varying the component functionals – for example, by substituting the Perdew-Wang 1991 gradient-corrected correlation function for LYP – and by adjusting the values of the three parameters.

2.1.4 Basis Sets

The wave equation (2.5) can only be solved analytically for one electron systems like the hydrogen atom or H_2^+. For larger systems of interest, further approximations need to be made. Since the wave equation covers an infinite dimensional space, this must be approximated by a finite dimensional subspace with a chosen set of basis functions for computational purposes. A basis set is a mathematical representation of the molecular orbitals within a molecule. The basis set can be interpreted as restricting each electron to a particular region of space.(Foresman and Frisch, 1996) For the *ab initio* molecular orbital approach, one generally considers the molecular orbitals to be linear combinations of the atomic orbitals:

$$\Psi_i = \sum_{\mu=1}^{n} c_{\mu i}\varphi_\mu \qquad (2.16)$$

Ψ_i is the i-th molecular orbital, $c_{\mu i}$ are the coefficients of the linear combination, φ_μ is the μ-th atomic orbital, and n is the number of atomic orbitals.(Levine, 2000) There are two types of basis functions (also referred to as atomic orbitals, AO), which are Slater Type Orbitals (STO) and Gaussian Type Orbitals (GTO). In the software used in this research, Gaussian 98 (Frisch et al., 1998), Gaussian-type orbitals are used in the calculations. A Gaussian-type orbital has the following form:

$$\chi_{\xi,a,b,c}(x,y,z) = N_{a,b,c,\xi} x^a y^b z^c e^{-\xi r^2} \qquad (2.17)$$

Where N is the normalization constant, a, b, and c are quantum numbers describing the angular shape and direction of the orbital (for example, $a+b+c=1$ is a *p*-orbital), and exponents ξ which apply to the radial size of the electron orbital. In general, a basis set is a linear combination of these Gaussian Type Orbitals.

In general, large basis sets impose fewer constraints on electrons and lead the solution to be closer to the "exact" solution. However, larger basis sets require more computational resources so there is always a trade-off in choosing the right basis set for a particular application. Again the discussion returns to the trade-off between accuracy and computational expense, which will guide many of the choices made in methodology. The effects of these choices on the results will be explored in various sections of later chapters.

Besides the basis sets just described, polarization and diffuse functions can be added to include effects that are outside the scope of just choosing the molecular orbital shapes where the electrons can be found. Polarization functions are functions of one higher orbital angular momentum than an atom actually has in its valence orbital space. The orbital exponent of the basis function, however, causes their radial sizes to be similar to the actual sizes of the true valence orbital. The purpose of adding the polarization functions is to provide additional angular flexibility to the linear combination of atomic orbitals in forming bonding orbitals. A diffuse basis function is one with a small orbital exponent in the range of 0.01 to 0.1. In general, the diffuse functions are added for anions and compounds which have lone electron pairs and significant density at large distances from the nucleus, aiding in the prediction of long range electronic effects.(Frank, 1999)

2.2 Computational Approaches in the Investigation of Hydrocarbon Heterogeneous Catalytic Reactions

2.2.1 Zeolite Catalyst Basics

Zeolites are widely used in such areas as oil refining for cracking in the petroleum industries, and as adsorbents and for gas separations. A zeolite is a crystalline aluminosilicate with a three-dimensional framework structure which forms uniformly sized pores of molecular dimension (Maesen and Marcus, 2001). There are

hundreds of different zeolite structures, among which 130 types have been identified and are described in the International Zeolite Association Database (http://www.iza-structure.org/databases/). A three letter framework type code is generally accepted to describe different zeolite structures, e.g. FAU for the mineral faujasite, LTA for Linde Type A, and MFI for ZSM-5 (Zeolite SOCONY Mobile – five).(McCusker and Baerlocher, 2001) The properties of the zeolite materials are essentially determined by their structures, especially by the size and dimension of the pores. Pore openings are characterized by the size of the ring, designated by an n-ring where n is the number of the tetrahedral atoms in the ring. An 8-ring is considered to be a small pore, a 10-ring a medium one, and a 12-ring a large one (Flanigen, 2001).

ZSM-5 has been most widely applied in the refinery and petrochemical processes.(Wojciechowski and Corma, 1986) Therefore, it will be the focus of this work. The structure of ZSM-5 is shown in Figure 2-2.

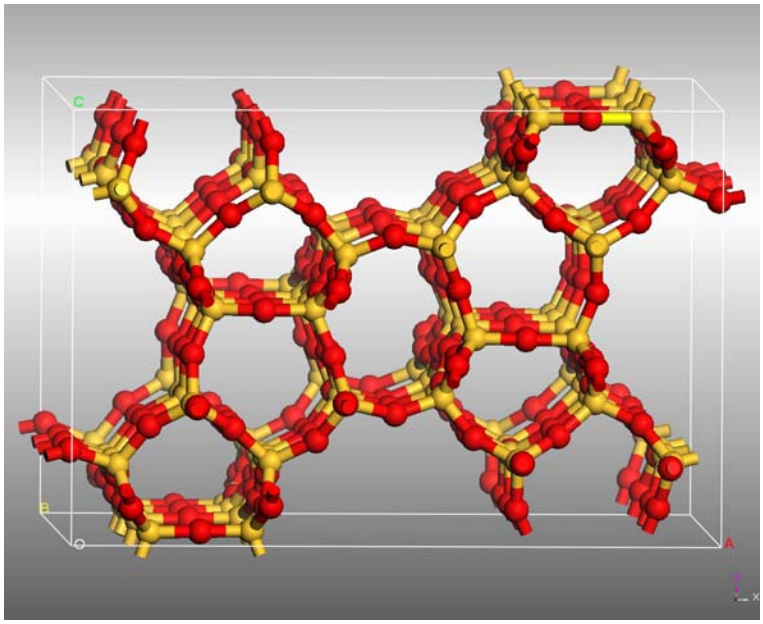

Figure 2-2. The ZSM-5 zeolite structure

The molecules in light color are silicon and those in dark color are oxygen atoms. ZSM-5 has a straight 10-ring pore channel along the direction perpendicular to the paper, which makes it a medium-pore structure. The character of ZSM-5 makes it able to break the center carbon-carbon bond of n-paraffins to produce propylene and butylene (Maxwell and Stork, 2001).

When all lattice ions are silicon, the zeolite lattice has the composition of SiO_2 and is a polymorph of quartz. At some places in the framework, Al^{3+} can replace Si^{4+}, and the framework will carry a negative charge. The loosely held cations stay within the cavities and preserve the electroneutrality of the zeolite. Brønsted acidic sites are formed when silicon, which has a formal valency of four, is replaced by a metal atom with a lower valency. A proton is attracted to the oxygen atom

connecting the silicon and aluminum atom neighbor, resulting in a chemically stable situation. In these situations, the oxygen atom becomes a three-coordinated structure. SiO and AlO bonds have considerable covalency, resulting in a relatively weak OH bond. This “onium” type coordination of oxygen is the fundamental reason for the high acidity of the attached proton.

2.2.2 The Cluster Approach and the Choice of a Zeolite Cluster Model

Heterogeneous catalytic reactions which occur on solid surfaces can be studied using the cluster approach, embedding methods, or periodic methods shown in Figure 2-3, depending upon the aspects of the reactions that are most important.(Neurock, 2003)

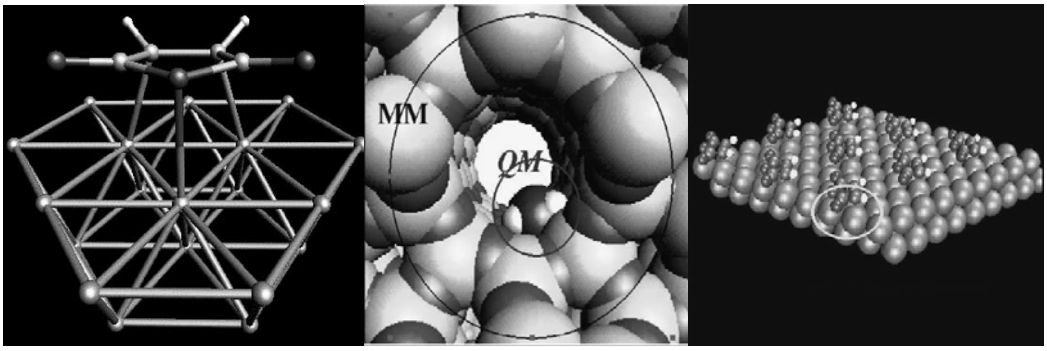

(a) Cluster **(b) Embedding** **(c) Periodic**

Figure 2-3. Three methods to model catalysts

Source: Adapted from, Neurock, M., 2003, “Perspectives on the first principles elucidation and the design of active sites”, Journal of Catalysis, 216(1-2): 73-88.

A cluster model is formed by cutting out a small portion of the catalyst's lattice and terminating open valences with hydroxyl or hydride bonds.(Curtiss and Gordon, 2004) The size of the cluster is chosen so that the reaction can be modeled using quantum mechanical methods (Bates and Van Santen, 1998). The embedding method is an extension of the cluster approach where one embeds the cluster into a low level quantum mechanical or molecular mechanical model. In periodic methods, one defines a unit cell which comprises a large enough surface ensemble. Periodic boundary conditions are then used to expand the cell in three dimensions.(Neurock, 2003) Properties that strongly depend on zeolite structure like heats of adsorption and diffusion rates need to be investigated using embedding methods. The aspects of a catalytic reaction which are only dependent on local properties, such as activation of adsorbates and any bond breaking or forming that may take place, are in the realm of the cluster approach (vanSanten, 1997a).

An important issue for obtaining high quality results is the use of clusters to model the local environment around the zeolitic proton (vanSanten, 1997b). This Brønsted acidic site is generally modeled by one of the following cluster models: H-(OH)-AlH_2-O-H, H_3Si-(OH)-AlH_2-O-SiH_3, H-(OH)-$Al(OH)_2$-O-H, or H_3Si-(OH)-$Al(OH)_2$-O-SiH_3. The structures of first two models are shown in Figure 2-4**.**

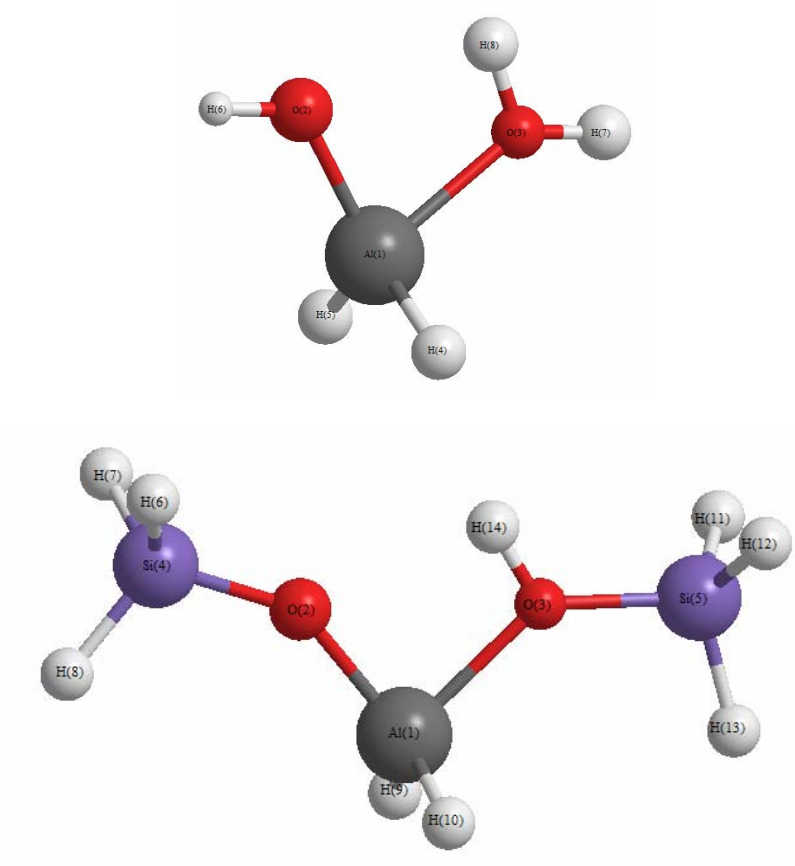

Figure 2-4. Commonly used zeolite cluster models

The silicon-containing cluster models on the bottom has a deprotonation energy close to that found for high-silica acidic zeolites (around 1250 kJ/mol), and leads to more accurate results than those obtained using non-silicon clusters. However, the computational requirement is greatly increased over the top case because of the two silicon atoms. Smaller silicon-free cluster models give higher deprotonation energies, indicating that they are less strongly acidic, and can be very useful when investigating reactions involving large reactant molecules or the dependence of

reaction properties on the cluster deprotonation energy. But smaller cluster models usually lead to higher activation energies.(Frash et al., 1998; Frash and van Santen, 1999)

The other two cluster models previously described just replace the terminal hydrogens with hydroxyls connecting to aluminum. Between the two silicon containing cluster models, H_3Si-(OH)-$Al(OH)_2$-O-SiH_3, is closer to the real zeolite surroundings with only slightly higher computational cost than H_3Si-(OH)-AlH_2-O-SiH_3. However, it has been proven that there is only a very small difference between the reaction characteristic properties of interest by using these two models (Blaszkowski et al., 1994; Blaszkowski et al., 1996). Additionally, computational problems are sometimes encountered when using the H_3Si-(OH)-$Al(OH)_2$-O-SiH_3 cluster. Therefore, the H_3Si-(OH)-AlH_2-O-SiH_3 cluster model is applied in this work to study cracking reactions on zeolites which is a main object of this work.

2.2.3 Computational Methods in Catalytic Reactions

In this section, we will discuss computational methods applied particularly for hydrocarbon catalytic reactions.

Density function theory and *ab-initio* quantum chemical methods have been applied to study catalytic reactions quantitatively by other researchers.(Frash et al., 1998; Frash and van Santen, 1999) Density function theory methods have been shown to give accurate protonation energies and errors are usually within 5 kJ/mol

compared to experiment. However, with the best results of the B3LYP method, the transition state energies may be underestimated by approximately 30 kJ/mol (van Santen et al., 2001).

The Hartree-Fock method, the least expensive method in the *ab initio* family, is used most commonly instead of DFT because of its relatively low computational cost. The average interaction between electrons adopted by the Hartree-Fock method leads it to fail for describing the motion of the individual electrons, especially for the computation of hydrogen bonds and protonation, where correlation is very important.(Frash and van Santen, 1999) The second order Møller-Plesset method (MP2) fits right into this situation to give better results with its MP2 correlation corrections.

However, Hartree-Fock calculations are still very useful to offer the initial geometry for the MP2 method, which is computationally more demanding. On the other hand, the Hartree-Fock geometries can be used so energies can be computed using higher level methods, as will be discussed when the composite energy methods are described in the next chapter.

2.3 Transition States

A transition state is an intermediate state between reactants and products, characterized by a combination of reacting molecules. In theories describing elementary reactions, it is usually assumed that there is a transition state of more

positive molar Gibbs energy between the reactants and the products through which an assembly of atoms (initially composing the molecular entities of the reactants) must pass on going from reactants to products in either direction (McNaught and Wilkinson, 1997).

Obtaining chemical reaction information requires locating appropriate transition states which link the reactants with the correct products. Unlike stable molecules whose geometries and energies can often be acquired experimentally, transition states can only be studied using computational methods.

2.3.1 General Approach for Locating Transition States

In general, there are three stages in locating transition states. The first is finding an initial structure which is between the reactants and products on the hyperdimensional potential energy surface (PES). Using a lower level optimization result as the initial guess for high level optimization calculation is always a reliable approach. An example would be in using a HF method first before doing a higher level optimization with an MP2 calculation.

The second step in finding a transition state is computing a refined transition state structure from the initial guess. In this step, the choice of appropriate level of theory is essential. A frequency calculation on the stable structure found through the geometry optimization must have only one negative mode, indicating that the transition state is a first order saddle point.

The last step in finding a transition state is verifying the calculated transition state

links the correct reactants and products through and intrinsic reaction coordinate (IRC) calculation (Gonzalez and Schlegel, 1989).

The Gaussian 98 software package (Frisch et al., 1998) has included a new method for locating transition states using the keywords QST2 and QST3. By applying the Synchronous Transit-Guided Quasi-Newton (STQN) Method, the program searches for the actual transition structure by using an empirical estimate of the Hessian matrix and suitable starting structures. The reactant and product molecule specifications are required using QST2 as the keyword, while using QST3 requires an extra initial structure for the transition state. (http://www.gaussian.com/g_whitepap/qst2.htm, 2003)

2.3.2 A Hierarchical Approach for Narrowing Down Difficult Transition States

The QST tools offered by Gaussian 98, however, do not guarantee location of transition states except for small molecules with simple structures. Synchronous transit methods, constrained optimization algorithms, and Dewar-Healy-Stewart methods are only useful for some cases (Frash and van Santen, 1999). Therefore, the location of transition states is generally based on intuition and experience. The search for a viable initial transition state structure can be sped up by fixing several geometry parameters unrelated to the reaction coordinate while optimizing the other degrees of freedom. The fixed parameters can then be relaxed one at a time later to get better results. This strategy is extremely important for large and complex

molecular systems. The example given below illustrates the transition state location procedures:

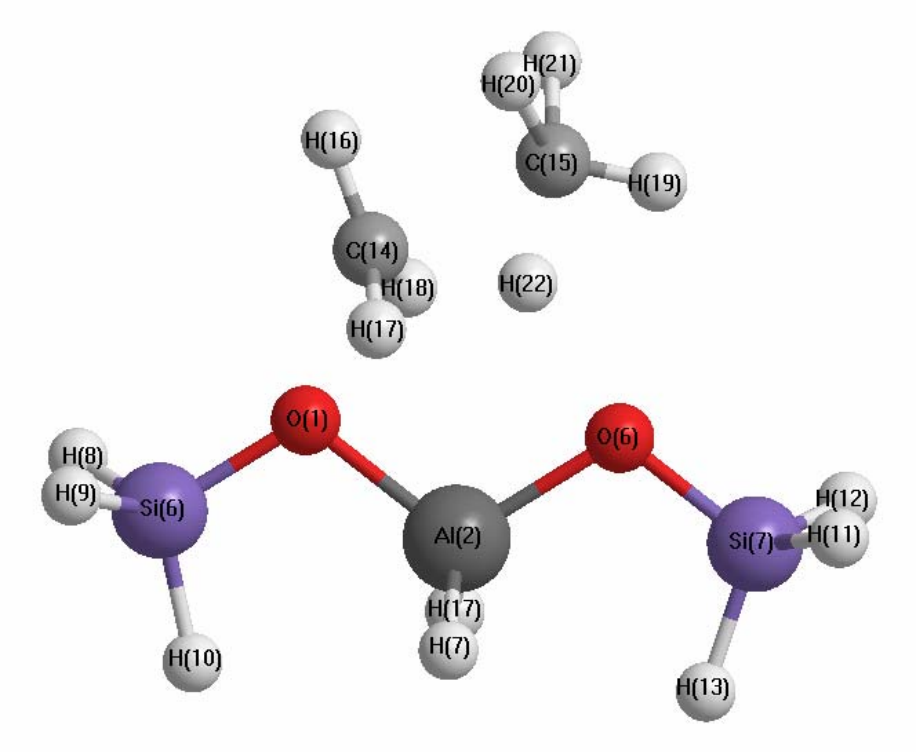

Figure 2-5. Transition state structure of ethane cracking reaction on the zeolite cluster

Figure 2-5 is the transition state structure of the ethane cracking reaction on a zeolite cluster. This large molecular system includes 1 aluminum, 2 oxygen, 2 silicon, 2 carbon, and 15 hydrogen atoms. The location of the transition state includes the following considerations (Frash and van Santen, 1999):

1. The choice of chemically sensible initial geometry for the transition state search.

The zeolite cluster (Si-O-Al-O-Si structure) serves as the catalyst in the example reaction so that the geometry parameters from the optimization calculation results of

the cluster can be directly applied as the initial guess to the transition state structure since they should not change during the reaction. The ethane structure and the H_{22} atom are considered to be the chemically sensible parts of the transition structure and need to be optimized thoroughly. After the transition state structure is located with the fixed zeolite cluster, a full optimization can be then performed to refine the transition state structure.

2. Stepwise optimization of geometry.

Optimization of all the geometry parameters simultaneously is more convenient than fixing some parameters and then relaxing them later on, but sometimes causes problems when locating transition state structures due to the complexity of the energetic hypersurface. This difficulty can be solved by dividing the geometry parameters into two groups: one small group that contributes essentially to the reaction coordinate and a second group that contributes very little. In the example above, the ethane molecule is treated as the first group and the cluster molecule as the second group. The second group is optimized as a local minimum and the first group is then optimized as the transition state (Kazansky et al., 1996).

3. Use of a transition geometry calculated from a lower computation level.

The convergence of the transition state search can converge faster at lower computational levels, but may not lead to good energies. Therefore, in order to find the transition state of this reaction at the MP2 level, the HF method is first employed to search for the transition state location. Then the results from the HF calculation

can be applied as initial geometry for the MP2 calculation.

2.3.3 Verification of Transition States

Once the transition state is located, it has to be proven to be a structure that connects the correct reactants and products. This can be verified with several main criteria:

Usually, a frequency calculation is performed once a geometry optimization is complete. This calculation uses the second derivative of the energy gradients to verify that the geometry of the species corresponds to a true saddle point on the potential energy surface. There is only one negative eigenvalue from the Hessian matrix for a first order transition state.

Although frequencies can be used, the most reliable method for verifying transition state structure is to perform the intrinsic reaction coordinate (IRC) calculation (Gonzalez and Schlegel, 1989). This calculation follows the reaction pathway toward the reactants and products from the transition state and will reveal if the structure is appropriate for the reaction being studied. However, this method is rarely used for large systems because it is extremely time-consuming.

Instead, as an inexpensive method, one can slightly distort the transition state structure in both directions of the negative eigenvector and perform a localized minimum optimization of the two distorted structures to reach the initial and final states involved.(Frash and van Santen, 1999) This will reveal the reactant and product structures but will not give the intermediate points the IRC calculation would

give.

In this work, frequency and IRC calculations will be used to test the transition state structures for all the reactions except in some cases, the distort geometry method will be used.

2.4 Partition Functions

The partition functions of a system play an important role in statistical thermodynamics. The concept was first introduced by Boltzmann, who gave it the German name *Zustandssumme*, i.e., a sum over states (Foresman and Frisch, 1996). The partition function is important because it enables the calculation of the energy and entropy of a molecule, its equilibrium, as well as the reaction rate constants in which the molecule is involved.(van Santen and Niemantsverdriet, 1995)

The partition function for a single molecule is usually denoted q and is defined as a sum of the exponential terms involving all possible quantum energy states.

$$q = \sum_{i}^{\text{all states}} e^{-\varepsilon_i / k_B T} \qquad (2.18)$$

where ε_i is the energy of the quantum energy state i and k_B is the Boltzmann's constant. The partition function can be described as the product of translational, rotational, vibrational and electronic partition functions.

$$q_{tot} = q_{trans} q_{rot} q_{vib} q_{elec} \qquad (2.19)$$

The translational partition function can then be calculated as:

$$q_{trans} = \left(\frac{2\pi M k_B T}{h^2} \right)^{3/2} V \tag{2.20}$$

The only molecular parameter in the equation above is the total molecular mass M, while V is the volume of one mole of gas.

The rotational partition function can be described as:

$$q_{rot} = \frac{8\pi^2 I k_B T}{h^2 \sigma} \tag{2.21}$$

where I is the moment of inertia and σ is the symmetry index which is 2 for a homonucelar and 1 for a heteronuclear diatomic molecule.

The vibrational partition function can be obtained by:

$$q_{vib} = \prod_{i=1}^{n} \frac{e^{-\frac{h\nu_i}{2k_B T}}}{1 - e^{\frac{-h\nu_i}{k_B T}}} \tag{2.22}$$

where ν_i is the vibration frequency in units of cm^{-1} and n is the total number of vibrations. n is 3N-5 for linear molecules and 3N-6 for non-linear molecules, where N is the total number of atoms. For transition states, n is 3N-6 for linear structures and 3N-7 for non-linear structures excluding the one negative frequency which corresponds to the reaction coordinate (Levine, 2000).

The electronic partition function involves a sum over electronic quantum states and can be calculated as:

$$q_{elec}^{\text{reactant}} = g \tag{2.23}$$

$$q_{elec}^{TS} = g e^{-\frac{\Delta E^{\mp}}{k_B T}} \tag{2.24}$$

where $\Delta E^{\mp}$ is the difference in the electronic energy between the reactant and TS and g is the electronic degeneracy of the wave function. The degeneracy, g, is 1 for a singlet, 2 for a doublet, and 3 for a triplet. The large majority of stable molecules have non-degenerate ground-state wave functions where $g = 1$.

The partition functions just described here will be applied extensively to the reaction rate constants prediction which will be discussed in detail in a later section.

2.5 Reaction Rate Constant Estimation Theory

2.5.1 Rice-Ramsperger-Kassel-Marcus (RRKM) Theory

RRKM theory is the most commonly used method for predicting reaction rates for unimolecular reactions of polyatomic molecules (Gilbert and Smith, 1990). The reaction rate constant for unimolecular reaction can be modeled as:

$$k_{uni} = \frac{LQ_1^+ \exp(-E_0/kT)}{hQ_1Q_2} \int_{E^+=0}^{\infty} \frac{W(E^+)\exp(-E^+/kT)dE^+}{1+k_a(E^*)/\beta_c Z_{LJ}[M]} \quad (2.25)$$

$$k_a(E^*) = \frac{LQ_1^+ W(E^+)}{hQ_1\rho(E^*)} \quad (2.26)$$

where L is the statistical factor; E^*, the total vibrational and rotational energy; E^+, the total energy of a given state; E_0, the activation energy; Q_1^+, the partition function for the rotation of A^+; Q_1, the partition function for the rotation of A; Q_2, the partition function for non-rotational modes; β_c, the collision efficiency; Z_{LJ} the Lennard-Jones collision frequency; k, Boltzmann's constant; h, Plank's constant;

$[M]$, the concentration of bath gas; $W(E^+)$, the sum of states; and $\rho(E^*)$, the density of states (Holbrook et al., 1996).

The bath gas influences the rate constant through the Lennard-Jones collision frequency term, Z_{LJ}, which can be obtained with:

$$Z_{LJ} = N_A \sigma^2{}_{A-M} \sqrt{\frac{8RT}{\pi \mu_{A-M}}} \Omega_{A-M} \tag{2-27}$$

where N_A is the Avagadro's constant, A denotes the reactant, and M is the bath gas. σ_{A-M}, the collision distance can be calculated as:

$$\sigma_{A-M} = \frac{1}{2}(\sigma_A + \sigma_M) \tag{2-28}$$

μ_{A-M}, the reduced mass, can be calculated as:

$$\mu_{A-M} = \frac{MW_A \times MW_M}{MW_A + MW_M} \tag{2.29}$$

Ω_{A-M}, the collisional integral, is only a function of reduced temperature $T^* = \frac{k_B T}{\varepsilon_{A-M}}$ and can be calculated as:

$$\Omega_{A-M} = (0.636 + 0.567 \log_{10} T^*)^{-1} \tag{2.30}$$

where ε_{A-M} .is the well depth. Physical constants which were not available in the literature were estimated from group additivity methods in Perry's handbook (Perry and Green, 1997).

All the parameters listed can be obtained from quantum theory except for the collisional efficiency β_c, which is usually taken as a fitting parameter between zero and unity. In this work, the sum of states $W(E^+)$ and the density of states $\rho(E^*)$

were calculated using the Beyer-Swinehart algorithm (Beyer and Swinehart, 1973).

2.5.2 Canonical Transition State Theory (CTST)

Canonical transition state theory is broadly used to predict reaction rate constants using the computational results. One of the main assumptions of CTST is that transition states are effectively in equilibrium with reactant molecules. It is argued that the rate of reaction is given by the product of the concentration of transition states passing over the energy barrier located at the point dividing reactants from products on the potential energy surface and the frequency associated with this motion. This frequency is found to be given by kT/h and the concentration of transition states is calculated from the statistical-mechanical expression for the equilibrium constant $k^{\mp}$ in terms of the appropriate partition functions. (Holbrook et al., 1996)

For a reaction, $A + B \Leftrightarrow AB \rightarrow products$, the overall rate constant $k^{\mp}$ is given by the equation:

$$k^{\mp} = \frac{-d[A]/dt}{[A][B]} = \frac{kT}{h}\frac{Q^{\mp}}{Q_A Q_B}\exp(-E_0/kT) \qquad (2.31)$$

Where E_0 is the critical energy, Q_A and Q_B are the complete partition functions per unit volume for the reactants and $Q^{\mp}$ is the partition function for all the degrees of freedom of the transition state except the reaction coordinate. The motion along the reaction coordinate has been considered separately and its partition function included in the factor, kT/h.

At high pressure limit conditions, the unimolecular rate constant does not depend

on pressure and the above expression simplifies to CTST. For a unimolecular reaction, there is only one reactant and the CTST expression becomes:

$$k_{\infty} = \frac{kT}{h}\frac{Q^{\mp}}{Q}\exp(-E_0 / RT) \qquad (2.32)$$

2.5.3 General Steps for Obtaining Reaction Rate Constants

1. Perform geometry optimization of reactants, transition states, and verify structures with frequency and IRC calculations;
2. Perform vibrational frequency calculations;
3. Possibly do a higher level geometry optimization calculation to refine the geometries or obtain energies at a higher level;
4. Obtain activation barriers from the energy calculations, possibly with composite energy methods as described in the next chapter;
5. Obtain partition function from the vibrational frequency calculations;
6. Apply RRKM or CTST to calculate reaction rate constants

From the chapters later on, these steps will be repeated to predict the reaction rate constants of hydrocarbon cracking reactions.

References:

Andzelm, J. and Wimmer, E., 1992. Density Functional Gaussian-Type-Orbital Approach To Molecular Geometries, Vibrations, And Reaction Energies. *Journal Of Chemical Physics*, 96(2): 1280-1303.

Bates, S.P. and Van Santen, R.A., 1998. The molecular basis of zeolite catalysis: a review of theoretical simulations. *Advances in Catalysis*, 42: 1-114.

Becke, A.D., 1993. Density-Functional Thermochemistry .3. The Role Of Exact Exchange. *Journal Of Chemical Physics*, 98(7): 5648-5652.

Beyer, T. and Swinehart, D.F., 1973. Number of Multiply-Restricted Partitions. *Communications of the Acm*, 16(6): 379-379.

Blaszkowski, S.R., Jansen, A.P.J., Nascimento, M.A.C. and Vansanten, R.A., 1994. Density-Functional Theory Calculations of the Transition-States for Hydrogen-Exchange and Dehydrogenation of Methane by a Bronsted Zeolitic Proton. *Journal of Physical Chemistry*, 98(49): 12938-12944.

Blaszkowski, S.R., Nascimento, M.A.C. and vanSanten, R.A., 1996. Activation of C-H and C-C bonds by an acidic zeolite: A density functional study. *Journal of Physical Chemistry*, 100(9): 3463-3472.

Bloch, F., 1927. The Electron Theory of Ferromagnetism and Electrical Conductivity. *Z. Physik*, 57: 545.

Cizek, J., 1966. On Correlation Problem In Atomic And Molecular Systems . Calculation Of Wavefunction Components In Ursell-Type Expansion Using Quantum-Field Theoretical Methods. *Journal Of Chemical Physics*, 45(11): 4256-&.

Curtiss, L.A. and Gordon, M.S., 2004. *Computational materials chemistry methods and applications*. Kluwer academic publishers, Dordrecht ; Boston ; London.

Dickson, R.M. and Becke, A.D., 1993. Basis-Set-Free Local Density-Functional Calculations Of Geometries Of Polyatomic-Molecules. *Journal Of Chemical Physics*, 99(5): 3898-3905.

Filatov, M. and Thiel, W., 1997. A new gradient-corrected exchange-correlation density functional. *Molecular Physics*, 91(5): 847-859.

Flanigen, E.M., 2001. Zeolites and molecular sieves: An historical perspective. *Studies in Surface Science and Catalysis*, 137(Introduction to Zeolite Science and Practice (2nd Edition)): 11-35.

Foresman, J.B. and Frisch, E., 1996. *Exploring Chemistry with Electronic Structure Methods*. Gaussian, Inc., Pittsburgh, PA.

Frank, J., 1999. *Introduction to Computational Chemistry*. Wiley, West Sussex, England.

Frash, M.V., Kazansky, V.B., Rigby, A.M. and van Santen, R.A., 1998. Cracking of hydrocarbons on zeolite catalysts: Density functional and Hartree-Fock calculations on the mechanism of the beta-scission reaction. *Journal of Physical Chemistry B*, 102(12): 2232-2238.

Frash, M.V. and van Santen, R.A., 1999. Quantum-chemical modeling of the hydrocarbon transformations in acid zeolite catalysts. *Topics in Catalysis*, 9(3-4): 191-205.

Frisch, M.J. et al., 1998. *Gaussian 98, Revision A.7*. Gaussian, Inc., Pittsburgh PA.

Gilbert, R.G. and Smith, S.C., 1990. *Theory of unimolecular and recombination reactions*. Blackwell Scientific Publications, Oxford, England.

Gonzalez, C. and Schlegel, H.B., 1989. An Improved Algorithm For Reaction-Path Following. *Journal Of Chemical Physics*, 90(4): 2154-2161.

Hehre, W.J., Stewart, R.F. and Pople, J.A., 1969. Self-Consistent Molecular-Orbital Methods .I. Use Of Gaussian Expansions Of Slater-Type Atomic Orbitals. *Journal Of Chemical Physics*, 51(6): 2657-&.

Holbrook, K.A., Pilling, M.J. and Robertson, S.H., 1996. *Unimolecular reactions*. John Wiley & Sons, New York.

http://www.gaussian.com/g_whitepap/qst2.htm, 2003. *Transition State Optimizations with Opt=QST2*.

http://www.iza-structure.org/databases/.

Johnson, B.G., Gill, P.M.W. and Pople, J.A., 1993. The Performance Of A Family Of Density Functional Methods. *Journal Of Chemical Physics*, 98(7): 5612-5626.

Jursic, B.S., 1997. Quadratic Complete Basis Set ab initio and Hybrid Density Functional Theory studies of the stability of HNC, HCN, H2NCH, and HNCH2, their isomerizations, and the hydrogen insertion reactions for HCN and HNC. *Abstracts of Papers of the American Chemical Society*, 214: 141-COMP.

Kazansky, V.B., Frash, M.V. and vanSanten, R.A., 1996. Quantumchemical study of the isobutane cracking on zeolites. *Applied Catalysis a-General*, 146(1): 225-247.

Koch, W. and Holthausen, M.C., 2001. *A chemist's guide to density functional theory*. Wiley-VCH, Weinheim ; New York.

Leach, A.R., 1998. *Molecular Modelling*. Longman, Essex, England.

Lee, C.T., Yang, W.T. and Parr, R.G., 1988. Development Of The Colle-Salvetti Correlation-Energy Formula Into A Functional Of The Electron-Density. *Physical Review B*, 37(2): 785-789.

Levine, I.N., 2000. *Quantum Chemistry*. Prentice Hall, Upper Saddle River, New Jersey.

Lynch, B.J. and Truhlar, D.G., 2001. How well can hybrid density functional methods predict transition state geometries and barrier heights? *Journal of Physical Chemistry A*, 105(13): 2936-2941.

Maesen, T. and Marcus, B., 2001. The zeolite scene - an overview. *Studies in Surface*

Science and Catalysis, 137(Introduction to Zeolite Science and Practice (2nd Edition)): 1-9.

Maxwell, I.E. and Stork, W.H.J., 2001. Hydrocarbon processing with zeolites. *Studies in Surface Science and Catalysis*, 137(Introduction to Zeolite Science and Practice (2nd Edition)): 747-819.

McCusker, L.B. and Baerlocher, C., 2001. Zeolite structures. *Studies in Surface Science and Catalysis*, 137(Introduction to Zeolite Science and Practice (2nd Edition)): 37-67.

McNaught, A.D. and Wilkinson, A., 1997. *IUPAC Compendium of Chemical Terminology*. Royal Society of Chemistry, Cambridge, England.

Moller, C. and Plesset, M.S., 1934. Note on an approximation treatment for many-electron systems. *Physical Review*, 46(7): 0618-0622.

Neurock, M., 2003. Perspectives on the first principles elucidation and the design of active sites. *Journal Of Catalysis*, 216(1-2): 73-88.

Perdew, J.P., 1986. Density-Functional Approximation For The Correlation-Energy Of The Inhomogeneous Electron-Gas. *Physical Review B*, 33(12): 8822-8824.

Perdew, J.P., 1991. *Unified Theory of Exchange and Correlation Beyond the Local Density Approximation Electronic structure of Solids*. Akademie Verlag, Berlin.

Perdew, J.P. and Wang, Y., 1992. Accurate And Simple Analytic Representation Of The Electron-Gas Correlation-Energy. *Physical Review B*, 45(23): 13244-13249.

Perry, R. and Green, D.W., 1997. *Perry's chemical engineers' handbook*. McGraw-Hill, New York.

Pople, J.A., Headgordon, M., Fox, D.J., Raghavachari, K. and Curtiss, L.A., 1989. Gaussian-1 Theory - a General Procedure for Prediction of Molecular-Energies. *Journal of Chemical Physics*, 90(10): 5622-5629.

Pople, J.A., Seeger, R. and Krishnan, R., 1977. Variational Configuration Interaction Methods And Comparison With Perturbation-Theory. *International Journal Of Quantum Chemistry*: 149-163.

Reddy, S.P. and Prasad, C.V.V., 1989. The Baldet-Johnson (B Sigma-2+-A Pi-2i) System Of (Co)-C-13-O-18+. *Journal Of Chemical Physics*, 91(4): 1972-1977.

Saeys, M., Reyniers, M.F. and Marin, G.B., 2003. Ab initio calculations for hydrocarbons: Enthalpy of formation, transition state geometry, and activation energy for radical reactions. *Journal of Physical Chemistry A*, 107(43): 9147-9159.

Truong, T.N., 2000. Reaction class transition state theory: Hydrogen abstraction reactions by hydrogen atoms as test cases. *Journal of Chemical Physics*, 113(12): 4957-4964.

Truong, T.N. and Truong, T.T.T., 1999. A reaction class approach with the integrated molecular orbital plus molecular orbital methodology. *Chemical Physics Letters*, 314(5-6): 529-533.

van Santen, R.A. and Niemantsverdriet, J.W., 1995. *Chemical kinetics and catalysis* Plenum Press, New York.

van Santen, R.A., van de Graaf, B. and Smit, B., 2001. Introduction to zeolite theory and modelling. *Studies in Surface Science and Catalysis*, 137(Introduction to Zeolite Science and Practice (2nd Edition)): 419-466.

vanSanten, R.A., 1997a. The cluster approach to molecular heterogeneous catalysis. *Journal of Molecular Catalysis a-Chemical*, 115(3): 405-419.

vanSanten, R.A., 1997b. Quantum-chemistry of zeolite acidity. *Catalysis Today*, 38(3): 377-390.

Vosko, S.H., Wilk, L. and Nusair, M., 1980. Accurate Spin-Dependent Electron Liquid Correlation Energies For Local Spin-Density Calculations - A Critical Analysis. *Canadian Journal Of Physics*, 58(8): 1200-1211.

Wojciechowski, B.W. and Corma, A., 1986. *Catalytic cracking : catalysts, chemistry,*

and kinetics. Dekker, New York.

Wong, M.W., Pross, A. and Radom, L., 1994. Comparison of the Addition of Ch3-Center-Dot, Ch2oh-Center-Dot, and Ch2cn-Center-Dot Radicals to Substituted Alkenes - a Theoretical-Study of the Reaction-Mechanism. *Journal of the American Chemical Society*, 116(14): 6284-6292.

Wong, M.W. and Radom, L., 1995. Radical-Addition to Alkenes - an Assessment of Theoretical Procedures. *Journal of Physical Chemistry*, 99(21): 8582-8588.

Wong, M.W. and Radom, L., 1998. Radical addition to alkenes: Further assessment of theoretical procedures. *Journal of Physical Chemistry A*, 102(12): 2237-2245.

Xiao, Y.T., Longo, J.M., Hieshima, G.B. and Hill, R.J., 1997. Understanding the kinetics and mechanisms of hydrocarbon thermal cracking: An ab initio approach. *Industrial & Engineering Chemistry Research*, 36(10): 4033-4040.

Zheng, X. and Paul, B., 2005. The investigation of hydrocarbon cracking reaction energetics using composite energy method. *Molecular Simulation*: (in press).

Zhou, X.F., Wheeless, C.J.M. and Liu, R.F., 1996. Density functional theory study of vibrational spectra .1. Performance of several density functional methods in predicting vibrational frequencies. *Vibrational Spectroscopy*, 12(1): 53-63.

CHAPTER 3
THE CHOICE AND DEVELOPMENT OF A NEW COMPOSITE ENERGY METHOD

3.1 Introduction to Composite Energy Methods

Electronic structure energy calculations traditionally consist of a single computation. However, in order to reach high accuracy compared to experimental energetics, the calculation generally requires a very large basis set and high level method which takes a significantly long time to complete.(Foresman and Frisch, 1996; Hehre, 1986; Jensen, 1998; Leach, 1998; Levine, 2000) This leads to a trade-off between computational methods, basis sets, and the accuracies of the results that can be achieved. Compound models, also referred to as composite energy methods, were proposed in order to reach a high level of energetic accuracy at a reduced computational cost. They are defined as a series of single point calculation steps where the results are combined to obtain the final electronic energy value. For instance, the G3 method developed by Pople and coworkers has shown great promise for predicting heats of reaction, ionization potentials, and other phenomena (Baboul et

al., 1999; Curtiss et al., 1995; Curtiss et al., 1998a; Curtiss et al., 1997c; Kedziora et al., 1999) at a relatively low computational cost compared to its G2 ancestor. However, the single point calculation using the G3Large basis set is very expensive for larger species of interest. More recently, another series of compound models named the Complete Basis Set (CBS) methods have been developed (Mayer et al., 1998; Montgomery et al., 1999; Montgomery et al., 2000; Montgomery et al., 1994; Morihovitis et al., 1999; Ochterski et al., 1996; Petersson and Allaham, 1991; Petersson et al., 1988; Petersson et al., 1991). These methods eliminate some of the empirical correlations that are included in the Gaussian-n series of methods while still giving very accurate predictions of heats of formation and enthalpies of reaction.

In this chapter, the most popularly used composite energy methods will be discussed in detail, including G2, G3, and CBS. The calculated results for activation energies and heats of reactions will be compared with the available experimental data to evaluate the performance of these methods for predicting energetics of hydrocarbon cracking reactions. A brief history of each method will first be described before moving on to the development of a new method used extensively in this work.

3.1.1 Gaussian-2 (G2) Composite Energy Method

3.1.1.1 Gaussian-2 (G2) theory

Gaussian-2 (G2) theory was developed by Pople and Curtiss in 1991 (Curtiss et al., 1991; Curtiss et al., 1992) as a well-defined composite method of predicting

accurate molecular energies (atomization energies, ionization potentials, electron affinities, and proton affinities). As the successor of G1 theory (Curtiss et al., 1990; Pople et al., 1989), G2 theory improves G1 theory by eliminating some of the deficiencies in G1.

The procedures of G1 theory are briefly described below. First, initial equilibrium structures are obtained using the Hartree-Fock level with the 6-31G* basis set (HF/6-31G*). Then the equilibrium geometries are found using the second-order Moller-Plesset theory (MP2) with the 6-31G* basis set. All electron correlation, including inner shell electrons, are consider using MP2(FU)/6-31G* during this step. Then, a series of higher level single point energy calculations are performed using the equilibrium geometry obtained from the lower level optimization. Only valence electrons are treated in these higher level calculations so the frozen core (FC) designation is used.

The starting energy is obtained with the full fourth-order Moller-Plesset theory (MP4SDTQ) and the 6-311G** basis set, MP4SDTQ(FC)/6-311G**. While this energy is still not accurate enough to give satisfactory electronic energies, modifications are made through other corrections to refine the results.

First, diffuse *sp* basis functions, which are important for ions and molecules with lone pairs of electrons, are included:

$$E(+)=E(MP4/6\text{-}311+G^{**})-E(MP4/6\text{-}311G^{**}) \qquad (3.1)$$

Second, higher polarization functions on nonhydrogen atoms are added. A (*2df*)

augmentation replaces the single set of *d*-polarization functions with an inner and outer set and includes a single set of *f*-functions:

$$E(2df)=E[MP4/6\text{-}311G^{**}(2df)]\text{-}E(MP4/6\text{-}311G^{**}) \quad (3.2)$$

Next, a correlation for residual correlation effects is added in order to account for deficiencies of truncating the MP theory at the fourth order. This improvement to the energy is realized with the quadratic configuration interaction method because it incorporates parts of the fifth and higher order contributions.

$$E(QCI)=E[QCISD(T)/6\text{-}311G^{**}]\text{-}E(MP4/6\text{-}311G^{**}) \quad (3.3)$$

Still, because of remaining deficiencies in the basis set, we need to add an overall "higher level correction" (HLC) to account for the correlation between spin-paired electrons. Based on the analysis of the hydrogen atom and the hydrogen molecule, it is given as:

$$E(HLC)=-0.19n_{\alpha}-5.95n_{\beta} \quad (3.4)$$

Where the n_{α} and n_{β} designate the number of spin up and spin down electrons, and the total correction is in millihartrees. This is a purely empirical correction that does not have a fundamental basis in theory, like the other changes made so far.

In the final step, the zero-point energy (ZPE) correction is added to get the total energy. The ZPE is obtained by optimizing the geometry at the HF/6-31G* level and finding the frequencies of that molecule. Then, in order to take into account the known frequency calculation deficiencies at that level, a factor of 0.8929 is used to scale the energy (Pople et al., 1981).

Therefore, the G1 energy is obtained by:

$$E_0(G1)=E[MP4SDTQ(FC)/6\text{-}311G^{**}]+\Delta E(+)+\Delta E(2df)+\Delta E(QCI)$$
$$+\Delta E(HLC)+\Delta E(ZPE) \quad (3.5)$$

Based on the G1 test set species, agreement within 2 kcal/mol was found in most cases for compounds including only first-row elements. For those containing second-row elements, agreement was found to be within 3 kcal/mol. G1 theory has been applied to various molecular systems (Curtiss et al., 1991; Curtiss and Pople, 1988a; Curtiss and Pople, 1988b; Curtiss and Pople, 1988c; Curtiss and Pople, 1989a; Curtiss and Pople, 1989b; Raghavachari et al., 1989; Ruscic et al., 1989) and has provided valuable information.

However, some deficiencies in G1 theory were found that may cause discrepancies between computational results and experiment. G1 theory does poorly for ionic molecule dissociation energies, triplet molecules, singlet-triplet energy separations, some hydrides and hypervalent species. In G2 theory, a correction, Δ, is added to the G1 method in order to overcome these deficiencies.

First, the assumption of separate basis set extensions for diffuse function *sp*(+) and higher polarization 2*df* basis sets in G1 theory is eliminated by adding the first part of the correction, Δ_1.

$$\Delta_1=D(+2df)-D(+)-D(2df) \quad (3.6)$$

Where, $$D(+2df)=E[MP2/6\text{-}311+G(2df,p)]-E[MP2/6\text{-}311G(d,p)] \quad (3.7)$$

$$D(+)=E[MP2/6\text{-}311+G(d,p)]-E[MP2/6\text{-}311G(d,p)] \quad (3.8)$$

$$D(2df)=E[MP2/6\text{-}311G(2df,p)]-E[MP2/6\text{-}311G(d,p)] \quad (3.9)$$

Second, a third *d*-function on nonhydrogen atoms and a second *p*-function on hydrogen is added as a correction, Δ_2.

$$\Delta_2=E[MP2/6\text{-}311+G(3df,2p)]-E[MP2/6\text{-}311+G(2df,p)] \quad (3.10)$$

Finally, an improvement to the higher level correction is made by adding 1.14 times the number of electron pairs to the total energy as a purely empirical correction.

$$E(HLC)=-0.19n_{\alpha}-4.81n_{\beta} \quad (3.11)$$

The G2 energy is obtained by:

$$E_0(G2)=E_0(G1)+\Delta_1+\Delta_2+\Delta E(HLC)+1.14n_{pair} \quad (3.12)$$

G2 theory is a significant improvement over G1 theory. The average absolute deviation from experiment of atomization energies of 39 first-row compounds is reduced from 1.42 to 0.92 kcal/mol. And for the G2 test set of 125 species, the average absolute deviation is 1.21 kcal/mol.

3.1.1.2 New developments in the G2 theory

Although the G2 method is quite accurate, it's application is limited by the prohibitive computational cost of the fourth-order Moller-Plesset calculation, MP4(SDTQ), using the 6-311G(2*df*,*p*) basis set. There are several research groups that have lately modified the G2 theory to eliminate the highest level single point energy calculation step or improve the accuracy of the energy calculations. In 1992, Curtiss and Pople (Curtiss et al., 1993) proposed to replace the MP4/6-311G(2*df*,*p*) calculation with the 2nd order Moller-Plesset (MP2) or 3rd Moller-Plesset (MP3) level

for the basis-set-extension energy corrections, which are referred as G2(MP2) and G2(MP3) theories.

In G2(MP2) theory, the basis-set-extension step is replaced by an MP2 level single point correction:

$$\Delta_{MP2}=E[MP2/6\text{-}311+G(3df,2p)]-E[MP2/6\text{-}311G(d,p)] \quad (3.13)$$

And the G2(MP2) energy is given by:

$$E_0[G2(MP2)]=E[QCISD(T)/6\text{-}311G(d,p)+\Delta_{MP2}+HLC+E(ZPE) \quad (3.14)$$

In G2(MP3) theory, the basis-set-extension steps are replaced by MP3 level single point corrections:

$$\Delta_{MP3}(+)=E[MP3/6\text{-}311+G(d,p)]-E[MP3/6\text{-}311G(d,p)] \quad (3.15)$$

$$\Delta_{MP3}(2df)=E[MP3/6\text{-}311G(2df,p)]-E[MP3/6\text{-}311G(d,p)] \quad (3.16)$$

And the G2(MP3) energy is given by:

$$E_0[G2(MP3)]=E[QCISD(T)/6\text{-}311G(d,p)+\Delta_{MP3}(+)+\Delta_{MP3}(2df)+\Delta+HLC+E(ZPE) \quad (3.17)$$

For the G2 test set of 125 species, the average absolute deviation of G2(MP2) is 1.57 kcal/mol and 1.52 kcal/mol for G2(MP3). The replacement of the MP4 level calculation in G2 with lower level MP2 or MP3 significantly reduces computational time and disk storage. Therefore, G2(MP2) and G2(MP3) methods can handle larger systems that were impossible to handle with the G2 method. The G2(MP3) method has only a slight energetic advantage over G2(MP2), so the latter is recommended for large molecules systems.

In 1995, Glukhovsev and coworkers proposed the G2(+) method (Glukhovtsev et al., 1995a; Glukhovtsev et al., 1995b; Glukhovtsev et al., 1996a; Glukhovtsev et al., 1996b). In order to have a better description of anions and simplify computation, some modifications were made to the original G2 method. The geometry and frequency calculations are performed with a basis set that includes diffuse functions, 6-31+G(*d*), rather than 6-31G(*d*). For simplification, the MP2/6-31+G(*d*) optimization method is applied with the frozen-core approximation and the frequencies are calculated at the HF/6-31+G(*d*) level instead of HF/6-31G(*d*).

On the other hand, Mebel *et al*. developed a family of modified G-2 methods (G2M) in 1995, which applied hybrid density-functional theory for geometry optimization and frequency calculations, and electron correlation evaluated at the coupled-cluster methods (Mebel et al., 1995). G2M(RCC), the most accurate method in this family, gives an average absolute deviation of 0.88 kcal/mol for 32 first-row compounds atomization energy calculations. Korchowiec applied the G2M method to methane and hydrofluoromethanes with hydroxyl radical reactions (Korchowiec et al., 1999). The average absolute errors of the reaction enthalpies and activation energies calculated were smaller than 1 kcal/mol.

In 1999, Fast and coworkers modified the G2 method by deleting the empirical high-level correction and applying empirical coefficients to extrapolate to full configuration interaction and an infinite basis set (Fast et al., 1999b). This is referred to as multicoefficient Gaussian-2 (MCG2), which is useful for calculating

continuous global potential energy surfaces. The equation representing this method is:

$$E(MCG2)=c_1E[HF/(d,p)]+c_2\Delta E[HF/a(3df,2p)|(d,p)]+c_3\Delta E[MP2|HF/(d,p)]+c_3\Delta E[MP2|HF/(d,p)]+c_4\Delta E[MP2|HF/a(3df,2p)|(d,p)]+c_5\Delta E[MP4SDQ|MP2/(d,p)]+c_6\Delta E[MP4SDQ|MP2/(2df,p)|(d,p)]+c_7\Delta E[MP4|MP4SDQ/(d,p)]+c_8\Delta E[MP4|MP4SDQ/(2df,p)|(d,p)]+c_9\Delta E[QCISD(T)|MP4/(d,p)]+E_{SO}+E_{CC} \quad (3.18)$$

Where the pipe "|" is defined as

$$E(L/B2|B1)=E(L/B2)-E(L/B1), \quad (3.19)$$

$$E(L2|L1/B)=E(L2/B)-E(L1/B), \quad (3.20)$$

$$E(L1|L2/B2|B1)=E(L2|L1/B2)-E(L2|L1/B1), \quad (3.21)$$

And E_{SO} and E_{CC} are spin-orbit and core-correlation energy described elsewhere (Fast et al., 1999c).

A "minimal" MCG2 method (MMCG2) is defined without the inclusion of spin-orbit and core-correlation effects. The coefficients for both MCG2 and MMCG2 methods are listed in Table 3-1.

Table 3-1. Optimized coefficients for G2 composite method

Method	c_1	c_2	c_3	c_4	c_5	c_6	c_7	c_8	c_9
MCG2	0.9911	1.0329	1.1498	1.0160	1.0242	3.4914	0.3824	3.1698	1.0826
MMCG2	0.9949	0.9462	1.1414	1.0396	1.0784	3.6766	0.6666	3.3428	1.1427

3.1.2 Gaussian-3 (G3) Composite Energy Method

3.1.2.1 Gaussian-3 (G3) theory

Gaussian-3 (G3) theory was the third in the series of Gaussian-n theories. It makes a significant improvement over G2 theory and eliminates many of the deficiencies in G2 theory. The steps in G3 theory are described next.

First, the initial geometry structure, frequencies and zero point energy E(ZPE) are calculated using HF/6-31G(*d*), and a scaling factor of 0.8929 (Pople et al., 1981) is applied to the obtained frequency results.

Second, the equilibrium geometry is optimized with the second order Moller-Plesset method with all electrons and a 6-31G(*d*) basis set, MP2(full)/6-31G(*d*). This is the geometry used in the following single point energy calculation steps.

The starting energy of G3 theory is obtained using fourth order Moller-Plesset perturbation theory with the 6-31G(*d*) basis set, MP4/6-31G(*d*). Also, several corrections are added to improve the results.

First, a diffuse function correction is added, ΔE(+):

$$\Delta E(+)=E[MP4/6\text{-}31+G(d)]\text{-}E[MP4/6\text{-}31G(d)] \quad (3.22)$$

A higher polarization function correction is then done, ΔE(2df,p):

$$\Delta E(2df,p)=E[MP4/6\text{-}31G(2df,p)]\text{-}E[MP4/6\text{-}31G(d)] \quad (3.23)$$

Correlation effects for corrections beyond fourth order perturbation theory using the quadratic configuration method are done, ΔE(QCI):

$$\Delta E(QCI)=E[QCISD(T)/6\text{-}31G(d)]\text{-}E[MP4/6\text{-}31G(d)] \quad (3.24)$$

Large basis set effect corrections are computed, ΔE(G3large):

$$\Delta E(G3large)=E[MP2(full)/G3large]\text{-}E[MP2/6\text{-}31G(2df,p)]\text{-}E[MP2/6\text{-}31+G(d)] + E[MP2/6\text{-}31G(d)] \quad (3.25)$$

Then, a "higher level correction", E(HLC), which accounts for the remaining deficiencies in the energy calculation is added, again as an empirical correction.

$$E(HLC)=-6.386n_{\beta}-2.977(n_{\alpha}-n_{\beta}) \text{ for molecules} \quad (3.26)$$

$$E(HLC)=-6.219n_{\beta}-1.185(n_{\alpha}-n_{\beta}) \text{ for atoms (including atomic ions)} \quad (3.27)$$

Where n_{α} and n_{β} are the numbers of α and β electrons, with units of mhartrees.

Finally, the total G3 composite energy is obtained by:

$$E_0(G3)=E[MP4/6\text{-}31G(d)]+\Delta E(+)+\Delta E(2df,p)+\Delta E(QCI)+\Delta E(G3large) + \Delta E(SO)+E(HLC)+E(ZPE) \quad (3.28)$$

where the spin-orbit correction, ΔE(SO), is taken from experiment. This factor commonly is not included in G3 theory because experimental data are not available for all of the elements.

For the 299 energies from the G2/97 basis set (Curtiss et al., 1997a; Curtiss et al., 1998b) including enthalpies of formation, ionization potentials, electron affinities, and proton affinities, the overall average absolute deviation decreases from 1.48 kcal/mol for G2 theory to 1.02 kcal/mol for G3 theory. For a larger experimental test set, G3/99 which includes 376 energies, G3 theory has a mean absolute deviation of 1.07 kcal/mol (Curtiss et al., 2000a)

Besides the accuracy improvement in energies, the computational cost of the G3 method is nearly a factor of 2 to 3 less than that of the G2 method for two sample molecules, benzene and $SiCl_4$ (Curtiss et al., 1998a).

3.1.2.2 New developments in G3 theory

Because the correction methods in G3 theory are still very computationally intensive, some modifications have been made to reduce the computational cost so that larger systems can be studied. In 1999, Curtiss *et al*. proposed a new modification to the G3 theory, where the basis set extension is calculated using second-order Moller-Plesset perturbation theory (MP2) instead of the computationally demanding MP4 method. This is referred to as G3(MP2) (Curtiss et al., 1999b).

$$E_0[G3(MP2)]=QCISD(T)/6\text{-}31G(d)+\Delta E_{MP2}+\Delta E(SO)+E(HLC)+E(ZPE) \quad (3.29)$$

Where:

$$\Delta E_{MP2}=[E(MP2/G3MP2large)]-[E(MP2)/6\text{-}31G(d)] \quad (3.30)$$

$$E(HLC)=-9.279n_\beta-4.471(n_\alpha-n_\beta) \text{ for molecules} \quad (3.31)$$

$$E(HLC)= -9.345n_\beta-2.021(n_\alpha-n_\beta) \text{ for atoms (including atomic ions)} \quad (3.32)$$

G3(MP2) theory gives significant improvement over G2(MP2) theory. For the 299 energies in the G2/97 test set, the absolute average deviation from experiment is decreased from 1.89 kcal/mol for the G2(MP2) method to 1.30 kcal/mol for the G3(MP2) method. Additionally, significant savings of computational time and disk storage are achieved with the G3(MP2) method.

Similarly, another variation of Gaussian-3 (MP3) theory was developed by Curtiss and coworkers at almost the same time (Curtiss et al., 1999a). It replaces the fourth-order perturbation theory in G3 theory with third-order perturbation theory and is referred as G3(MP3) theory.

$$E_0[\text{G3(MP3)}]=\text{QCISD(T)/6-31G(}d\text{)}+\Delta E_{MP3}+\Delta E_{MP2}+\Delta E(\text{SO})+E(\text{HLC})+E(\text{ZPE}) \quad (3.33)$$

Where:

$$\Delta E_{MP3}=[\text{E(MP3)(FC)/6-31G(2}df,p\text{)}]-[\text{E(MP3)(FC)/6-31G(}d\text{)}] \quad (3.34)$$

$$\Delta E_{MP2}=[\text{E(MP2(FU)/G3large)}]-[\text{E(MP2)(FC)/6-31G(}2df,p\text{)}] \quad (3.35)$$

$$E(\text{HLC})=-7.902n_\beta-3.684(n_\alpha-n_\beta) \text{ for molecules} \quad (3.36)$$

$$E(\text{HLC})= -7.368n_\beta-1.983(n_\alpha-n_\beta) \text{ for atoms (including atomic ions)} \quad (3.37)$$

Only three single-point energy calculations are required, which are QCISD(T)/6-31G(d), MP3(FC)/6-31G(2df,p), and MP2(FU)/G3large. For the 299 energies of G2/97 test set, the average absolute deviation from experiment decreases from 1.30 kcal/mol for the G3(MP2) theory to 1.22 kcal/mol for the G3(MP3) theory. And, for ionization potentials and electron affinity calculations, G3(MP3) theory

performs much better than G3(MP2). Additionally, G3(MP3) theory is about four times faster than G3 theory.

Baboul *et al.* proposed a new modification to the G3 and G3(MP2) theories by substituting the geometry and zero-point energy calculation method with B3LYP density functional theory B3LYP/6-31G(d) instead of MP2(FU)/6-31G(d).(Baboul et al., 1999) The zero point energy scaling factor used for B3LYP with this basis set is 0.96 (Curtiss et al., 1997b). The new methods are referred to as G3//B3LYP and G3(MP2)//B3LYP theories, respectively. All other calculational steps are identical to G3 or G3(MP2) theories, where the high level correction term HLC is $-An_\beta-B(n_\alpha-n_\beta)$ for molecules and $-Cn_\beta-D(n_\alpha-n_\beta)$ for atoms (including atomic ions). For G3//B3LYP theory, A=6.760 mhartrees, B=3.233 mhartrees, C=6.786 mhartrees, and D=1.269 mhartrees. For G3(MP2)//B3LYP theory, A=10.041 mhartrees, B=4.995 mhartrees, C=10.188 mhartrees, and D=2.323 mhartrees. From the G2/97 test set of 299 energies, the average absolute deviation from experiment is 0.99 kcal/mol for G3//B3LYP theory compared to 1.01 kcal/mol for G3 theory. G3(MP2)//B3LYP theory has an average absolute deviation of 1.25 kcal/mol compared with 1.30 kcal/mol for G3(MP2) theory.

In 1999, Fast and coworkers provided a multi-coefficient modification (MCG3) of the G3 method which is fitted for continuous potential energy surface calculations (Fast et al., 1999a; Fast et al., 1999c). Curtiss *et al.* also modified the G3 theory with multiplicative scale factors, referred to as G3S (Curtiss et al., 2000b). Six

parameters are obtained by fitting to the G2/97 test set, and the G3S method has a mean absolute deviation of 0.99 kcal/mol, compared with G3 at 1.01 kcal/mol.

3.1.3 Complete Basis Set (CBS) Composite Energy Method

Because one of the major error sources in *ab initio* calculations of molecular energies is from basis set truncation, in 1988, Petersson and coworkers proposed a complete basis set (CBS) model chemistry which is defined to include the basis set truncation errors (Petersson et al., 1988). The CBS model chemistry requires three components: basis sets for each atom, the CBS self-consistent-field (SCF) energy, and the CBS correlation energy. The atomic pair natural orbitals (APNO) basis sets for the atoms from H to Ne are based on the optimized primitive Gaussian basis sets of Van Duijneveldt (van Duijneveldt, 1971). Double zeta plus polarization level atomic pair natural orbital basis sets are used to calculate SCF energies and correlation energies.

The total energies of the closed-shell atoms and hydrides of the first-row elements obtained using $CBS^{(\infty,3)}$ (full)/atomic pair natural orbital (APNO) model chemistry were in very good agreement with experiment. The root mean square errors were within ±0.0014 Hartrees, which was the most accurate energy calculation method for molecules at that time.

In 1991, the CBS model chemistry was extended to include open-shell species by including *f* functions in the basis set (Petersson and Allaham, 1991). Localization of the occupied orbitals was introduced. Moreover, the higher-order correlation is

treated using the quadratic configuration interaction singles and doubles with the fourth-order triples QCISD(T) method (Pople et al., 1987). By those modifications, the CBS method is self-consistent and applicable to any geometry of any state of a polyatomic molecule. The energies of first row atoms calculated using the CBS-QCI(full)/APNO model were in very good agreement with experiment. The root mean square errors were within ±0.0012 Hartrees compared to experiment, which were the most accurate energy calculations for molecules containing first row atoms at that time.

A sequence of CBS-QCI family of methods were then developed successively (Petersson et al., 1991). CBS-QCI/APNO is the most accurate method among this family and serves as a benchmark to test other methods. And, the CBS2(FC)/6-31G++ model chemistry has about 2.5 times larger errors compared with CBS-QCI. The CPU time is two orders of magnitude less than the G1 method and one order of magnitude less than CBS2(FC)/6-311G**-QCI/6-31G** method, which has similar accuracy compared to the G1 method.

Because of the prohibitive computational cost of the CBS-QCI/APNO method, some modifications were made in 1993 so it can be applied to a wider range of molecular systems (Montgomery et al., 1994). The geometry is optimized at the QCISD/6-311G** level and the zero point energy is evaluated using an unrestricted Hartree-Fock UHF/6-311G** calculation with a scaling factor of 0.9251 (Grev et al., 1991). The higher-order correlation energy is obtained at the

QCISD(T)/6-311^{++}G(*2df,p*) level, except in cases where $\Delta<S^2>$ is larger than 0.11 where the APNO basis set is retained. Also, a size-consistent empirical correction is introduced to improve calculated results. For the 64 first-row species from the G2 test set, the root mean square error for the CBS-QCI/APNO method is 0.68 kcal/mol compared with 1.37 kcal/mol for the G2 method.

Although CBS-QCI/APNO models gave a very good improvement over other *ab initio* calculations, the method is limited by its prohibitive computational cost. Petersson *et. al* continued to modify the original theory to reach a compromise of accuracy and CPU time. In 1995, three new computational models, CBS-4, CBS-q, CBS-Q, were introduced (Ochterski et al., 1996). The CBS-4 method has the best efficiency through using smaller basis sets for some of the calculations. The mean absolute deviation of 125 energies from the G2 test set is 2.0 kcal/mol. CBS-q and CBS-Q performs increasing better by using larger basis sets and including core correlation. The mean absolute deviations are 1.7 and 1.0 kcal/mol, respectively.

The popularly applied CBS-Q method is composed of the following calculation steps:

1. Geometry optimization and frequencies calculation at the UHF/6-31G* level
2. Geometry optimized at MP2(FC)/6-31G*
3. UMP2/6-311+G(*3d2f,2df,2p*) energy and CBS extrapolation
4. MP4(SDQ)/6-31+G(*d(f),p*) single point energy

5. QCISD(T)/6-31+G* single point energy

The CBS-Q energy is obtained by:

$$E(CBS\text{-}Q)=E(UMP2)+\Delta E(CBS)+\Delta E(MP4)+\Delta E(QCI)+\Delta E(ZPE)+\Delta E(emp)+\Delta E(spin) \quad (3.38)$$

Where, $\Delta E(MP4)=E[MP4(SDQ)/6\text{-}31+G(d(f),p)]-E[MP2/6\text{-}31+G(d(f),p)]$ (3.39)

$\Delta E(QCI)=E[QCISD(T)/6\text{-}31+G^*]-E[MP4(SDQ)/6\text{-}31+G^*]$ (3.40)

$\Delta E(ZPE)$ is obtained at step 1, with a scaling factor of 0.91844

$\Delta E(spin)=-9.20mE_h\Delta\langle S^2\rangle$ (3.41)

$$\Delta E(emp) = -5.33mE_h \sum_{i=1}^{n_\beta} \left[\sum_{\mu=1}^{N_{virt}+1} C_{\mu_{ii}} \right]^2 |S|_{ii}^2 \quad (3.42)$$

Where $|S|_{ii} = \int |{}^{\alpha}\varphi_i^{\beta}\varphi_i| d\tau$ (3.43)

Later in 1999, Montgomery and coworkers modified the CBS-Q method using density functional geometry and frequencies, referred to as the CBS-QB3 method (Montgomery et al., 1999). This method has similar steps to the CBS-Q method, while the geometries and frequencies are obtained at the B3LYP/6-311G(*2d,d,p*) level. Furthermore, the QCISD(T) single point energy calculation step in the CBS-Q method is replaced by CCSD(T) in the CBS-QB3 method. The empirical parameters for final corrections were then re-optimized. The zero point scaling factor is 0.99. The coefficient of the overlap interference term is $-5.79mE_h$ to replace the $-5.33mE_h$. term in Eq. (3.42). And, $-9.54mE_h$ is used for the spin correction parameter to replace the $-9.20mE_h$ term in Eq.(3.41). For the G2 test set of first-row molecules, the mean

absolute error in energies is decreased to 0.87 kcal/mol for CBS-QB3 method.

For free radical molecules, spin contamination becomes a serious problem. To deal with this problem, Mayer and coworkers proposed the CBS-RAD method which is a modification of the CBS-Q method to treat free radicals and yield reliable results (Mayer et al., 1998). The geometry and zero point energies are obtained using the QCISD/6-31G(d) method, and the quadratic configuration interaction method in the CBS-Q single point energy calculation is replaced by coupled-cluster theory. The CSB-RAD method scheme is composed of 5 steps:

1. Geometry optimization and frequencies calculation at the QCISD(fc)/6-31G(d) level; scaling factor for zero point energy is 0.9776 (Scott and Radom, 1996)
2. CCSD(T)(fc)/6-31+G* single point energy calculation
3. MP4(SDQ)(fc)/CBSB4 single point energy calculation
4. MP2(fc)/CBSB3 single point energy calculation

The CBS-RAD energy is obtained by:

$$E(\text{CBS-RAD})=E(\text{SCF})+\Delta E(\text{MP2})+\Delta E(\text{CC})+\Delta E(\text{MP3,4})+\Delta E(\text{CBS}) +\Delta E(\text{INT})+\Delta E(\text{EMP})+\Delta E(\text{SPIN})+\text{ZPE} \quad (3.44)$$

Where, E(SCF)=HF/CBSB3:

$\Delta E(\text{MP2})=\text{MP2/CBSB3-HF/CBSB3}$

$\Delta E(\text{CC})=\text{CCSD(T)/6-31+G*-MP4(SDQ)/6-31+G*}$

$\Delta E(\text{MP3,4})=\text{MP4(SDQ)/CBSB4-MP2/CBSB4}$

$\Delta E(CBS)=E2(CBS)/CBSB3-DE(UMP2)$

$\Delta E(INT)=CBS-INT/CBSB3-E2(CBS)/CBSB3$

$\Delta E(EMP)=-0.00533*OIii$

$\Delta E(SPIN)=-0.0092*\Delta<S^2>$

CBS-4, CBS-q, CBS-Q, CBS-QB3, and CBS-APNO methods have already been built into the Gaussian 98 software package (Frisch et al., 1998). It should be noted that CBS-4, CBS-q, CBS-Q and CBS-QB3 are available for first and second row atoms while the APNO method is available for first row atoms only.

The errors of different composite energy methods for the G2 test set are summarized in Table 3-2.

Table 3-2. Summary of error measurements for composite energy methods

Composite Energy Method	Mean Absolute Deviation (kcal/mol)	
	G2 test set of 125 energies	G2 expanded test set of 299 energies
G2	1.21	1.48
G2(MP2)	1.57	1.89
G2(MP3)	1.52	1.30
G3	-	1.02
G3(MP2)	-	1.30
G3(MP3)	-	1.22
CBS-QCI/ANPO	0.5	-
CBS-QB3	0.87	-
CBS-Q	0.98	-
CBS-4	2.0	-

The CBS composite energy method family has the least mean absolute deviation errors compared with the G2 and G3 series, which shows the importance of reducing

basis set truncation errors. However, the CBS calculations always have very high computational costs and take a considerably long time to run. In the next section, we will analyze the CBS method in order to modify and find a composite energy method that fits the accuracy requirement of studying hydrocarbon thermal cracking reactions with reasonable computational costs.

3.2 The Development and Evaluation of a New Composite Energy Method

3.2.1 The Development of a new Composite Method

Blowers, *et al.* (Blowers et al., 2003) showed that, for 17 ligand transfer reactions, the CBS-RAD method decreased the root mean square(RMS) error by about 10% compared with the G2 method for activation energy calculations. However, this increase in accuracy caused the CPU time to increase by 400%, which limits the application of the CBS-RAD method to systems with a small number of first and second row atoms.

To reduce the computational cost while maintaining high accuracy, we proposed replacing the time consuming QCISD(fc)/6-31g* geometry optimization and frequency calculation method in the CBS-RAD method with the MP2(full)/6-31g* method and basis set, and the resulting method is named the CBS-RAD(MP2) method (Zheng and Blowers, 2005).

The purpose of the work in the rest of this chapter is to test the performance of the composite energy methods on hydrocarbon cracking reaction energetics with reactions that have reliable experimental data. Based on the results of this work, the specific method can be applied to the estimation of large hydrocarbon cracking reaction energetics where there is no experiment information.

3.2.2 Computational Methods

All of the *ab initio* calculations were performed with the GAUSSIAN98 software package (Frisch et al., 1998). Geometries were optimized at the MP2(full)/6-31g* level of calculation instead of the larger QCISD(fc)/6-31g* method recommended in the CBS-RAD method to reduce computational costs, as was just discussed. A comparison of calculations needed for the G2, G3, CBS-QB3, and CBS-RAD(MP2) composite energy methods is shown in Table 3-3.

Table 3-3. Brief description of the composite energy methods used in this chapter

Method	G2	G3	CBS-QB3	CBS-RAD(MP2)
Geometry Optimization	MP2(full)/6-31G*	MP2(full)/6-31G*	B3LYP/6-311G(*2d,d,p*)	MP2(full)/6-31G*
Single Point Calculations	MP4SDTQ(fc)/6-311G** MP4SDTQ(fc)/6-311+G** MP4SDTQ(fc)/6-311+G**(*2df,p*) QCISD(T)/6-311G** MP2/6-311+G(*3df,2p*)	MP4SDTQ(fc)/6-31G* MPSDTQ(fc)/6-31+G* MP4SDTQ(fc)/6-31G(*2df,p*) QCISD(T)/6-31G* MP2=(full)/big basis	CCSD(T)/6-31+G(*d(f),p*) MP4SDQ/CBSB4 MP2/CBSB3	CCSD(T)(fc)/6-31+G* MP4SDQ(fc)/CBSB4 MP2(fc)/CBSB3
Frequency	MP2(full)/6-31G*	MP2(full)/6-31G*	B3LYP/6-311G(*2d,d,p*)	MP2(full)/6-31G*
Empirical Corrections	E(SO) Higher Level Correction Scaled ZPE	E(SO) Higher Level Correction Scaled ZPE	Spin Contamination Empirical Correction Scaled ZPE	Spin Contamination Empirical Correction Scaled ZPE

All products and reactants were verified to be stable structures with frequency calculations and all transition states were found to be first order saddle points with only one negative eigenvalue. Additionally, IRC (intrinsic reaction coordinate) calculations showed that each reaction linked the correct products with reactants. For the CBS-RAD(MP2) method, ZPVEs (zero point vibrational energies) were obtained from harmonic vibrational frequencies calculated at the MP2(full)/6-31g* level with a scaling factor of 0.9661 (Scott and Radom, 1996). Frequencies were scaled with a factor of 0.9427 at the MP2(full)/6-31g* level, and a factor of 0.9537 at the QCISD(fc)/6-31g* level (Scott and Radom, 1996). For heats of reaction, an additional temperature correction was added to convert from internal energy to enthalpy with the change in number of moles. This term changes the energy by a factor of $+\Delta nRT$, where $\Delta n = 1$.

3.2.3 Results and Discussion

Before considering the heats of reaction and activation energy calculations, we compare geometries and frequencies obtained by the QCISD(fc)/6-31g* and MP2(full)/6-31g* methods in Tables 3-4, 3-5, and 3-6 for the propyl radical ($CH_2CH_2CH_3$), the neopentyl radical ($CH_2C(CH_3)_3$), and the transition state structure for the propyl radical β-scission reaction ($CH_2CH_2CH_3 \rightarrow CH_2CH_2 + CH_3$). These comparisons are important because changes in structure affect partition functions, which may affect reaction rates estimated through transition state theory, as discussed in Chapter 2.

From Table 3-4, the geometries and frequencies obtained by the two different computational methods for the propyl radical show that the largest bond length difference is 0.005 Å for carbon – carbon bonds and the carbon – hydrogen bond lengths are all identical. Meanwhile, the largest deviation in angle is 0.32^{o} from A(9H-3C-2C). The scaled frequency results obtained by QCISD(fc)/6-31g* are lower than the MP2(full)/6-31g* results, but the largest difference is 10%.

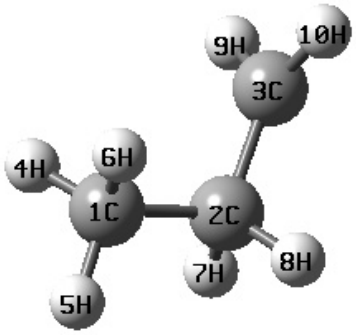

Table 3-4. Geometry and frequency calculation results obtained by MP2(full)/6-31g* and QCISD(fc)/6-31g* methods for the propyl radical ($CH_2CH_2CH_3$)

	R(1C-2C)	R(2C-3C)	R(4H-1C)	R(9H-3C)	A(1C-2C-3C)	A(9H-3C-2C)
mp2(full)/6-31g*	1.536	1.490	1.090	1.080	112.760	120.320
qcisd(fc)/6-31g*	1.541	1.490	1.090	1.080	112.950	120.640
	frequency (cm^{-1})					
mp2(full)/6-31g*	98, 253, 322, 499, 725, 872, 884, 1022, 1074, 1176, 1278, 1311 1378, 1446, 1465, 1474, 1481, 2925, 2928, 2973, 3012, 3020, 3047, 3149					
qcisd(fc)/6-31g*	88, 250, 320, 499, 725, 872, 883, 1024, 1073, 1179, 1282, 1313 1386, 1443, 1468, 1475, 1484, 2912, 2920, 2950, 2992, 2998, 3028, 3121					

For the geometry calculation results of the neopentyl radical in Table 3-5, the largest bond length difference is 0.008 Å for carbon – carbon bonds and the carbon – hydrogen bond lengths are again all identical. The largest angle difference is for A(2H-1C-4C), which is 0.19^{o}. However, the frequency calculations using the QCISD(fc)/6-31g* method were computationally demanding and were not complete after 64 hours of CPU time using the IBM pSeries 655 supercomputer at Boston University. This highlights why the original CBS-RAD method using the QCISD geometry optimization is too expensive for larger species and shows our motivation for changing to a lower level for the geometry optimization and frequency calculations.

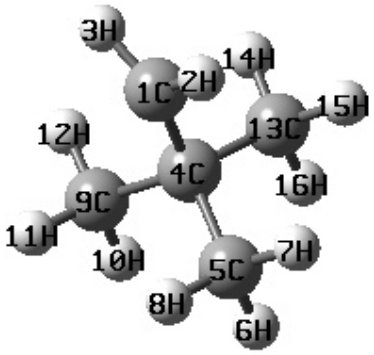

Table 3-5. Geometry and frequency calculation results obtained by MP2(full)/6-31g* and QCISD(fc)/6-31g* methods for the neo-pentyl radical ($CH_2C(CH_3)_3$)

	R(1C-4C)	R(2H-1C)	R(6H-5C)	A(1C-4C-5C)	A(2H-1C-4C)	A(9C-4C-13C)
mp2(full)/6-31g*	1.497	1.080	1.090	109.770	120.180	109.110
qcisd(fc)/6-31g*	1.505	1.080	1.090	109.710	120.370	109.140
	frequency (cm^{-1})					
mp2(full)/6-31g*	153, 233, 281, 286, 301, 324, 376, 402, 405, 536, 726, 900, 913, 930, 935, 938 1012, 1049, 1196, 1253, 1267, 1393, 1370, 1391, 1436, 1455, 3007, 3008, 3028, 3130					
qcisd(fc)/6-31g*	not calculated					

In Table 3-6, the transition state structure of the propyl radical β-scission reaction is shown, and the largest bond deviation is 0.02 Å for carbon – carbon bonds and the carbon – hydrogen bonds are still all identical. The largest deviation in angle is 0.15^{o} for A(4H-1C-2C). From the frequency calculation results, all the differences are within 10% between the two methods.

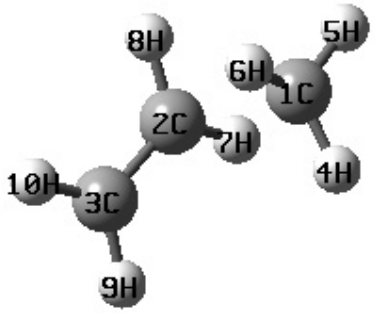

Table 3-6. Geometry and frequency calculation results obtained by MP2(full)/6-31g* and QCISD(fc)/6-31g* methods for the transition state of the propyl radical β-scission reaction ($CH_2CH_2CH_3 \rightarrow CH_2CH_2 + CH_3$)

	R(1C-2C)	R(2C-3C)	R(4H-1C)	R(7H-2C)	A(1C-2C-3C)	A(4H-1C-2C)
mp2(full)/6-31g*	2.260	1.340	1.080	1.080	109.520	101.660
qcisd(fc)/6-31g*	2.272	1.360	1.080	1.080	109.580	101.510
	frequency (cm^{-1})					
mp2(full)/6-31g*	591i, 108, 230, 368, 504, 532, 791, 805, 888, 964, 1047, 1211, 1277 1408, 1413, 1439, 1558, 3000, 3042, 3050, 3123, 3144, 3155, 3167					
qcisd(fc)/6-31g*	535i, 104, 220, 355, 502, 525, 766, 795, 827, 930, 979, 1205, 1252 1402, 1407, 1435, 1539, 2983, 3026, 3037, 3100, 3122, 3128, 3138					

With the results above, we see that geometries and frequencies obtained by QCISD(fc)/6-31g* and MP2(full)/6-31g* calculations did not differ substantially from each other. This is the reason we propose replacing the QCISD(fc)/6-31g* method in the CBS-RAD method with the MP2(full)/6-31g* method in the new CBS-RAD(MP2) method.

We next show the performance of the new CBS-RAD(MP2) composite energy method by comparing results for 13 hydrocarbon radical cracking reactions energetics with the G2 and G3 composite methods and experimental data in Table 3-7. Both carbon-carbon bond cracking and carbon-hydrogen bond cracking reactions were investigated.

Table 3-7. Comparison of computed composite heats of reaction (units in kcal/mol)

Reaction	G2	G3	CBS-QB3	CBS-RAD(MP2)	Experiment *
$CH_2CH_3 \rightarrow CH_2CH_2 + H$	33.63	34.51	35.00	34.17	*36.24*
$CH_3CH_3 \rightarrow CH_2CH_3 + H$	101.34	99.65	100.20	100.49	*100.67*
$CH_3CH_2CH_2 \rightarrow CH_3CHCH_2 + H$	30.73	31.58	31.08	31.33	*33.05*
$CH_3CHCH_3 \rightarrow CH_2CHCH_3 + H$	33.67	34.25	34.56	34.31	*35.50*
$CH_3CH_2CH_3 \rightarrow CH_2CH_2CH_3 + H$	101.77	100.40	101.43	101.02	*101.12*
$CH_3CH_2CH_2CH_3 \rightarrow CH_2CH_2CH_2CH_3 + H$	103.63	99.99	100.94	100.69	*101.56*
$CH_3CH_2CH_2CH_3 \rightarrow CH_3CHCH_2CH_3 + H$	99.06	97.63	98.17	98.16	*98.71*
$CH_3C(CH_3)_2 \rightarrow CH_2C(CH_3)_2 + H$	33.77	34.20	34.51	34.43	*36.39*
$CH_2CH_3 \rightarrow CH_2 + CH_3$	98.69	97.49	100.79	98.53	*98.82*
$CH_2CH_2CH_3 \rightarrow CH_2CH_2 + CH_3$	24.21	20.96	22.77	21.76	*23.48*
$CH_2CH_2CH_2CH_3 \rightarrow CH_2CH_2 + CH_2CH_3$	21.25	21.10	21.85	22.16	*21.67*
$CH_2CH(CH_3)_2CH_3 \rightarrow CH_3 + CH_2CHCH_3$	19.27	20.19	22.21	21.20	*22.99*
$CH_3CHCH_2CH_3 \rightarrow CH_3 + CH_2CHCH_3$	21.30	21.05	23.43	22.32	*23.23*
Maximum Absolute Deviation	3.72	2.52	1.96	2.06	-
Root Mean Square Error	1.88	1.70	1.06	1.22	-

* - (Linstrom and Mallard, 2003)

The experimental heats of reaction data were calculated with data from the National Institute of Standards and Technology (NIST) database (Linstrom and Mallard, 2003). The composite energy methods give similar results and the errors are within 4 kcal/mol compared to experimental values. The G2 energy has an RMS (root mean square) error of 1.88 kcal/mol, the maximum absolute deviation is 3.72 kcal/mol, while the RMS error of G3 is 1.70 kcal/mol with a maximum absolute deviation of 2.52 kcal/mol. The CBS-QB3 method has an RMS error of 1.06 kcal/mol with a maximum absolute deviation of 1.96 kcal/mol. The CBS-RAD(MP2) method has an RMS error of 1.22 kcal/mol and the maximum absolute deviation is 2.06 kcal/mol. From the heats of reaction calculations of 13 hydrocarbon cracking reactions, the CBS-QB3 method has the lowest RMS error and the lowest maximum absolute deviation. The CBS-RAD(MP2) has slightly larger errors. However, the two CBS methods have smaller errors compared to the G2 and G3 methods.

Table 3-8 is a comparison of the composite energy results of activation energies for the hydrocarbon cracking reactions with the experimental values from the NIST Chemical Kinetics Database (Mallard et al., 1993). In general, experimental error estimates of the activation energy are ± 0.5 kcal/mol.

Table 3-8. Comparison of computed composite activation energy (units in kcal/mol)

Reaction	G2	G3	CBS-QB3	CBS-RAD(MP2)	Experiment *
$CH_2CH_3 \rightarrow CH_2CH_2 + H$	37.58	37.19	36.60	40.76	*40.98*
$CH_3CHCH_3 \rightarrow CH_2CHCH_3 + H$	36.78	36.16	35.19	35.74	*35.80*
$CH_3CH_2CH_2 \rightarrow CH_3CHCH_2 + H$	35.63	35.26	34.00	34.52	*37.40*
$CH_3C(CH_3)_2 \rightarrow CH_2C(CH_3)_2 + H$	35.76	35.16	34.55	34.92	*37.59*
$CH_2CH_2CH_3 \rightarrow CH_2CH_2 + CH_3$	30.90	30.40	28.93	29.55	*30.23*
$CH_2CH_2CH_2CH_3 \rightarrow CH_2CH_2 + CH_2CH_3$	29.87	29.43	28.10	28.62	*27.85*
$CH_3CHCH_2CH_3 \rightarrow CH_3 + CH_2CHCH_3$	30.64	30.07	29.34	29.49	*29.24*
$CH_2CH(CH_3)_2 \rightarrow CH_3 + CH_2CHCH_3$	31.04	30.54	29.53	29.66	*30.04*
$CH_2C(CH_3)_3 \rightarrow CH_2C(CH_3)_2 + CH_3$	30.51	30.08	29.53	29.35	*29.84*
Maximum Absolute Deviation	3.40	3.79	4.38	2.88	-
Root Mean Square Error	1.73	1.78	2.17	1.37	-

* - (Mallard et al., 1993)

From the results, the G2 energy has an RMS error of 1.73 kcal/mol, and the maximum absolute deviation is 3.40 kcal/mol. The RMS error of the G3 energy is 1.78 kcal/mol, with a maximum absolute deviation of 3.79 kcal/mol. The CBS-QB3 method has an RMS error of 2.17 kcal/mol, with the maximum absolute deviation of 4.38 kcal/mol. The CBS-RAD(MP2) method shows the least RMS error of 1.37 kcal/mol; the maximum absolute deviation is 2.88 kcal/mol. From the calculated results, the CBS-QB3 method performs most poorly for the activation energy calculations. The reason appears to be that B3LYP density functional theory tends to underestimate the transition state structure energies for chemical reactions and this may have some effect on the composite energies through structure optimizations. Moreover, there can be cases where the B3LYP method completely fails to find a transition state structure for a reaction (Montgomery et al., 1999).

Transition state structures of three carbon-carbon bond cracking reactions are compared with Saeys, *et al*'s work (Saeys et al., 2003) and listed in Table 3-9 so that the geometry optimization we have selected can be compared to high quality results from IRCmax calculations (Malick et al., 1998). Since transition state structures can not be measured experimentally, high level theory optimized transition state geometries are expected to be more accurate. However, transition state structures locations using high level method are always computationally prohibitive. In 1998, Malick *et al*. proposed performing single point calculations using a high level method for the maximum of energy along the intrinsic reaction coordinate (IRC) obtained

with a low level method, which is called the IRCMax method. Using this method, errors of the transition state geometries can be reduced by a factor of 4 to 5. The geometries obtained by the MP2(full)/6-31g* method are closer to the IRCmax results than the B3LYP/6-311G(*d,p*) results. In fact, the bond difference between the two is less than 3 pm, suggesting that the MP2 level of theory used in this work is adequate for reactions involving hydrocarbon species. The B3LYP optimization has larger errors, explaining that the results from the CBS-QB3 composite energy method, which uses the B3LYP geometry optimization method, is less accurate for transition states.

Table 3-9. Carbon-carbon bond cracking reaction calculation results compared with Saeys, *et al.*'s work (distance in units of pm)

	IRCMax*	QCISD/6-31G(*d*)*	MP2(full)/6-31G(*d*)	B3LYP/6-311G(*d*,*p*)	QCISD(fc)/6-31G(*d*)
$CH_3^{\cdot} + CH_2{=}CH_2$	*229.2*	*227.2*	226.0	223.2	227.2
$CH_3CH_2^{\cdot} + CH_2{=}CH_2$	*227.*	*226.5*	225.4	230.5	226.2
$CH_3^{\cdot} + CH_3CH{=}CH_2$	*228.0*	*not calcd*	225.1	233.2	not calculated

* Obtained from Saeys, *et al.*'s work (Saeys et al., 2003)

One can conclude from the calculated results in this chapter that for heats of reaction, the CBS-RAD(MP2) method has a comparable performance with CBS-QB3 which has the least RMS error. For activation energy calculations, the CBS-RAD(MP2) method has the lowest RMS error, while the G2 ,G3 and CBS-QB3 methods have larger errors. However, the computational demands of the G2, G3, CBS-QB3, and CBS-RAD(MP2) methods are quite different. A comparison of computational costs of the G2, G3, CBS-QB3 and CBS-RAD(MP2) methods for the single point and vibrational frequencies of t-butyl radical using the Gaussian98 program on the National Partnership for Advanced Computational Infrastructure supercomputer at Boston University is illustrated in Figure 3-1. It shows that, for tert-butyl energy calculations, the G2 method required 73.22 hours of CPU time, while the G3 method required only 34.83 hours, which is 48% of the G2 time. The computational cost for the CBS-RAD(MP2) method is 11.1 hours, which is only 15% of the requirements for the G2 calculations. This is a large savings of 85% with an improvement in accuracy for predicting heats of reaction and activation energies for hydrocarbon reactions involving radicals. The CBS-QB3 method is composed of similar single point energy calculation steps. However, because of the large basis set used in the geometry optimization and frequency calculations, it takes 13.66 hours, 23% more than CBS-RAD(MP2). These relative times are similar for the other species covered throughout this work. Because of the computational savings and the increased accuracy of the results, the CBS-RAD(MP2) method is recommended for

the study of larger hydrocarbon cracking reactions where computational cost is a concern.

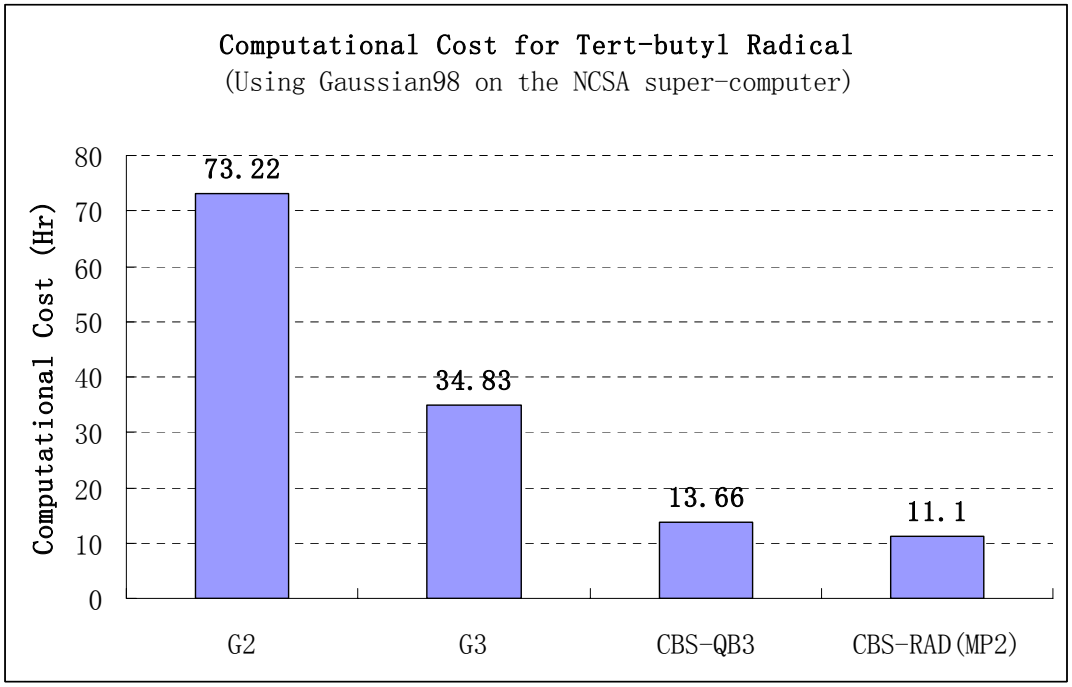

Figure 3-1. Computational cost of *tert*-butyl radical calculations using G2, G3, CBS-Q and CBS-RAD(MP2) methods

3.3 Conclusions

In this chapter, the G2, G3, CBS-QB3, and new CBS-RAD(MP2) composite energy methods are applied to calculations of the heats of reaction and activation energies of 14 hydrocarbon radical cracking reactions where reliable experimental data are available. The new CBS-RAD(MP2) method has the second least RMS error of 1.22 kcal/mol for heats of reaction calculations, very close to CBS-QB3 method which has the least RMS error of 1.06 kcal/mol. For the cracking reaction

activation energy calculation results, the new CBS-RAD(MP2) method has the least RMS error of 1.37 kcal/mol. In addition, the computational cost of the CBS-RAD(MP2) method is 81% of CBS-QB3, 32% of the G3 composite energy methods, and only 15% of the G2 composite energy method. Because of the high accuracy and low computational cost, the CBS-RAD(MP2) composite energy method is useful for large hydrocarbon species.

In the following chapters, we will apply the invented CBS-RAD(MP2) composite energy method to investigate hydrocarbon reaction energetics and kinetics.

References:

Baboul, A.G., Curtiss, L.A., Redfern, P.C. and Raghavachari, K., 1999. Gaussian-3 theory using density functional geometries and zero-point energies. *Journal of Chemical Physics*, 110(16): 7650-7657.

Blowers, P., Zheng, X.B. and Homan, K., 2003. Assessment of the suitability of using the composite G2, G3, and CBS-RAD methods for predicting activation energies. *Chemical Engineering Communications*, 190(9): 1233-1248.

Curtiss, L.A., Brand, H., Nicholas, J.B. and Iton, L.E., 1991. Predicted Proton Affinities of H3sio-, H3sioh, H3siosih3, and H3sioalh3. *Chemical Physics Letters*, 184(1-3): 215-220.

Curtiss, L.A., Carpenter, J.E., Raghavachari, K. and Pople, J.A., 1992. Validity of additivity approximations used in GAUSSIAN-2 theory. *Journal of Chemical Physics*, 96(12): 9030-9034.

Curtiss, L.A., Jones, C., Trucks, G.W., Raghavachari, K. and Pople, J.A., 1990. Gaussian-1 Theory of Molecular-Energies for 2nd-Row Compounds. *Journal of Chemical Physics*, 93(4): 2537-2545.

Curtiss, L.A. and Pople, J.A., 1988a. Theoretical-Study of B2h-5(+), B2h-6(+), and B2h6. *Journal of Chemical Physics*, 89(8): 4875-4879.

Curtiss, L.A. and Pople, J.A., 1988b. Theoretical-Study of Structures and Energies of Acetylene, Ethylene, and Vinyl Radical and Cation. *Journal of Chemical Physics*, 88(12): 7405-7409.

Curtiss, L.A. and Pople, J.A., 1988c. A Theoretical-Study of the Energies of Bhn Compounds. *Journal of Chemical Physics*, 89(1): 614-615.

Curtiss, L.A. and Pople, J.A., 1989a. Theoretical-Study of the C-H Bond-Dissociation Energy of Acetylene. *Journal of Chemical Physics*, 91(4): 2420-2423.

Curtiss, L.A. and Pople, J.A., 1989b. A Theoretical-Study of the Dissociation-Energy of Bh Using Quadratic Configuration-Interaction. *Journal of Chemical Physics*, 90(4): 2522-2523.

Curtiss, L.A., Raghavachari, K. and Pople, J.A., 1993. Gaussian-2 Theory Using Reduced Moller-Plesset Orders. *Journal of Chemical Physics*, 98(2): 1293-1298.

Curtiss, L.A., Raghavachari, K. and Pople, J.A., 1995. Gaussian-2 Theory - Use of Higher-Level Correlation Methods, Quadratic Configuration-Interaction Geometries, and 2nd-Order Moller-Plesset Zero-Point Energies. *Journal of Chemical Physics*, 103(10): 4192-4200.

Curtiss, L.A., Raghavachari, K., Redfern, P.C. and Pople, J.A., 1997a. Assessment of Gaussian-2 and density functional theories for the computation of enthalpies of formation. *Journal of Chemical Physics*, 106(3): 1063-1079.

Curtiss, L.A., Raghavachari, K., Redfern, P.C. and Pople, J.A., 1997b. Investigation of the use of B3LYP zero-point energies and geometries in the calculation of enthalpies of formation. *Chemical Physics Letters*, 270(5-6): 419-426.

Curtiss, L.A., Raghavachari, K., Redfern, P.C. and Pople, J.A., 2000a. Assessment of Gaussian-3 and density functional theories for a larger experimental test set. *Journal of Chemical Physics*, 112(17): 7374-7383.

Curtiss, L.A., Raghavachari, K., Redfern, P.C. and Pople, J.A., 2000b. Gaussian-3 theory using scaled energies. *Journal of Chemical Physics*, 112(3): 1125-1132.

Curtiss, L.A., Raghavachari, K., Redfern, P.C., Rassolov, V. and Pople, J.A., 1998a. Gaussian-3 (G3) theory for molecules containing first and second-row atoms. *Journal of Chemical Physics*, 109(18): 7764-7776.

Curtiss, L.A., Redfern, P.C., Raghavachari, K., Bassolov, V. and Pople, J.A., 1997c. Gaussian-3 theory using reduced M?ller-Plesset order. *Journal of Chemical Physics*, 110: 4703.

Curtiss, L.A., Redfern, P.C., Raghavachari, K. and Pople, J.A., 1998b. Assessment of Gaussian-2 and density functional theories for the computation of ionization

potentials and electron affinities. *Journal of Chemical Physics*, 109(1): 42-55.

Curtiss, L.A., Redfern, P.C., Raghavachari, K. and Pople, J.A., 1999a. Gaussian-3 theory: a variation based on third-order perturbation theory and an assessment of the contribution of core-related correlation. *Chemical Physics Letters*, 313(3-4): 600-607.

Curtiss, L.A., Redfern, P.C., Raghavachari, K., Rassolov, V. and Pople, J.A., 1999b. Gaussian-3 theory using reduced Moller-Plesset order. *Journal of Chemical Physics*, 110(10): 4703-4709.

Fast, P.L., Corchado, J.C., Sanchez, M.L. and Truhlar, D.G., 1999a. Multi-coefficient correlation method for quantum chemistry. *Journal of Physical Chemistry A*, 103(26): 5129-5136.

Fast, P.L., Sanchez, M.L., Corchado, J.C. and Truhlar, D.G., 1999b. The Gaussian-2 method with proper dissociation, improved accuracy, and less cost. *Journal of Chemical Physics*, 110(24): 11679-11681.

Fast, P.L., Sanchez, M.L. and Truhlar, D.G., 1999c. Multi-coefficient Gaussian-3 method for calculating potential energy surfaces. *Chemical Physics Letters*, 306(5-6): 407-410.

Foresman, J.B. and Frisch, E., 1996. *Exploring Chemistry with Electronic Structure Methods*. Gaussian, Inc., Pittsburgh, PA.

Frisch, M.J. et al., 1998. *Gaussian 98, Revision A.7*. Gaussian, Inc., Pittsburgh PA.

Glukhovtsev, M.N., Pross, A. and Radom, L., 1995a. Gas-Phase Identity S(N)2 Reactions of Halide-Ions at Neutral Nitrogen - a High-Level Computational Study. *Journal of the American Chemical Society*, 117(35): 9012-9018.

Glukhovtsev, M.N., Pross, A. and Radom, L., 1995b. Gas-Phase Identity S(N)2 Reactions of Halide Anions with Methyl Halides - a High-Level Computational Study. *Journal of the American Chemical Society*, 117(7): 2024-2032.

Glukhovtsev, M.N., Pross, A. and Radom, L., 1996a. Gas-phase non-identity S(N)2 reactions of halide anions with methyl halides: A high-level computational study.

Journal of the American Chemical Society, 118(26): 6273-6284.

Glukhovtsev, M.N., Pross, A., Schlegel, H.B., Bach, R.D. and Radom, L., 1996b. Gas-phase identity S(N)2 reactions of halide anions and methyl halides with retention of configuration. *Journal of the American Chemical Society*, 118(45): 11258-11264.

Grev, R.S., Janssen, C.L. and Schaefer, H.F., 1991. Concerning Zero-Point Vibrational-Energy Corrections to Electronic Energies. *Journal of Chemical Physics*, 95(7): 5128-5132.

Hehre, W.J., 1986. *Ab initio molecular orbital theory*. Wiley, New York.

Jensen, F., 1998. *An introduction to computational chemistry*. Wiley, New York.

Kedziora, G.S. et al., 1999. The relativistic Dirac-Coulomb-Fock effect on atomization energies. *Journal of Chemical Physics*, 110(15): 7123-7126.

Korchowiec, J., Kawahara, S., Matsumura, K., Uchimaru, T. and Sugie, M., 1999. Hydrogen abstraction from methane and hydrofluoromethanes by center dot OH radical: Modified GAUSSIAN-2 study. *Journal of Physical Chemistry A*, 103(18): 3548-3553.

Leach, A.R., 1998. *Molecular Modelling*. Longman, Essex, England.

Levine, I.N., 2000. *Quantum Chemistry*. Prentice Hall, Upper Saddle River, New Jersey.

Linstrom, P.J. and Mallard, W.G., 2003. *NIST Chemistry WebBook, NIST Standard Reference Database Number 69, March 2003, National Institute of Standards and Technology*, Gaithersburg MD, 20899 (http://webbook.nist.gov).

Malick, D.K., Petersson, G.A. and Montgomery, J.A., 1998. Transition states for chemical reactions I. Geometry and classical barrier height. *Journal of Chemical Physics*, 108(14): 5704-5713.

Mallard, W.G., Westley, F., Herron, J.T., Hampson, R.F. and Frizzell, D.H., 1993.

NIST Chemical Kinetics Database - Ver. 6.0. NIST Standard Reference Data, Gaithersburg, MD.

Mayer, P.M., Parkinson, C.J., Smith, D.M. and Radom, L., 1998. An assessment of theoretical procedures for the calculation of reliable free radical thermochemistry: A recommended new procedure. *Journal of Chemical Physics*, 108(2): 604-615.

Mebel, A.M., Morokuma, K. and Lin, M.C., 1995. Modification of the Gaussian-2 Theoretical-Model - the Use of Coupled-Cluster Energies, Density-Functional Geometries, and Frequencies. *Journal of Chemical Physics*, 103(17): 7414-7421.

Montgomery, J.A., Frisch, M.J., Ochterski, J.W. and Petersson, G.A., 1999. A complete basis set model chemistry. VI. Use of density functional geometries and frequencies. *Journal of Chemical Physics*, 110(6): 2822-2827.

Montgomery, J.A., Frisch, M.J., Ochterski, J.W. and Petersson, G.A., 2000. A complete basis set model chemistry. VII. Use of the minimum population localization method. *Journal of Chemical Physics*, 112(15): 6532-6542.

Montgomery, J.A., Ochterski, J.W. and Petersson, G.A., 1994. A Complete Basis Set Model Chemistry .4. An Improved Atomic Pair Natural Orbital Method. *Journal of Chemical Physics*, 101(7): 5900-5909.

Morihovitis, T., Schiesser, C.H. and Skidmore, M.A., 1999. An ab initio study of beta-fragmentation reactions in some alkoxyacyl (alkoxycarbonyl) and related radicals. *Journal of the Chemical Society-Perkin Transactions 2*(10): 2041-2047.

Ochterski, J.W., Petersson, G.A. and Montgomery, J.A., 1996. A complete basis set model chemistry .5. Extensions to six or more heavy atoms. *Journal of Chemical Physics*, 104(7): 2598-2619.

Petersson, G.A. and Allaham, M.A., 1991. A Complete Basis Set Model Chemistry .2. Open-Shell Systems and the Total Energies of the 1st-Row Atoms. *Journal of Chemical Physics*, 94(9): 6081-6090.

Petersson, G.A. et al., 1988. A Complete Basis Set Model Chemistry .1. The Total Energies of Closed-Shell Atoms and Hydrides of the 1st-Row Elements. *Journal of*

Chemical Physics, 89(4): 2193-2218.

Petersson, G.A., Tensfeldt, T.G. and Montgomery, J.A., 1991. A Complete Basis Set Model Chemistry .3. The Complete Basis Set-Quadratic Configuration-Interaction Family of Methods. *Journal of Chemical Physics*, 94(9): 6091-6101.

Pople, J.A., Headgordon, M., Fox, D.J., Raghavachari, K. and Curtiss, L.A., 1989. Gaussian-1 Theory - a General Procedure for Prediction of Molecular-Energies. *Journal of Chemical Physics*, 90(10): 5622-5629.

Pople, J.A., Headgordon, M. and Raghavachari, K., 1987. Quadratic Configuration-Interaction - a General Technique for Determining Electron Correlation Energies. *Journal of Chemical Physics*, 87(10): 5968-5975.

Pople, J.A. et al., 1981. Molecular-Orbital Studies of Vibrational Frequencies. *International Journal of Quantum Chemistry*: 269-278.

Raghavachari, K., Trucks, G.W., Pople, J.A. and Replogle, E., 1989. Highly Correlated Systems - Structure, Binding-Energy and Harmonic Vibrational Frequencies of Ozone. *Chemical Physics Letters*, 158(3-4): 207-212.

Ruscic, B., Berkowitz, J., Curtiss, L.A. and Pople, J.A., 1989. The Ethyl Radical - Photoionization and Theoretical-Studies. *Journal of Chemical Physics*, 91(1): 114-121.

Saeys, M., Reyniers, M.F. and Marin, G.B., 2003. Ab initio calculations for hydrocarbons: Enthalpy of formation, transition state geometry, and activation energy for radical reactions. *Journal of Physical Chemistry A*, 107(43): 9147-9159.

Scott, A.P. and Radom, L., 1996. Harmonic vibrational frequencies: An evaluation of Hartree-Fock, Moller-Plesset, quadratic configuration interaction, density functional theory, and semiempirical scale factors. *Journal of Physical Chemistry*, 100(41): 16502-16513.

van Duijneveldt, F.B., 1971. *IBM Publ. RI 945*. Yorktown Hts., New York.

Zheng, X. and Blowers, P., 2005. The investigation of hydrocarbon cracking reaction

energetics using composite energy method. *Molecular Simulation*: (in press).

CHAPTER 4

HYDROCARBON RADICAL GAS PHASE (THERMAL) CRACKING REACTIONS: CARBON-CARBON BOND SCISSION

In hydrocarbon gas phase (thermal) cracking, high temperatures (typically in the range of 450°C to 750°C) and pressures (up to about 70 atmospheres) are used to the break large hydrocarbons into smaller ones (Gardiner and Burcat, 1984; Olah and Molnar, 2003). Thermal cracking is the dominant method for petroleum refining processes and its mechanisms are generally accepted to be free-radical chain reactions. The most important elementary steps are: chain initiation reactions where a hydrocarbon molecule is decomposed into two radicals, which can be represented by $RH \rightarrow *R + *H$; hydrogen transfer reactions which can be represented by $*R_1 + HR_2 \rightarrow HR_1 + *R_2$; and radical decomposition reactions where a hydrocarbon radical decomposes into an olefin and a smaller radical, which can be represented by $*R \rightarrow *R_1 + R_2$.

State-of-the-art kinetic modeling of hydrocarbon thermal cracking is done by means

of a free-radical reaction scheme like the one just described. This scheme can involve hundreds of elementary reactions and therefore makes qualitative application difficult.(Xiao, 2001)

In general, radicals are highly reactive species that have very short lifetimes, which makes experimental study of their reaction kinetics very difficult. The experimental kinetic information for hydrocarbon radical cracking reactions is only available for several simple species (Bencsura et al., 1992; Knyazev et al., 1994a; Knyazev et al., 1994b; Knyazev and Slagle, 1996; Knyazev and Tsang, 2000; Slagle et al., 1991; Yamauchi et al., 1999). Under high temperatures, the lifetimes for radicals are very short and the product radicals are difficult to isolate before reacting further. Even these experimental data are limited to moderate temperatures. In the petroleum industry, the cracking reactions always take place at high temperatures where the measured data may not be applicable.

In this chapter, hydrocarbon radical gas phase cracking reactions will be investigated using *ab initio* quantum mechanical methods. The reactions of interest will include propyl, butyl, *sec*-butyl, and *neo*-pentyl radical cracking reactions which have been listed in Table 1-2. This chapter will cover four carbon-carbon bond scission reactions and the next chapter will include the other corresponding carbon-hydrogen bond scission reactions. Using the new CBS-RAD(MP2) composite energy method discussed in the previous chapter, the calculated results of reaction energetics and kinetics will be evaluated by comparing them with the available experimental data. Most importantly,

kinetic models will be proposed with extended conditions which can be easily applied to different reaction conditions without performing additional costly calculations.

The G3 and CBS composite energy methods were applied in this chapter to study the reaction energetics and kinetics of hydrocarbon radical cracking reactions. All of the *ab initio* calculations were performed with the GAUSSIAN98 software package (Frisch et al., 1998). Geometries were optimized at the MP2(full)/6-31G* level of calculation. All products and reactants were verified with frequency calculations be stable structures, and all transition states were found to be first order saddle points with only one negative eigenvalue. Additionally, intrinsic reaction coordinate (IRC) calculations (Gonzalez and Schlegel, 1989) showed that each reaction linked the correct products with reactants. Zero point vibrational energies (ZPVE) were obtained from harmonic vibrational frequencies calculated at the MP2(full)/6-31G* level with a scaling factor of 0.9661(Scott and Radom, 1996). Frequencies were scaled with a factor of 0.9427 at the MP2(full)/6-31G* level (Scott and Radom, 1996).

4.1 Propyl Radical Cracking Reaction:

$$*CH_2CH_2CH_3 \rightarrow CH_2CH_2 + *CH_3$$

This is a reaction for which experimental information is available (Bencsura et al., 1992). Therefore, this relatively simple reaction can be applied as a benchmark to evaluate the accuracy of various theoretical methodologies. With the accuracy of methods proven by this gauge reaction, the methods can then be implemented for larger

hydrocarbon species where experimental data are currently unavailable.

Bencsura *et al.* studied the kinetics of this reaction using the master equation approach.(Bencsura et al., 1992) $<\Delta E>_{down}$, the average energy transferred in deactivations, was given with a large uncertainty of ±20%. The Master equation approach with a large uncertainty range of $<\Delta E>_{down}$ constrains the ability of extending their results to new conditions where one may want kinetic data. In this work, a generalized kinetic model is proposed which can be applied to different reaction conditions to reduce the uncertainties in predictions and improve the previous calculations.(Zheng and Blowers, 2005b)

4.1.1 Reaction Pathway and Energetics

The optimized structures of propane, propyl radical, and the transition state of the propyl radical β-scission reaction optimized at the MP2/6-31G* level are shown in Table 4-1.

Propane **Propyl** **Propyl β-scission TS**

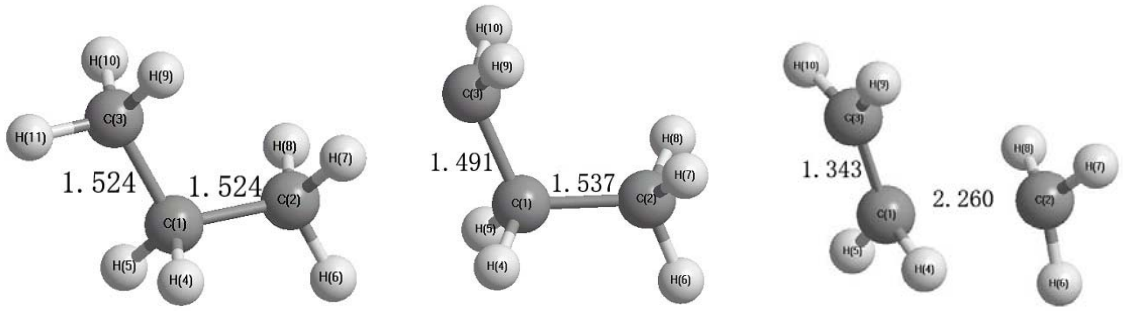

Table 4-1. Comparison of calculated geometries of propane, propyl, and the propyl β-scission transition state structure (Structures are optimized at MP2/6-31G* level. Units are in Å for bond lengths and degrees for angles)

	Propane	Propyl	TS
R(C1C2)	1.524	1.537	2.260
R(C1C3)	1.524	1.491	1.343
R(C1H4)	1.096	1.096	1.084
R(C2H6)	1.093	1.094	1.084
R(C3H9)	1.093	1.083	1.084
A(C3C1C2)	112.336	112.766	109.504
A(H4C1H5)	106.292	106.607	115.681
A(H7C2H8)	107.905	108.195	116.394
A(H9C3H10)	107.868	117.118	116.543

The calculated C-C bond lengths in propane are both 1.524 Å, which is in excellent agreement with the experimental value, 1.526 Å (Hellwege and Hellwege, 1976). For the propyl radical, the C1-C3 (α) bond length decreases to 1.491 Å because of the unsaturated carbon atom and the C1-C2 (β) bond length increases slightly to 1.537 Å. This is an indication that the β-bond is weaker than the α-bond and prone to break. As the reaction takes place, the β-bond length increases and reaches 2.260 Å at the transition state, revealing the bond rupture mode; the α-bond length decreases and reaches 1.343 Å, which is close to 1.331 Å, the equilibrium bond length of ethylene. Meanwhile, the C1-C3 and C2 tetrahedral structures become mostly planar, suggesting the formation of ethylene and methyl radical products. Less experimental information is available for radicals because of their short residence times. Therefore, the calculated geometry results are impossible to compare directly to experimental measurements for many radicals. However, the calculated methyl product C-H bond length is 1.080 Å, compared with the experimental value of 1.079 Å (Herzberg, 1966).

The calculated energies of the reactant, transition state, and products as well as the heat of reaction and activation barrier are listed in Table 4-2. G3 and CBS composite energy methods were chosen because of their proven compromise between accuracy and computational cost for hydrocarbon cracking reactions (Zheng and Blowers, 2005c).

Table 4-2. Calculated energies for the propyl β-scission reaction (Units are in Hartrees for reactant, TS and products; Units are in kcal/mol for heats of reaction and activation energy)

	Propyl	TS	Ethene	Methyl	Heats of reaction	Activation energy
G3	-118.3299918	-118.2815394	-78.50608889	-39.79143797	20.00	30.03
CBS	-118.1931868	-118.146095	-78.41548449	-39.74397279	21.16	29.55
Experiment	-	-	-	-	23.48 [a]	30.0 ~ 33.0 [b]

a - (Linstrom and Mallard, 2003)

b - (Dean, 1985; Tsang, 1988)

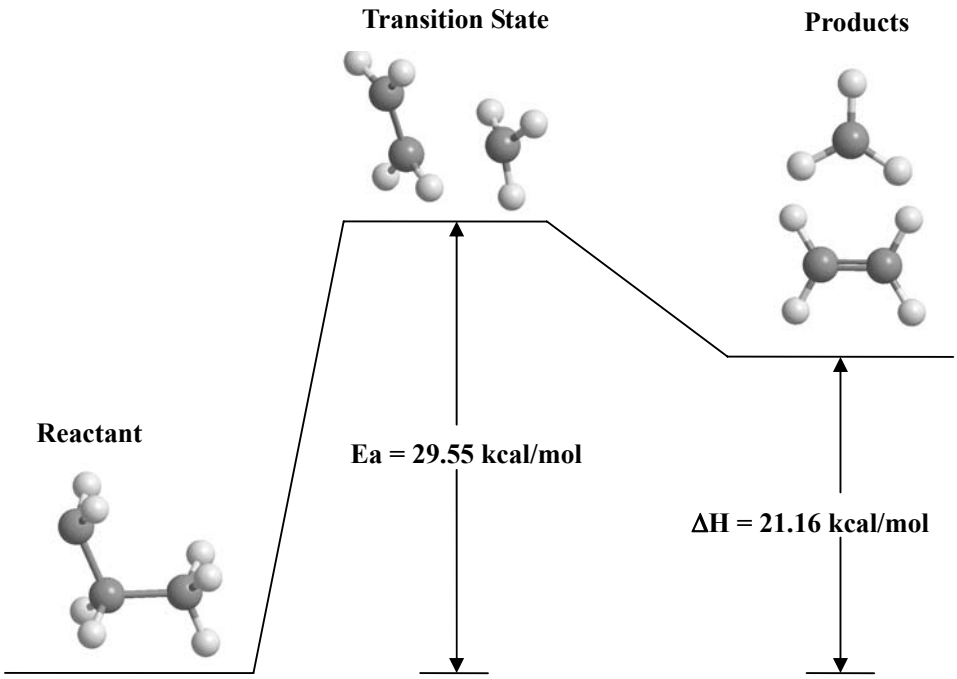

Figure 4-1. Calculated reaction coordinate of the propyl radical β-scission reaction (Structures are optimized at MP2/6-31G* level and energies listed are calculated using the CBS method)

Figure 4-1 shows the calculated reaction pathway of the reaction. The activation energy of the propyl β-scission reaction is 30.03 kcal/mol using the G3 method and 29.55 kcal/mol using the CBS method. Both results agree very well with the experimental activation energy results, which range from 30 to 33 kcal/mol (Dean, 1985; Tsang, 1988). The reaction is exothermic and the heat of reaction is 20.00 kcal/mol using the G3 method and 21.16 kcal/mol using the CBS method, indicating that the transition state is product-like. Compared with heats of reaction from NIST

(Linstrom and Mallard, 2003), 23.48 kcal/mol, the CBS method again agrees well with a relative error less than 10% and the G3 method underestimates the heat of reaction by 3.48 kcal/mol. The activation energies of the reverse radical recombination results can be calculated as 10.03 kcal/mol and 8.39 kcal/mol using the G3 and CBS methods. They agree very well with the experimental values, which range from 7.35 kcal/mol to 7.72 kcal/mol (Baulch et al., 1992; Tsang and Hampson, 1986).

4.1.2 Reaction Kinetic Modeling

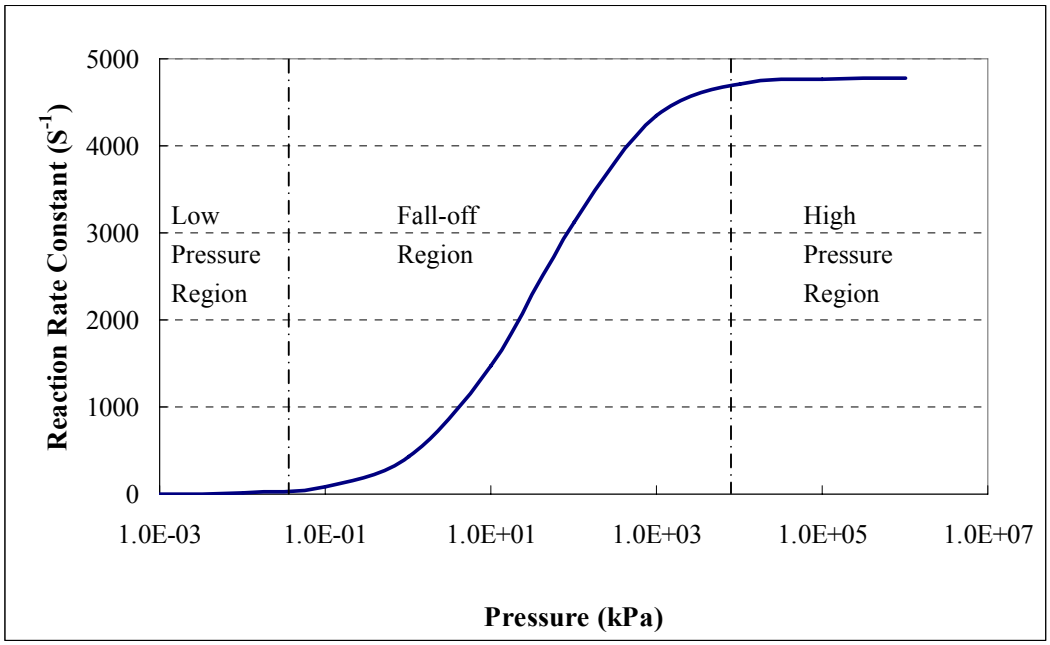

Figure 4-2. Propyl radical β-scission reaction rate constant calculated results as a function of pressure at T = 680 K.

The pressure effect of the reaction rate constant is illustrated in Figure 4-2, which is usually referred to as an S-curve. The calculations were performed at a temperature of 680K using the CBS compound model. RRKM theory and CTST discussed in Chapter 2 were applied in the rate constants estimations. The curve can be divided into three different regions according to the rate dependence on pressure. The region in the middle is the fall-off region where the reaction rate is a strong function of pressure. RRKM theory is implemented in this region to obtain the theoretical rate constants. The region on the right is the high pressure region where the reaction rate constant does not depend on pressure. CTST is implemented in this region to obtain the theoretical rate constants. The region on the left is the low pressure region, where the reaction rate is so slow that it does not have any practical applications. Therefore, this region is not the object of this research.

In the fall-off region, the reaction rate constants are calculated using both G3 and CBS methods. The results, together with the available experimental data (Bencsura et al., 1992), are shown in Figure 4-3.

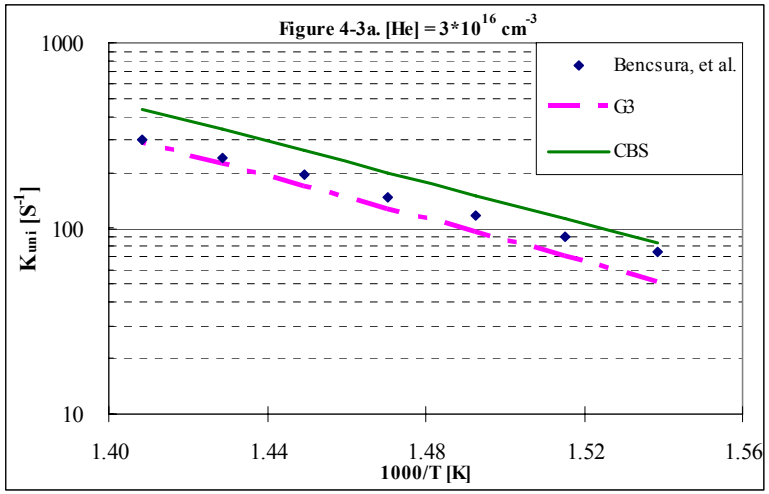

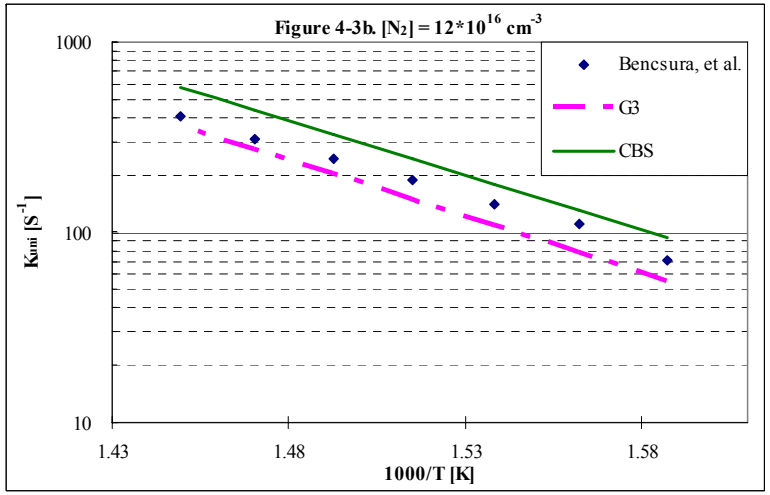

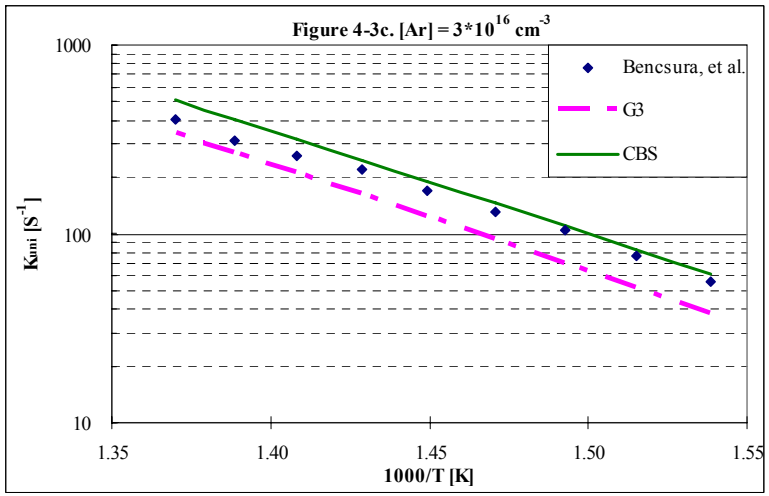

Figure 4-3a. – 4-3c. RRKM theory rate constants for the propyl β-scission reaction with different bath gases compared with experimental data from Bencsura, *et al.* (Bencsura et al., 1992)

In this research, the collisional efficiency in the RRKM expression is taken as 0.1 and kept constant for all the calculations. Three bath gases--He, N_2, and Ar--with different concentrations are considered in this research. The bath gas influences the rate constant through the Lennard-Jones collision frequency term, Z_{LJ}. Both G3 and CBS methods successfully predict the rate constants under all conditions (different bath gases and concentrations) and the errors are within a factor of two compared with the experiment. The CBS method estimates a slightly larger rate constant compared with G3 because the activation energy obtained by CBS is 0.48 kcal/mol lower than G3.

In the high pressure region, the reaction rate is estimated using CTST and compared with experimental data (Warnatz et al., 1984). As shown in Figure 4-4, the CBS method shows very good agreement with the experiments, while the calculated results using the G3 method are somewhat lower.

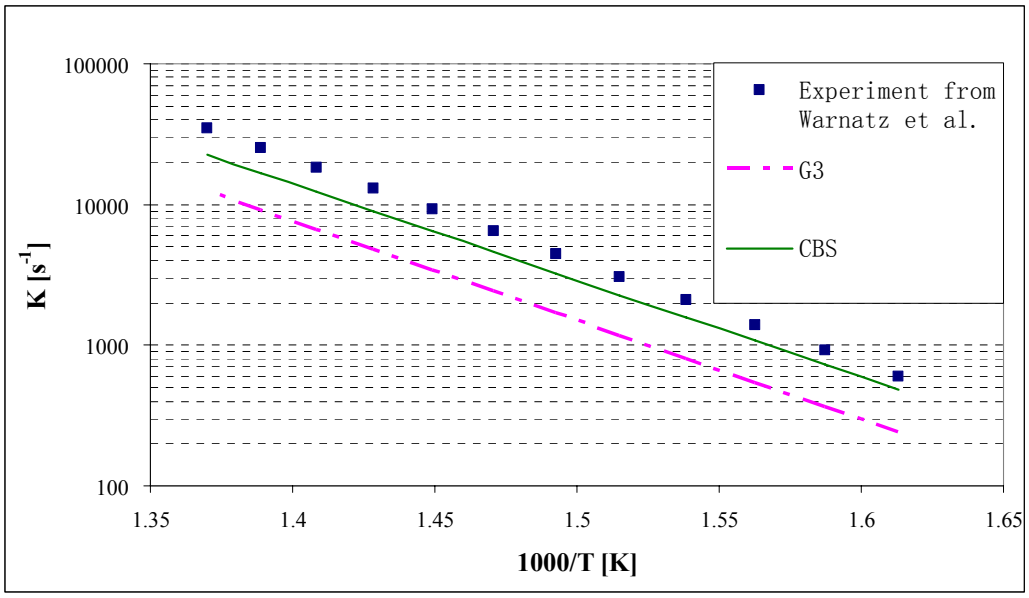

Figure 4-4. High pressure canonical transition state theory rate constant calculation results for the propyl β-scission reaction compared with experimental data from Warnatz, *et al.* (Warnatz et al., 1984)

Rate constants were then calculated in the pressure range of 10kPa to 10000kPa and the temperature range of 680K to 1000K using N_2 as bath gas to extend the RRKM predictions to a wide range of conditions. The data in the fall-off region were modeled using the SAS software program package (SAS Institute, 1999) and the model is shown below.

$$k\ [s^{-1}] = 2.59\times10^{11}\times P^{0.40} e^{(-13618.16/T)} \qquad \text{when } P \le P_0 \qquad (4.1\text{-}1)$$

$$k\ [s^{-1}] = 2.70\times10^{13}\times e^{(-15117.33/T)} \qquad \text{when } P > P_0 \qquad (4.1\text{-}2)$$

where P is in kPa and T is in Kelvin. Model (4.1-1) describes the reaction rates in the fall-off region, while model (4.1-2) is in the high pressure region and derived from

the high pressure limit TST. Then, P_0, the switching pressure, is obtained by equalizing model (4.1-1) and (4.1-2) where $P_0 = 1.10\times10^5\times e^{(-3747.92/T)}$. The model, together with the calculated results, is shown in Figure 4-5 at 800K. 800K is chosen because it is in the middle of the model temperature range. The calculated results indicate this model is a very good description of the complicated quantum chemical-based kinetics simulation data.

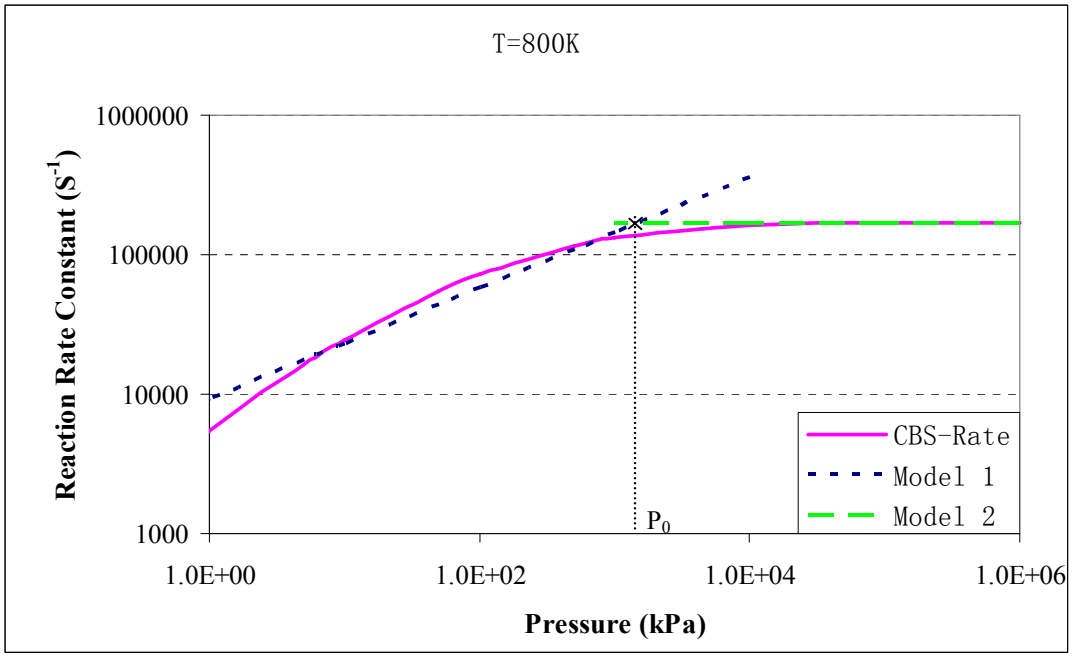

Figure 4-5. Propyl radical β-scission reaction kinetic model at T = 800 K

The model data are then compared with the calculated results and the relative errors are shown in Figure 4-6. The errors are always within ±20% with the exception of high temperatures close to 1000K and low pressures close to 10 kPa, which is a very uncommon condition rarely encountered in industrial applications. Even in this range, the relative errors are less than 65%. The advantage of the simple model is that it can be easily applied even under conditions where pressure is a factor, meaning it has broad applications to the petroleum industry.

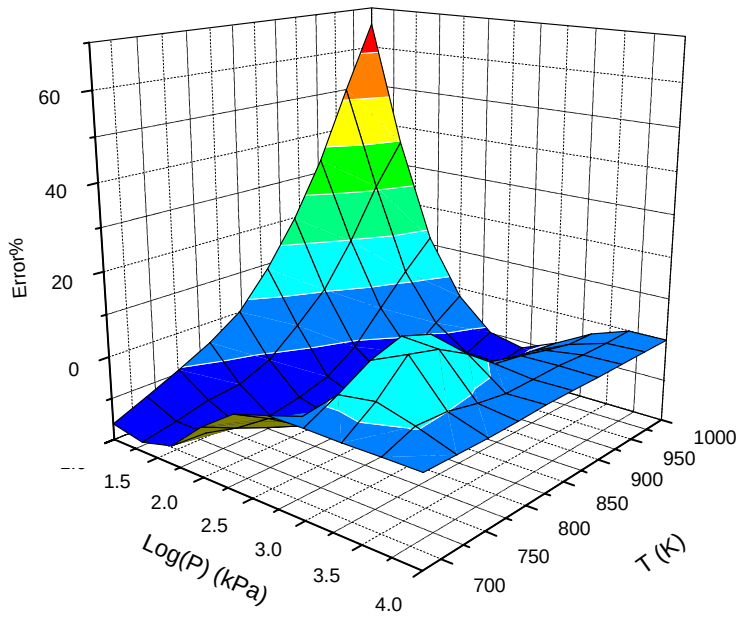

Figure 4-6. Error analysis of the propyl radical β-scission reaction kinetic model compared to full computational chemistry predictions

The CBS compound model has now been tested to give accurate energetic results for a sample hydrocarbon cracking reaction. This method will be applied next to other hydrocarbon cracking reactions.

4.2 Butyl Radical Cracking Reaction:

$$*CH_2CH_2CH_2CH_3 \rightarrow CH_2CH_2 + *CH_2CH_3$$

In this section, *ab initio* methods were applied to investigate the butyl radical β-scission reaction. Knyazev, *et al.*, studied the kinetics of this reaction using the theoretical master equation approach (Knyazev and Slagle, 1996). $<\Delta E>_{down}$, the average energy transferred in deactivation collisions, was given with an uncertainty of ±30%. The master equation approach with a large uncertainty range of $<\Delta E>_{down}$ constrains the ability of extending their results to industrially relevant conditions.

In this section, a generalized kinetic model is proposed which can be applied to different reaction conditions to reduce the uncertainties in reaction rate constant predictions.(Zheng and Blowers, 2005a)

4.2.1 Reaction Pathway and Energetics

Table 4-3 shows the structures of butane, butyl radical, and the transition state of butyl radical β-scission reaction optimized at the MP2/6-31G* level. For butane, the calculated C-C bond lengths are all identical at 1.525 Å. They are in excellent agreement with the experimental value, 1.526 Å (Hellwege and Hellwege, 1976).

For the butyl radical, because of the unsaturated C1 atom, the C1-C2 (α) bond length decreases to 1.49 Å, and the C2-C3 (β) bond length increases slightly to 1.529 Å. This information indicates that the β-bond is weaker than the α-bond and is prone to break. As the reaction takes place, the β-bond length increases and reaches 2.534 Å at the transition state, revealing the bond breaking mode. The α-bond length decreases and reaches 1.342 Å, which is close to the equilibrium C-C double bond length of ethylene, 1.331 Å. Meanwhile, the C1-C2 structure becomes mostly planar, suggesting the formation of ethylene products.

Butane Butyl Butyl β-scission TS

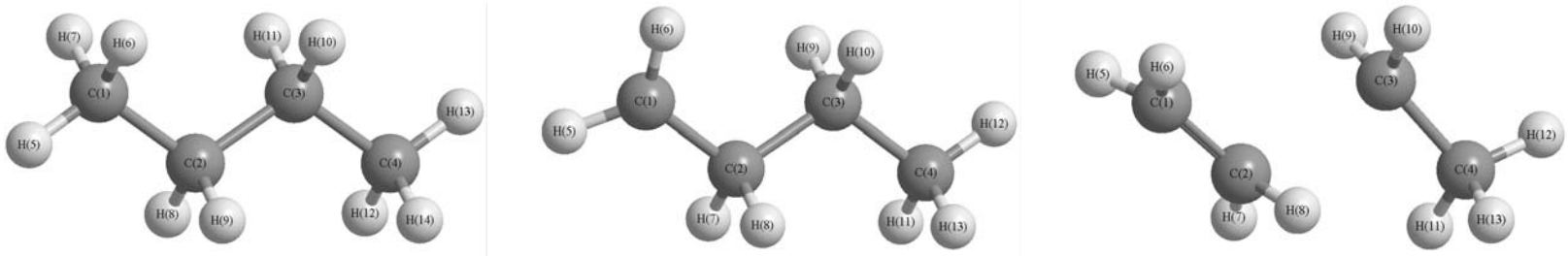

Table 4-3. Comparison of calculated geometry of butane, butyl and the butyl β-scission transition state structure (Structures are optimized at MP2/6-31G* level. Units are in Å for bond lengths and degrees for angles)

	Butane	Butyl	TS
R(C2C1)	1.525	1.490	1.342
R(C3C2)	1.525	1.529	2.534
R(C4C3)	1.525	1.524	1.497
R(H5C1)	1.094	1.083	1.084
R(H8C2)	1.097	1.103	1.084
R(H10C3)	1.097	1.083	1.085
A(C3C2C1)	112.871	113.213	110.988
A(C4C3C2)	112.861	112.623	104.521
A(H5C1H6)	107.868	117.353	116.482

Table 4-4 lists the calculated energies of the reactant, transition state, and products as well as heats of reaction and activation energy of the reaction. G3 and CBS compound models were chosen because of their proven compromise between accuracy and computational cost for hydrocarbon cracking reactions (Zheng and Blowers, 2005c). Figure 4-7 shows the calculated reaction pathway of the reaction. The calculated activation energy of the butyl β-scission reaction is 29.43 kcal/mol using the G3 method and 28.62 kcal/mol using the CBS method. Compared with the experimental activation energy from Knyazev, *et al*, 27.82 kcal/mol (Knyazev and Slagle, 1996), the CBS method has the best agreement with a relative error less than 3%, while the G3 method overestimates the activation energy by 1.61 kcal/mol. The calculated heat of reaction is 20.51 kcal/mol using the G3 method and 21.57 kcal/mol using the CBS method. Compared with heats of reaction from NIST (Linstrom and Mallard, 2003), 21.67 kcal/mol, the CBS method again has an excellent agreement with a relative error less than 1% and the G3 method slightly underestimates the heat of reaction by 1.16 kcal/mol. These comparisons clearly show that the CBS and G3 compound models successfully predict the butyl β-scission reaction energies.

Table 4-4. Calculated energies of the butyl β-scission reaction (Units are in Hartrees for reactant, TS and products; Units are in kcal/mol for heats of reaction and activation energy)

	Butyl	TS	Ethene	Ethyl	Heats of reaction	Activation energy
G3	-157.5999126	-157.553005	-78.506089	-79.061142	20.51	29.43
CBS	-157.4188053	-157.373193	-78.41548449	-78.96895229	21.57	28.62
Experiment	-	-	-	-	21.67 [a]	27.82 [b]

a. - (Linstrom and Mallard, 2003)

b. - (Knyazev and Slagle, 1996)

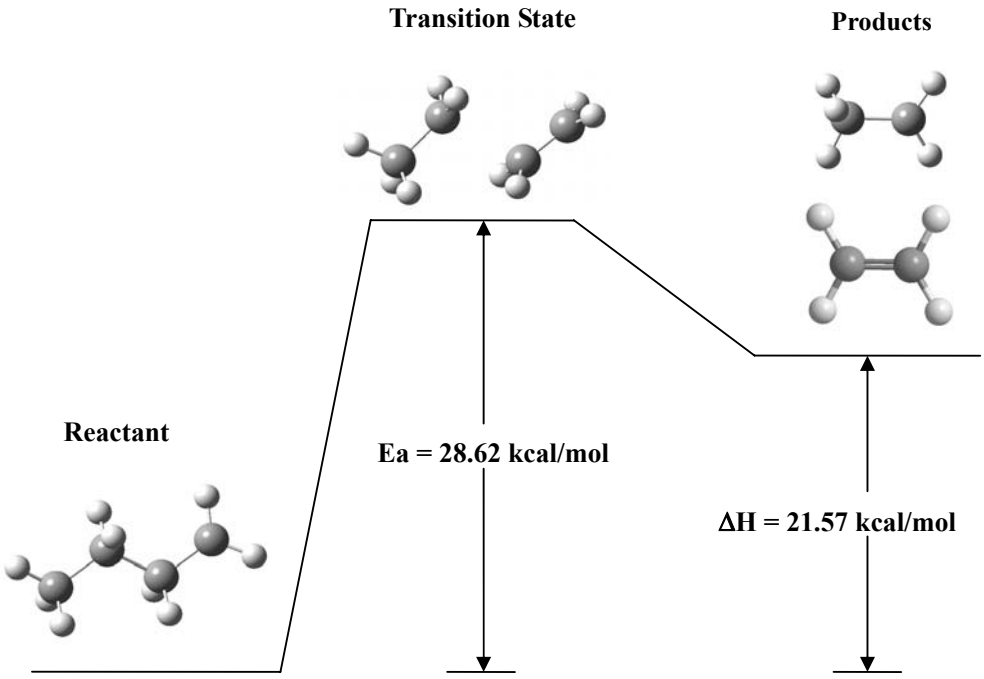

Figure 4-7. Calculated reaction coordinate of the butyl radical β-scission reaction (Structures are optimized at MP2/6-31G* level and energies listed are calculated using the CBS method)

4.2.2 Reaction Kinetic Modeling

Similarly as in the propyl radical kientics modeling, RRKM theory is applied in the fall-off region to calculate the reaction rate using both G3 and CBS methods. The results, together with the available experimental data (Knyazev and Slagle, 1996) are shown in Figure 4-8. Two bath gases—He and N_2--with different concentrations are considered in this work for comparison to the experimental results. The bath gas influences the rate constant through the Lennard-Jones collision frequency term, Z_{LJ}, in the RRKM expression (2.25). It can be seen from Figure 4-8 that the CBS method successfully predicts the reaction rate constants and the errors are almost negligible compared with the experimental results. The G3 method estimates a slightly lower rate constant compared with the CBS method because the activation energy obtained by G3 is 0.81 kcal/mol higher than the CBS one.

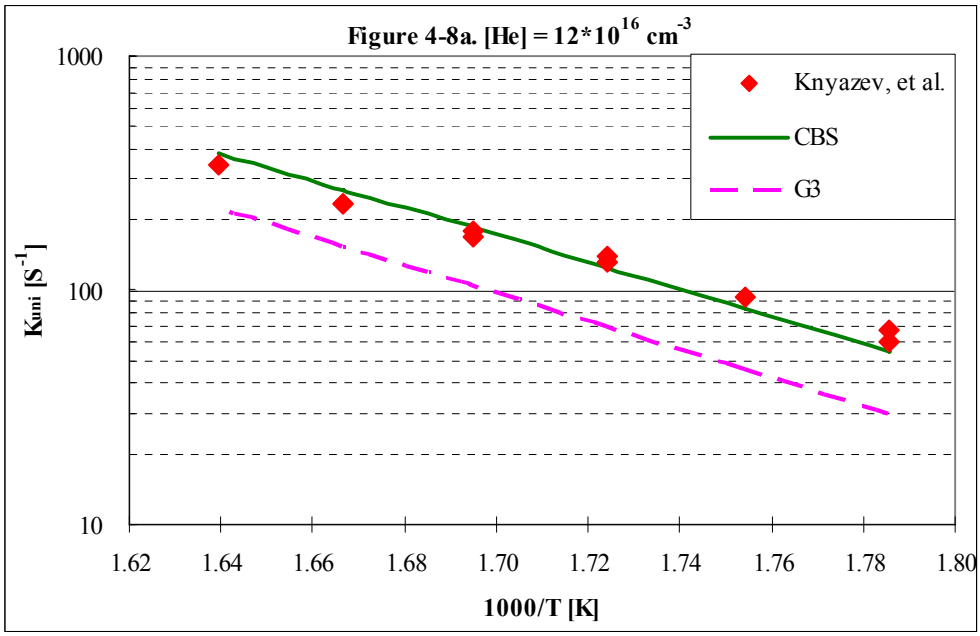

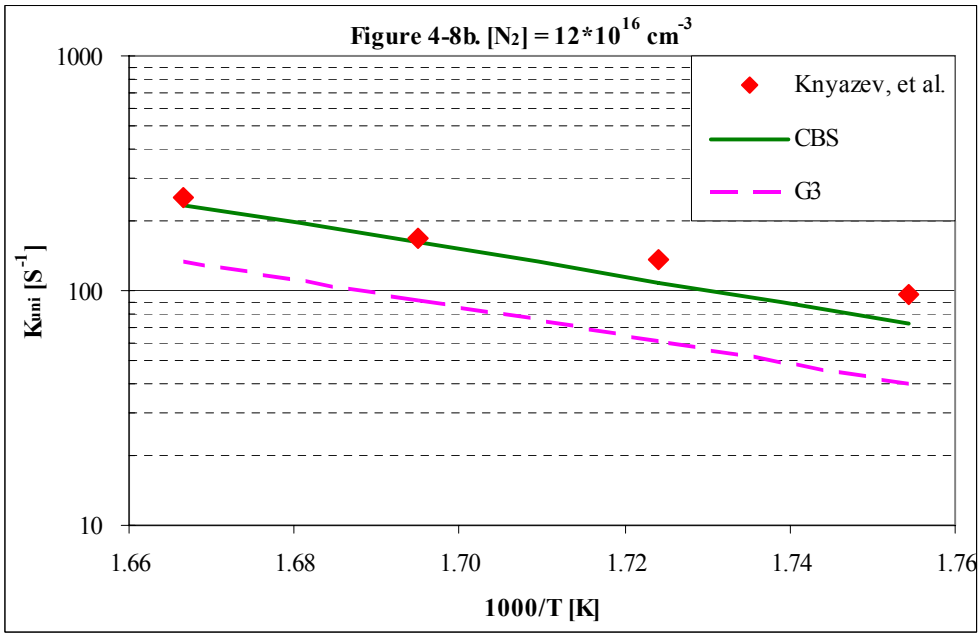

Figure 4-8a. – 4-8b. RRKM theory rate constants for the butyl β- scission reaction under different bath gases compared with experimental data from Knyazev, *et al.* (Knyazev and Slagle, 1996)

In the high pressure region, the reaction rate is estimated using CTST and compared with experimental data from Gierczak *et al*. (Gierczak et al., 1998). As shown in Figure 4-9, the CBS method shows excellent agreement with experiment, while the calculated results using the G3 method are somewhat lower.

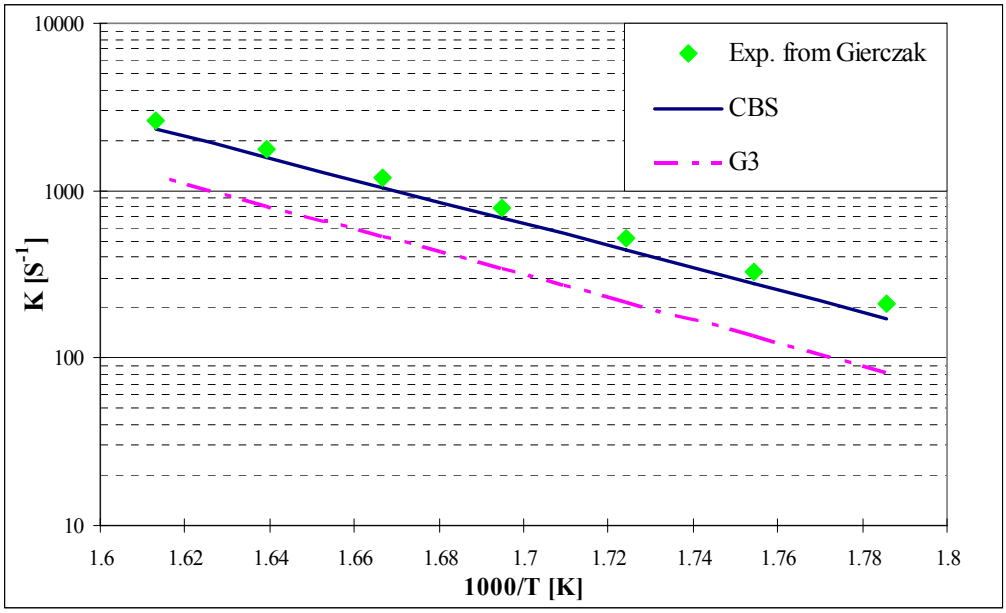

Figure 4-9. High pressure canonical transition state theory rate constant calculation results for the butyl β-scission reaction compared with experimental data from Gierczak, *et al.* (Gierczak et al., 1998)

Rate constants were then calculated in the pressure range of 0.1kPa to 10000kPa and the temperature range of 500K to 1000K using N_2 as bath gas to extend the predictions to a wide range of conditions that could be encountered in hydrocarbon pyrolysis reactors. The data in the fall-off region were modeled using the SAS software program package (SAS Institute, 1999) and the models are shown below:

$$k\,[s^{-1}] = 2.04\times10^{9}\times P^{0.51}\times e^{(-9745.70/T)} \qquad \text{when } P \le P_0 \qquad (4.2\text{-}1)$$

$$k\ [s^{-1}] = 9.43\times10^{13}\times e^{(-15135.70/T)} \qquad \text{when } P > P_0 \qquad (4.2\text{-}2)$$

where P is pressure in kPa and T is temperature in Kelvin. Model (4.2-1) describes the reaction rate constants in the fall-off region, while model (4.2-2) is in the high pressure region and derived from the high pressure limit CTST. P_0, the switching pressure, is obtained by equalizing model (4.2-1) and (4.2-2) where $P_0 = 1.53\times10^{9}\times e^{(-10610.24/T)}$. The model, together with the calculated results at 600K, is shown in Figure 4-10. 600K is chosen because it is in the middle of the experimental temperature range. The calculated results indicate this model is a very good description of the complicated quantum chemical-based chemical kinetics simulation data.

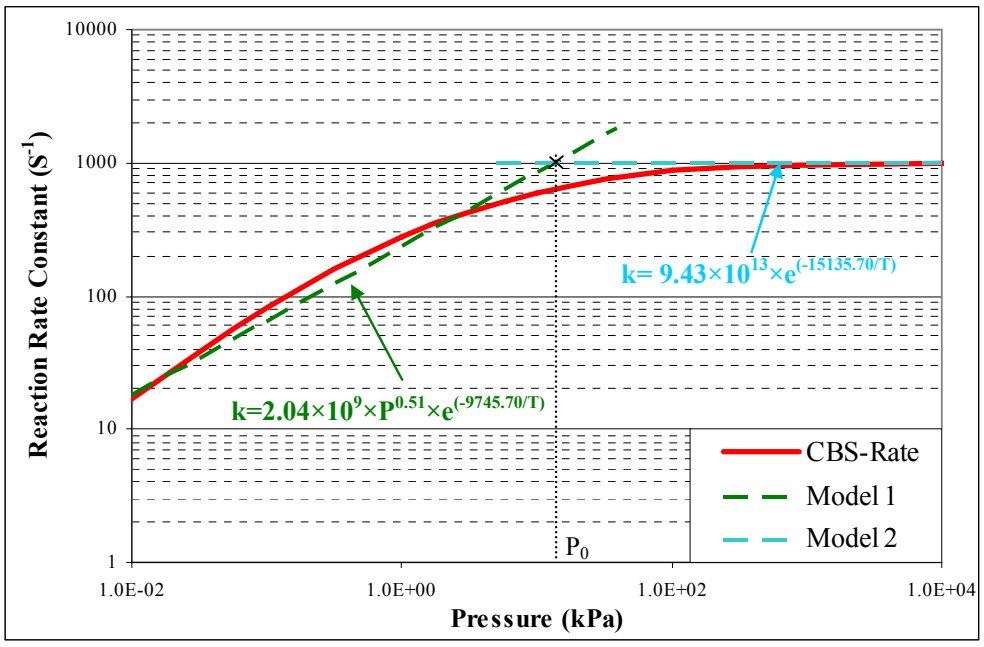

Figure 4-10. Butyl radical β-scission reaction kinetic model at T = 600 K

4.3 *Sec*-butyl Radical Cracking Reaction:

$$CH_3{}^*CHCH_2CH_3 \rightarrow CH_2CHCH_3 + {}^*CH_3$$

4.3.1 Reaction Pathway and Energetics

This section will follow the same format as the previous sections so language will be reduced to just highlight details and the final results. The optimized structure of butane, *sec*-butyl radical, and the transition state of the *sec*-butyl radical β-scission reaction optimized at the MP2/6-31G* level are shown in Table 4-5.

For butane, the calculated C-C bond lengths are all identical at 1.525 Å. For the *sec*-butyl radical, because of the unsaturated C2 atom, the C3-C2 (α) bond length decreases to 1.492 Å, and the C4-C3 (β) bond length increases slightly to 1.527 Å. This information indicates that the β-bond is weaker than the α-bond and is prone to break. As the reaction takes place, the β-bond length increases and reaches 2.254 Å at the transition state, revealing this bond scission mode. The α-bond length decreases and reaches 1.343 Å, which is close to the calculated equilibrium C-C double bond length of propylene, 1.333 Å. The C4 fragment becomes almost planar, indicating the formation of the methyl radical product.

Butane *Sec*-butyl *Sec*-butyl β-scission TS

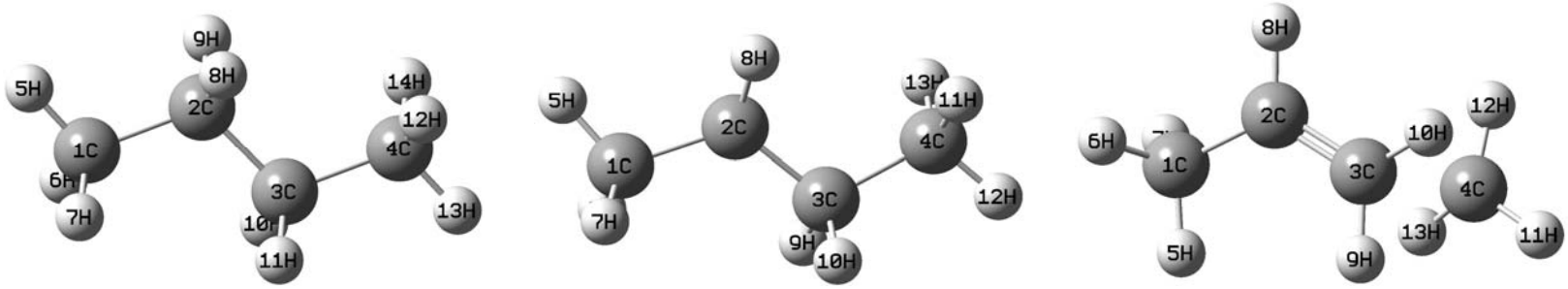

Table 4-5. Comparison of calculated geometry of butane, *sec*-butyl and the *sec*-butyl β-scission transition state structure (Structures are optimized at MP2/6-31G* level. Units are in Å for bond lengths and degrees for angles)

	Butane	*Sec*-butyl	TS
R(C2C1)	1.525	1.491	1.495
R(C3C2)	1.525	1.492	1.343
R(C4C3)	1.525	1.527	2.254
R(H5C1)	1.094	1.093	1.093
R(H8C2)	1.097	1.087	1.088
R(H13C4)	1.094	1.093	1.083
A(C3C2C1)	112.87	120.60	124.12
A(C4C3C2)	112.86	113.25	109.17
A(H8C2C3)	109.08	117.74	119.03
A(H12C4H13)	107.87	107.89	116.00

Table 4-6 lists the calculated energies of the reactant, transition state, and products as well as heats of reaction and activation energy of the reaction. The calculated activation energy of the butyl β-scission reaction is 30.07 kcal/mol using the G3 method and 29.49 kcal/mol using the CBS method. Compared with the experimental activation energy from Tsang, 29.21 kcal/mol (Tsang, 1985), the CBS method has the best agreement with a relative error less than 1%, while the G3 method overestimates the activation energy by 0.86 kcal/mol. The calculated heat of reaction is 20.46 kcal/mol using the G3 method and 21.72 kcal/mol using the CBS method. Compared with heats of reaction from NIST (Linstrom and Mallard, 2003), 23.23 kcal/mol, the CBS method again has an better agreement with a relative error less than 7% and the G3 method underestimates heats of reaction by 2.77 kcal/mol. These comparisons clearly show that the CBS and G3 compound models successfully predict the *sec*-butyl β-scission reaction energies. Figure 4-11 shows the calculated reaction pathway of the reaction. The reaction is exothermic and the heat of reaction, 21.72 kcal/mol, is close to the activation energy, 29.49, indicating the transition state is product like.

Table 4-6. Calculated energies of the *sec*-butyl β-scission reaction (Units are in Hartrees for reactant, TS and products; Units are in kcal/mol for heats of reaction and activation energy)

	sec-Butyl	TS	Propylene	Methyl	Heats of reaction	Activation energy
G3	-157.6036633	-157.5557372	-117.7796156	-39.79143797	20.46	30.07
CBS	-157.4228406	-157.3758419	-117.6442481	-39.74397279	21.72	29.49
Experiment	N/A	N/A	N/A	N/A	23.23 [a]	29.21 [b]

a. - (Linstrom and Mallard, 2003)

b. - (Tsang, 1985)

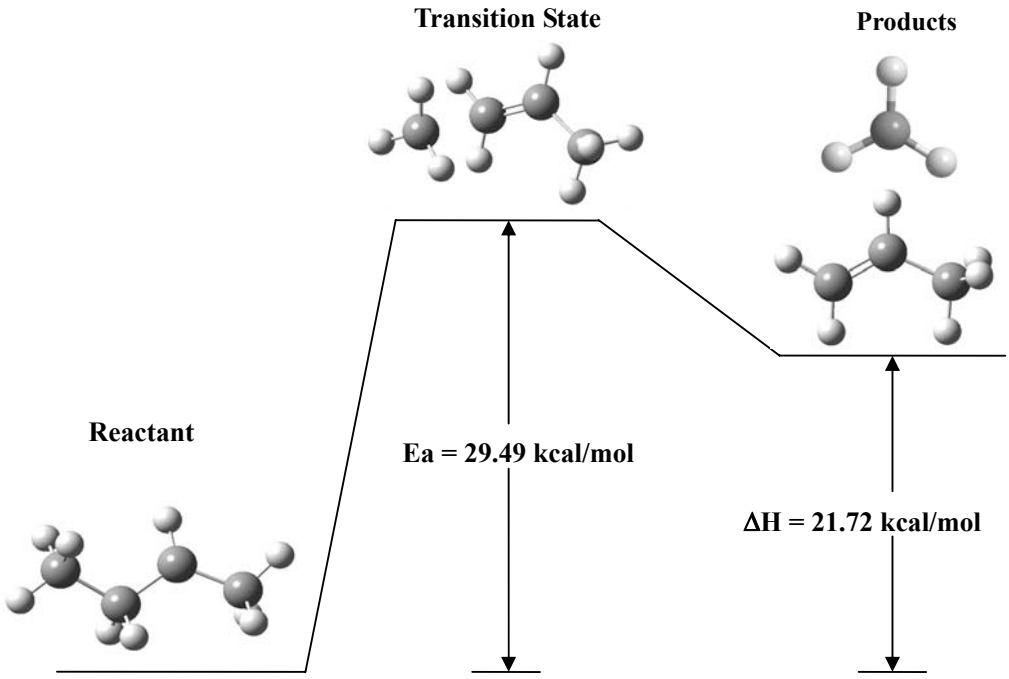

Figure 4-11. Calculated reaction coordinate of the *sec*-butyl radical β-scission reaction (Structures are optimized at MP2/6-31G* level and energies listed are calculated using the CBS method)

4.3.2 Reaction Kinetic Modeling

In the fall-off region, RRKM theory is applied to calculate the reaction rate constants using both G3 and CBS methods. The calculated results, together with the available experimental data (Knyazev et al., 1994a), are shown in Figure 4-12. Three bath gases—He, Ar, and N_2--with different concentrations are considered in this work for comparison to the experimental results. The bath gas influences the rate constants through the Lennard-Jones collision frequency term, Z_{LJ}, in the RRKM expression (2.25). It can be seen from Figure 4-12 that the G3 method predicts

slightly more accurate reaction rate constants than the CBS method for He and Ar bath gases. The rate constants calculated using CBS method are slightly higher than the experimental results considering the fact that the activation energy obtained by CBS is 0.58 kcal/mol lower than the G3 one. For N_2 as the bath gas, which is most common in industrial applications, the rate constant predicted using the CBS method is in excellent agreement with experiment and the errors are almost negligible.

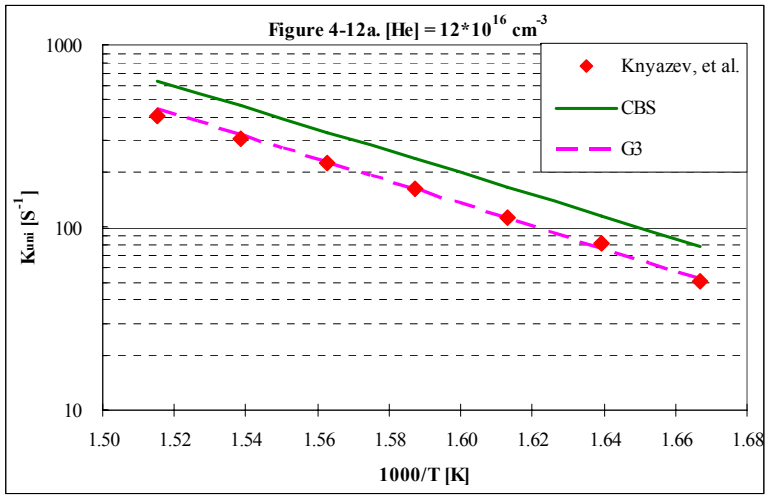

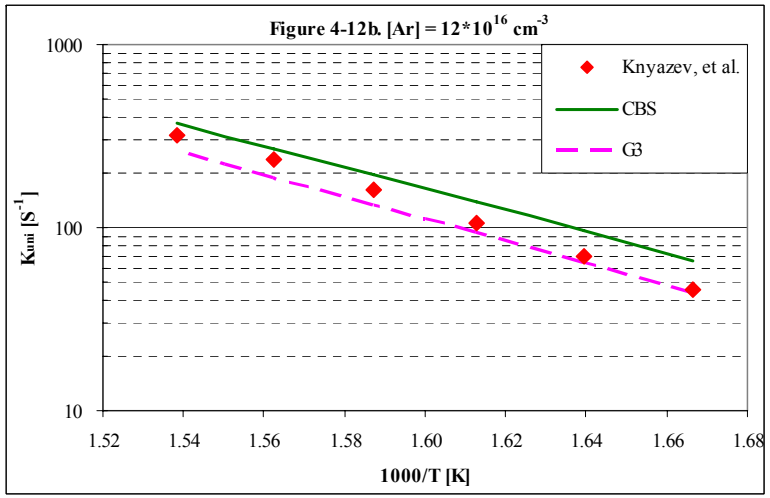

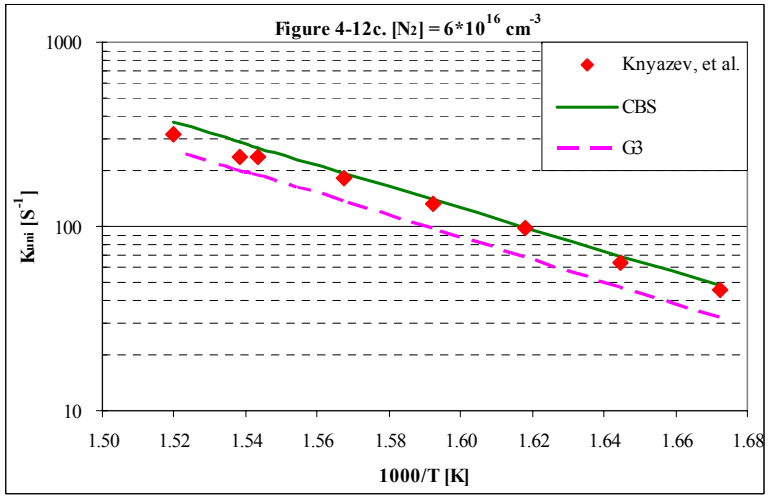

Figure 4-12a. – 4-12c. RRKM theory rate constants for the *sec*-butyl β-scission reaction using different bath gases compared with experimental data from Knyazev, *et al.* (Knyazev and Tsang, 2000)

In the high pressure region, the reaction rate is estimated using a CTST expression (2.26) and compared with experimental data from Marshall *et al*. (Marshall, 1990) and Tsang (Tsang, 1985). As shown in Figure 4-13, even the two experiment results have significant differences; the rate constants estimated using CBS method show good agreement with both experiments, and the calculated data is in the middle of the two experimental results. On the other hand, the calculated results using the G3 method are somewhat lower since its activation energy is slightly higher than that of CBS.

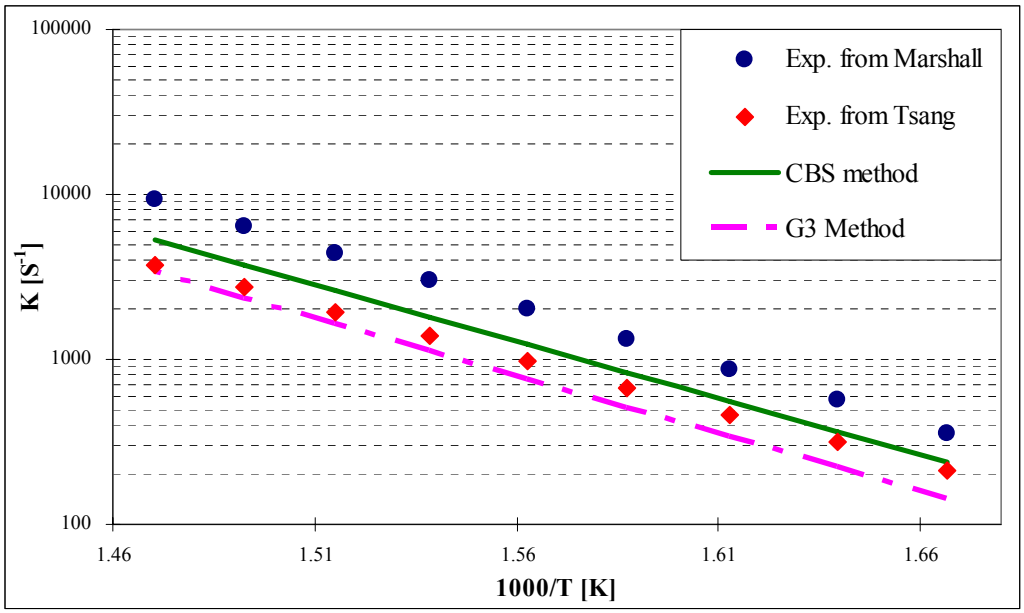

Figure 4-13. High pressure canonical transition state theory rate constant calculation results for the *sec*-butyl β-scission reaction compared with experimental data from Marshall, *et al.* (Marshall, 1990) and Tsang (Tsang, 1985).

Rate constants were then calculated in the pressure range of 0.1kPa to 10000kPa and the temperature range of 500K to 800K using N_2 as the bath gas to extend the predictions to a wide range of industrially relevant conditions. The calculated data in the fall-off region were modeled using the SAS software program package (SAS Institute, 1999) and the models are shown below.

$$k\ [s^{-1}] = 1.82\times10^{11}\times P^{0.51}\times e^{(-13023.70/T)} \qquad \text{when } P \le P_0 \qquad (4.3\text{-}1)$$

$$k\ [s^{-1}] = 7.18\times10^{13}\times e^{(-15916.50/T)} \qquad \text{when } P > P_0 \qquad (4.3\text{-}2)$$

where P is pressure in kPa and T is in Kelvin. Model (4.3-1) describes the reaction rate constants in the fall-off region, while model (4.3-2) is in the high pressure region and derived from the high pressure limit CTST. P_0, the switching pressure, is obtained by equalizing model (4.3-1) and (4.3-2) where $P_0 = 1.23\times10^{5}\times e^{(-5672.16/T)}$. The model, together with the calculated results at 640K, is shown in Figure 4-14. The calculated results indicate this model is a very good description of the complicated quantum chemical-based chemical kinetics simulation data.

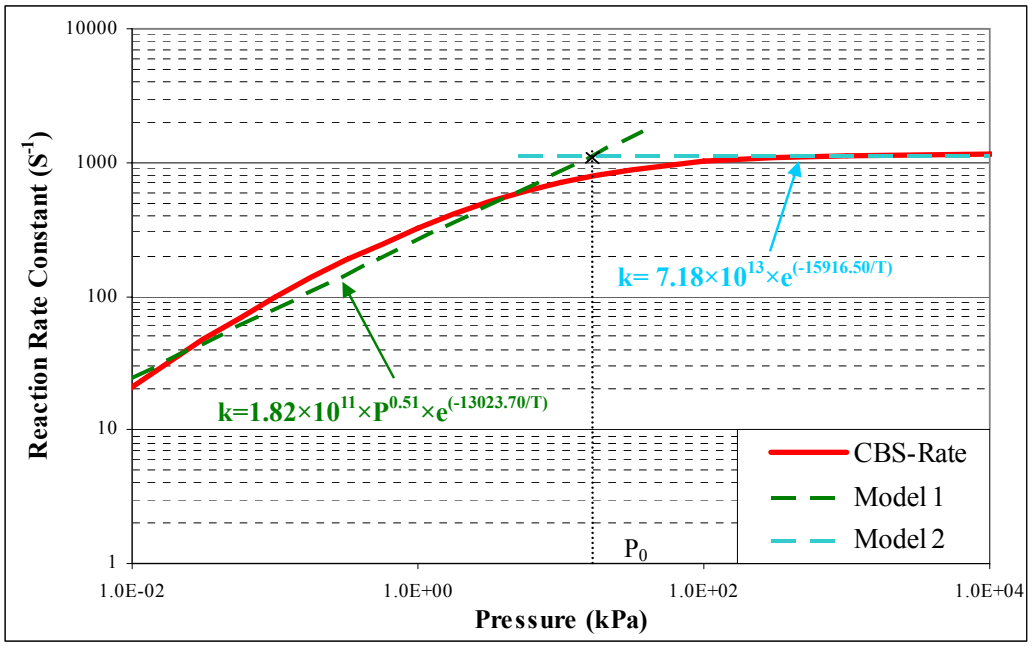

Figure 4-14. *Sec*-butyl radical β-scission reaction kinetic model at T =640 K

4.4 *Neo*-pentyl Radical Cracking Reaction:

$$*CH_2C(CH_3)_3 \rightarrow CH_2C(CH_3)_2 + *CH_3$$

This is a reaction where only limited experimental information is available (Slagle et al., 1991). Therefore, this reaction is applied as another benchmark to evaluate the accuracy of various theoretical methodologies. With the accuracy of methods proven by this reaction, the methods can be implemented for other hydrocarbon species where experimental data are currently unavailable. Slagle *et al.* have studied the kinetics of the β-scission reaction using the master equation approach (Slagle et al., 1991). The master equation approach is one method to treat collisional energy transfer to obtain unimolecular reaction rates. $\langle \Delta E \rangle_{down}$, the average energy

transferred in deactivations, was derived with a large uncertainty of ±30% and it requires the high pressure limit experimental reaction rates. In this chapter so far, our own theoretical work only requires the estimation of the collisional efficiency, as described in section 3.1, which we have kept constant at 0.1. On the other hand, $<\Delta E>_{down}$ greatly depends on experimental conditions and constrains the ability of extending past results to other conditions outside the scope of their work. In this section, a generalized kinetic model is proposed which can be applied to different reaction conditions while reducing the uncertainties in the predictions. (Zheng et al., 2005)

4.4.1 Reaction Pathway and Energetics

The structures of the *neo*-pentyl radical and the transition state of the *neo*-pentyl radical β-scission reaction optimized at the MP2/6-31G* level are shown in Table 4-7. For the *neo*-pentyl radical, the C1-C4 (α) bond length is 1.497Å and the C13-C4 (β) bond length, 1.537Å, is slightly larger. This is an indication that the β-bond is weaker than the α-bond and prone to break. As the reaction takes place, the β-bond length increases and reaches 2.255Å at the transition state, revealing the bond rupture mode; the α-bond length decreases and reaches 1.349Å, which is close to 1.321Å, the equilibrium bond length of *iso*-butene. Meanwhile, the C1-C4-C5-C9 and C13 structures become mostly planar, suggesting the formation of isobutene and methyl radical products.

***Neo*-pentyl** **_Neo_-pentyl β-scission TS**

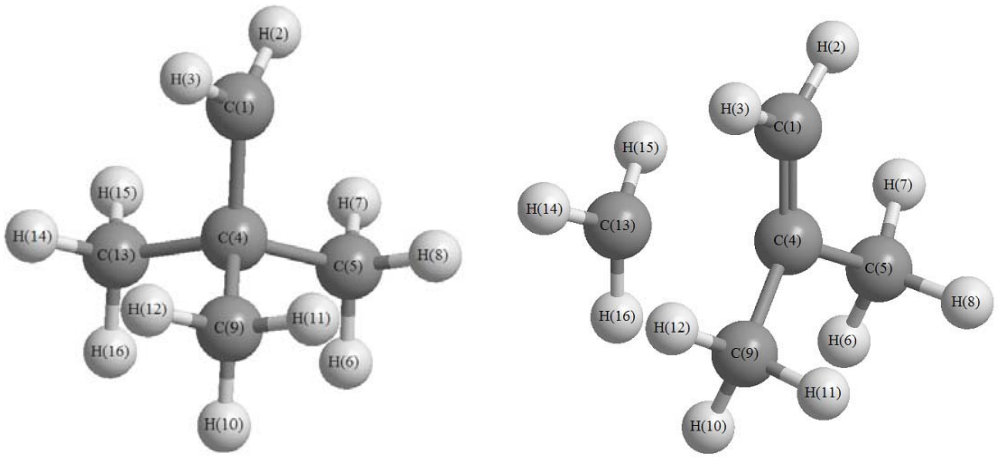

Table 4-7. Comparison of the calculated geometry of *neo*-pentyl and the *neo*-pentyl β-scission transition state structure (Structures are optimized at MP2/6-31G* level. Units are in Å for bond lengths and degrees for angles)

	Neopentyl	Transition State
R(C1C4)	1.497	1.349
R(C5C4)	1.537	1.510
R(C13C4)	1.537	2.255
R(H2C1)	1.085	1.085
R(H7C5)	1.095	1.092
R(H14C13)	1.094	1.083
A(C5C4C1)	109.8	119.9
A(C13C4C1)	109.4	100.6
A(C5C4C9)	109.6	115.1
A(H2C1H3)	117.2	116.7
A(H7C5H8)	108.1	108.1
A(H14C13H15)	108.1	115.6
D(H9C4C1C5)	120.5	153.3

Table 4-8. Calculated energies of the *neo*-pentyl β-scission reaction (Units are in Hartrees for the reactant, TS and products; Units are in kcal/mol for heat of reaction and activation energy)

	Neo-pentyl	TS	*Iso*-butene	Methyl	Heat of reaction	Activation energy
G3	-196.8761157	-196.8274672	-157.0549963	-39.791438	18.63	30.53
CBS	-196.6504753	-196.6025667	-156.8746801	-39.74397279	19.97	30.06
Experiment	-	-	-	-	-	29.81 [a]

a - (Tsang, 1985)

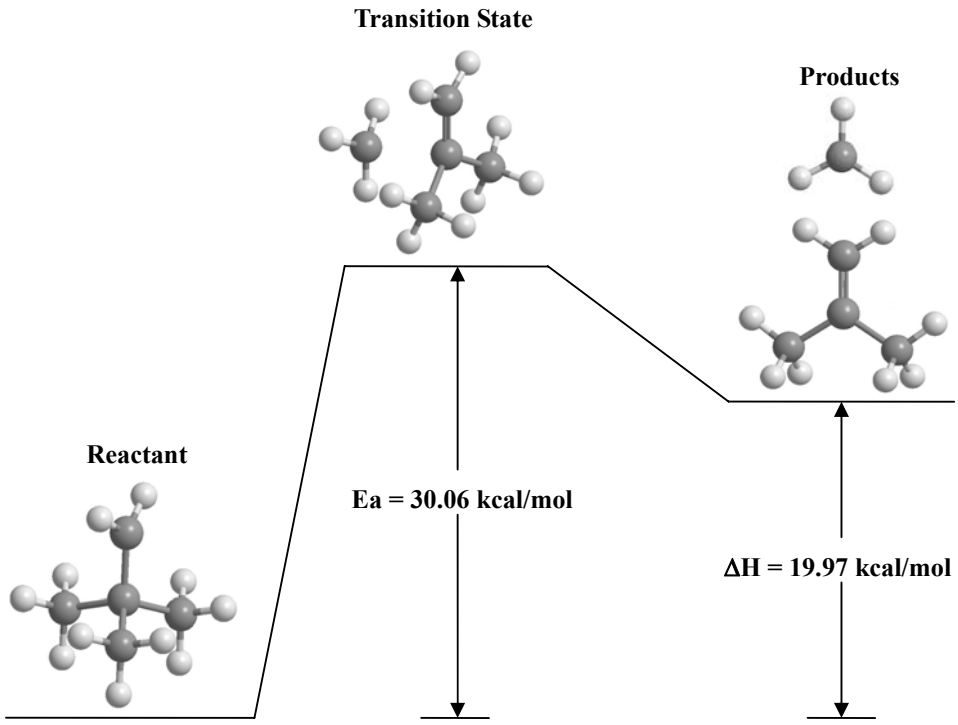

Figure 4-15. The calculated reaction coordinate of the *neo*-pentyl radical β-scission reaction (Structures are optimized at MP2(full)/6-31G* level and energies listed are calculated using the CBS method).

Table 4-8 lists the calculated energies of the reactant, transition state, and products as well as the heat of reaction and the activation energy. Figure 4-15 shows the calculated reaction pathway of the reaction. The activation energy of the *neo*-pentyl β-scission reaction is 30.53 kcal/mol using the G3 method and 30.06 kcal/mol using the CBS method. Compared with the experimental activation energy obtained by Tsang et al. (Tsang, 1985), 29.81 kcal/mol, the relative error is only 0.83% for the CBS method and 2.4% for the G3 method. This proves that the CBS composite energy method can accurately predict reaction energetics. The heat of reaction is

18.63 kcal/mol using the G3 method and 19.97 kcal/mol using the CBS method. The activation energies of the reverse radical recombination results can be calculated as 11.90 kcal/mol and 10.09 kcal/mol using the G3 and CBS methods respectively.

Table 4-9. Computational cost comparison of the single point calculations using the G3 and CBS composite energy methods

	Neo-pentyl	Transition State	*Iso*-butene
G3	8 hours 44 minutes	9 hours 11 minutes	3 hours 30 minutes
CBS	2 hours 48 minutes	3 hours 19 minutes	1 hour 34 minutes

The supercomputer time cost for G3 and CBS composite energy calculations for this reaction system are listed in Table 4-9. The calculations were performed using the IBM pSeries 690 and pSeries 655 at Boston University and the p4-long queue which has 16GB of memory and 36GB of disk space. From the computational cost of the composite energy of *neo*-pentyl, transition state structure, and isobutene species, the CBS compound method only takes one third of the supercomputer time compared to the G3 method, which is why this method was developed in Chapter 3. This difference will be crucial when investigating large hydrocarbon species in the future, not even considering that the accuracy of CBS method is better than that of G3.

4.4.2 Reaction Kinetic Modeling

In the fall-off region, the reaction rate is calculated using both G3 and CBS methods. The results, together with the available experimental data (Slagle et al., 1991), are shown in Figure 4-16. In this research, the collisional efficiency in the RRKM expression is taken as 0.1 and kept constant for all calculations. Three bath gases--He, N_2, and Ar--with different concentrations are considered. The bath gas influences the reaction rate through the Lennard-Jones collision frequency term, Z_{LJ}. It can be seen from Figure 4-16 that the CBS method successfully predicts the reaction rate under all conditions (different bath gases and concentrations), and the errors are almost negligible compared with the experimental results. The G3 method estimates a slightly lower reaction rate compared with the CBS method because the activation energy obtained by the G3 method is 0.47 kcal/mol higher than CBS.

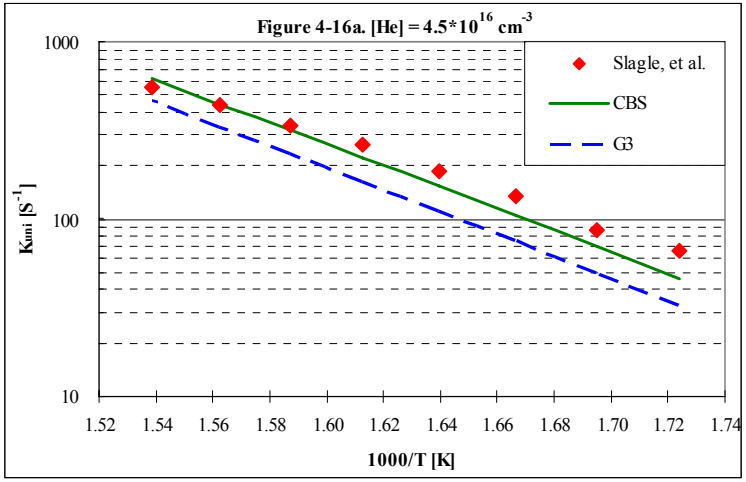

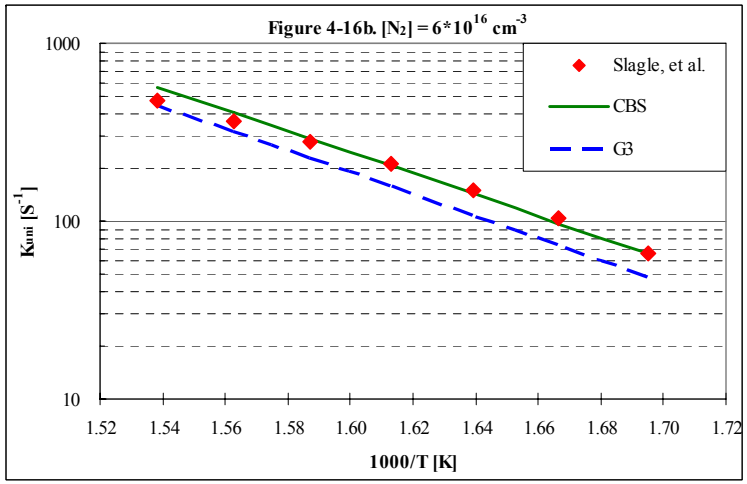

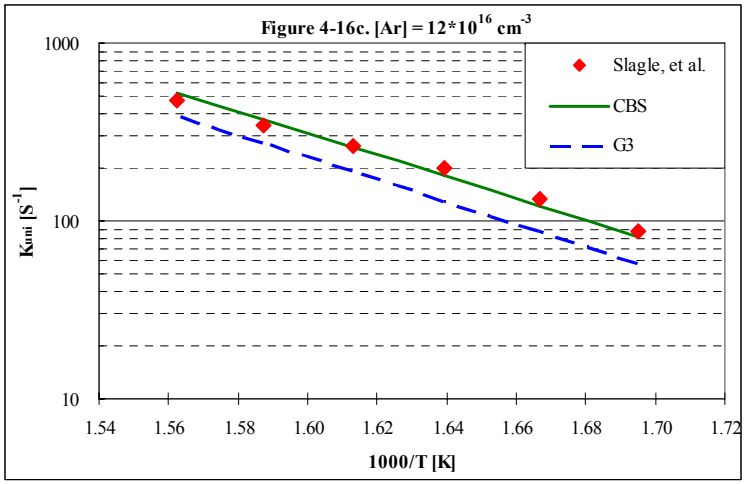

Figure 4-16a. – 4-16c. RRKM theory reaction rates for the *neo*-pentyl β-scission reaction using different bath gases compared with experimental data from Slagel, *et al.* (Slagle et al., 1991)

In the high pressure region, the reaction rate is estimated using CTST and compared with experimental data from Tsang *et al.* (Tsang, 1985) and Baldwin *et al.* (Baldwin et al., 1982). As shown in Figure 4-17, the CBS method results show very good agreement with the experiments, while the calculated results using the G3 method are relatively lower.

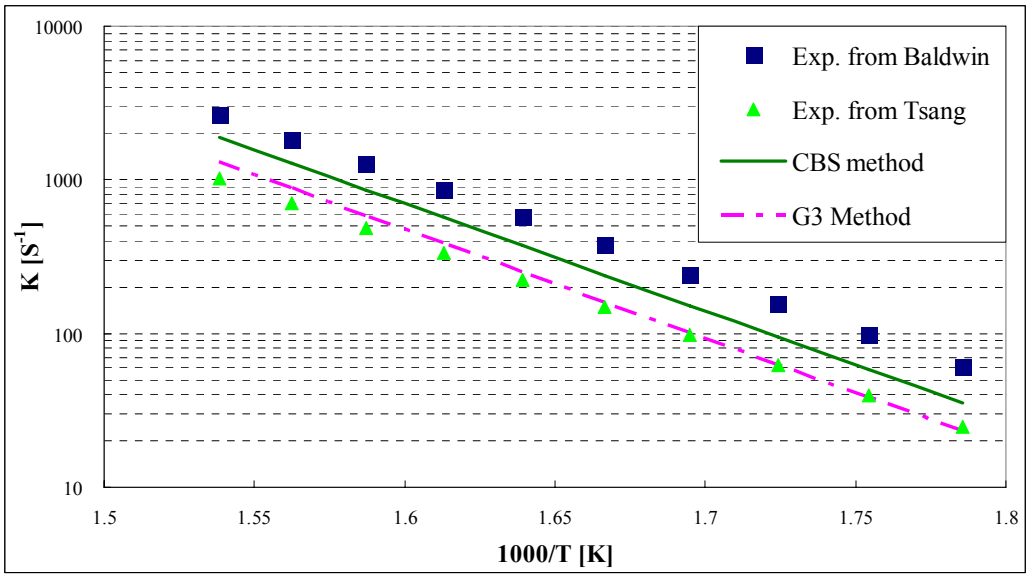

Figure 4-17. High pressure canonical transition state theory rate constant results for the *neo*-pentyl β-scission reaction compared with experimental data from Baldwin (Baldwin et al., 1982) and Tsang (Tsang, 1985)

The reaction rate was then calculated in the pressure range of 0.1kPa to 1000kPa and the temperature range of 500K to 1000K using N_2 as the bath gas to extend the predictions to a wide range of conditions. In order to accommodate chemists and engineers who would like to utilize the kinetic calculation results without going into

the details of the complicated theories, the data were regressed using the SAS software program package (SAS Institute, 1999). A linear relationship of log(k) with respect to log(P) and 1/T is introduced. An R-squared value of 0.995 indicates a good fit of the resulting model with the quantum chemical calculation results. The obtained models are shown below.

$$k\ [s^{-1}] = 1.44\times10^{12}\times P^{0.29}\times e^{(-13890.20/T)} \qquad \text{when } P \le P_0 \qquad (4.4\text{-}1)$$

$$k\ [s^{-1}] = 1.04\times10^{14}\times e^{(-16075.80/T)} \qquad \text{when } P > P_0 \qquad (4.4\text{-}2)$$

where P is in kPa and T is in degrees Kelvin. Model (4.4-1) describes the reaction rate in the fall-off region, while model (4.4-2) applies in the high pressure region and is derived from the high pressure limit CTST. P_0 is switching pressure where the behavior of the reaction changes from the fall off region to the high pressure limit. This pressure was obtained by equalizing models (4.4-1) and (4.4-2), leading to $P_0 = 2.54\times10^{6}\times e^{(-7536.55/T)}$. At T=610K, the model and the calculated results are shown in Figure 4-18. The calculated results indicate the model is a good description of the complicated quantum chemical-based chemical kinetic simulation data. The advantage of this simple model is that it can be easily applied even under conditions where pressure is a factor, meaning it has broad applications to the petroleum industry.

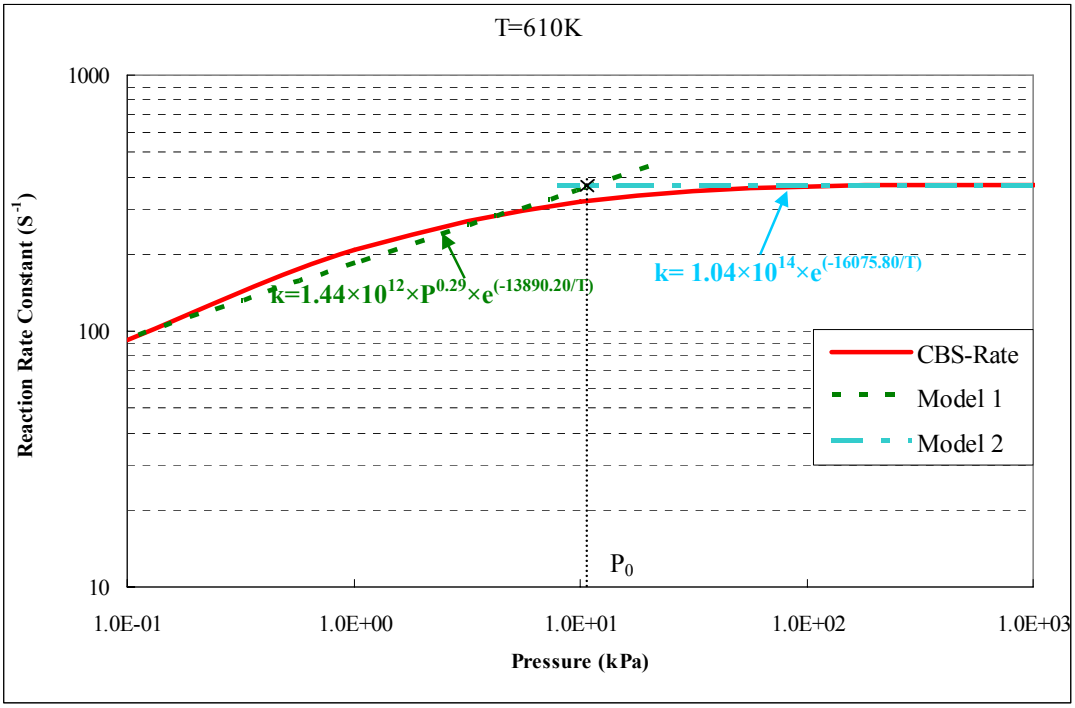

Figure 4-18. Neopentyl radical β-scission reaction kinetic models at T = 610 K

4.5 Conclusions

In this chapter, four hydrocarbon radical carbon-carbon bond thermal scission reactions were studied, including propyl, butyl, *sec*-butyl, and *neo*-pentyl radicals. These are reactions for which experimental information is available to validate the calculation results. From the calculational results using G3 and CBS-RAD(MP2) methods, the heats of reaction and activation barriers agree well with the available experimental data. With the reaction energetics accurately obtained, RRKM and CTST expressions were applied to estimate the reaction kinetics over a much broader range of experimental conditions. Compared with the experimental data,

CBS-RAD(MP2) method successfully predicted the reaction rate constants almost in all cases. Also, the computational cost of CBS-RAD(MP2) is considerably less than that of G3. In order to facilitate engineers who would like to use the kinetic data without going through the complicated theory details, analytic formula of the kinetic model was proposed for each reaction. The advantage of the models is that they include the pressure as independent variable which is important since most of the prolysis reactors in the petroleum industry operate at low pressure where reaction rate is directly related to pressure.

In industrial applications, the free-radical reaction scheme in the hydrocarbon cracking can involve hundreds of elementary reactions, some of which might no have experimental information available. With the accuracy of the methods proven by these gauge reaction, this computational approaches here can be extrapolated to many other hydrocarbon radical cracking reactions, especially those without experimental data.

References:

Baldwin, R.R., Hisham, M.W.M. and Walker, R.W., 1982. Arrhenius Parameters of Elementary Reactions Involved in the Oxidation of Neopentane. *Journal of the Chemical Society-Faraday Transactions I*, 78: 1615-1627.

Baulch, D.L. et al., 1992. Evaluated Kinetic Data for Combustion Modeling. *Journal of Physical and Chemical Reference Data*, 21(3): 411-734.

Bencsura, A., Knyazev, V.D., Xing, S.B., Slagle, I.R. and Gutman, D., 1992. Kinetics of the thermal decomposition of the n-propyl radical. *Symposium (International) on Combustion, [Proceedings]*, 24th: 629-35.

Dean, A.M., 1985. Predictions of Pressure and Temperature Effects Upon Radical-Addition and Recombination Reactions. *Journal of Physical Chemistry*, 89(21): 4600-4608.

Frisch, M.J. et al., 1998. *Gaussian 98, Revision A.7*. Gaussian, Inc., Pittsburgh PA.

Gardiner, W.C. and Burcat, A., 1984. *Combustion chemistry*. Springer-Verlag, New York.

Gierczak, T., Gawlowski, J. and Niedzielski, J., 1998. Isomerization Of Chemically Activated Secondary Butyl Radical. *Reaction Kinetics And Catalysis Letters*, 36(2): 435-440.

Gonzalez, C. and Schlegel, H.B., 1989. An Improved Algorithm For Reaction-Path Following. *Journal Of Chemical Physics*, 90(4): 2154-2161.

Hellwege, K.H. and Hellwege, A.M., 1976. *Atomic and Molecular Physics Volume 7: Structure Data of Free Polyatomic Molecules*. Springer-Verlag, Berlin.

Herzberg, G., 1966. *Electronic spectra and electronic structure of polyatomic molecules*. Van Nostrand, New York.

Knyazev, V.D., Dubinsky, I.A., Slagle, I.R. and Gutman, D., 1994a. Experimental and Theoretical-Study of the Sec-C4h9-Reversible-Arrow-Ch3+C3h6 Reaction. *Journal of Physical Chemistry*, 98(43): 11099-11108.

Knyazev, V.D., Dubinsky, I.A., Slagle, I.R. and Gutman, D., 1994b. Unimolecular Decomposition of T-C4h9 Radical. *Journal of Physical Chemistry*, 98(20): 5279-5289.

Knyazev, V.D. and Slagle, I.R., 1996. Unimolecular decomposition of n-C4H9 and iso-C4H9 radicals. *Journal of Physical Chemistry*, 100(13): 5318-5328.

Knyazev, V.D. and Tsang, W., 2000. Chemically and thermally activated decomposition of secondary butyl radical. *Journal of Physical Chemistry A*, 104(46): 10747-10765.

Linstrom, P.J. and Mallard, W.G., 2003. *NIST Chemistry WebBook, NIST Standard Reference Database Number 69, March 2003, National Institute of Standards and Technology*, Gaithersburg MD, 20899 (http://webbook.nist.gov).

Marshall, R.M., 1990. The Rate-Constant for the Intramolecular Isomerization of Pentyl Radicals. *International Journal of Chemical Kinetics*, 22(9): 935-950.

Olah, G.A. and Molnar, A., 2003. *Hydrocarbon Chemistry*. John Wiley & Sons, Inc., New York.

SAS Institute, I., version 8, 1999.

Scott, A.P. and Radom, L., 1996. Harmonic vibrational frequencies: An evaluation of Hartree-Fock, Moller-Plesset, quadratic configuration interaction, density functional theory, and semiempirical scale factors. *Journal of Physical Chemistry*, 100(41): 16502-16513.

Slagle, I.R., Batt, L., Gmurczyk, G.W., Gutman, D. and Tsang, W., 1991. Unimolecular Decomposition of the Neopentyl Radical. *Journal of Physical*

Chemistry, 95(20): 7732-7739.

Tsang, W., 1985. The Stability of Alkyl Radicals. *Journal of the American Chemical Society*, 107(10): 2872-2880.

Tsang, W., 1988. Chemical Kinetic Data-Base for Combustion Chemistry .3. Propane. *Journal of Physical and Chemical Reference Data*, 17(2): 887-952.

Tsang, W. and Hampson, R.F., 1986. Chemical Kinetic Database for Combustion Chemistry .1. Methane and Related-Compounds. *Journal of Physical and Chemical Reference Data*, 15(3): 1087-1279.

Warnatz, J., Gardiner, W.C. and Burcat, A., 1984. *Combustion Chemistry*. Springer-Verlag, New York.

Xiao, Y., 2001. Modeling the kinetics and mechanisms of petroleum and natural gas generation: A first principles approach. *Reviews in Mineralogy & Geochemistry*, 42(Molecular Modeling Theory): 383-436.

Yamauchi, N., Miyoshi, A., Kosaka, K., Koshi, M. and Matsui, N., 1999. Thermal decomposition and isomerization processes of alkyl radicals. *Journal of Physical Chemistry A*, 103(15): 2723-2733.

Zheng, X. and Blowers, P., 2005a. The application of composite energy methods to n-butyl radical β-scission reaction kinetic estimations. *Theoretical Chemistry Accounts*, (in press).

Zheng, X. and Blowers, P., 2005b. Evaluate of compound models for estimating rate constants of hydrocarbon thermal cracking reactions: Propyl radical β-scission reaction. *Industrial Engineering Chemistry & Research*, (in press).

Zheng, X. and Blowers, P., 2005c. The investigation of hydrocarbon cracking reaction energetics using composite energy method. *Molecular Simulation*: (in press).

Zheng, X., Blowers, P. and Zhang, N.L., 2005. Application of compound models for estimating rate constants of hydrocarbon thermal cracking reactions: The neopentyl radical beta-scission reaction. *Molecular Simulation*, 31(9): 615-621.

CHAPTER 5
HYDROCARBON RADICAL GAS PHASE (THERMAL) CRACKING REACTIONS: CARBON-HYDROGEN BOND SCISSION

In this chapter, hydrocarbon radical gas phase carbon-hydrogen bond scission reactions will be investigated using *ab initio* quantum mechanical methods. The reactions of interest have been listed in Table 1-2. Using the new CBS-RAD(MP2) composite energy method from Chapter 3, the calculated results of reaction energetics and kinetics will be evaluated by comparing them with the available experimental information. Most importantly, kinetic models will be proposed with extended conditions which can be easily applied to different reaction conditions without performing additional costly calculations.

The G3 and CBS composite energy methods were used in this chapter to investigate the reaction energetics and kinetics of hydrocarbon radical cracking reactions. All of the *ab initio* calculations were performed with the GAUSSIAN98 software package (Frisch et al., 1998). Geometries were optimized at the

MP2(full)/6-31G* level of calculation. All products and reactants were verified with frequency calculations to be stable structures, and all transition states were found to be first order saddle points with only one negative eigenvalue. Additionally, intrinsic reaction coordinate (IRC) calculations (Gonzalez and Schlegel, 1989) showed that each transition state linked the correct products with reactants. Zero point vibrational energies (ZPVE) were obtained from harmonic vibrational frequencies calculated at the MP2(full)/6-31G* level with a scaling factor of 0.9661 (Scott and Radom, 1996). Frequencies were scaled with a factor of 0.9427 at the MP2(full)/6-31g* level (Scott and Radom, 1996).

5.1 1-Cloroethyl Radical Cracking Reaction:

$$^{*}CHClCH_3 \rightarrow CHClCH_2 + {}^{*}H$$

Chlorinated hydrocarbons (CHCs) are important species in the treatment of the hazardous compounds in combustion processes (Gardiner and Burcat, 1984). They are also crucial for the incineration of natural gas. Therefore, understanding of CHC reaction energetics and kinetics has broad application in the combustion and petrochemical industry.

In this section, the focus will be on the 1-chloroethyl radical decomposition reaction: $^{*}CHClCH_3 \rightarrow CHClCH_2 + {}^{*}H$, where * denotes an unpaired electron present in the radical species. This is a reaction where limited experimental information is available. Knyazev *et al.* have studied the kinetics of the decomposition reaction

using the master equation approach (Knyazev et al., 1994a). The master equation approach is one method to treat collisional energy transfer to obtain unimolecular reaction rates. $<\Delta E>_{down}$, the average energy transferred in deactivations, was derived with a large uncertainty of ±30% and it requires the high pressure limit experimental reaction rates for prediction of reaction rates. $<\Delta E>_{down}$ greatly depends on experimental conditions, which constrains the ability of extending the previous results to other conditions outside the scope of their work. In this work, a generalized kinetic model is proposed which can be applied to different reaction conditions while reducing the uncertainties in the reaction rate predictions.(Zheng and Blowers, 2005d)

5.1.1 Reaction Pathway and Energetics

Table 5-1 shows the structures of the 1-chloroethane, 1-chloroethyl radical, and the transition state of the 1-chloroethyl radical decomposition reaction calculated at the MP2/6-31G* level. For the 1-chloroethyl, carbon C2 has one unpaired electron which is the reason for the high activity of this radical. The C1-C2 bond length is 1.484 Å, and is slightly shorter than that of 1-cloroethane, indicating a stronger C-C bond compared with that of 1-choroethane. As the decomposition reaction takes place, the H4-C1 bond length increases from 1.082 Å for the 1-chloroetyl radical and reaches 1.844 Å at the transition state, showing the bond rupture mode. The C1-C2 bond length decreases and reaches 1.332 Å at the transition state, which is very close to the equilibrium bond length of 1-chloroethene, 1.331 Å. Meanwhile, the C1-C2 structure becomes mostly planar, indicating the formation of the 1-chloroethene

product. The negative frequency corresponding to the bond rupture mode is 1218 cm^{-1}, a typical value for C-H bond scission reactions.

1-choloroethane **1-chloroethyl** **Transition State**

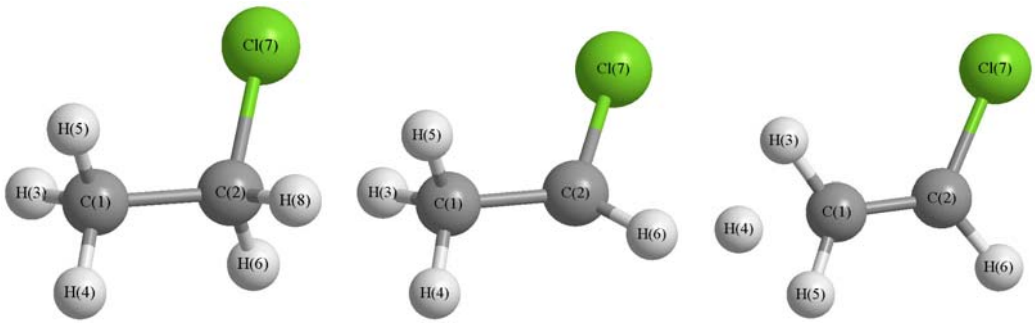

Table 5-1. Comparison of the calculated geometry of 1-choroethane, 1-chloroethyl, and the 1-chloroethyl decomposition transition state structure (Structures are optimized at MP2/6-31G* level. Units are in Å for bond lengths and degrees for angles)

	1-chloroethane	1-chloroethyl	Transition State
R(C1C2)	1.514	1.484	1.332
R(Cl7C2)	1.788	1.717	1.722
R(H6C2)	1.090	1.082	1.082
R(H4C1)	1.094	1.093	1.844
A(Cl7C2C1)	111.30	118.56	122.97
A(H6C2C1)	111.51	122.32	123.47
A(H4C1C2)	109.50	109.68	107.36
D(Cl7C2C1H4)	180.04	171.10	88.69
D(H6C2C1H5)	180.58	204.53	9.93

Table 5-2 lists the calculated energies of the reactant, transition state, and products as well as the heat of reaction and the activation energy for the 1-chloroethyl decomposition reaction. The G3 and CBS composite energy methods were chosen

because of their proven compromise between accuracy and computational cost for hydrocarbon cracking reactions (Zheng and Blowers, 2005c). The calculated reaction pathway is shown in Figure 5-1. The activation energy of the 1-chloroethyl decomposition reaction is 39.50 kcal/mol using the G3 method and 38.94 kcal/mol using the CBS method. Compared with the experimental activation energy obtained by Manion *et al.* (Manion and Louw, 1988), 40.14 kcal/mol, the relative error is only 1.59% for the G3 method and 2.99% for the CBS method. This proves that both composite energy methods can accurately predict reaction energetics. The heat of reaction is 36.70 kcal/mol using the G3 method and 36.73 kcal/mol using the CBS method.

Table 5-2. Calculated energies of 1-chloroethyl decomposition reaction (Units are in Hartrees for the reactant, TS and products; Units are in kcal/mol for heat of reaction and activation energy)

	1-chloroethyl	TS	1-chloroethene	H	Heat of reaction	Activation energy
G3	-538.5307607	-538.4678137	-537.9712769	-0.501	36.70	39.50
CBS	-538.1344765	-538.0724292	-537.5759866	-0.49995	36.73	38.94
Experiment	-	-	-	-	-	40.14

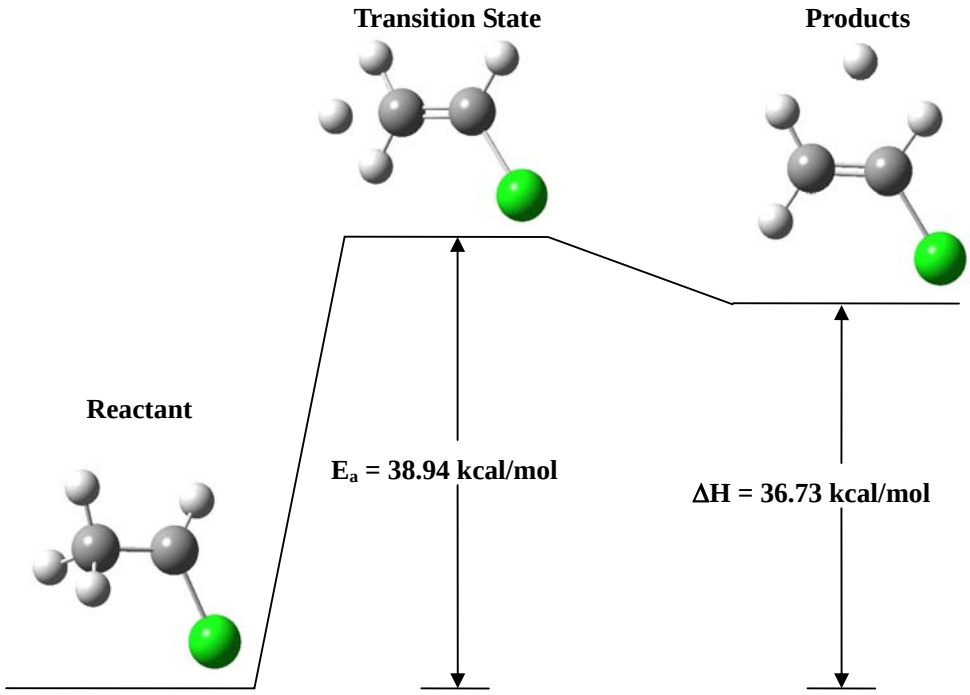

Figure 5-1. The calculated reaction coordinate of the 1-chloroethyl radical decomposition reaction (Structures are optimized at the MP2(full)/6-31G* level and energies listed are calculated using the CBS method).

5.1.2 Reaction Kinetic Modeling

In the fall-off region, the reaction rate constant is calculated applying RRKM theory and using G3 and CBS composite energy methods. The calculated results, together with the available experimental data (Knyazev et al., 1994a), are shown in Figures 5-2. In this work, β_c, the collisional efficiency in the RRKM expression is taken as 0.1 and kept constant for all calculations (Zheng and Blowers, 2005a; Zheng and Blowers, 2005b; Zheng et al., 2005). He, N_2, and Ar bath gases with different concentrations are considered. The bath gas influences the reaction rate through the

Lennard-Jones collision frequency term, Z_{LJ}. It can be seen from Figure 5-2 that the G3 and CBS composite energy methods successfully predict the reaction rate under all conditions (different bath gases and concentrations) compared with the experimental results. The G3 method estimates a slightly lower reaction rate compared with the CBS method because the activation energy obtained by the G3 method is 0.56 kcal/mol higher than the one from the CBS method.

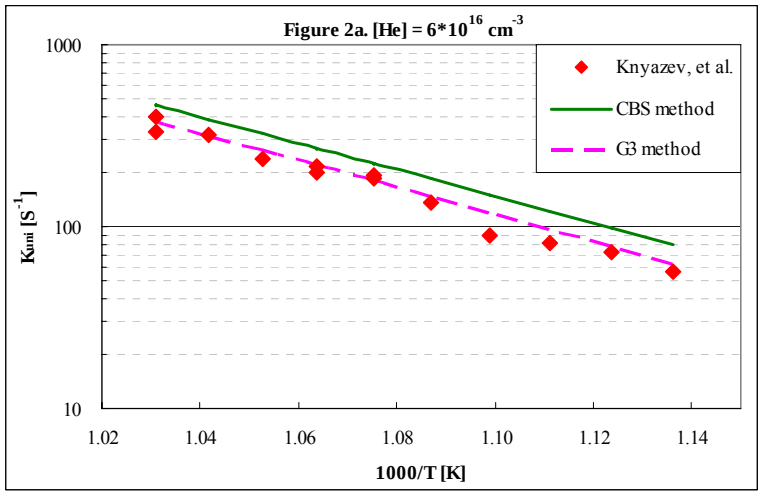

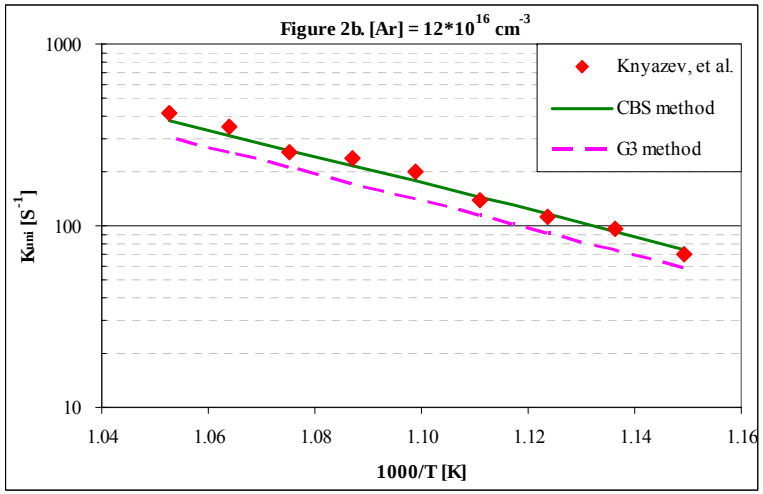

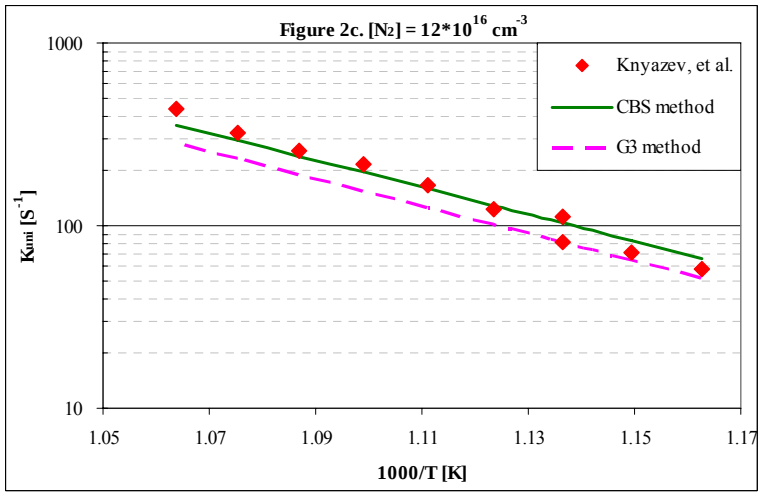

Figure 5-2a. – 5-2c. RRKM theory reaction rates for the 1-chloroethyl decomposition reaction using different bath gases compared with experimental data from Knyazev, *et al.* (Knyazev et al., 1994a)

In the high pressure region, the reaction rate is estimated using CTST and compared with experimental data from Manion *et al.* (Manion and Louw, 1988). As shown in Figure 5-3, the G3 and CBS composite energy method results show very good agreement with the experiments, while the calculated results using the CBS method are relatively higher.

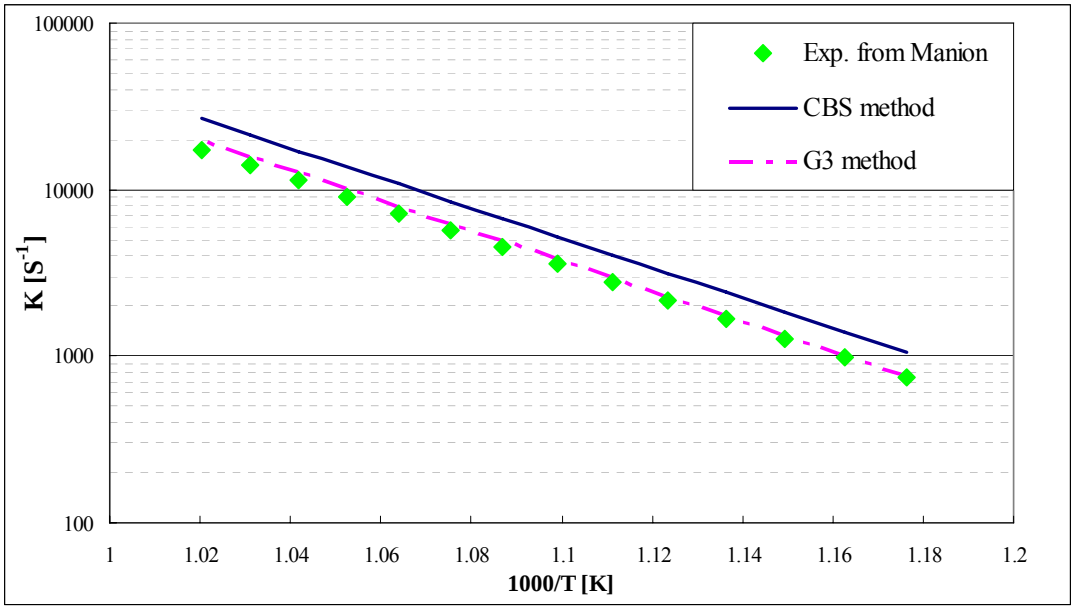

Figure 5-3. High pressure canonical transition state theory rate constant results for the 1-chloroethyl decomposition reaction compared with experimental data from Manion (Manion and Louw, 1988)

The reaction rate constants were then calculated in the pressure range of 0.1 kPa to 1000 kPa and the temperature range of 600 K to 1000 K using N_2 as the bath gas to extend the predictions to a wide range of pressure and temperature conditions. In

order to facilitate predictions by chemists and engineers who would like to apply the kinetic results over a wide range of conditions without going into the details of the complicated theories, the kinetic data were regressed using the SAS software program package (SAS Institute, 1999). A linear relationship of log(k) with respect to log(P) and 1/T is introduced. An R-squared value of 0.995 indicates a good fit of the resulting model with the quantum chemical calculation results. The obtained kinetic models are shown below.

$$k\ [s^{-1}] = 7.32\times10^{10}\times P^{0.69}\times e^{(-18727.10/T)} \qquad \text{when } P \le P_0 \qquad (5.1\text{-}1)$$

$$k\ [s^{-1}] = 3.74\times10^{13}\times e^{(-20648.10/T)} \qquad \text{when } P > P_0 \qquad (5.1\text{-}2)$$

where P is in units of kPa and T is in units of degrees Kelvin. Model (5.1-1) describes the reaction rate in the fall-off region, while model (5.1-2) applies in the high pressure region and is derived from the high pressure limit CTST. P_0 is switching pressure where the reaction rate changes from the fall off region to the high pressure limit. This pressure was obtained by equalizing models (5.1-1) and (5.1-2), leading to $P_0 = 8.42\times10^{3}\times e^{(-2782.61/T)}$. At T=950K, the model and the calculated results are shown in Figure 5-4.

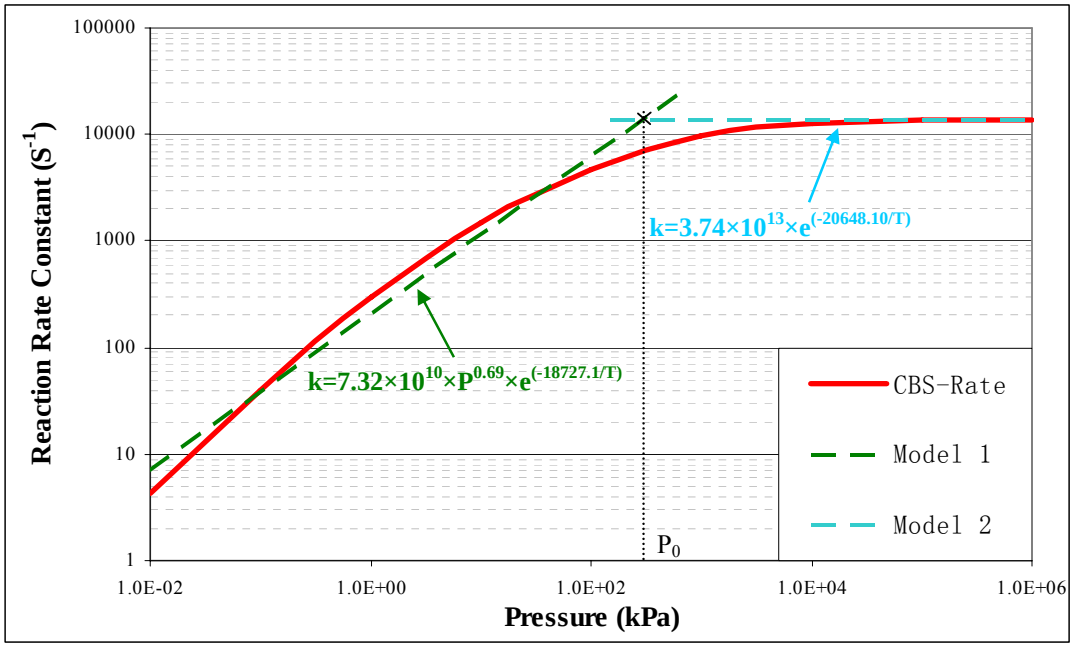

Figure 5-4. 1-chloroethyl radical decomposition reaction kinetic models at T = 950 K

This figure indicates the model to be a good description of the complicated quantum chemical-based kinetic simulation data. The advantage of this simple model is that it can be easily applied, even under conditions where pressure is a factor, meaning it has broad applications in industrial settings.

5.2 *Tert*-butyl Radical Cracking Reaction:

$$CH_3{}^*C(CH_3)_2 \rightarrow CH_2C(CH_3)_2 + {}^*H$$

In this section, the focus will be on the *tert*-butyl radical decomposition reaction: $CH_3{}^*C(CH_3)_2 \rightarrow CH_2C(CH_3)_2 + {}^*H$, where * denotes an unpaired electron. This is another reaction where limited experimental information is available (Knyazev et al.,

1994b). Knyazev *et al.* have studied the kinetics of the decomposition reaction using the master equation approach. The average energy transferred in deactivations, $<\Delta E>_{down}$, was derived with a significantly large uncertainty of ± 200%. $<\Delta E>_{down}$ greatly depends on experimental conditions and constrains the ability of extending their results to other conditions outside the scope of their work. In this work, a generalized kinetic model is proposed which can be applied to different reaction conditions while reducing the uncertainties in the predictions.

5.2.1 Reaction Pathway and Energetics

Table 5-3 shows the structures of the *tert*-butane, *tert*-butyl radical and the transition state of the *tert*-butyl radical decomposition reaction calculated at the MP2/6-31G* level. For *tert*-butane, all three C-C bond lengths are identical, 1.526 Å, because of its C_{3v} symmetry. For the *tert*-butyl reactant, carbon C2 has one unpaired electron, which is the reason for the high activity of this radical. The radical keeps the symmetry, and the three C-C bond lengths are still identical, 1.493 Å, slightly shorter than that of *tert*-butane, which indicates stronger C-C bonds. As the decomposition reaction takes place, the H11-C4 bond length increases from 1.102 Å for *tert*-butyl radical and reaches 1.824 Å at the transition state, showing this C-H bond rupture mode. Meanwhile, the C2-C4 bond length decreases from 1.493 Å for *tert*-butyl reactant and reaches 1.341 Å at the transition state, which is very close to the equilibrium bond length of *tert*-butene, 1.339 Å. Meanwhile, the C1-C2-C3-C4 structure becomes mostly planar, indicating the formation of the *tert*-butene product.

The negative frequency corresponding to the bond rupture mode is 1210 cm^{-1}, a typical value for C-H bond scission reactions.

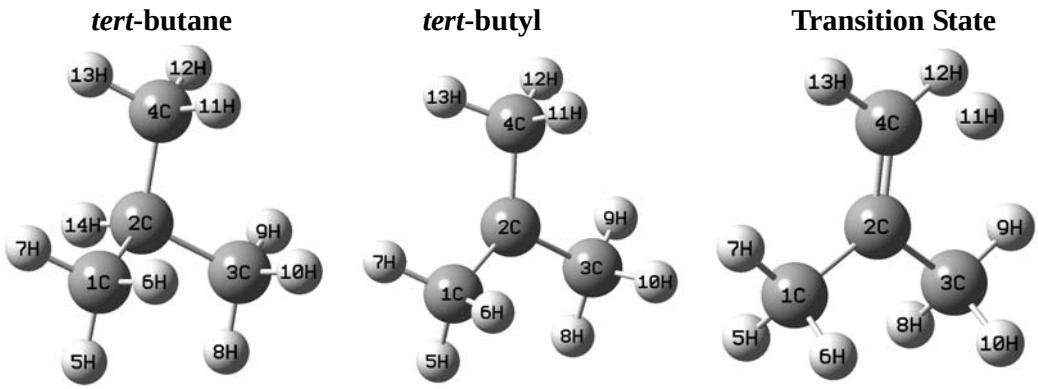

Table 5-3. Comparison of the calculated geometries of *tert*-butane, *tert*-butyl, and the *tert*-butyl decomposition reaction transition state structures (Structures are optimized at the MP2/6-31G* level. Units are in Å for bond lengths and degrees for angles)

	tert-butane	*tert*-butyl	Transition State
R(C2C4)	1.526	1.493	1.341
R(ClC2)	1.526	1.493	1.498
R(H11C4)	1.095	1.102	1.824
A(C4C2C1)	110.84	118.01	121.89
A(C1C2C3)	110.82	118.01	115.97
A(H13C4H12)	108.03	108.29	116.07
D(C4C2C1C3)	-123.50	-152.45	-174.52

Table 5-4 lists the calculated energies of the reactant, transition state, and products as well as the heat of reaction and the activation energy for the *tert*-butyl decomposition reaction. The G3 and CBS compound models were chosen because of their proven compromise between accuracy and computational cost for hydrocarbon cracking reactions (Zheng and Blowers, 2005c). The calculated

reaction pathway is shown in Figure 5-5. The heat of reaction is 33.60 kcal/mol using the G3 method and 33.83 kcal/mol using the CBS method. Compared with the experimental data from NIST (Linstrom and Mallard, 2003), our calculated numbers are slightly lower by 3 kcal/mol. The activation energy of the *tert*-butyl decomposition reaction is 35.16 kcal/mol using the G3 method and 34.92 kcal/mol using the CBS method. Compared with the experimental activation energy obtained by Knyazev (Knyazev et al., 1994a), 35.97 kcal/mol, both methods have excellent agreement. For this reaction, the heats of reaction and activation energies obtained using G3 and CBS methods are very close to each other. Also, the comparison with the experiment data proves that both composite energy methods can accurately predict reaction energetics.

Table 5-4. Calculated energies of *tert*-butyl decomposition reaction (Units are in Hartrees for the reactant, TS and products; Units are in kcal/mol for heat of reaction and activation energy)

	tert-butyl	TS	*tert*-butene	H	Heat of reaction	Activation energy
G3	-157.6095464	-157.5535231	-157.0549963	-0.501	33.60	35.16
CBS	-157.4285471	-157.3729011	-156.8746801	-0.49995	33.83	34.92
Experiment	-	-	-	-	36.33 [a]	35.97 [b]

a – (Linstrom and Mallard, 2003)

b – (Knyazev et al., 1994b)

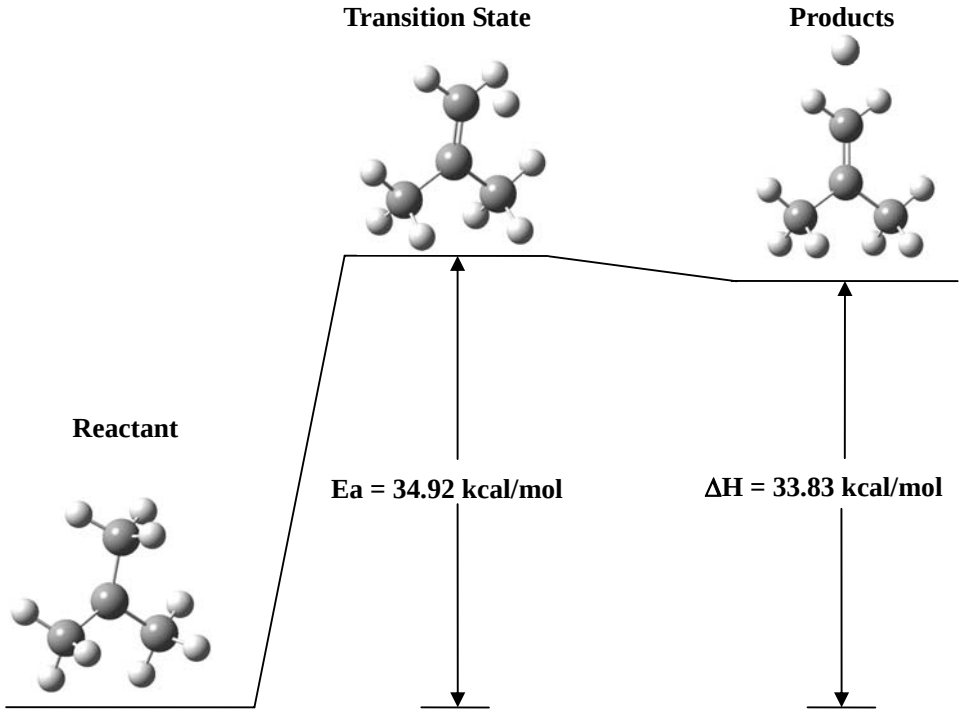

Figure 5-5. The calculated reaction coordinate of the *tert*-butyl radical decomposition reaction (Structures are optimized at the MP2(full)/6-31G* level and energies listed are calculated using the CBS method).

5.2.2 Reaction Kinetic Modeling

In the fall-off region, the reaction rate constant is calculated applying RRKM theory and using G3 and CBS composite energy methods. The calculated results, together with the available experimental data (Knyazev et al., 1994b), are shown in Figures 5-6. In this work, β_c, the collisional efficiency in the RRKM expression is taken as 0.1 and kept constant for all calculations. Only the He bath gas with different concentrations is considered because it is the only bath gas studied in the experiments. It can be seen from Figure 5-6 that the G3 and CBS composite energy methods successfully predict the reaction rate under different He concentrations compared with the experimental results. The G3 method estimates a slightly lower reaction rate compared with the CBS method because the activation energy obtained by the G3 method is 0.24 kcal/mol higher than CBS.

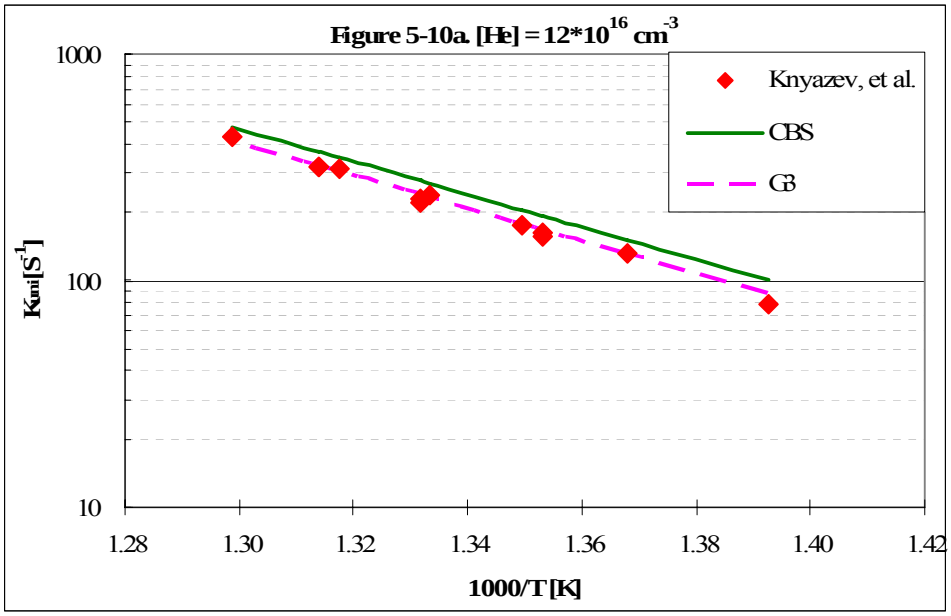

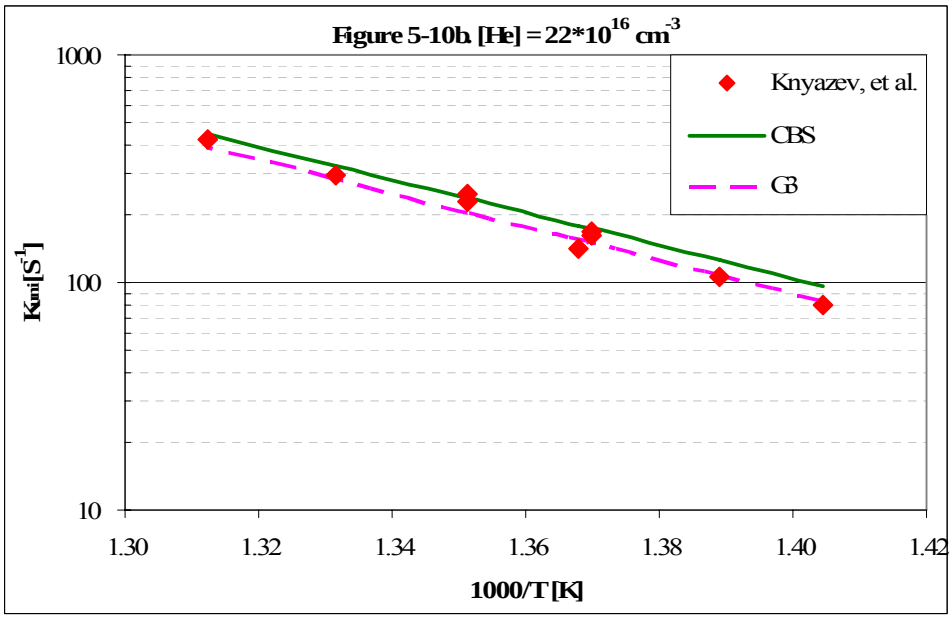

Figure 5-6a. – 5-6b. RRKM theory reaction rates for the *tert*-butyl decomposition reaction using He bath gas compared with experimental data from Knyazev, *et al.* (Knyazev et al., 1994b)

In the high pressure region, the reaction rate is estimated using CTST and compared with experimental data from Tsang (Tsang, 1990). As shown in Figure 5-7, the G3 and CBS composite energy method results show very good agreement with the experiments, while the calculated results using the CBS method are relatively higher.

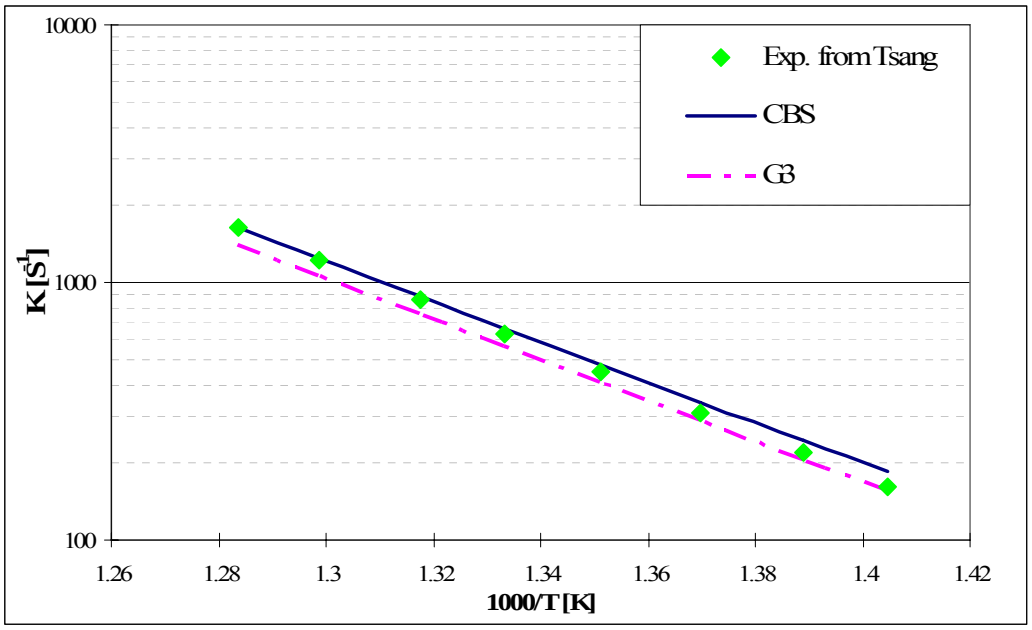

Figure 5-7. High pressure canonical transition state theory rate constant results for the *tert*-butyl decomposition reaction compared with experimental data from Tsang (Tsang, 1990)

The reaction rate constants were then calculated in the pressure range of 0.1kPa to 1000 kPa and the temperature range of 600 K to 1000 K using N_2 as the bath gas to extend the predictions to a wide range of pressure and temperature conditions. The

kinetic data were then regressed using the SAS software program package (SAS Institute, 1999). A linear relationship of log(k) with respect to log(P) and 1/T is introduced. The obtained kinetic models are shown below.

$$k\ [s^{-1}] = 3.93\times10^{12}\times P^{0.35}\times e^{(-17878.5/T)} \qquad \text{when } P \le P_0 \qquad (5.2\text{-}1)$$

$$k\ [s^{-1}] = 2.0\times10^{13}\times e^{(-18096.0/T)} \qquad \text{when } P > P_0 \qquad (5.2\text{-}2)$$

where P is in units of kPa and T is in units of degrees Kelvin. Model (5.2-1) describes the reaction rate in the fall-off region, while model (5.2-2) applies in the high pressure region and is derived from the high pressure limit CTST. P_0 is switching pressure where the reaction rates change from the fall off region to the high pressure limit. This pressure was obtained by equalizing models (5.2-1) and (5.2-2), leading to $P_0 = 1.04\times10^{2}\times e^{(-621.43/T)}$. At T=750K, the model and the calculated results are shown in Figure 5-8.

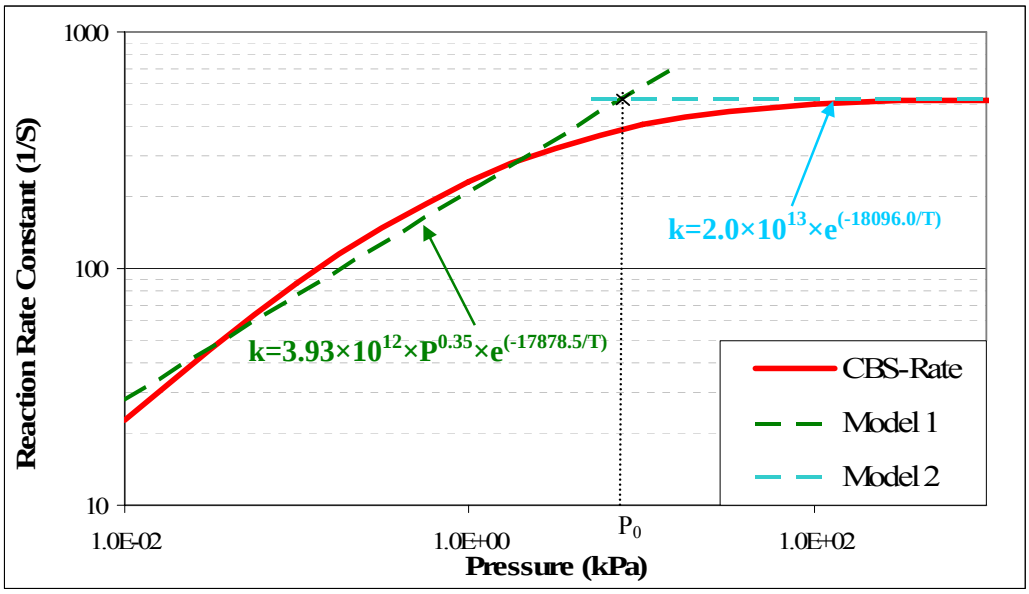

Figure 5-8. *tert*-butyl radical decomposition reaction kinetic models at T = 750 K

This figure indicates the model to be a good description of the complicated quantum chemical-based kinetic simulation data. The advantage of this simple model is that it can be easily applied even under conditions where pressure is a factor.

5.3 Conclusions

In this chapter, 1-chloroethyl and *tert*-butyl radical carbon-hydrogen bond scission reactions were investigated using G3 and CBS-RAD(MP2) methods. These are reactions for which experimental information is available. From the calculational results using G3 and CBS-RAD(MP2) methods, the heats of reaction and activation barriers agree well with the available experimental data. RRKM and CTST

expressions were then applied to estimate the reaction kinetics. Compared with the experimental data, the CBS method successfully predicted the reaction rate constants in all cases. In order to facilitate predictions by engineers who would like to use the kinetic data without going through the complicated theoretical details presented here, analytic formulas of the kinetic models were proposed for each reaction.

REFERENCES:

Frisch, M.J. et al., 1998. *Gaussian 98, Revision A.7*. Gaussian, Inc., Pittsburgh PA.

Gardiner, W.C. and Burcat, A., 1984. *Combustion chemistry*. Springer-Verlag, New York.

Gonzalez, C. and Schlegel, H.B., 1989. An Improved Algorithm For Reaction-Path Following. *Journal Of Chemical Physics*, 90(4): 2154-2161.

Knyazev, V.D., Bencsura, A., Dubinsky, I.A., Gutman, D. and Senkan, S.M., 1994a. The unimolecular decomposition of 1-chloroethyl radical. *Symposium (International) on Combustion, [Proceedings]*, 25th: 817-24.

Knyazev, V.D., Dubinsky, I.A., Slagle, I.R. and Gutman, D., 1994b. Unimolecular Decomposition of T-C4h9 Radical. *Journal of Physical Chemistry*, 98(20): 5279-5289.

Linstrom, P.J. and Mallard, W.G., 2003. *NIST Chemistry WebBook, NIST Standard Reference Database Number 69, March 2003, National Institute of Standards and Technology*, Gaithersburg MD, 20899 (http://webbook.nist.gov).

Manion, J.A. and Louw, R., 1988. Studies In Gas-Phase Hydrogenolysis .5. Gas-Phase Hydrogenolysis Of Chloroethene - Rates, Products, And Computer Modeling. *Journal Of The Chemical Society-Perkin Transactions 2*(8): 1547-1555.

SAS Institute, I., version 8, 1999.

Scott, A.P. and Radom, L., 1996. Harmonic vibrational frequencies: An evaluation of Hartree-Fock, Moller-Plesset, quadratic configuration interaction, density functional theory, and semiempirical scale factors. *Journal of Physical Chemistry*, 100(41): 16502-16513.

Tsang, W., 1990. Chemical Kinetic Data-Base for Combustion Chemistry .4. Isobutane. *Journal of Physical and Chemical Reference Data*, 19(1): 1-68.

Zheng, X. and Blowers, P., 2005a. The application of composite energy methods to n-butyl radical β-scission reaction kinetic estimations. *Theoretical Chemistry Accounts*, (in press).

Zheng, X. and Blowers, P., 2005b. Evaluate of compound models for estimating rate constants of hydrocarbon thermal cracking reactions: Propyl radical β-scission reaction. *Industrial Engineering Chemistry & Research*, (in press).

Zheng, X. and Blowers, P., 2005c. The investigation of hydrocarbon cracking reaction energetics using composite energy method. *Molecular Simulation*: (in press).

Zheng, X. and Blowers, P., 2005d. Kinetic modeling of 1-chloroethtyl unimolecular decomposition reaction with composite energy methods. *Industrial Engineering Chemistry & Research*, (in review).

Zheng, X., Blowers, P. and Zhang, N.L., 2005. Application of compound models for estimating rate constants of hydrocarbon thermal cracking reactions: The neopentyl radical beta-scission reaction. *Molecular Simulation*, 31(9): 615-621.

CHAPTER 6

HYDROCARBON HETEROGENEOUS REACTIONS ON ZEOLITE CATALYSTS

Zeolites are microporous crystalline aluminosilicates with a three-dimensional framework structure which forms uniformly sized pores of molecular dimension. They are broadly used as catalysts in the oil refining and petroleum industries; the world wide total annual zeolite catalyst consumption rate was 360 million tons in 1998 (Maesen and Marcus, 2001). There are 130 different types of zeolite structures identified and described in the International Zeolite Association Database (http://www.iza-structure.org/databases/), 16 of which are of commercial interest and are produced synthetically. Among them, H-ZSM-5 is broadly used in the petrochemical industry for cracking of hydrocarbons because of its interesting catalytic properties including shape selectivity and high acid strength (McCusker and Baerlocher, 2001).

The catalytic function of zeolites is realized by their Brønsted acidic sites. These active sites are formed when a silicon atom, which has a formal valency of four, is replaced by an aluminum atom with a valency of three. A proton is attached to the

oxygen atom connecting the silicon and its aluminum atom neighbor, resulting in a chemically stable structure, Al(OH)Si, where the oxygen atom becomes a three-coordinated structure. SiO and AlO bonds have considerable covalency, resulting in a relatively weak OH bond. The "onium" type coordination of oxygen is the fundamental reason for the high acidity of the attached proton, which makes a zeolite a good catalyst (Flanigen, 2001).

Because of the complicated reaction mechanisms and various simultaneous reaction pathways, hydrocarbon catalytic reactions on zeolites are very difficult to study experimentally (Curtiss and Gordon, 2004; van Santen et al., 2001). On the other hand, the dramatic increase of computer speed has greatly increased the ability to apply computational tools for investigating large systems in the last decade. Density functional theory and *ab initio* quantum chemical methods have been applied by many researchers to study zeolite catalytic reactions quantitatively (Blaszkowski et al., 1994; Blaszkowski et al., 1996; Collins and Omalley, 1994; Collins and Omalley, 1995; Frash et al., 1998; Frash and van Santen, 1999; Hay et al., 1999; Himei et al., 1995; Kazansky, 1999; Kazansky et al., 1994a; Kazansky et al., 1996b; Kazansky et al., 1996c; Kazansky et al., 1994b; Klier, 2002; Rigby and Frash, 1997; Rigby et al., 1997; Viruelamartin et al., 1993; Zygmunt et al., 2000). The results have demonstrated great relevance for understanding the reaction mechanisms and their kinetic and thermodynamic implications.

The aspects of a catalytic reaction which are only dependent on local properties, such as activation of adsorbates and any bond breaking or forming that may take place, are

generally studied with the cluster approach. A cluster model is formed by theoretically cutting out a portion of the catalyst lattice and terminating the open valences with hydroxyl or hydride bonds. The cluster size is chosen so that the reaction can be modeled using quantum methods (Bates and Van Santen, 1998). $H_3Si\text{-}O\text{-}AlH_2\text{-}(OH)\text{-}SiH_3$, a T3 cluster model cluster model, has been applied extensively to investigate hydrocarbon heterogeneous reactions (Furtado et al., 2001; Milas and Nascimento, 2001; Okulik et al., 2004; Okulik et al., 2001; Zheng and Blowers, 2005a), which will also be the cluster of choice for this work to simulate the zeolite surface.

6.1 Methane Reactions

Catalytic conversion of methane to liquid fuels or desired products is currently one of the great challenges in catalysis science.(Vollmer and Truong, 2000) Also, methane catalytic conversion reactions are among the simplest elementary reactions which can be studied experimentally. By comparing theoretical results with the experimental data, these reactions can be used as a benchmark to evaluate the choice of computational methods.

For many years, researchers have used quantum chemical tools to investigate the structure, stability, reaction kinetics and mechanisms of different molecular systems.(Blowers and Masel, 2000; Jursic, 1997; Lynch and Truhlar, 2001; Saeys et al., 2003; Truong, 2000; Truong and Truong, 1999; Wong et al., 1994; Wong and Radom, 1995; Wong and Radom, 1998; Xiao et al., 1997) Particularly, density functional theory and *ab initio* methods have been applied by other researchers to study catalytic reactions

quantitatively.(Abbot and Dunstan, 1997; Collins and Omalley, 1994; Collins and Omalley, 1995; Frash et al., 1998; Hay et al., 1999; Kazansky, 1999; Kazansky et al., 1996a; Kazansky et al., 1994a; Kazansky et al., 1996b; Kazansky et al., 1994b; Rigby et al., 1997; Viruelamartin et al., 1993; Zheng and Blowers, 2005a; Zygmunt et al., 2000) Kramer, *et al.,* studied the methane hydrogen exchange reaction using HF/6-31g** calculations, a low level *ab initio* method with a modest basis set.(Kramer et al., 1993) Evleth, *et al.,* investigated the methane hydrogen exchange reaction using MP2/6-31++g*//HF/3-21g (energy calculation method//geometry optimization method) with a silicon-free T1 cluster.(Evleth et al., 1994) The activation energies obtained are relatively high in that work, reflecting the inability of a T1 cluster to represent a zeolite catalyst. In 1999, Esteves, *et al.,* studied the methane hydrogen exchange reaction using B3LYP/6-31g** and MP2/6-31g**//HF/6-31g** methods.(Esteves et al., 1999) The activation energies for the methane hydrogen exchange reaction are 32.3 kcal/mol and 31.1 kcal/mol using these methods. In 2000, Ryder, *et al.,* studied the methane hydrogen exchange reaction using the BH&HLYP/6-31++g** method.(Ryder et al., 2000) The activation barrier obtained with this method was 38.4 kcal/mol. Kazansky, *et al.,* also investigated methane hydrogen exchange and dehydrogenation reactions using a small T1 cluster and the low level HF/3-21g method.(Kazansky et al., 1994a) The activation energies obtained were 37.1 kcal/mol for hydrogen exchange and 104.5 kcal/mol for dehydrogenation. With a T3 cluster model, Blaszkowski, *et al*., studied the methane reaction using BP/DZPV, a nonlocal density functional theory method.(Blaszkowski et al., 1994) The resulting activation energies were relatively

low, 29.85 kcal/mol for hydrogen exchange and 82.03 kcal/mol for dehydrogenation, because the BP/DZPV method tends to underestimate reaction barriers for this type of reaction.(Zhang et al., 1995) Larson, *et al.,* investigated the CD_4 H/D reaction using silica-alumina catalysts experimentally and reported an activation barrier of 33.4 kcal/mol.(Larson and Hall, 1965)

In this section, a silicon-containing T3 cluster is used to simulate the zeolite catalyst, and a composite energy method is implemented to investigate the methane hydrogen exchange and dehydrogenation reactions energetics. The results are then compared with the experimental data and computational results from other researchers. Furthermore, the influence of the zeolite acidity on methane conversion reaction activation energies is studied quantitatively. Calculations of the reaction rate constants using canonical transition state theory are also proposed.

6.1.1 Computational Methods

Density functional theory (DFT) has been widely applied by physicists to study the electronic structure of solids in the past 30 years.(Bhan et al., 2003; Blaszkowski and Vansanten, 1995; Bottoni, 1996; Broclawik et al., 1995; Frash et al., 1998; Gonzales et al., 1998; Hay et al., 1999; Jursic, 1997; Lins and Nascimento, 1996; Nicholas, 1997; Rozanska et al., 2003; Truong, 2000; Truong and Truong, 1999) Computational studies of chemical reaction systems have become very popular because the methods are quite reliable and only have medium computational demands compared to *ab intio* molecular orbital theory. The geometry optimizations of the reactants, products and transition state structures in this work were carried out using Becke's three-parameter density

functional(Becke, 1993) and the Lee, Yang, and Parr functional(Lee et al., 1988) to describe gradient-corrected correlation effects, which leads to the well-known B3LYP method combined with a moderate basis set, 6-31g*. The B3LYP method has been validated to give results similar to that of the more expensive MP2 theory for molecular geometry and frequency calculations.(Bauschlicher and Partridge, 1995; Johnson et al., 1993)

It has been pointed out by many researchers that the calculated activation energies strongly depend on the level of the final energy calculations and less on the level of the geometry optimization.(Frash et al., 1998; Frash et al., 1997; Kazansky et al., 1997) Therefore, it is useful to perform the geometry optimizations at a relatively lower level, B3LYP/6-31g* in this work, and the final energy calculations at a higher level, CBS-QB3, a complete basis set composite energy method discussed in Chapter 3 earlier.

The calculations are performed with the GAUSSIAN98 software package (Frisch et al., 1998). All the structures were fully optimized without geometry constraints. The products and reactants were verified with frequency calculations to be stable structures, and the transition states were tested to ensure they were first order saddle points with only one negative eigenvalue. Additionally, intrinsic reaction coordinate (IRC) calculations proved that each reaction linked the correct products with reactants. Zero point vibrational energies (ZPVE) were obtained from harmonic vibrational frequencies calculated at the B3LYP/6-31g* level with a scaling factor of 0.9806 and the frequencies were scaled by 0.9945 (Scott and Radom, 1996). These frequencies were used in the partition functions for the prediction of reaction rates using transition state theory (Gilbert

and Smith, 1990; Holbrook et al., 1996; Masel, 1996; Masel, 2001). Also, thermal corrections were included in addition to the ZPVE at all temperatures where reaction rate constants were calculated.

6.1.2 Hydrogen Exchange Reaction

$CH_4 + H_3SiOAlH_2(OH')SiH_3 \rightarrow CH_3H' + H_3Si(OH)AlH_2OSiH_3$

The hydrogen exchange reaction consists of the cleavage of one methane C-H bond and the formation of another C-H' bond to the zeolite acidic proton. Figure 6-1(a) shows the calculated transition state structure for the hydrogen exchange reaction of methane using the B3LYP method. The structure clearly shows the C_s symmetry obtained without any symmetry constraints applied for the optimization calculation. The protonated carbon, C(15), stays in the main plane of zeolite cluster and becomes a penta-coordinated structure. The acidic proton H(14) and the hydrogen atom from the methane molecule H(19) stay in the middle of the carbon and oxygen atoms, indicating formation of one C-H bond and breaking of the other. In the reaction process, the right oxygen of the cluster acts as a Brønsted acid which donates a proton. The left oxygen acts as a Lewis base which receives the hydrogen atom from methane.

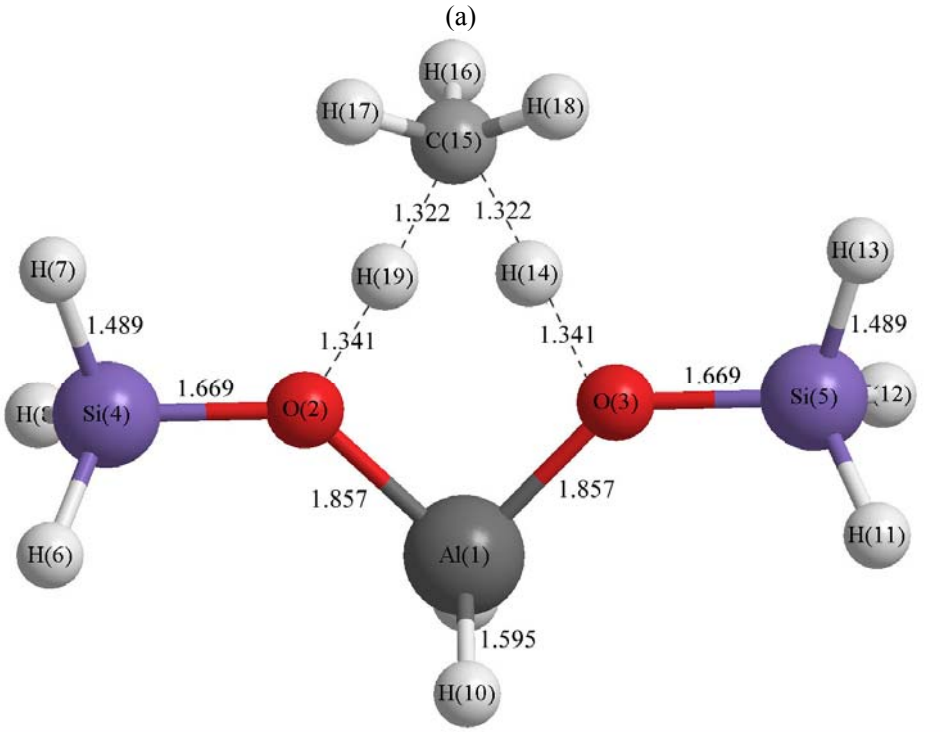

Figure 6-1(a). Transition state structure for the methane hydrogen exchange reaction on a T3 zeolite cluster (Units in Å)

Table 6-1. Activation barrier calculation results for methane reactions on zeolites (Units in kcal/mol)

	This Work	Kramer [a]	Evleth1994 [b]	Esteves1999 [c]	Ryder [d]	Kazansky [e]	Blaszkowski [f]	Experiment [g]
Cluster Model	T3	T3	T1	T3	T5	T1	T3	
Geometry Optimization Method	B3LYP /6-31g*	HF /6-31g**	HF /6-31g*	B3LYP /6-31g**	BH&HLYP /6-31++g**	HF/3-21g	BP/DZVP	
Energy Calculation Method	CBS-QB3	HF /6-31g**	MP2 /6-31++g*	B3LYP /6-31g**	BH&HLYP /6-31++g**	HF/3-21g	BP/DZVP	
Hydrogen Exchange	33.53	35.90	39.90	32.30	38.40	37.10	29.85	33.40
Dehydrogenation	90.08	-	-	-	-	104.50	82.03	-

a - (Kramer et al., 1993) b - (Evleth et al., 1994)

c. - (Esteves et al., 1999) d. - (Ryder et al., 2000)

e. - (Kazansky et al., 1994a) f. - (Blaszkowski et al., 1994)

g. - (Larson and Hall, 1965)

The activation barrier calculated using the CBS-QB3 composite energy method is 33.53 kcal/mol. As listed in Table 6-1, the result is compared with experimental data and computational results from other researchers. An experimental study from Larson, *et al.,* determined the activation energy for the deuterium exchange reaction of CD_4 with zeolite type H-ZSM-5 to be 33.4 kcal/mol. The difference between our calculated result with the experimental value is only 0.13 kcal/mol, which shows our choice of zeolite cluster model and computational method can reproduce experiment very well. In 1993, Kramer, *et al.,* studied the methane hydrogen exchange reaction using HF/6-31g** calculations and a T3 cluster. The activation barrier obtained, 35.90 kcal/mol, is higher than the experiment. The reason is that the HF energy calculations tend to overestimate barrier heights.(Lee and Masel, 1995; Lee and Masel, 1996; Willis and Jensen, 1998; Yamataka et al., 1986) In 1994, Evleth, *et al.,* performed a similar calculation using MP2/6-31++g*//HF/3-21g (energy calculation method//geometry optimization method) and a silicon-free T1 cluster.(Evleth et al., 1994) The activation barrier obtained, 39.90 kcal/mol, is relatively high, reflecting that the T1 cluster cannot represent the zeolite catalyst properly because it does not contain important characteristics of a real zeolite, including the Si-O-Al bridge.(Milas and Nascimento, 2001) In 1999, Evleth, *et al.,* extended their early work by using B3LYP/6-31g** and MP2/6-31g**//HF/6-31g** methods with the T3 cluster model.(Esteves et al., 1999) The activation energies for the methane hydrogen exchange reaction are 32.3 kcal/mol and 31.1 kcal/mol respectively. Kazansky, *et al.,* investigated the methane hydrogen exchange reaction using a small T1 cluster and the low level HF/3-21g method.(Kazansky et al., 1994a) The activation

energy obtained was 37.1 kcal/mol, again overestimating the barrier like HF methods often do. With a T3 cluster model, Blaszkowski, *et al*., studied the methane reaction using BP/DZPV, a nonlocal density functional theory method. The resulting activation energy is relatively low, 29.85 kcal/mol, because the BP/DZPV method tends to underestimate reaction barriers in this type of reactions.(Zhang et al., 1995) With a large T5 cluster model, Ryder, *et al.,* studied the methane hydrogen exchange reaction using the BH&HLYP/6-31++G** method.(Ryder et al., 2000) The activation barrier calculation result is 38.4 kcal/mol, which did not show much improvement by introducing a larger cluster model. Compared with the more accurate result of this work using a relatively smaller T3 cluster model, this highlights the importance of energy calculation method over geometry affects due to basis set or cluster type. Without further increasing the zeolite cluster size, accurate results can be obtained as long as the energy is obtained at a high level, CBS-QB3 in this work.

6.1.3 Dehydrogenation Reaction

$$CH_4 + H_3SiOAlH_2(OH)SiH_3 \rightarrow H_2 + H_3Si(OCH_3)AlH_2OSiH_3$$

The dehydrogenation reaction consists of cleavage of a C-H bond by the zeolite Brønsted acid proton. The fully optimized transition state structure of the reaction is shown in Figure 6-1(b). The H(16)-C(15)-H(18)-H(19) structure becomes planar. A six member ring, O(2)-Al(1)-O(3)-H(14)-H(17)-C(15), is formed. With the H(17)-C(15) and H(14)-O(3) distances greatly extended, a di-hydrogen molecule is almost formed, whereas the CH_3 group binds to the zeolite oxygen, O(2). In this reaction, the right

oxygen O(3) acts as a Brønsted acid which donates a proton and the left oxygen O(2) acts as a Lewis base which receives the CH_3 group.

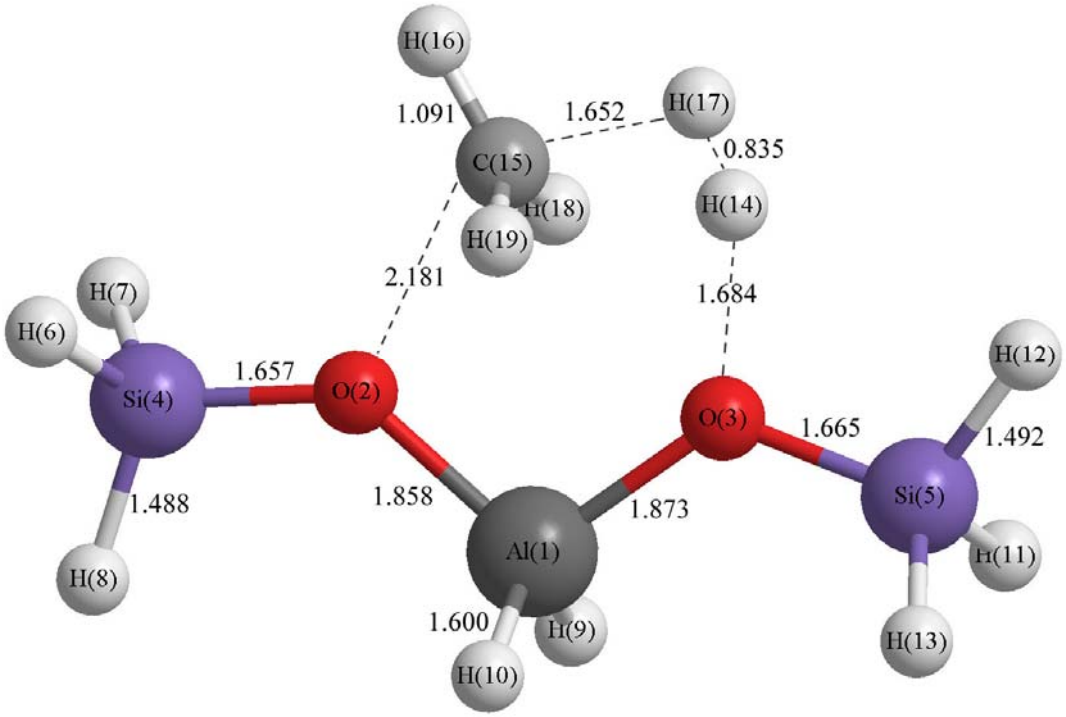

Figure 6-1(b). Transition state structure for the methane dehydrogenation reaction on a T3 zeolite cluster (Units in Å)

The activation barrier obtained from the B3LYP geometry optimization with the CBS energy is 90.08 kcal/mol. This barrier is much higher than the hydrogen exchange reaction activation barrier, indicating the reaction is more difficult to take place. Unfortunately, direct comparison to experiment cannot be accomplished for this reaction because there are no experimental data available. The result obtained in this work is compared with the computational results from other researchers instead in Table 6-1. Blaszkowski, *et al*., studied the reaction using BP/DZPV, a nonlocal density functional

theory method and a T3 cluster. The resulting activation barrier, 82.03 kcal/mol, is relatively low for dehydrogenation because the BP/DZPV method tends to underestimate reaction barriers in this type of reaction.(Zhang et al., 1995) The activation barrier obtained by Kazansky, *et al.*, using HF/3-21g and a T1 cluster is 104.5 kcal/mol. This is relatively higher than the result of this work because the small T1 cluster is unable to represent the zeolite catalyst and because the HF method tends to overestimate activation energies.(Lee and Masel, 1995; Lee and Masel, 1996; Willis and Jensen, 1998; Yamataka et al., 1986) Our result falls between these two values and is expected to be closer to the true value due to the limitations of the other methods used previously.

6.1.4 Acidity Effects

The zeolite acidity plays a very important role in studying reaction properties. In this work, we investigated the effect of zeolite acidity for the methane conversion reactions. The deprotonation energy (E_{dep}) is a theoretical measurement of zeolite acidity and is defined as the energy difference between the protonated (ZH) and unprotonated (Z^-) clusters (Brand et al., 1993).

$$E_{dep} = E(Z^-) - E(ZH)$$

In real zeolite catalysts, the deprotonation energy varies over a range of 20 to 50 kcal/mol among different zeolite structures.(van Santen et al., 1991; van Santen et al., 2001) Kramer, *et al.*,(Evleth et al., 1994; Kramer et al., 1993) have shown that the acidity effect of zeolite catalysts can be simulated by modifying the length of the terminal Si-H bonds of the cluster model with all other geometry parameters fully optimized, and our previous work has followed this methodology successfully (Zheng and Blowers,

2005a). Figure 6-2 shows the effect of the terminal Si-H distance on the zeolite cluster geometries. The geometry shown is obtained at the B3LYP/6-31g* level. The neighbor Si-O bond length decreases from 1.72 Å to 1.698 Å and the protonic hydrogen and acidic oxygen bond distance, H(14)-O(3), increases slightly from 0.975Å to 0.979Å as the Si-H bond length changes from 1.30 Å to 1.70 Å. This indicates that this O-H bond becomes weaker with the increasing distance of the Si-H bond. Therefore, the zeolite cluster becomes more acidic. Increasing the Si-H bond length on the left side of the cluster only has a slight effect on the O-H bond because the Si and H atoms are so far apart.

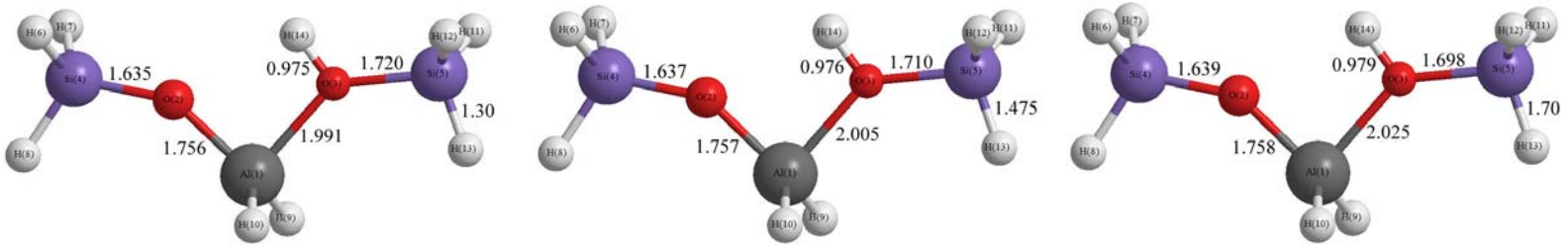

(a) R_{Si-H} = 1.3 Å (less acidic) (b) R_{Si-H} = 1.47 Å (Equilibrium) (c) R_{Si-H} = 1.7 Å (more acidic)

Figure 6-2. H_3Si-O-AlH_2-(OH)-SiH_3 cluster structures with changing terminal Si-H bond distances (Units in Å)

The changes of the zeolite acidity also affect the transition state structures and activation energies of the reactions. Figure 6-3 shows the transition state structures of the methane hydrogen exchange reaction as the Si-H distance changes from 1.3 Å to 1.9 Å. With a Si-H bond length increase, the distance of the protonic hydrogen and acidic oxygen, H(14)-O(3), increases from 1.329 Å to 1.361 Å. Similarly, the distance between the exchanging hydrogen and Lewis basic oxygen, H(19)-O(2), increases from 1.313 Å to 1.407 Å and the CH_5 group moves further away from the cluster. Meanwhile, the two exchanging hydrogens, H(14) and H(19), stay closer to the CH_3 group.

Similar acidic studies were applied to the methane dehydrogenation reaction as well. However, a transition state cannot be located as the Si-H distance increases to 1.9 Å. The transition state structures of the methane dehydrogenation reaction as the Si-H distance changes to 1.3 Å and 1.7 Å are shown in Figure 6-4. As the Si-H distance increases, the distance between the carbon atom and Lewis basic oxygen, C(15)-O(2), increases from 2.151 Å to 2.229 Å and the distance between the protonic hydrogen and acidic oxygen, H(14)-O(3), increases from 1.615 Å to 1.811 Å. Meanwhile, the bi-hydrogen, H(14) and H(17), atoms move closer to each other from 0.849 Å to 0.818 Å, which is more like the structure of a hydrogen molecule, and the entire CH_5 group moves further away from the cluster.

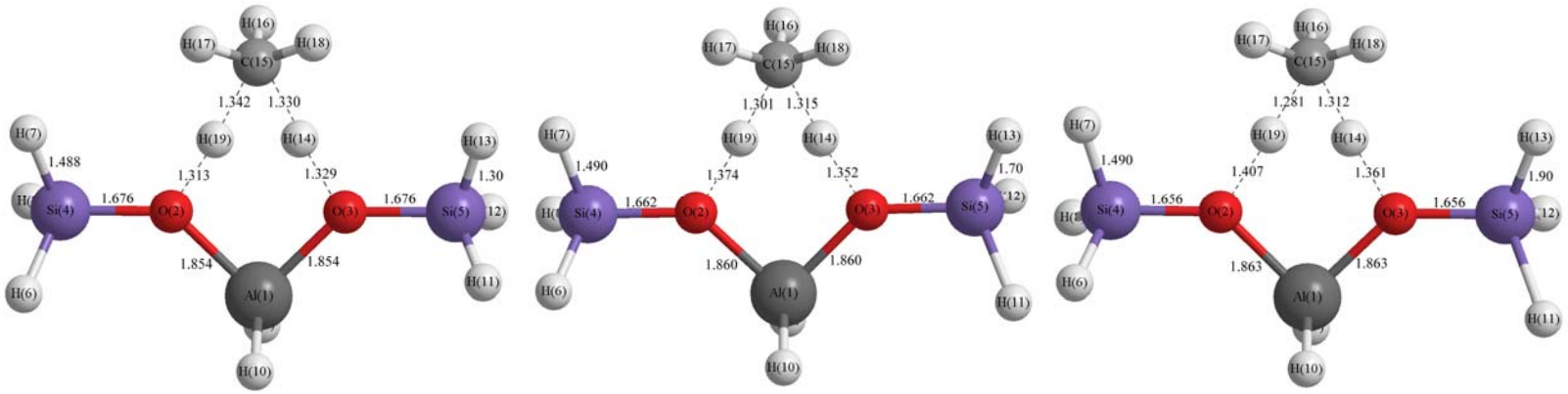

(a) R_{Si-H} = 1.3 Å (less acidic) (b) R_{Si-H} = 1.7 Å (more acidic) (c) R_{Si-H} = 1.9 Å (most acidic)

Figure 6-3. Transition state structures of methane hydrogen exchange reaction with changing terminal Si-H bond distances (Units in Å)

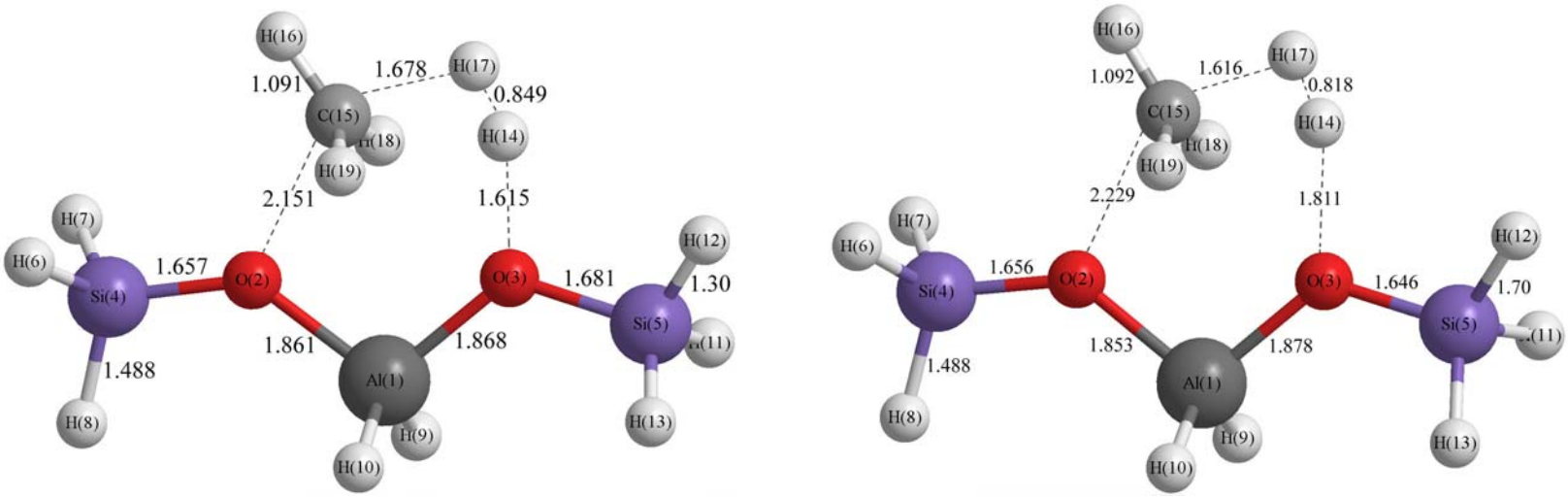

(a) R_{Si-H} = 1.3 Å (less acidic) (b) R_{Si-H} = 1.7 Å (more acidic)

Figure 6-4. Transition state structures for the methane dehydrogenation reaction with changing terminal Si-H bond distances (Units in Å)

Table 6-2 shows the change in activation energies of methane conversion reactions as the zeolite cluster Si-H bond distances are varied. With the Si-H distance increasing, the activation energies decrease for the reactions because of the increased acidity of the zeolite cluster. As long as the reaction mechanism does not alter, the change in activation barrier is linearly correlated to the change in deprotonation energy. Therefore, the Brøsted-Polanyi principle can be applied (van Santen and Kramer, 1995):

$$\Delta E_a = c\Delta E_{dep} \quad \text{or} \quad E_a = c\Delta E_{dep} + b$$

Table 6-2. Effects of Si-H distances on methane reaction activation barriers (Units in kcal/mol)

	Activation Energy (E_a)		Deprotonation Energy (E_{dep})
	Dehydrogenation	Hydrogen Exchange	
R_{Si-H} = 1.30Å	93.31	35.61	303.99
R_{Si-H} = 1.47Å	90.08	33.53	297.93
R_{Si-H} = 1.70Å	85.33	31.16	291.59
R_{Si-H} = 1.90Å	-	29.25	285.81
"Average" Zeolite *	88.01	32.58	295.40
Relationship	$E_a = 0.6453E_{dep} - 102.61$	$E_a = 0.3525E_{dep} - 71.55$	

* - (Frash and van Santen, 1999; van Santen et al., 2001)

The linear relationship of the activation barriers with cluster deprotonation energies is illustrated in Figure 6-5. Applying the average zeolite catalyst deprotonation energy, 295.40 kcal/mol (Frash and van Santen, 1999; van Santen et al., 2001), the activation energies are then calculated and listed in Table 6-2. For the dehydrogenation reaction, the ratio of the change in activation barrier to the change in zeolite deprotonation energy is 0.6453, which is almost identical to that from previous work on ethane conversion reactions on zeolite (Zheng and Blowers, 2005a), 0.6509. For hydrogen exchange, the ratio becomes 0.3523, slightly less than that of ethane, 0.403. Further work needs to verify if these ratios hold for other and larger n-alkane reactions.

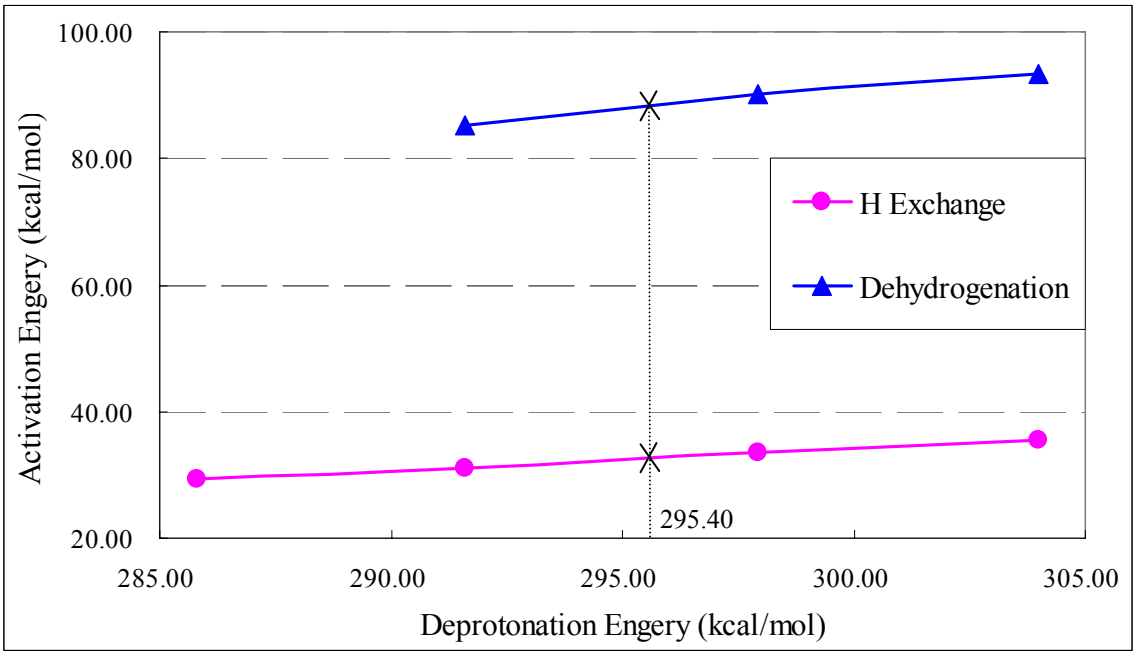

Figure 6-5. Corrections to the calculated methane conversion reactions activation energies for the acidity effect

The acidity effect study has shown the correlations between the deprotonation energies and activation energies for methane conversion reactions. Because deprotonation energies are significantly easier to calculate than activation energies due to the difficulty in performing transition state optimizations for large complexes with many degrees of freedom, using the correlations, activation energies can be easily obtained for different zeolite catalysts as long as their deprotonation energies are first acquired from theory or experiment.

6.1.5 Reaction Rate Constant Estimations

Canonical transition state theory (CTST) (Gilbert and Smith, 1990; Holbrook et al., 1996; Masel, 1996; Masel, 2001) can be applied to calculate reaction rate constants for systems like the ones in this work where pressure is not a factor. For methane conversion reactions, the rate constants can be expressed as:

$$k_r = \left(\frac{k_B T}{h}\right) N_A \frac{q_{TS}^{\mp}}{q_{CH_4} q_{T3}} \exp(-E_{act} / k_B T)$$

where h, k_B and N_A are the Boltzmann, Planck and Avogadro constants; $q_{TS}^{\mp}$, q_{CH_4} and q_{T3} are the partition functions of the transition state structure, methane reactant, and zeolite T3 cluster, which include electronic, translational, rotational, and vibrational partition functions. Since the zeolite cluster is part of a solid, translational and rotational partition functions for the zeolite are assumed to be equal in the reactant and transition state. Therefore, the rate constants are expressed as:

$$k_r = \left(\frac{k_B T}{h}\right) N_A \frac{q_{TS,vib}^{\mp}}{q_{CH_4} q_{T3,vib}} \exp(-E_{act} / k_B T)$$

Tunneling is a quantum effect where reactant molecules that do not have enough energy to cross the barrier can still sometimes react. Tunneling effects can be calculated with the following formula:(Duncan et al., 1998)

$$\kappa(T) = 1 + \frac{1}{24}\left(\frac{h\nu c}{k_B T}\right)^2$$

where c is the speed of light; ν is the imaginary frequency that accounts for the vibrational motion along the reaction path; and, $\kappa(T)$ is the tunneling coefficient. Therefore, the reaction rate constants can be calculated as: $k = \kappa(T)k_r$.

The pre-exponential factor, $A = \left(\frac{k_B T}{h}\right) N_A \frac{q^{\mp}_{TS,vib}}{q_{CH_4} q_{T3,vib}}$, and activation energy E_{act} of the methane hydrogen exchange reaction and dehydrogenation reactions under different temperatures are listed in Table 6-3. The partition functions and activation energies were produced particularly at each temperature point. One can see that the activation energies increase as temperature increases so it is very important to include the thermal corrections in the activation energy calculations for this system in order to obtain accurate kinetic information.

Table 6-3. Rate constants of methane conversion reactions (Units in $m^3\ mol^{-1}\ s^{-1}$ for A and k; in kcal/mol for E_{act})

T	Hydrogen Exchange Reaction				Dehydrogenation Reaction		
	A	E_{act}	k		A	E_{act}	k
300	1.15E+05	33.99	1.92E-20		7.84E+03	90.08	1.67E-62
400	2.42E+05	34.58	3.00E-14		9.08E+03	90.61	2.61E-46
500	3.32E+05	35.30	1.20E-10		1.22E+04	91.25	1.48E-36
800	1.06E+06	37.93	4.54E-05		3.65E+04	93.49	1.01E-21
1000	2.30E+06	39.84	4.45E-03		7.33E+04	95.02	1.22E-16
1250	5.62E+06	42.26	2.27E-01		1.60E+05	96.89	1.78E-12

The reaction rate constant plot is shown in Figure 6-6. The rate constants of hydrogen exchange reaction are much higher than the dehydrogenation reaction because its activation barrier is much lower.

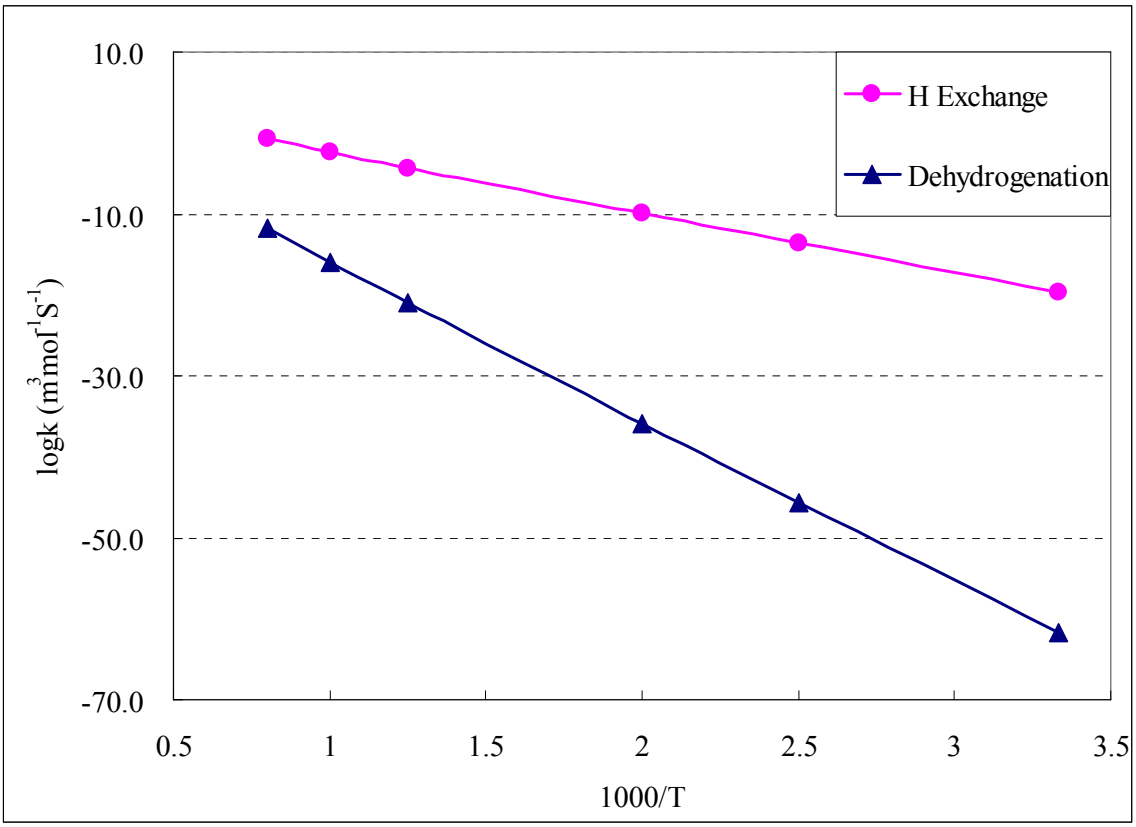

Figure 6-6. Reaction rate constant predictions of methane reactions on zeolite catalysts using the B3LYP/6-31G* geometry optimization and CBS-QB3 energy calculations with canonical transition state theory.

A linear relationship of log(k) with respect to 1/T is regressed and the kinetic models are described as:

$k = 1.41 \times 10^5 \exp(-17221.96/T)$ for the hydrogen exchange reaction

$k = 6.28 \times 10^3 \exp(-45409.28/T)$ for the dehydrogenation reaction

The advantage of these simple models is that they can be easily applied even under different temperatures, and they have broad applications to the modern oil and chemical industries where methane conversion reaction kinetics are of concern.

6.2 Ethane Reactions

Kazansky *et al.* investigated the ethane cracking and dehydrogenation reactions using the small 3-21 basis set with a silicon-free T1 cluster (Kazansky et al., 1994b). The activation energies obtained are very high, bringing into question the validity of the results. With a T3 cluster model, Rigby *et al*. studied the ethane cracking reaction using MP2/6-31g*//HF/3-21g (energy calculation method//geometry optimization method). The results are relatively high because of the small basis set applied in both geometry and energy calculation methods. More recently, Zygmunt *et al*. investigated the ethane cracking and dehydrogenation reactions using a T5 cluster. After higher level theory corrections and long-range corrections, the activation energies obtained are 54.1 kcal/mol and 53.6 kcal/mol, respectively.

In this section, a silicon-containing T3 cluster is used to simulate the zeolite surface, and *ab initio* methods are implemented to investigate the three ethane conversion reactions including protolytic cracking, hydrogen exchange, and dehydrogenation. The results here are then compared with those from previous research. Furthermore, the influence of the zeolite cluster size and acidity on ethane conversion reaction activation energies is studied quantitatively. Also analytical formulas are provided so activation

energies can be obtained for different zeolite catalysts.

6.2.1 Computational Methods

In this section, the CBS-RAD(MP2) compound model was used to investigate ethane conversion energetics on a zeolite cluster because it was shown to be accurate in Chapter 3. All of the *ab initio* calculations were performed with the GAUSSIAN98 software package (Frisch et al., 1998). Geometries were optimized at the HF/6-31g* and MP2(full)/6-31g* levels of calculation. Initial geometries for MP2(full)/6-31g* were obtained using HF/6-31g* optimization results. In some cases, a planar symmetry constraint of the carbon atoms of ethane with five cluster atoms (one Al, two O and two Si) was imposed in order to accelerate calculation and reach convergence. All products and reactants were verified with frequency calculations to be stable structures, and all transition states were found to be first order saddle points with only one negative eigenvalue. Additionally, intrinsic reaction coordinate (IRC) calculations (Gonzalez and Schlegel, 1989) showed that each reaction linked the correct products with reactants. Zero point vibrational energies (ZPVE) were obtained from harmonic vibrational frequencies calculated at the MP2(full)/6-31g* level with a scaling factor of 0.9661(Scott and Radom, 1996). Frequencies were scaled with a factor of 0.9427 at the MP2(full)/6-31g* level.

Table 6-4. Calculated geometry results using MP2/6-31g* compared to experimental data

	$H_3SiOAlH_2(OH)SiH_3$ [a]	Experimental Data
H-Al distance (Å)	2.39	2.43±0.03, 2.48±0.04 [b]
O-H vibrational frequency (cm^{-1})	3708	3600-3623 [c]

a – calculated results using MP2/6-31g*

b – (Freude et al., 1988; Kenaston et al., 1994)

c – (Kustov et al., 1987; Makarova et al., 1994; Trombetta et al., 2000)

In order to verify the computational methods used in this work, the zeolite cluster--$H_3SiOAlH_2(OH)SiH_3$ geometry and frequency calculation results, together with the available experimental results, are compared and listed in Table 6-4. By NMR spectroscopy, the distances between acidic hydrogen and aluminum atom are measured to be 2.43±0.03Å and 2.48±0.04Å, respectively, by Freude (Freude et al., 1988) and Kenaston (Kenaston et al., 1994). The calculated result using MP2/6-31g* is 2.39Å, which is in excellent agreement with the experimental data. The vibrational frequency of the acidic H-O bond is 3496 cm^{-1} using the same method. Compared with an experimental value between 3600-3623 cm^{-1} (Kustov et al., 1987; Makarova et al., 1994; Trombetta et al., 2000), the relative error is within 3%. This supports the geometry optimization level and basis set choice for representing the molecular geometry well.

6.2.2 Protolytic Cracking Reaction

$$CH_3CH_3 + H_3SiOAlH_2(OH)SiH_3 \rightarrow CH_4 + H_3Si(OCH_3)AlH_2OSiH_3$$

The cracking reaction consists of the C-C bond cleavage of ethane by the zeolite Brønsted acid proton. The proton attaches to one methyl group of the ethane reactant and forms methane and a surface oxide. The calculated transition state structure using the MP2/6-31g* method is shown in Figure 6-7(a). The acidic proton has been transferred to the right carbon of ethane and a methane molecule is almost formed. The left methyl group of ethane becomes a planar structure and forms a carbenium ion together with the cluster structure. The zeolite cluster plays an important role in this reaction. The right oxygen of the cluster acts as a Brønsted acid which donates a proton while the left oxygen acts as a Lewis base which receives the methyl group.

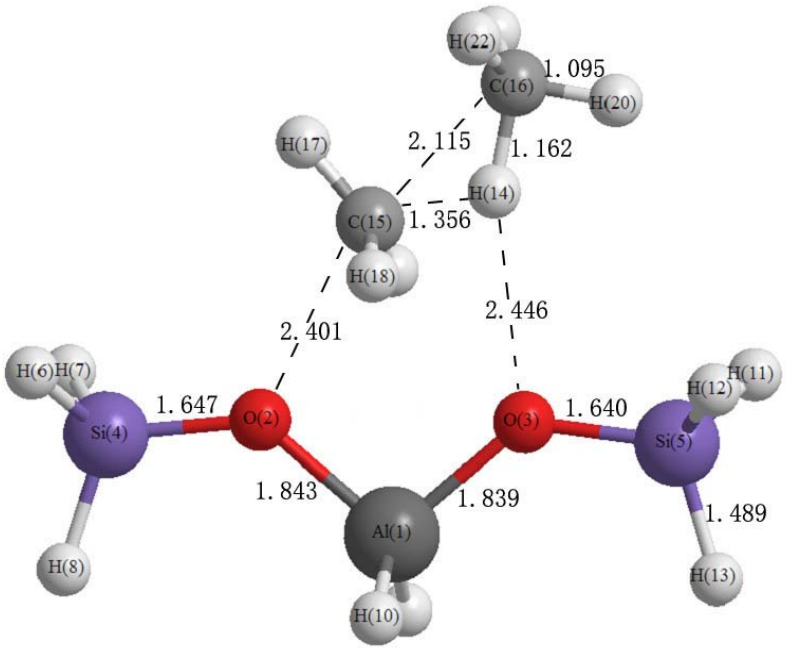

Figure 6-7(a). Transition state structures for the ethane protolytic cracking reaction on a T3 zeolite cluster (Units in Å)

The activation energies obtained from the MP2 geometry optimization method with CBS energy calculations is 71.39 kcal/mol as listed in Table 6-5. Unfortunately, direct comparison to experiment cannot be accomplished because there are no experimental activation energies available. The experimental activation energy for the propane and n-butane cracking reactions are 47 kcal/mol (Narbeshuber et al., 1995), and for the iso-butane cracking reaction is 57 kcal/mol (Stefanadis et al., 1991). Considering the fact that the protonation of ethane is certainly more difficult than that of propane and butane (Kazansky et al., 1994b), the experimental activation energies for ethane cracking reaction should be larger.

Table 6-5. Activation energy calculational results for ethane conversion reactions on zeolites using the CBS method (Units in kcal/mol)

	This Work		Blaszkowski [c]	Kazansky [d]	Kazansky [e]	Rigby [f]	Zygmunt [g]
Cluster Model	T3	T3	T3	T1	T1	T3	T5
Geometry Optimization Method	HF/ 6-31g*	MP2(full)/ 6-31g*	LDA/ DZPV	HF/ 3-21g	HF/ 6-31g*	HF/ 3-21g	MP2(fc)/ 6-31g*
Energy Calculation Method	CBS-RAD (MP2)	CBS-RAD (MP2)	LDA/ DZPV	HF/ 3-21g	MP2/ 6-31++g**	MP2/ 6-31g*	MP2(fc)/ 6-31g*
Protolytic Cracking	71.29	71.39	69.78	93.38	80.30	78.00	73.70/54.10 [a]
Hydrogen Exchange	32.90	31.39	28.28	-	-	-	-
Dehydrogenation	75.91	75.95	70.98	94.80	83.80	-	71.60/53.60 [a,b]

a – after corrections

b – obtained by B3LYP/6-31g*//B3LYP/6-311+g**

c. - (Blaszkowski et al., 1996)

d. - (Kazansky et al., 1994a; Kazansky et al., 1994b)

e. - (Kazansky et al., 1996b)

f. - (Rigby et al., 1997)

g. - (Zygmunt et al., 2000)

The result obtained in this work is compared with the computational results from other researchers also listed in Table 6-5. The activation energy obtained by Blaszkowski *et al.* (Blaszkowski et al., 1996) using the LDA density functional method is 69.76 kcal/mol, which is relatively lower because density functional theory has been known to often underestimate activation energies relative to experiment (Durant, 1996; Goldstein et al., 1998; Johnson et al., 1993; Lynch and Truhlar, 2001; Porezag and Pederson, 1995; Torrent et al., 1996) Another reason for the discrepancy in energies could be that their transition state structure is not fully optimized and four imaginary frequencies modes were present in their work. The result from Kazansky using HF/3-21g//HF/3-21g (Kazansky et al., 1994b), 93.38 kcal/mol, is high because of the small T1 cluster used and the fact that MP2 energy calculations tend to overestimate barrier heights (Lee and Masel, 1995; Lee and Masel, 1996; Willis and Jensen, 1998; Yamataka et al., 1986). Another result from Kazansky (Kazansky et al., 1996a) upgraded the geometry optimization method to MP2(fc)/6-31++g**//HF/6-31g*. The activation energy obtained, 75.23 kcal/mol, is still high, mostly because the MP2 method is known for over-predicting activation energies (Lee and Masel, 1995; Lee and Masel, 1996; Willis and Jensen, 1998; Yamataka et al., 1986). Rigby *et al.* applied MP2/6-31g*//HF/3-21g calculations where the basis set is less than that of Kanzansky. But the application of a larger T3 cluster instead of T1 used by Kanzansky gives an activation energy of 78.00 kcal/mol. More recently, Zygmunt studied the reaction with a large T5 cluster. The result obtained MP2(fc)/6-31g*//MP2(fc)/6-31g* is 73.70 kcal/mol. The authors then included higher level theory corrections by using

MP2(fc)/6-311+g**//MP2(fc)/6-31g* and reduced the activation energy by 2.0 kcal/mol. The long-range correction obtained by the HF/6-31g* correction for the 58T cluster model then reduces the activation energy by 14.50 kcal/mol. Including both corrections together with the zero point energy correction and thermal corrections brings the activation energy to 54.10 kcal/mol.

6.2.3 Hydrogen Exchange Reaction

$CH_3CH_3 + H_3SiOAlH_2(OH')SiH_3 \rightarrow CH_3CH_2H' + H_3Si(OH)AlH_2OSiH_3$

Figure 6-7(b) shows the calculated transition state structure for the hydrogen exchange reaction of ethane using the MP2 method. It shows clearly the C_s symmetry obtained without any symmetry constraints applied for the optimization step. The carbon in the main plane of zeolite structure, C(15), is protonated and becomes a penta-coordinated structure. The other carbon atom keeps its tetrahedral structure. The two hydrogen atoms, H(14) and H(19), stay in the middle of the carbon and oxygen atoms, indicating formation of one C-H bond and breaking of the other. The right oxygen of the cluster acts as a Brønsted acid which donates a proton. The left oxygen acts as a Lewis base which receives the hydrogen atom from ethane.

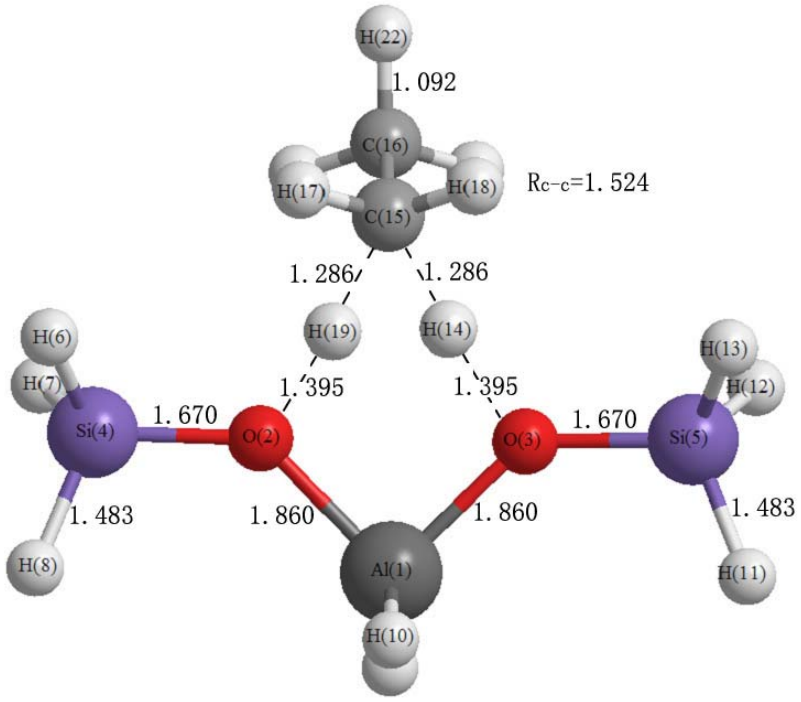

Figure 6-7(b). Transition state structure for the ethane hydrogen exchange reaction on a T3 zeolite cluster (Units in Å)

As shown in Table 6-5, the activation energy obtained from the MP2 geometry optimization and the CBS energy is 31.39 kcal/mol. This barrier is the lowest among the three ethane conversion reactions, indicating it is the easiest reaction to take place. The activation energy obtained by Blaszkowski *et al.* (Blaszkowski et al., 1996) using LDA density functional theory, 28.28 kcal/mol, is somewhat lower than ours. There are no additional calculated results available for comparison.

6.2.4 Dehydrogenation Reaction

$$CH_3CH_3 + H_3SiOAlH_2(OH)SiH_3 \rightarrow H_2 + H_3Si(OC_2H_5)AlH_2OSiH_3$$

The dehydrogenation reaction consists of cleavage of a C-H bond by the zeolite Brønsted acid proton. The transition state structure of the reaction is shown in Figure 6-7(c). The carbon atom attached to the acidic proton becomes a planar structure and the other carbon keeps the tetrahedral structure. A six member ring, O(2)-Al(1)-O(3)-H(14)-H(20)-C(15), is formed. With the H(20)-C(15) and H(14)-O(3) distances greatly extended, a di-hydrogen molecule is almost formed whereas the C_2H_5 binds to the zeolite oxygen, O(2), which acts as a Lewis base. This is very similar to the methane reaction in the previous sections.

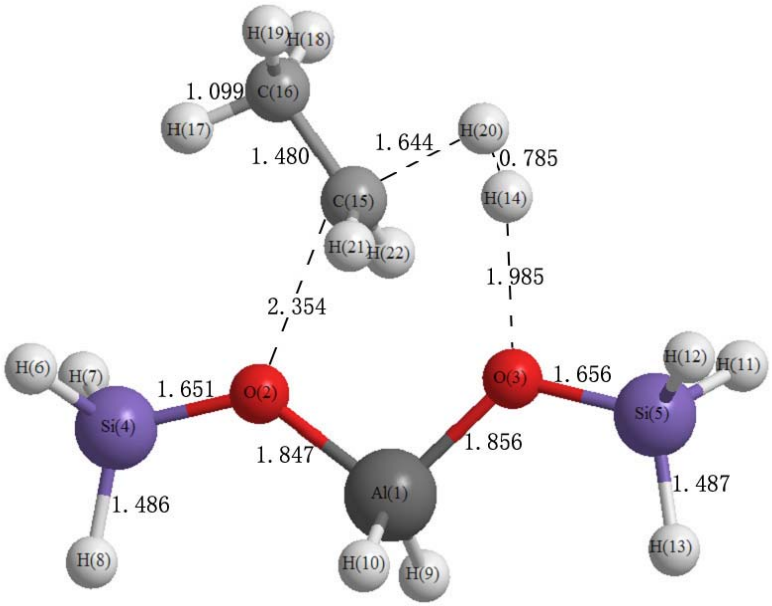

Figure 6-7(c). Transition state structure for the ethane dehydrogenation reaction on a T3 zeolite cluster (Units in Å)

The activation energies obtained from the MP2 geometry optimization with the CBS energy is 75.95 kcal/mol. This barrier is the highest among all three ethane conversion

reactions, indicating it is the most difficult reaction to take place. Compared with other researchers' work listed in Table 6-5, this result is higher than the result obtained by Blaszkowski *et al.* (Blaszkowski et al., 1996) using LDA density functional theory, and much less than the results obtained by Kazansky (Kazansky et al., 1996a; Kazansky et al., 1994b) using HF/3-21g//HF/3-21g and MP2/6-31++g**//HF/6-31g* calculations.

Zygmunt studied this reaction with a large T5 cluster. The result obtained B3LYP/6-31g*//B3LYP/6-311g** is 71.60 kcal/mol. Similar to the study of the ethane cracking reaction, the authors then included the long-range correction obtained by the HF/6-31g* correction for the 58T cluster model and reduced the activation energy to 53.6 kcal/mol.

6.2.5 The Effects of Geometry Optimization Methods

In this work, both HF and MP2 optimization methods combined with the same basis set, 6-31G*, were used to obtain the geometries of the reactants and transition states. The energies were then obtained by using the composite CBS method. As shown in Table 6-5, there is little difference between the activation energies obtained using these two different geometry optimization methods, with the maximum difference within 1 kcal/mol. The Hartree-Fock method, the most economical method in the *ab initio* family, is described by other researchers to fail in describing the motion of individual electrons, especially for the computation of hydrogen bonds and protonation (van Santen, 1997). However, this was not encountered in this work. Therefore, we find that the calculated activation energies depend greatly on the level of energy calculation method and depend less on the level of geometry optimization method. Using high level

calculations to obtain the activation energies through the CBS energy calculation method is crucial in this situation. Therefore, the geometry optimized using the HF method is adequate for activation barriers as long as the final energy is obtained using a high level method like CBS. Because of the low computational cost of the HF geometry optimization method, it is recommended for studying other zeolite catalytic reactions of large hydrocarbon species.

6.2.6 Cluster Size Effects

The choice of cluster to represent the zeolite surface plays a very important role in studying reaction properties. In this work, we investigated the effect of the cluster size for the ethane cracking reaction. The smallest cluster chosen is H-O-AlH_2-(OH)-H, a silicon-free T1 cluster.

The deprotonation energy (E_{dep}) of a cluster is a good indication of its chemical properties, and is defined as the energy difference between the protonated (ZH) and unprotonated (Z^-) clusters (Brand et al., 1993).

$$E_{dep} = E(Z^-) - E(ZH)$$

The deprotonation energy of this small T1 cluster, 318.26 kcal/mol, is much higher than the average zeolite value, 295.40 kcal/mol (Frash and van Santen, 1999; van Santen et al., 2001), which indicates a stronger bonding between the acidic hydrogen and its oxygen neighbor. Therefore, for small clusters, it takes more energy to break the H-O bond so the cracking reaction can take place, which means a higher activation barrier.

The activation energies of the reaction and the corresponding deprotonation energies of the clusters are listed in Table 6-6 together with those obtained using the larger T3 cluster--H_3Si-O-AlH_2-(OH)-SiH_3.

Table 6-6. Calculated activation energies for the ethane cracking reaction with different cluster sizes and the average zeolite catalyst (Units in kcal/mol)

	Deprotonation Energy	Activation Energy
$HOAlH_2(OH)H$	318.26	78.02
$H_3SiOAlH_2(OH)SiH_3$	298.02	71.39
Average Zeolite *	295.40	70.52

* - (Frash and van Santen, 1999; van Santen et al., 2001)

Since the clusters do not have exactly the same deprotonation energy as real zeolite catalysts, corrections can be made in order to obtain accurate activation energies. Applying the Brøsted-Polanyi principle, the following relationship can be used (van Santen and Kramer, 1995):

$$\Delta E_a = c\Delta E_{dep}$$

As long as the reaction mechanism does not alter, the change in activation energy is linearly correlated to the change in deprotonation energy.

Figure 6-8 is a plot of the activation energy change against deprotonation energy of the clusters. A linear extrapolation is made to extend the curve to the average real zeolite catalyst deprotonation energy point, 295.40 kcal/mol, and the activation energy obtained is 70.52 kcal/mol. The relationship can be described as:

$$\Delta E_a = 0.3279 E_{dep} - 104.37$$

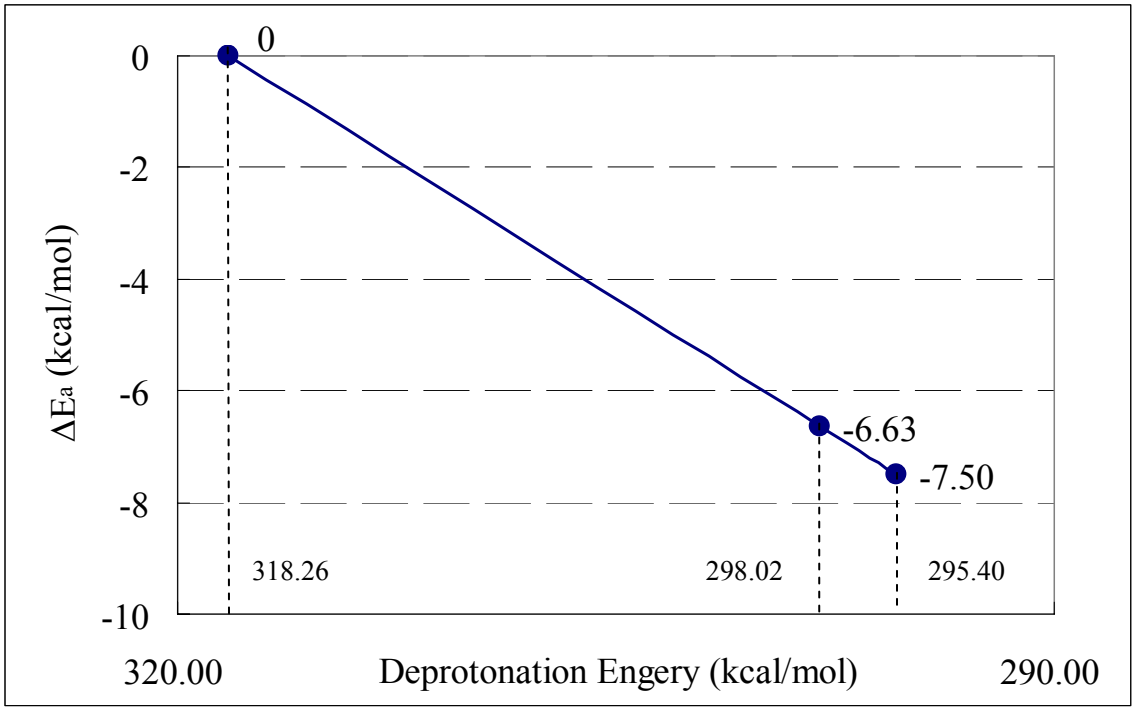

Figure 6-8. Corrections to the calculated ethane cracking reactions activation energies for the cluster effect

Kazansky *et al.* studied the cluster size effect of the cracking reaction using the smaller $HOAl(OH)_2(OH)H$ and larger $H_3SiOAlH_2(OH)SiH_3$ clusters (Frash and van Santen, 1999; Kazansky et al., 1996a). They reported the relationship between ΔE_a and E_{dep} to be: $\Delta E_a = 0.3213 E_{dep} - 102$. The slope is almost identical between the work of Kanzansky and this work, even though the energy calculation methods are very different (MP2 for Kanzansky and CBS for this work). The difference of the constant term is caused by the deprotonation energy difference between the $HOAl(OH)_2(OH)H$ cluster

used by Kanzansky and the $HOAlH_2(OH)H$ cluster used in this work. Therefore, the slope between the reaction activation energy and the cluster deprotonation energy is a constant that does not depend on the energy calculation method chosen, even while the deprotonation energy may depend on the method.

6.2.7 Acidity Effects

Figure 6-9 shows the effect of Si-H distance on the zeolite cluster geometries. With increases in the Si-H bond length, the neighbor Si-O bond length decreases. The O-H bond length increases slightly from 0.978Å to 0.982Å as the Si-H bond length changes from 1.30 Å to 1.70 Å. This indicates that the O-H bond becomes weaker with the increasing distance of the Si-H bond. Therefore, the zeolite cluster becomes more acidic. The Al-O and O-Si distances on the far end of the changing Si-H bonds vary almost negligibly because the atoms are too far away. Increasing the Si-H bond length on the left side of the cluster only has a slight effect on the O-H bond because the Si and H atoms are so far apart.

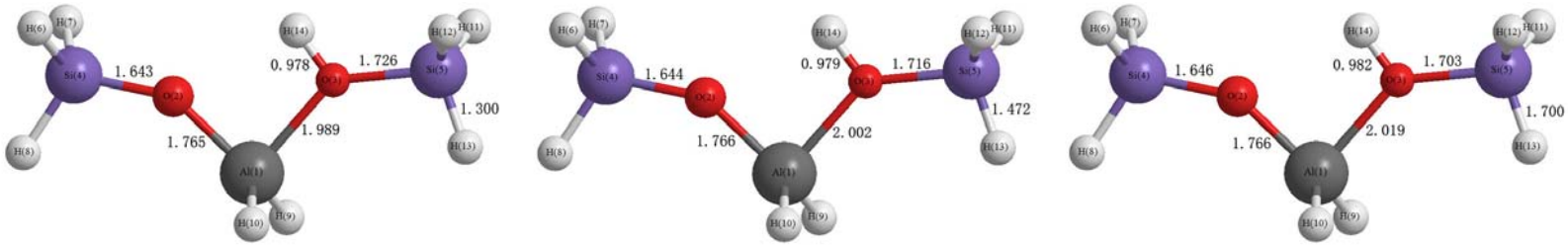

(a) R_{Si-H} = 1.3 Å (less acidic) (b) R_{Si-H} = 1.47 Å (Equilibrium) (c) R_{Si-H} = 1.7 Å (more acidic)

Figure 6-9. H_3Si-O-AlH_2-(OH)-SiH_3 cluster structures with changing terminal Si-H bond distances (Units in Å)

The changes of the zeolite acidity also affect the transition state structures and activation energies of the reactions. Figure 6-10 shows the transition state structures of the ethane cracking reaction as the Si-H distance changes. With the Si-H bond length increase, the CH_3 product moves closer to the cluster and the CH_4 product moves further from the cluster. Meanwhile, the CH_3 and CH_4 groups get closer to each other.

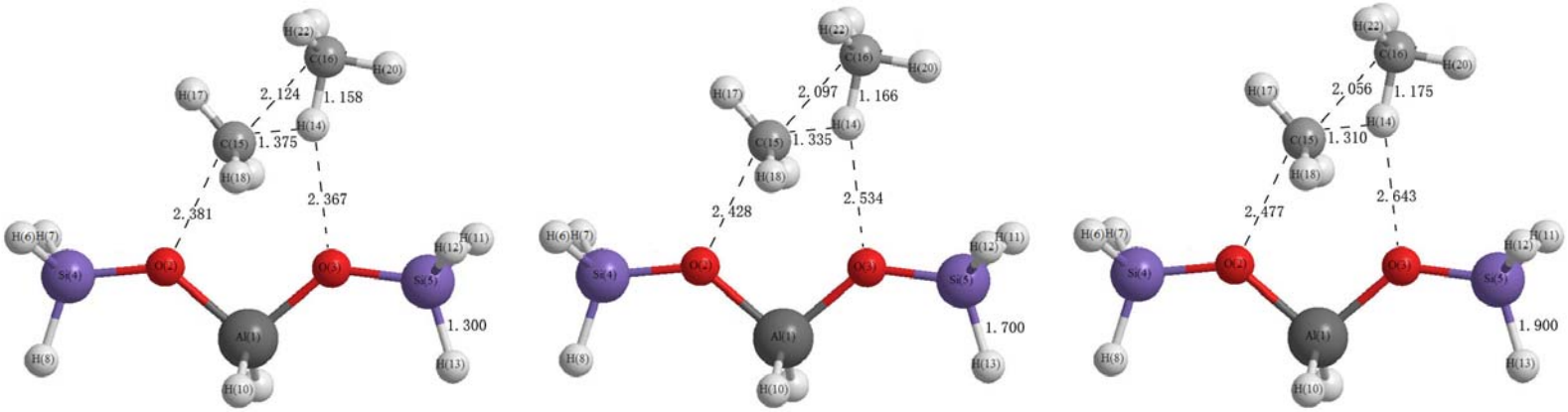

(a) R_{Si-H} = 1.3 Å (less acidic) (b) R_{Si-H} = 1.7 Å (more acidic) (c) R_{Si-H} = 1.9 Å (most acidic)

Figure 6-10. Transition state structures of the ethane cracking reaction with changing terminal Si-H bond distances (Units in Å)

Table 6-7 shows the change in activation energies as the Si-H bond distances for ethane cracking, dehydrogenation and hydrogen exchange reactions are varied. With the Si-H distance increasing, the activation energies decrease for all three reactions because of the increased acidity of the zeolite cluster. The relationship of the activation barriers with cluster deprotonation energies is illustrated in Figure 6-11. The linear dependence between these properties is seen, and the expressions are listed in Table 6-7. Applying the average zeolite catalyst deprotonation energy, 295.40 kcal/mol, the activation energies are then calculated and listed in Table 6-7. For the ethane cracking reaction, the activation barrier obtained is 69.08 kcal/mol using the expression $E_a = 0.7887E_{dep} - 163.90$. There is only a 1.50 kcal/mol difference with the results obtained from the cluster size effect correlation compared to the previous section 6.2.5, 70.52 kcal/mol. Because of the different types of zeolite catalysts used, the activation energies change slightly.

Table 6-7. Effects of Si-H distances on activation energies (Units in kcal/mol)

	Activation Energy (E_a)			Deprotonation Energy (E_{dep})
	Cracking	Dehydrogenation	Hydrogen Exchange	
R_{Si-H} = 1.30Å	75.74	79.52	33.64	303.97
R_{Si-H} = 1.47Å	71.39	75.95	31.39	298.02
R_{Si-H} = 1.70Å	66.12	71.71	28.70	291.76
R_{Si-H} = 1.90Å	62.03	68.16	26.63	286.44
Average Zeolite *	69.08	74.04	30.23	295.4
Empirical Correlation	$E_a = 0.7887E_{dep} - 163.90$	$E_a = 0.6509E_{dep} - 118.23$	$E_a = 0.403E_{dep} - 88.82$	

* - (Frash and van Santen, 1999; van Santen et al., 2001)

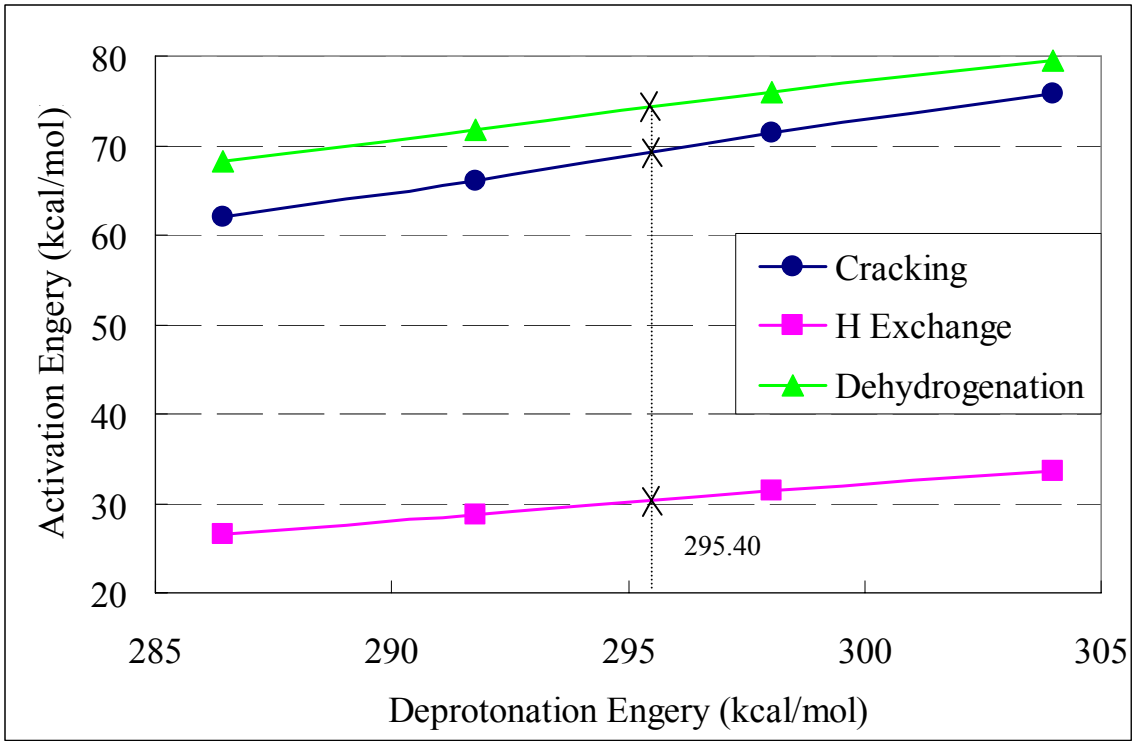

Figure 6-11. Corrections to the calculated ethane conversion reactions activation energies for the acidity effect

The acidity effect study has shown that there is a correlation between the deprotonation energy and activation energy for ethane conversion reactions. This is important because deprotonation energies are significantly easier to calculate than activation energies due to the difficulty in performing transition state optimizations for large complexes with many degrees of freedom. One correlation showed that the deprotonation energy can be varied by varying the cluster size, allowing one to now predict how ethane conversion reaction results may be extrapolated to larger cluster sizes. The second correlation showed how one could vary peripheral bonds on the cluster to change the deprotonation energy and influence the activation energy. Applying the

expressions, activation energies can be obtained for different zeolite catalysts as long as the experimental deprotonation energy is first acquired.

6.3 Propane Reactions

6.3.1 Computational Methods

All the calculations in this section were performed with the GAUSSIAN98 software package (Frisch et al., 1998), and all structures were obtained with Becke's three-parameter density functional (Becke, 1993) and the Lee, Yang, and Parr functional (Lee et al., 1988), the well-known B3LYP method, with a moderate 6-31G* basis set. The energies were obtained with CBS-QB3, a high-level complete basis set composite energy method (Montgomery et al., 1999). The products and reactants were verified with frequency calculations to be stable structures, and the transition states were tested to ensure they were first order saddle points with only one negative eigenvalue. Additionally, intrinsic reaction coordinate (IRC) calculations (Gonzalez and Schlegel, 1989) proved that each transition state linked the correct products with reactants. Zero point vibrational energies (ZPVE) were obtained from harmonic vibrational frequencies calculated at the B3LYP/6-31g* level with a scaling factor of 0.9806 (Scott and Radom, 1996).

6.3.2 Protolytic Cracking Reaction

$$CH_3CH_2CH_3 + H_3SiOAlH_2(OH)SiH_3 \rightarrow CH_4 + H_3Si(OC_2H_5)AlH_2OSiH_3$$

The protolytic cracking reaction consists of the C-C bond cleavage of propane by the zeolite Brønsted acid proton. The calculated transition state structure (TS1) using the B3LYP/6-31G* method is shown in Figure 6-12(a). This reaction is found to be similar to the protolytic cracking of ethane (Zheng and Blowers, 2005a) since it starts with a proton attaching to the C-C bond of propane. The acidic proton, H(14), attaches to the methyl group of the propane reactant, C(16), to form methane and a surface alkoxide product. In the transition state structure, the acidic proton has been transferred to carbon C(16), and a methane molecule is almost formed. The left ethyl group of propane becomes a carbenium ion, $C_2H_5^+$ with a Mulliken charge of 0.51, and is bonded to the zeolite cluster. In the transition state structure, the C(15)-C(16) structure stays in the same plane as the zeolite O(2)-Al(1)-O(3) plane and the C(15)-C(17) structure is perpendicular to the main zeolite cluster plane.

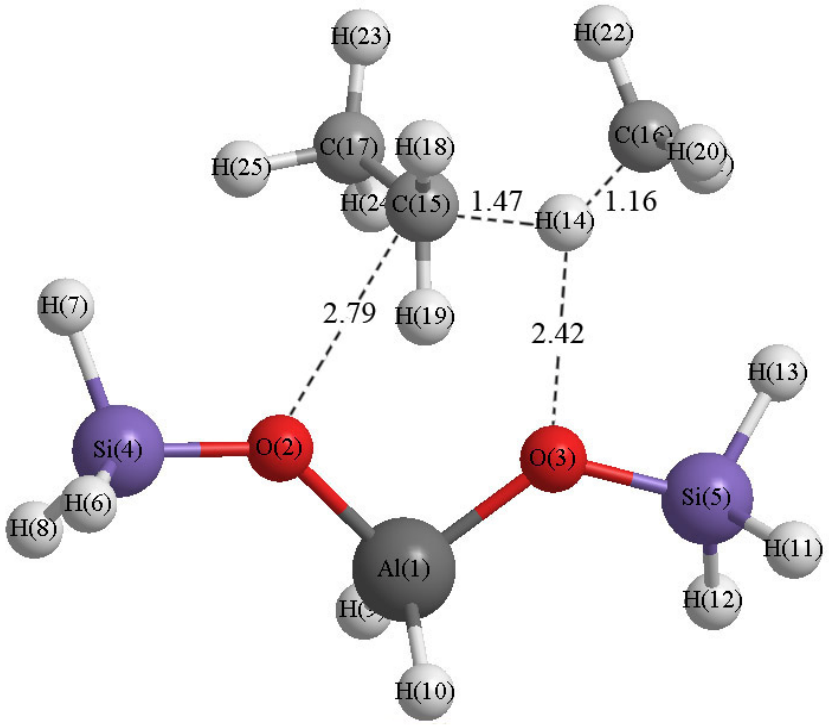

Figure 6-12(a). Transition state structure (TS1) for the propane protolytic cracking reaction on a T3 zeolite cluster (Units in Å)

The zeolite cluster plays an important role in this reaction. The right oxygen of the cluster, O(3), acts as a Brønsted acid which donates a proton, while the left oxygen, O(2), acts as a Lewis base which receives the ethyl group, demonstrating the bi-functional Brønsted acidic-Lewis basic nature of the zeolite catalyst.

The protolytic cracking reaction of propane is nearly thermo-neutral with an activation barrier of 62.1 kcal/mol calculated with the CBS-QB3 method. The activation barrier obtained in this work is compared with the computational results from Rigby *et al*. in Table 6-8.

Table 6-8. Activation barrier calculation results for propane conversion reactions on zeolites using the CBS method (Units in kcal/mol)

	Computational Results					Experiment		
	This Work	Rigby [a]	Furtado [b]	Esteves [c]	Ryder [d]	Narbeshuber [e]		Stepanov [f]
Cluster Model/Catalyst Type	T3	T3	T5	T3	T5	H-ZSM-5	HY-M	H-ZSM-5
Geometry Opt. Method	B3LYP /6-31G*	HF /3-21G	B3LYP /6-311G**	B3LYP /6-31G**	BH&HLYP /6-31++G**			
Energy Calculation Method	CBS-QB3	MP2 /6-31G*	B3LYP /6-311G**	B3LYP /6-31G**	BH&HLYP /6-31++G**			
Cracking	(62.1/62.6)*	68.0	-	-	-	37.1	39.5	-
Primary H-Exchange	30.4	-	-	32.2	40.5	-	-	25.8±1.7
Secondary H-Exchange	29.8	-	-	33.3	39.2	-	-	28.0±1.7
Dehydrogenation	76.7	-	73.0	-	-	22.7	15.6	-

a – (Rigby et al., 1997)

b – (Furtado et al., 2001)

c – (Esteves et al., 1999)

d – (Ryder et al., 2000)

e – (Narbeshuber et al., 1997; Narbeshuber et al., 1995)

f – (Stepanov et al., 1998)

The barrier obtained by Rigby using MP2/6-21G*//HF/3-21G (energy calculation method//geometry optimization method), 68.0 kcal/mol (Kazansky et al., 1994b), is much higher than the experimental result because MP2 energy calculations tend to overestimate barrier heights (Lee and Masel, 1995; Lee and Masel, 1996; Willis and Jensen, 1998; Yamataka et al., 1986). The experimental activation energies for the propane cracking reactions were reported to be 37.1 kcal/mol for the H-ZSM-5 zeolite and 39.5 kcal/mol for HY-M (Narbeshuber et al., 1997; Narbeshuber et al., 1995). Our calculated activation barrier is also higher than the experimental value. The difference could be caused by the fact that the T3 cluster applied in this work is only a partial representation of the zeolite catalyst which does not include long range interactions. Interestingly, Zygmunt recently studied the ethane protolytic cracking reaction with a T5 cluster (Zygmunt et al., 2000). The result obtained with MP2(fc)/6-31G*//MP2(fc)/6-31G* is even higher, 73.70 kcal/mol. The long-range correction obtained by the HF/6-31G* calculation for a 58T cluster model reduces the activation barrier by 14.50 kcal/mol. For the same scenario, long-range corrections could also lower our calculated barrier height and bring it much closer to the experimental value. The other reason for the high activation barrier obtained could be the moderate basis set 6-31G* used in the geometry optimization which will be tested in section 6.3.5 of this thesis. Moreover, the zeolite acidic effects could also reduce our calculated activation barrier by 2 kcal/mol, which will be discussed in Section 6.3.6.

We found another transition state (TS2) for the protolytic reaction and it is depicted in Figure 6-12(b). In this transition state, the C(17)-C(15)-C(16) plane becomes

perpendicular to the main zeolite cluster plane O(2)-Al(1)-O(3). Considering the cluster is only one part of the zeolite pore, this transition state structure represents the case where the propane molecule is perpendicular to the plane of the zeolite pores. This mechanism becomes more important when the reactant molecules become larger. For zeolites with small to medium pores, like ZSM-5, which is broadly used for hydrocarbon cracking, the reactant molecule becomes comparable to the zeolite pore diameter for those species larger than propane. They become too large to pass parallelly through the pores. As a result, the reaction can only take place when the reactant molecules are perpendicular to the zeolite pores. In other words, starting with n-butane as a reactant, the perpendicular transition state is the only reaction pathway for the protolytic cracking reaction.

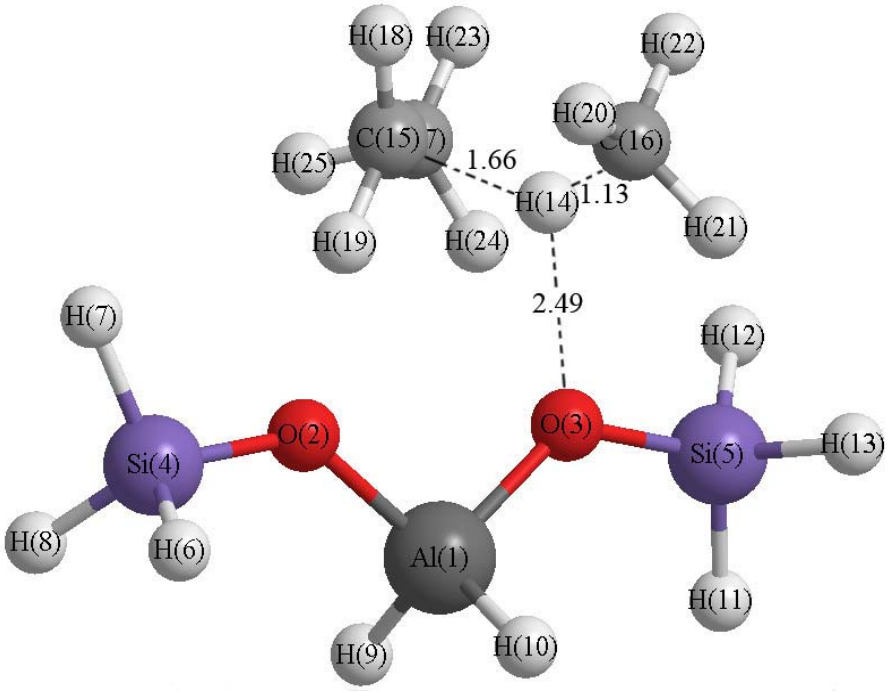

Figure 6-12(b). Transition state structure (TS2) for the propane protolytic cracking reaction on a T3 zeolite cluster (Units in Å)

The activation barrier of this protolytic cracking pathway is 62.6 kcal/mol calculated with the CBS-QB3 method. The barrier is similar to that of TS1, 62.1 kcal/mol, which indicates that the two competitive reaction pathways are comparable. Again, this activation barrier is higher than that obtained by the experiment (Narbeshuber et al., 1997).

6.3.3 Hydrogen Exchange Reactions

$CH_3CH_2\underline{C}H_3 + H_3SiOAlH_2(OH')SiH_3 \rightarrow CH_3CH_2\underline{C}H_2H' + H_3Si(OH)AlH_2OSiH_3$

$CH_3\underline{C}H_2CH_3 + H_3SiOAlH_2(OH')SiH_3 \rightarrow CH_3\underline{C}HH'CH_3 + H_3Si(OH)AlH_2OSiH_3$

The propane hydrogen exchange reaction can take place at either the primary carbon or the secondary carbon shown in the above reaction scheme. The underlined carbon atom indicates the place where hydrogen exchange takes place. The propane hydrogen exchange reactions were previously studied by this group (Zheng and Blowers, 2005b) and are briefly discussed here for completeness of this work. Figure 6-12(c) shows the calculated transition state structure for the primary hydrogen exchange reaction of propane using the B3LYP/6-31G* method. The structure clearly shows the C_s symmetry obtained without any symmetry constraints applied for the geometry optimization step. The carbon in the main plane of the zeolite structure, C(15), is protonated and becomes a penta-coordinated structure. The exchanging hydrogen atom from propane, H(19), and the acidic proton, H(14), stay in the middle of the carbon and two oxygen atoms, indicating formation of one C-H bond and breaking of the other.

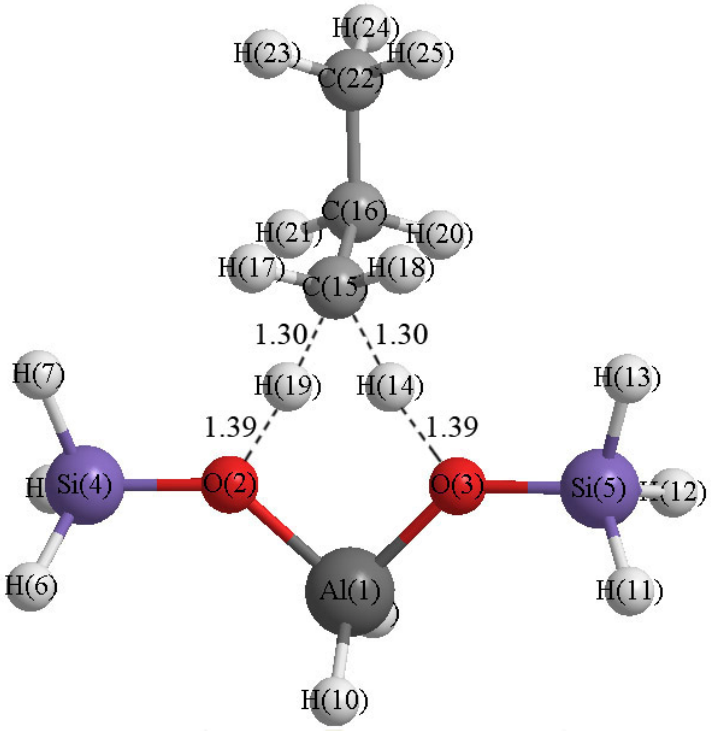

Figure 6-12(c). Transition state structure for the propane primary hydrogen exchange reaction on a T3 zeolite cluster (Units in Å)

The activation barrier obtained with the CBS-QB3 method is 30.4 kcal/mol. In Table 6-8, this activation barrier is compared with previous computational results from Esteves (Esteves et al., 1999) and Ryder (Ryder et al., 2000). The activation barrier obtained in this work is relatively lower than the calculated results from Esteves and Ryder which are 32.2 kcal/mol and 40.5 kcal/mol, respectively. The experimental activation energy reported by Stepanov *et al.* is 25.8 ± 1.7 kcal/mol (Stepanov et al., 1998). Our calculation is only 3 kcal/mol higher than the maximum experimental data and is much closer to experiment than those from Esteves and Ryder. This again

indicates our methodology is correct and able to reproduce experiment compared to previous work.

The calculated transition state structure for the propane secondary hydrogen exchange reaction with the B3LYP method is shown in Figure 6-12(d). The propane structure tilts to the right side of the zeolite cluster and pushes the acidic proton, H(14), further away from the C(15) atom. As a result, the C(15)-H(14) distance is slightly larger than the C(15)-H(19) distance, while the distance of H(14)-O(3) is slightly less than that of H(19)-O(2).

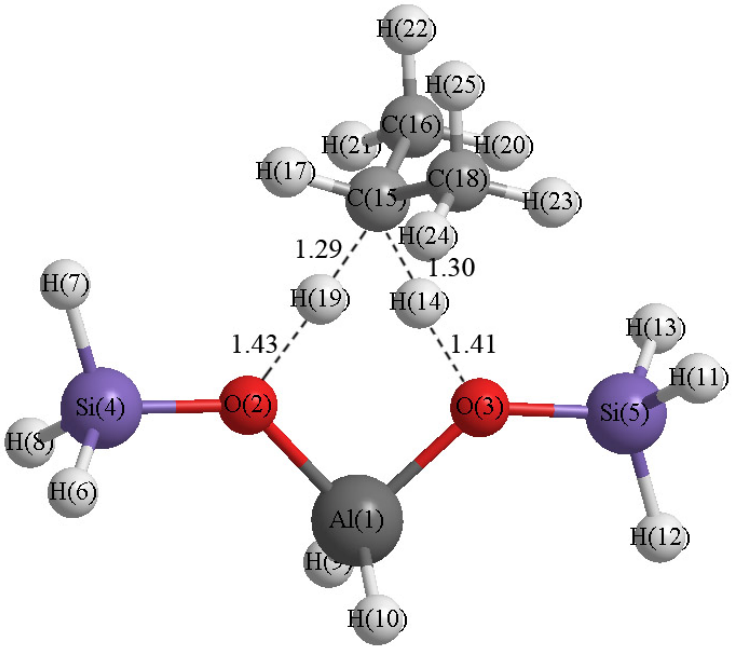

Figure 6-12(d). Transition state structure for the propane secondary hydrogen exchange reaction on a T3 zeolite cluster (Units in Å)

The activation barrier obtained with the CBS-QB3 method is 29.8 kcal/mol, which is very similar to the activation barrier for the primary hydrogen exchange reaction. The

result is again much lower than the calculated results from Esteves and Ryder which are 33.3 kcal/mol and 39.2 kcal/mol as listed in Table 6-8. Compared with the experimental activation energy of 28.0 ± 1.7 kcal/mol (Stepanov et al., 1998), our calculated result falls within the experimental error range.

Our calculated results show that the activation barrier of secondary carbon hydrogen exchange reaction is close to, but relatively lower than that of primary carbon. This trend is the same as that obtained by Ryder (Ryder et al., 2000), but contradictory to the experimental results of Stepanov (Stepanov et al., 1998). Since the experimental activation energy of primary and secondary exchange reactions only differs by 2.2 kcal/mol, the relative magnitude of these two activation energies could be reversed, considering the experimental error range is as large as ±1.7 kcal/mol for each reaction.

6.3.4 Dehydrogenation Reaction

$CH_3CH_2CH_3 + H_3SiOAlH_2(OH)SiH_3 \rightarrow H_2 + H_3Si(OC_3H_7)AlH_2OSiH_3$

The dehydrogenation reaction consists of cleavage of a C-H bond by the zeolite Brønsted acid proton. The transition state structure of the propane dehydrogenation reaction is shown in Figure 6-12(e). The carbon C(15) structure becomes almost planar and the other two carbons keep the tetrahedral structure. A six-member ring, O(2)-Al(1)-O(3)-H(14)-H(20)-C(15), is formed. With the H(20)-C(15) and H(14)-O(3) distances greatly extended to 1.81 Å and 1.82 Å, a di-hydrogen molecule, H(14)H(20), is almost formed, whereas the C_3H_7 fragment binds to the zeolite oxygen, O(2), which acts as a Lewis base.

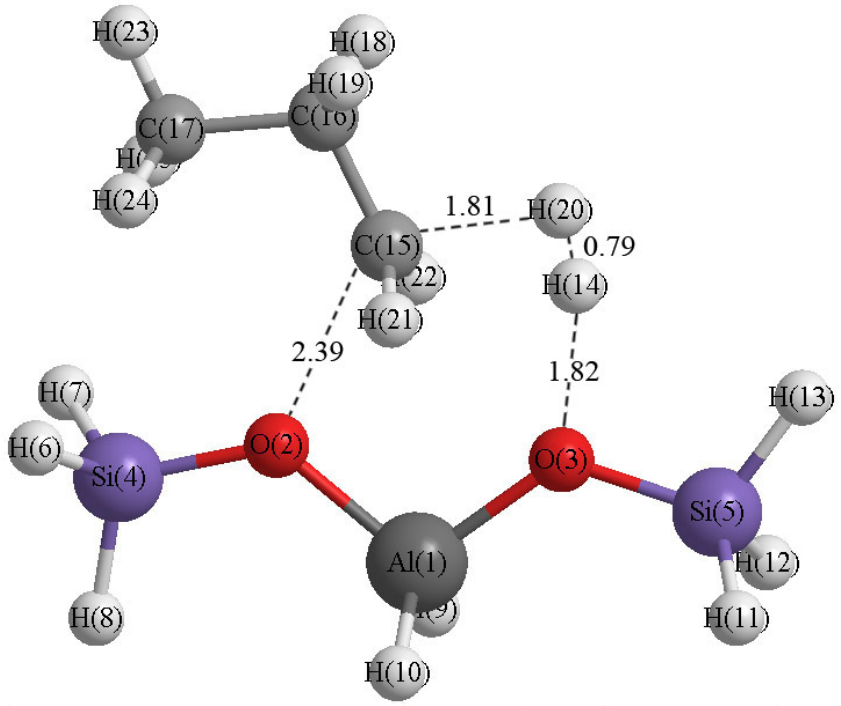

Figure 6-12(e). Transition state structure for the propane dehydrogenation reaction on a T3 zeolite cluster (Units in Å)

The activation barrier obtained with the CBS-QB3 method is 76.7 kcal/mol. This barrier is the highest among all of the propane conversion reactions, indicating it is the most difficult reaction to take place. Our result is 3.7 kcal/mol higher than the result obtained by Furtado *et al.* (Furtado et al., 2001) using B3LYP/6-311G**//B3LYP/6-31G**. However, B3LYP energy calculation methods have been well known for underestimation of activation barriers (Goldstein et al., 1998; Lynch and Truhlar, 2001; Truong, 2000; van Santen et al., 2001). The experimental study from Narbeshuber *et al.* reported activation energies of 22.7 kcal/mol and 15.5 kcal/mol for H-ZSM-5 and H-Y zeolites(Narbeshuber et al., 1997). It seems clear that the computational results are too high compared to these experimental values, which is

similar to the propane cracking reaction from Section 6.3.2. This discrepancy could be attributed to the relatively small cluster size and basis set choice for the optimization method. Furtado increased the cluster size to T5 and used a larger basis set to refine their results. However, the activation barriers obtained increased by 3 kcal/mol, which could eliminate the doubt of the choice of the cluster size and basis set.

Interestingly, Kanzansky found another two-step reaction pathway for the iso-butane dehydrogenation reaction.(Kazansky et al., 1996a) But the activation barrier obtained in their work was similar to that of the single-step pathway, which is still much higher than the experimental data. However, from previous experimental studies, the overall heat of reaction for the gas phase dehydrogenation reaction $C_3H_8 \rightarrow C_3H_6 + H_2$ is known to be about 30 kcal/mol, which is difficult to reconcile with the reported experimental barriers.(Curtiss and Gordon, 2004) Certainly, some discrepancy is caused by the failure of density functional theory to account for van der Waals interactions. But it is also possible that the experimental value is too low considering the gas phase heat of reaction value.

6.3.5 Basis Set Effects

In the investigation of propane reactions, the moderate 6-31G* basis set used in the geometry optimizations may seem inadequate. Therefore, the influence of the basis set on the activation barriers was investigated by increasing the basis set from 6-31G* to 6-31G** and 6-31++G** for the geometry optimization. The energies were then obtained using the composite CBS-QB3 method. As shown in Table 6-9, there is little difference between the activation barriers obtained using these three basis sets for the

propane reactions. The largest difference is for the dehydrogenation reaction where the activation barrier is reduced by less than 1 kcal/mol. Therefore, the diffuse and polarization functions added in the geometry optimization do not obtain better activation barriers with higher level calculated energies. This proves that the calculated activation barriers depend greatly on the level of the energy calculation method and depend less on the level of the geometry optimization method (Frash and van Santen, 1999; Zheng and Blowers, 2005a). Using high level calculations to obtain the activation barriers through the CBS-QB3 method is crucial in this situation. Therefore, the geometry optimized using the 6-31G* basis set is adequate for activation barriers as long as the final energy is obtained using a high level method like CBS-QB3.

Table 6-9. Calculated activation barriers for the propane protolytic cracking reaction with different basis sets used for the geometry optimization

Geometry Opt. Method	Cracking (TS1)	Cracking (TS2)	Primary H-Exchange	Secondary H-Exchange	Dehydrogenation
B3LYP/6-31G*	62.1	62.6	30.4	29.8	76.7
B3LYP/6-31G**	62.1	62.6	30.5	29.9	76.1
B3LYP/6-31++G**	62.3	62.6	30.6	30.1	75.8

6.3.6 Acidity Effects

Similar acidity effect studies as the methane and ethane reactions in previous sections are carried out here. Figure 6-13 shows the transition state structures of the propane protolytic cracking reaction as the Si-H distance changes from 1.3 Å to 1.9 Å. With a Si-H bond length increase, the distance of the protonic hydrogen and acidic oxygen, H(14)-O(3), increases from 2.36 Å to 2.55 Å. Similarly, the distance between the carbon atom and Lewis basic oxygen, C(15)-O(2), increases from 2.78 Å to 2.81 Å. The C_3H_9 group moves further away from the cluster while the two cracking carbon atoms, C(15) and C(16), move closer. Additionally, the oxygen and silicon distance, O(3)-Si(5), shrinks as the cluster acidity increases, indicating a stronger O-Si bond, which in turn causes a weak oxygen bond to the acidic proton.

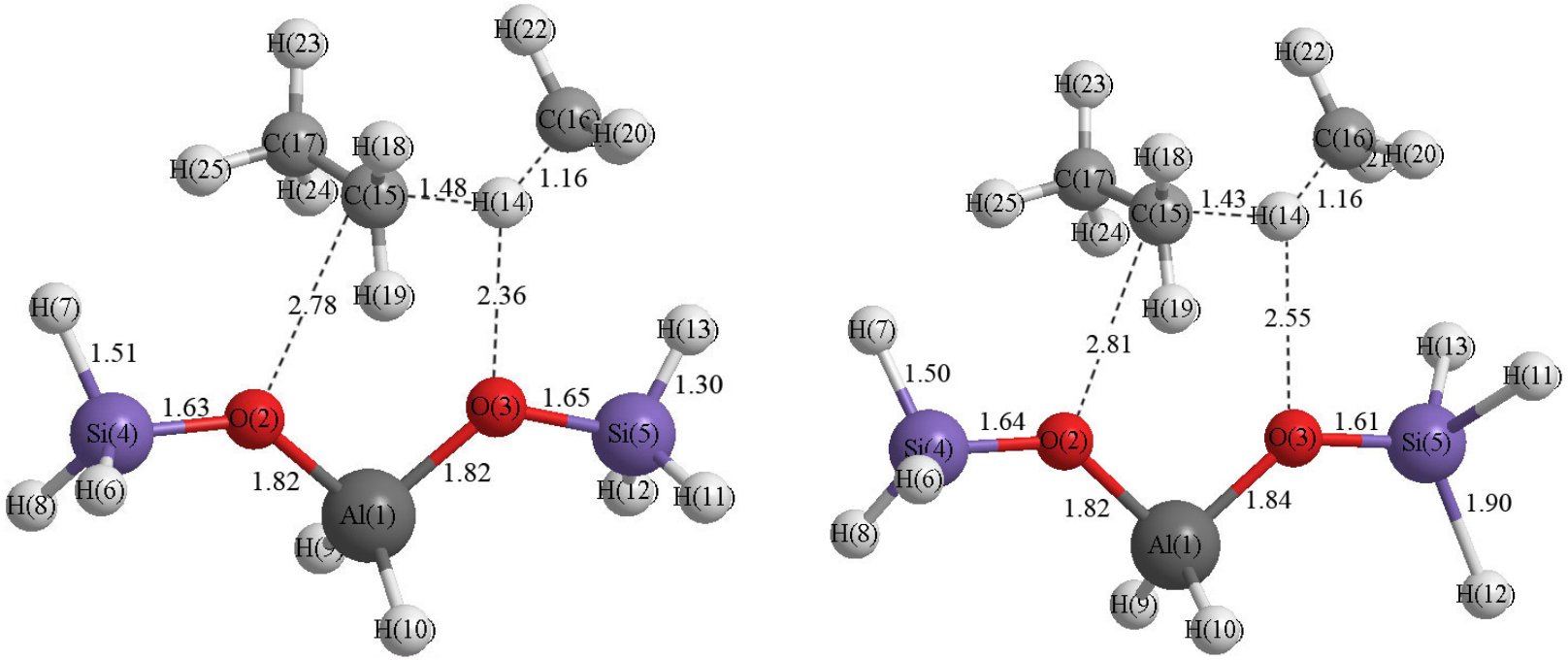

(a) R_{Si-H} = 1.3 Å (less acidic)

(b) R_{Si-H} = 1.9 Å (more acidic)

Figure 6-13. Transition state structures of propane cracking reaction with changing terminal Si-H bond distances (Units in Å)

Similar acidic effects were studied and applied to propane primary and secondary hydrogen exchange reactions shown in Figure 6-14 and 6-15. As the cluster acidity increases, the acidic hydrogen and oxygen distance, H(14)-O(3), increases. Meanwhile, the C_3H_9 structure moves away from the zeolite cluster, which is similar to protolytic cracking reaction. However, a transition state cannot be located for the propane dehydrogenation reaction as the Si-H distance increases to 1.9 Å. The transition state structures of the propane dehydrogenation reaction as the Si-H distance changes to 1.3 Å and 1.7 Å are shown in Figure 6-16. As the Si-H distance increases, the distance of the carbon atom and Lewis basic oxygen, C(15)-O(2), increases from 2.36 Å to 2.43 Å and the distance of protonic hydrogen and acidic oxygen, H(14)-O(3) increases from 1.76 Å to 1.90 Å. Meanwhile, the bi-hydrogen atoms, H(14) and H(20), move closer to each other, becoming more like the structure of a hydrogen molecule, and the entire C_3H_9 group moves farther away from the cluster.

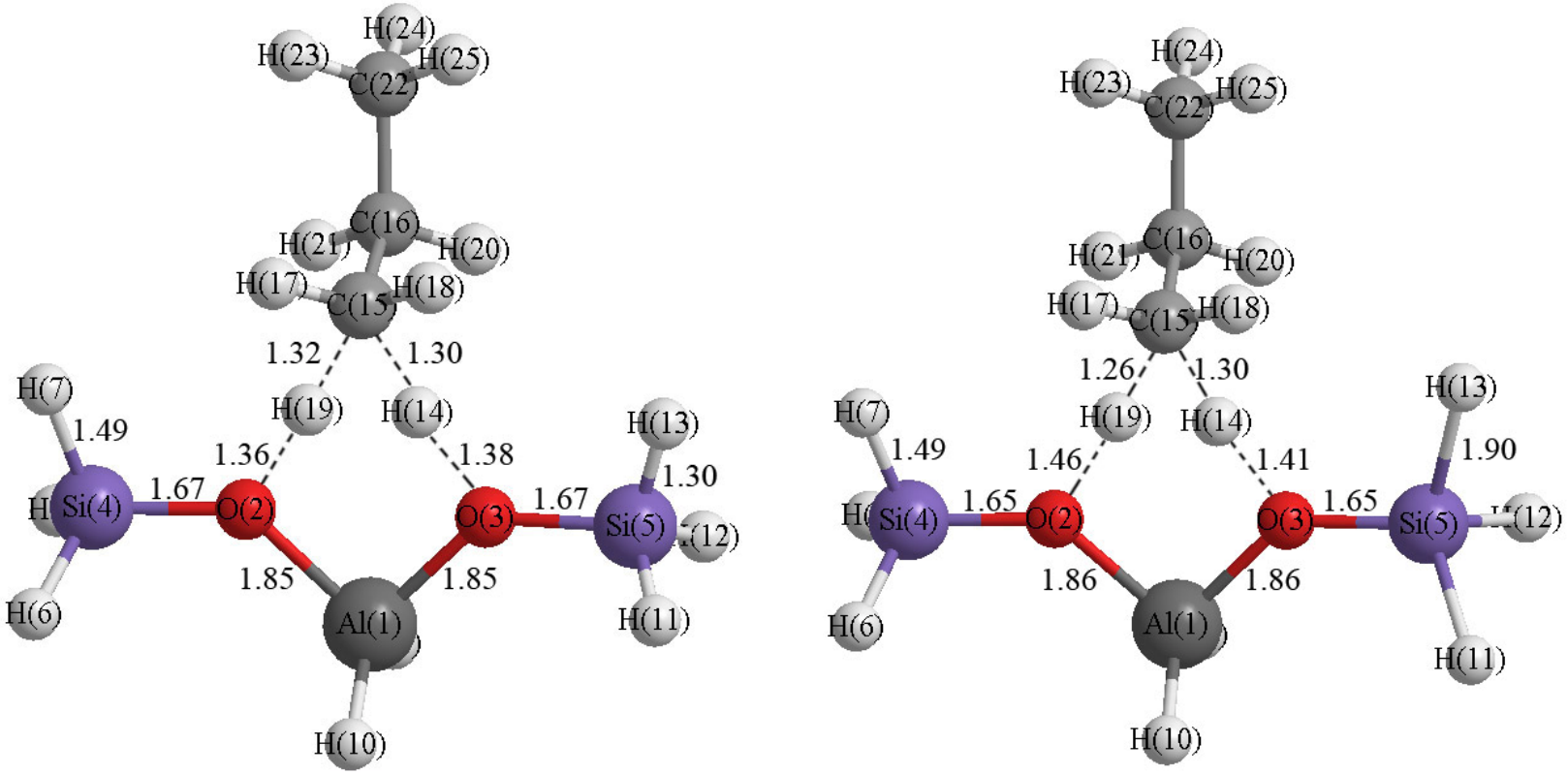

(a) R_{Si-H} = 1.3 Å (less acidic)

(b) R_{Si-H} = 1.9 Å (more acidic)

Figure 6-14. Transition state structures of propane primary hydrogen exchange reaction with changing terminal Si-H bond distances (Units in Å)

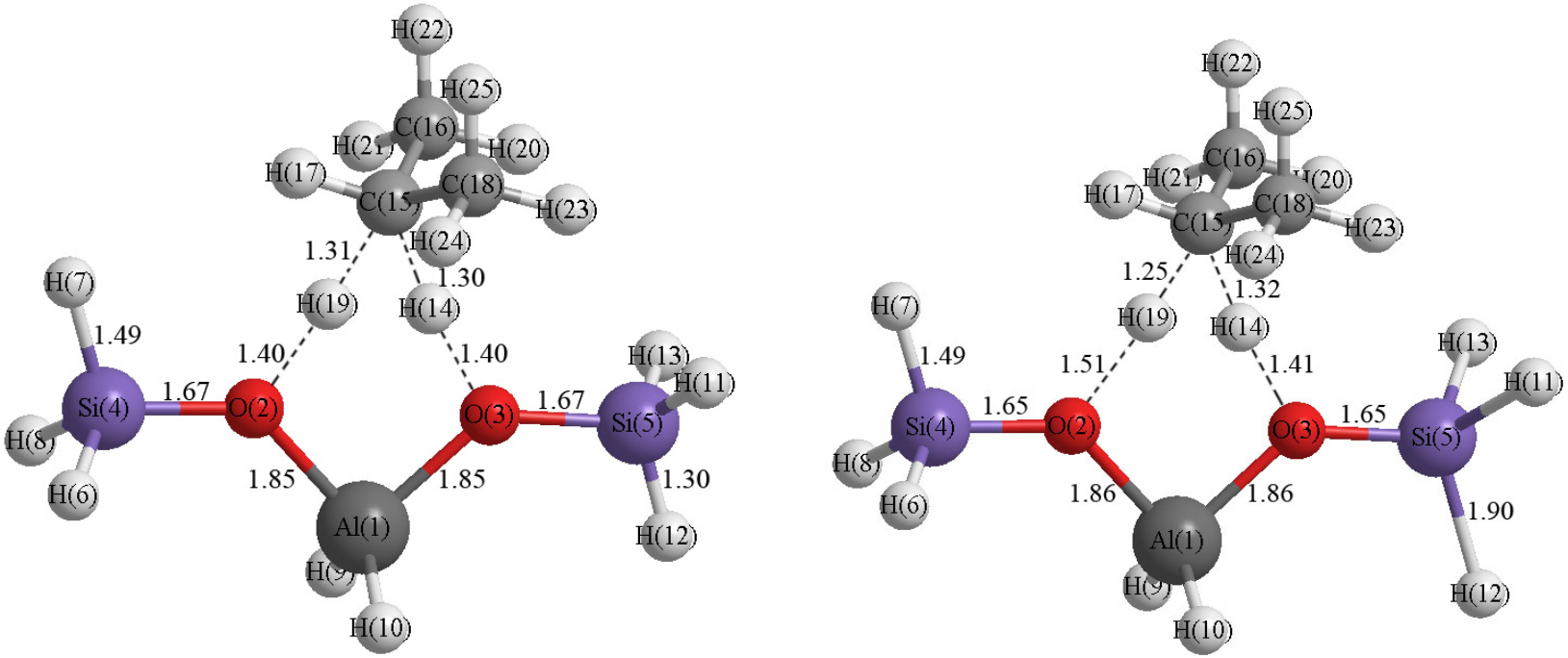

(a) R_{Si-H} = 1.3 Å (less acidic)

(b) R_{Si-H} = 1.9 Å (more acidic)

Figure 6-15. Transition state structures of propane secondary hydrogen exchange reaction with changing terminal Si-H bond distances (Units in Å)

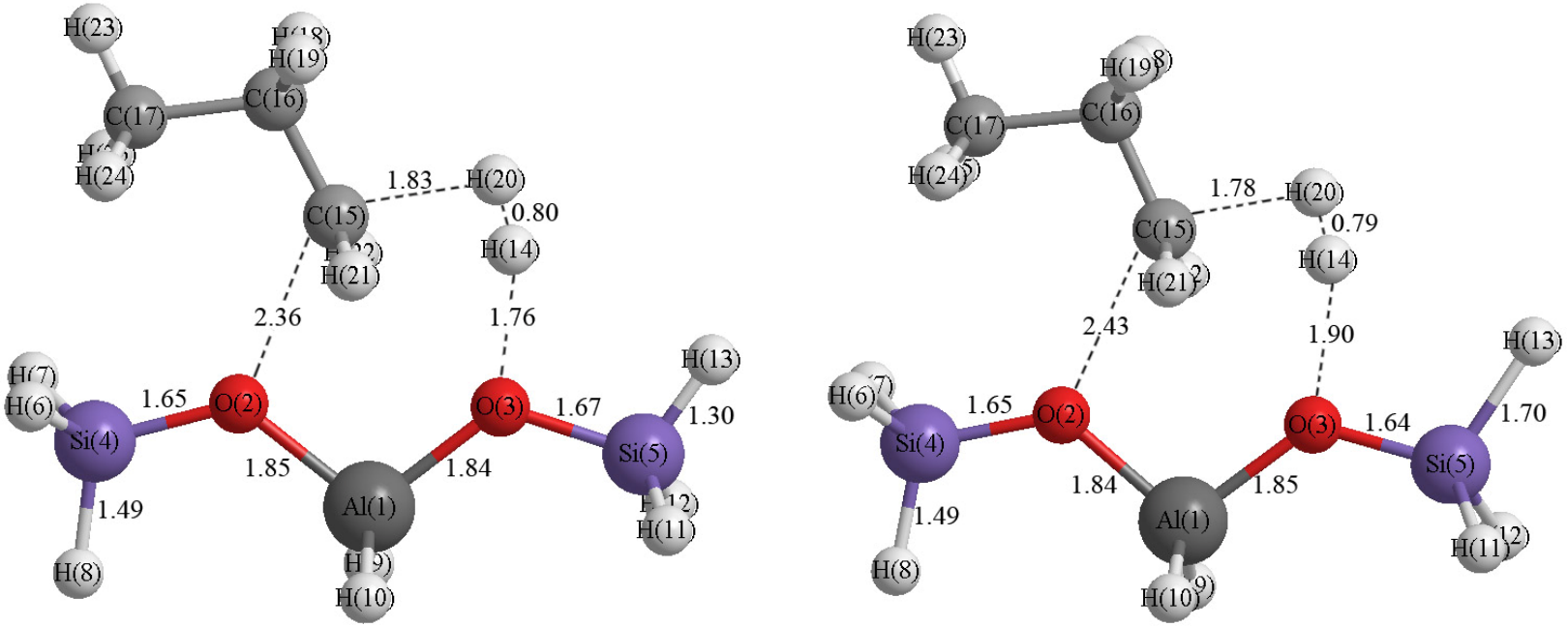

(a) R_{Si-H} = 1.3 Å (less acidic)

(b) R_{Si-H} = 1.7 Å (more acidic)

Figure 6-16. Transition state structures of propane dehydrogenation reaction with changing terminal Si-H bond distances (Units in Å)

Table 6-10 summarizes the change in activation barriers for propane protolytic cracking, primary, secondary hydrogen exchange, and dehydrogenation reactions as the Si-H bond distances are varied. With the Si-H distance increasing, the activation barriers decrease for all four reactions because of the increased acidity of the zeolite cluster. As long as the reaction mechanism does not alter, the change in activation barrier is linearly correlated to the change in zeolite cluster deprotonation energy. Therefore, the Brønsted-Polanyi principle can be applied (van Santen and Kramer, 1995):

$$\Delta E_a = c\Delta E_{dep} \quad \text{or} \quad E_a = c\Delta E_{dep} + b$$

Table 6-10. Effects of Si-H distances on activation barriers (Units in kcal/mol)

	Activation Barrier (E_a)				Deprotonation Energy (E_{dep})
	Protolytic Cracking	Primary H-Exchange	Secondary H-Exchange	Dehydrogenation	
R_{Si-H} = 1.30Å	66.1	32.8	32.2	80.5	304.0
R_{Si-H} = 1.47Å	62.1	30.4	29.8	76.7	297.9
R_{Si-H} = 1.70Å	57.3	27.7	27.0	72.0	291.6
R_{Si-H} = 1.90Å	53.4	25.6	24.9	N/A	285.8
H-ZSM-5 Zeolite	60.1	29.4	28.7	74.7	295.4
Expression	$E_a = 0.708E_{dep} - 148.9$	$E_a = 0.396E_{dep} - 87.6$	$E_a = 0.405E_{dep} - 90.8$	$E_a = 0.686E_{dep} - 127.9$	

The linear relationship of the activation barriers with cluster deprotonation energies is illustrated in Figure 6-17. Applying the H-ZSM-5 zeolite catalyst deprotonation energy, 295.4 kcal/mol (Sauer and Sierka, 2000), the activation barriers are then calculated and listed in Table 3. For the propane protolytic cracking reaction, the activation barrier obtained is 60.1 kcal/mol using the expression $E_a = 0.708E_{dep} - 148.9$. Therefore, with the acidity effect correction, the barrier height is reduced by 2.0 kcal/mol. Similarly, the barrier heights were lowered by 1.0 kcal/mol, 1.1 kcal/mol, and 2.0 kcal/mol for primary hydrogen exchange, secondary hydrogen exchange, and dehydrogenation reactions, respectively, which brings our computational results even closer to the experimental results.

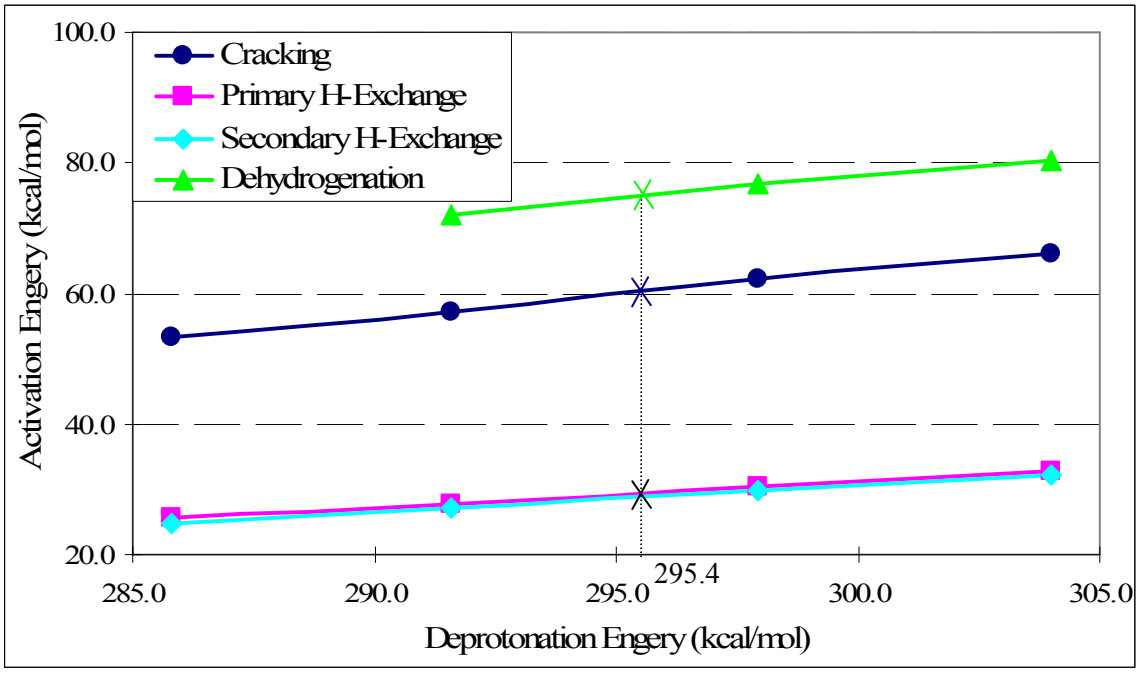

Figure 6-17. Corrections for the calculated propane conversion reactions activation barriers for the acidity effect

6.4 *Iso*-butane Reactions

6.4.1 Computational Methods

All of the calculations in this section were performed with the GAUSSIAN98 software package (Frisch et al., 1995). The geometries were optimized at the B3LYP/6-31G* level and the energies were obtained using CBS-QB3 (Montgomery et al., 1999), a complete basis set composite energy method. All products and reactants were verified with frequency calculations to be stable structures and all transition states were found to be first order saddle points with only one negative eigenvalue. Additionally, intrinsic reaction coordinate (IRC) calculations showed that each reaction linked the correct products with reactants. Zero point vibrational energies (ZPVE) were obtained from harmonic vibrational frequencies calculated at the B3LYP/6-31G* level with a scaling factor of 0.9806 (Scott and Radom, 1996).

6.4.2 Protolytic Cracking Reaction

$CH_3CH(CH_3)_2 + H_3SiOAlH_2(OH)SiH_3 \rightarrow CH_4 + H_3Si(OC_3H_7)AlH_2OSiH_3$

The *iso*-butane protolytic cracking reaction consists of the carbon-carbon bond cleavage of *iso*-butane by the zeolite Brønsted acid proton, leading to the formation of methane and a surface *sec*-propyl alkoxide products as shown in the reaction scheme above. The calculated transition state structure using the B3LYP/6-31G* method is shown in Figure 6-18(a).

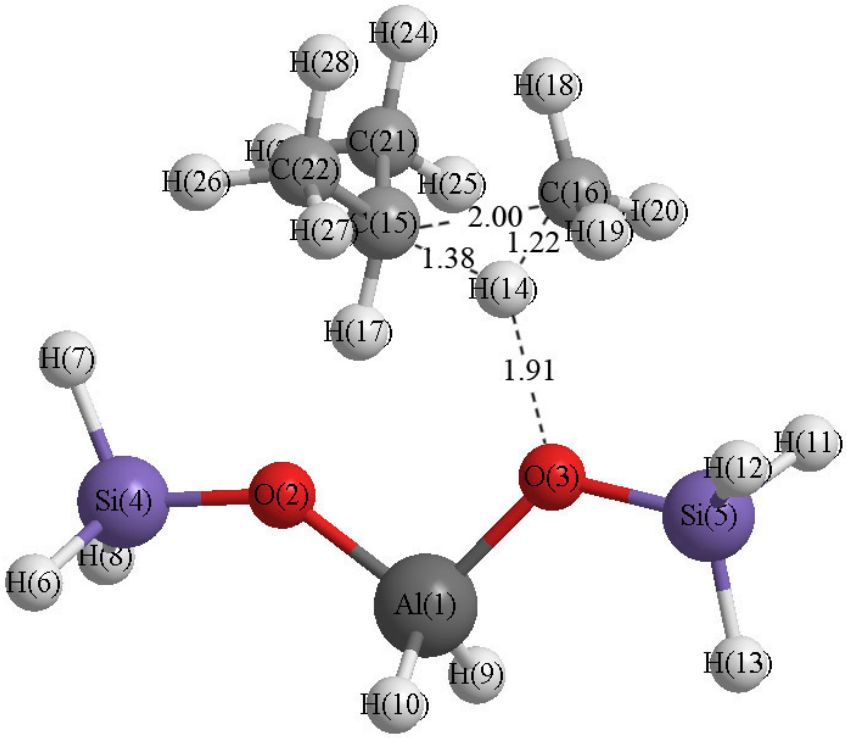

Figure 6-18(a). Transition state structures for the *iso*-butane protolytic cracking reaction on a T3 zeolite cluster (Units in Å)

The C_4H_{11} fragment has a Mulliken charge of +0.804 which makes it very similar to the non-classical $C_4H_{11}^+$ carbonium ion. In the transition state structure, the C(15)-C(16) distance is greatly extended from 1.54 Å in *iso*-butane to 2.00 Å, indicating the bond rupture mode. The acidic proton moves away from the zeolite cluster and the H(14)-O(3) distance reaches 1.91 Å compared with 0.98 Å for the zeolite-free cluster. The H(14)-C(16) distance is 1.22 Å, which is getting close to that of the methane product, 1.09 Å. The iso-propyl fragment, C_3H_7, is bonded to the zeolite oxygen, (O_2), and forms a surface alkoxide.

The zeolite cluster plays an important role in this reaction. The right oxygen of the cluster, O(3), acts as a Brønsted acid which donates a proton, while the left oxygen, O(2), acts as a Lewis base which receives the propyl group. This transition state structure demonstrates the typical bi-functional Brønsted acidic-Lewis basic nature of the zeolite catalyst.

The activation barrier for this protolytic reaction obtained with the CBS-QB3 method is 52.3 kcal/mol. It is much lower than those of other reactions from this group using similar methodology—71.4 kcal/mol for ethane (Zheng and Blowers, 2005a) and 62.1 kcal/mol for propane (Zheng and Blowers, 2005b). This indicates that the alkane protolytic reactions become easier to take place as the carbon chain length increases from C2 to C3 and C4.

The barrier calculated in this work is compared with the previous computational results and available experimental data, as listed in Table 6-11.

Table 6-11. Activation barrier calculation results for *iso*-butane conversion reactions on zeolites compared with previous computational and experimental studies

	Computational Studies				
	This Work	Kanzansky [a]	Rigby [b]	Esteves [c]	Furtado [d]
Cluster Model	T3	T1	T3	T3	T5
Geometry Optimization	B3LYP/6-31G*	HF/6-31G*	HF/3-21G	B3LYP/6-31G**	B3LYP/6-311G**
Energy Calculation	CBS-QB3	MP2/6-31++G**	MP2/6-31G*	B3LYP/6-31G**	B3LYP/6-311G**
Cracking	52.3	57.5	68	-	-
Primary H-Exchange	29.4	-	-	32.3	-
Tertiary H-Exchange	29.9	-	-	36.2	-
Dehydrogenation	59.4	66.9, 74.7	-	-	53.5
	This Work	**Experiment**			
		Stefanadis [e]	Sun [f]	Narbeshuber [g]	Corma [h]
Zeolite Catalyst Type		H-ZSM-5	H-ZSM-5	H-ZSM-5	USY
Cracking	52.3	57.0 (apparent)	29.0 ± 0.4	29.9	40.6 ± 0.4, 37.5 ± 4.5
Primary H-Exchange	29.4	-	-	-	-
Tertiary H-Exchange	29.9	-	-	-	-
Dehydrogenation	59.4	-	29.5 ± 0.3	23.9	28.0 ± 0.6, 39.6 ± 5.3

a – (Kazansky et al., 1996c) b – (Rigby et al., 1997)

c – (Esteves et al., 1999) d – (Furtado et al., 2001)

e – (Stefanadis et al., 1991) f – (Martin et al., 2000)

g – (Narbeshuber et al., 1995) h – (Corma et al., 1994)

Kanzansky reported an activation barrier of 57.5 kcal/mol using MP2/6-31++G**//HF/6-31G* (energy calculation method//geometry optimization method) and a small T1 zeolite cluster (Kazansky et al., 1996c). The barrier is relatively higher than that of this work because the small T1 cluster used is unable to include the important long-range interactions of the zeolite catalyst and MP2 energy calculations tend to overestimate barrier heights (Lee and Masel, 1995; Lee and Masel, 1996; Willis and Jensen, 1998; Yamataka et al., 1986). With a T3 cluster, Rigby studied the reaction using the MP2/6-31G*//HF/3-21G method, and the activation barrier obtained is even higher, 68.0 kcal/mol. Furthermore, several research groups conducted experimental studies of this reaction. The reported experimental activation energies are 29.0 kcal/mol from Sun (Martin et al., 2000) and 29.9 kcal/mol from Narbeshuber (Narbeshuber et al., 1995) using H-ZSM-5 zeolite as the catalyst. Corma *et al.* reported an activation energy of 37.5 and 40.6 kcal/mol using the USY zeolite with different Si/O ratios (Corma et al., 1994). The experimental apparent activation energy obtained by Stefanadis is 57.0 kcal/mol. Since the experimental adsorption energy of *iso*-butane on zeolites is in the range of 10 to 15 kcal/mol (Narbeshuber et al., 1995), the activation energy from Stefanadis is calculated to be 42 to 47 kcal/mol It can be found that the experimental results vary greatly from a low value of 29.0 kcal/mol to a much higher value of 47.0 kcal/mol. The great difference in the experimental value highlights the difficulty in measuring activation energies, especially when different reactor types are utilized.(Curtiss and Gordon, 2004) Also, the experimental results may depend on the *iso*-butane surface coverage ratio, Si/Al ratio, and temperature. The calculated

activation barrier from this work is slightly higher than the experimental data from Stefanadis and has better agreement than the computational works of Kanzansy and Rigby compared with the experimental results.

6.4.3 Hydrogen Exchange Reactions

$$\underline{\mathbf{C}}H_3CH(CH_3)_2 + H_3SiOAlH_2(OH')SiH_3 \rightarrow \underline{\mathbf{C}}H_2H'CH(CH_3)_2 + H_3Si(OH)AlH_2OSiH_3$$

$$CH_3\underline{\mathbf{C}}H(CH_3)_2 + H_3SiOAlH_2(OH')SiH_3 \rightarrow CH_3\underline{\mathbf{C}}H'(CH_3)_2 + H_3Si(OH)AlH_2OSiH_3$$

The *iso*-butane hydrogen exchange reaction can take place at either the primary carbon or the tertiary carbon shown in the above reaction scheme. The bold underlined carbon atom indicates the place where the hydrogen exchange takes place. Figure 6-18(b) shows the calculated transition state structure for the primary hydrogen exchange reaction of *iso*-butane optimized at the B3LYP/6-31G* level. The carbon in the main plane of the zeolite structure, C(15), is protonated and becomes a penta-coordinated structure. The exchanging hydrogen—H(19) and the acidic proton—H(14) stay in the middle of carbon and two oxygen atoms—(O2) and (O3), indicating the formation of one C-H bond and breaking of the other. The right oxygen of the cluster, O(3), acts as a Brønsted acid which donates a proton. The left oxygen, (O2), acts as a Lewis base which receives the hydrogen atom from *iso*-butane.

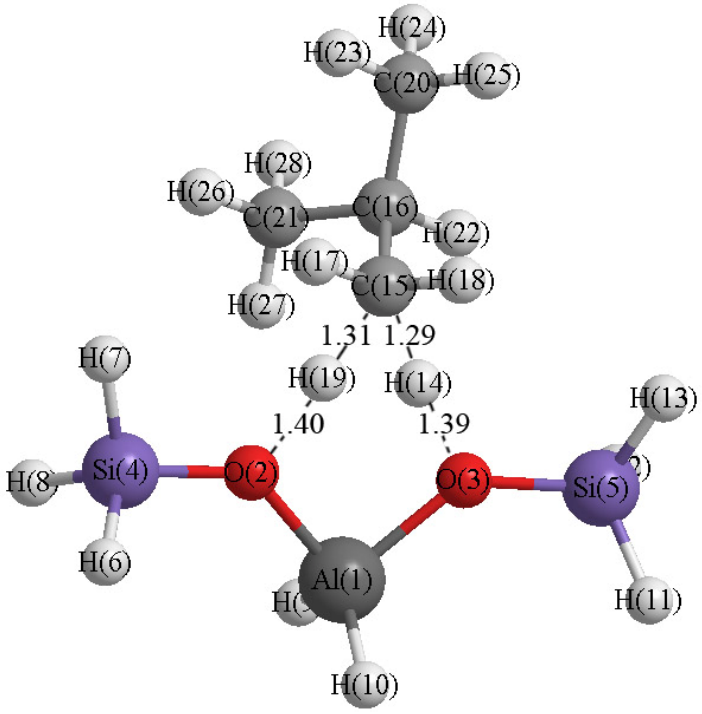

Figure 6-18(b). Transition state structure for the *iso*-butane primary hydrogen exchange reaction on a T3 zeolite cluster (Units in Å)

The activation barrier obtained with the CBS-QB3 method is 29.4 kcal/mol as listed in Table 6-11. Esteves *et al.* studied this reaction using the B3LYP/6-31G**//B3LYP/6-31G** method and a T3 cluster.(Esteves et al., 1999) The activation barrier reported is 32.3 kcal/mol, relatively higher than our value. Unfortunately, there is no experimental data to compare with directly. Stepanov reported the experimental activation energy of 25.8 ± 1.7 kcal/mol for the propane primary hydrogen exchange reaction (Stepanov et al., 1998). Considering the factor that the *iso*-butane hydrogen exchange should be similar to propane, our calculated activation barrier is expected to be quite reliable.

Figure 6-18(c) is the transition state structure for the *iso*-butane tertiary hydrogen exchange reaction optimized at the B3LYP/6-31G* level. The hydrogen exchange reaction takes place at the center carbon—C(15) which is protonated and becomes a penta-coordinated structure. The C(16)C(17)C(18) plane becomes almost flat and perpendicular to the cluster main plane, O(2)Al(1)O(3). The exchanging hydrogen—H(19), and the acidic hydrogen—H(14), stay in the middle of the carbon and two oxygen atoms—(O2) and (O3), indicating formation of one C-H bond and breaking of the other.

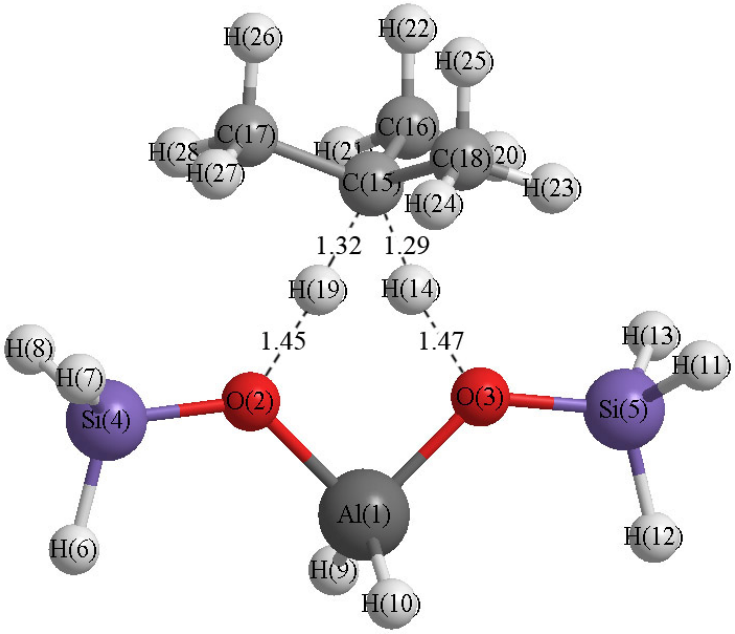

Figure 6-18(c). Transition state structure for the *iso*-butane tertiary hydrogen exchange reaction on a T3 zeolite cluster (Units in Å)

The activation barrier obtained with the CBS-QB3 method is 29.9 kcal/mol, which is similar to but slightly higher than that of the primary hydrogen exchange. Esteves reported a relatively higher barrier of 36.2 kcal/mol for this reaction using the B3LYP/6-31G**//B3LYP/6-31G** method and a T3 cluster. Again, there is no reported experimental study of this reaction. Considering that the experimental activation energy of the propane secondary hydrogen exchange is 28.0 ± 1.7 kcal/mol (Stepanov et al., 1998), our calculated result agrees well with it.

6.4.4 Dehydrogenation Reaction

$CH_3CH(CH_3)_2 + H_3SiOAlH_2(OH)SiH_3 \rightarrow H_2 + H_3Si(OC_4H_9)AlH_2OSiH_3$

For dehydrogenation, only the hydrogen attached to the tertiary carbon is available for attack by acidic zeolite sites (Martin et al., 2000), shown in the reaction scheme above. The dehydrogenation reaction consists of cleavage of a carbon-hydrogen bond by the zeolite Brønsted acid proton. The optimized transition state structure at the B3LYP/6-31G* level is shown in Figure 6-18(d). The carbon structure, C(15)C(16)C(21)C(22), becomes almost planar and a six-member ring, O(2)-Al(1)-O(3)-H(14)-H(20)-C(15), is formed. The H(20)-C(15) distance is greatly extended from 1.07 Å in *iso*-butane to 2.14 Å, indicating the bond rupture mode. The acidic proton, H(14), moves away from the zeolite cluster and the H(14)-O(3) distance reaches 1.85 Å compared with 0.98 Å for the zeolite free cluster. Meanwhile, these two hydrogens move closer to each other, and a di-hydrogen molecule is almost formed with a distance of 0.77 Å.

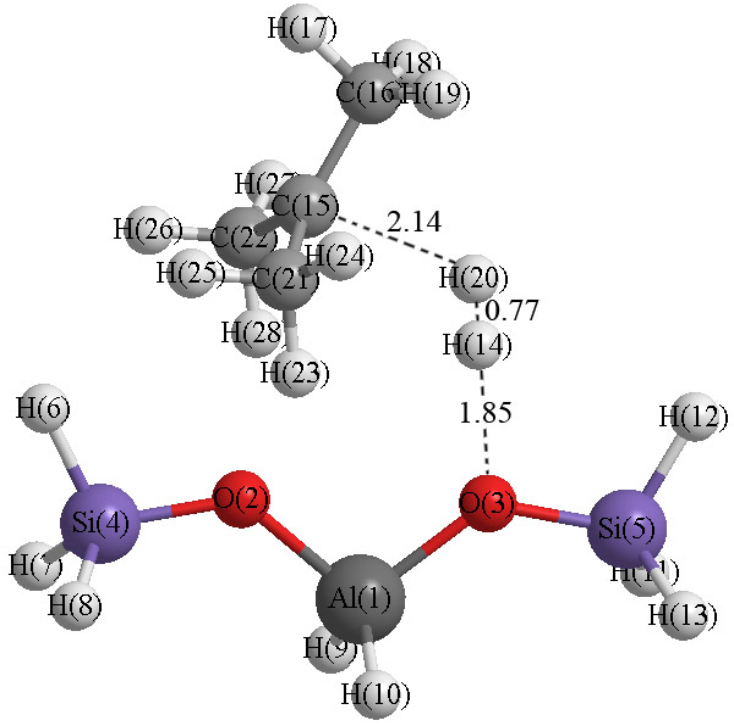

Figure 6-18(d). Transition state structure for the *iso*-butane dehydrogenation reaction on a T3 zeolite cluster (Units in Å)

The activation barrier obtained with the CBS-QB3 method is 59.4 kcal/mol. This barrier is the highest among the four *iso*-butane conversion reactions, indicating it is the most difficult reaction to take place. Compared with other researchers' computational work, this barrier is slightly higher than the result obtained by Furtado (Furtado et al., 2001) using B3LYP/6-311G**//B3LYP/6-311G** method and a T5 cluster, and much less than the results obtained by Kazansky, 66.9 and 74.7 kcal/mol, using the MP2/6-31++G**//HF/6-31G* method and a T1 cluster (Kazansky et al., 1996c). Several research groups have reported experimental studies of this reaction, and the activation energies vary from the low value of 23.0 kcal/mol by Narbeshuber (Narbeshuber et al., 1995) to a high value of 39.6 ± 5.3 kcal/mol by Croma (Corma et al.,

1994). It seems that the computational works overestimate activation barriers for this case.

This discrepancy could be caused by the limited size of the zeolite cluster used in this work since the T3 cluster did not include the long-range effects of the zeolite catalyst and led to the overestimation of barrier heights (Curtiss and Gordon, 2004). Zygmunt included the long-range correction for the ethane protolytic cracking reaction recently (Zygmunt et al., 2000), which was obtained with a HF/6-31G* correction for a 58T cluster model. This correction reduces the activation barrier by 14.50 kcal/mol. For the same scenario, a long-range correction could also lower our calculated barrier height and bring it much closer to the experimental value. Moreover, the zeolite acidic effect could also reduce our calculated activation barrier by 1.5 kcal/mol, which will be discussed in Section 6.4.5.

From the discussion above, the reactivity sequence found for zeolite catalytic reactions of *iso*-butane is:

dehydrogenation < protolytic cracking < hydrogen exchange

(59 kcal/mol) (52 kcal/mol) (29 kcal/mol)

6.4.5 Acidity Effects

Figure 6-19 shows the transition state structures of the *iso*-butane protolytic cracking reaction as the terminal Si-H distance changes from 1.3 Å to 1.9 Å. The acidic proton and oxygen distance—H(14)-O(3) decreases from 1.92 Å to 1.86 Å as cluster acidity increases. Meanwhile, the C(15)-C(16) distance decreases from 2.06 Å to 1.87 Å and the H(14)-C(16) distance slightly increases from 1.20 Å to 1.27 Å.

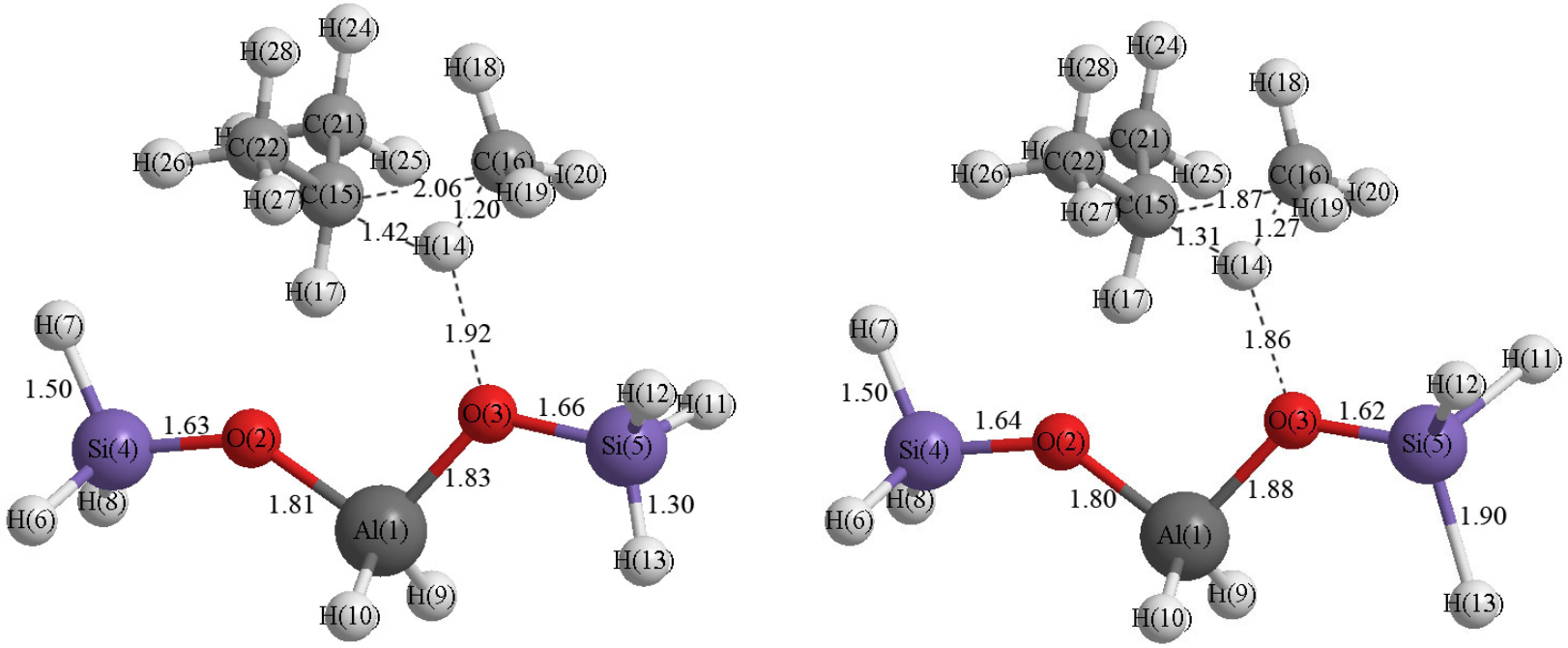

(a) R_{Si-H} = 1.3 Å (less acidic)

(b) R_{Si-H} = 1.9 Å (more acidic)

Figure 6-19. Transition state structures of *iso*-butane cracking reaction with changing terminal Si-H bond distances (Units in Å)

Similar acidic studies were applied to *iso*-butane primary and tertiary hydrogen exchange reactions, and the transition state structures are shown in Figures 6-20 and 6-21. In hydrogen exchange reactions, as the terminal Si-H distance increases from 1.3 Å to 1.9 Å, the acidic proton and oxygen distance—H(14)-O(3) increases and the exchanging hydrogen and oxygen distance—H(19)-O(2) increases as well. Meanwhile, the C_4H_{11} fragment moves away from the zeolite cluster. The transition state structures of the *iso*-butane dehydrogenation reaction as the Si-H distance changes to 1.3 Å and 1.9 Å are shown in Figure 6-22. The acidic proton and oxygen distance—H(14)-O(3) decreases slightly from 1.86 Å to 1.83 Å and the H(20)-C(15) distance decreases from 2.23 Å to 1.99 Å. Meanwhile, the H(14)-H(20) distance increases slightly from 0.768 Å to 0.772 Å.

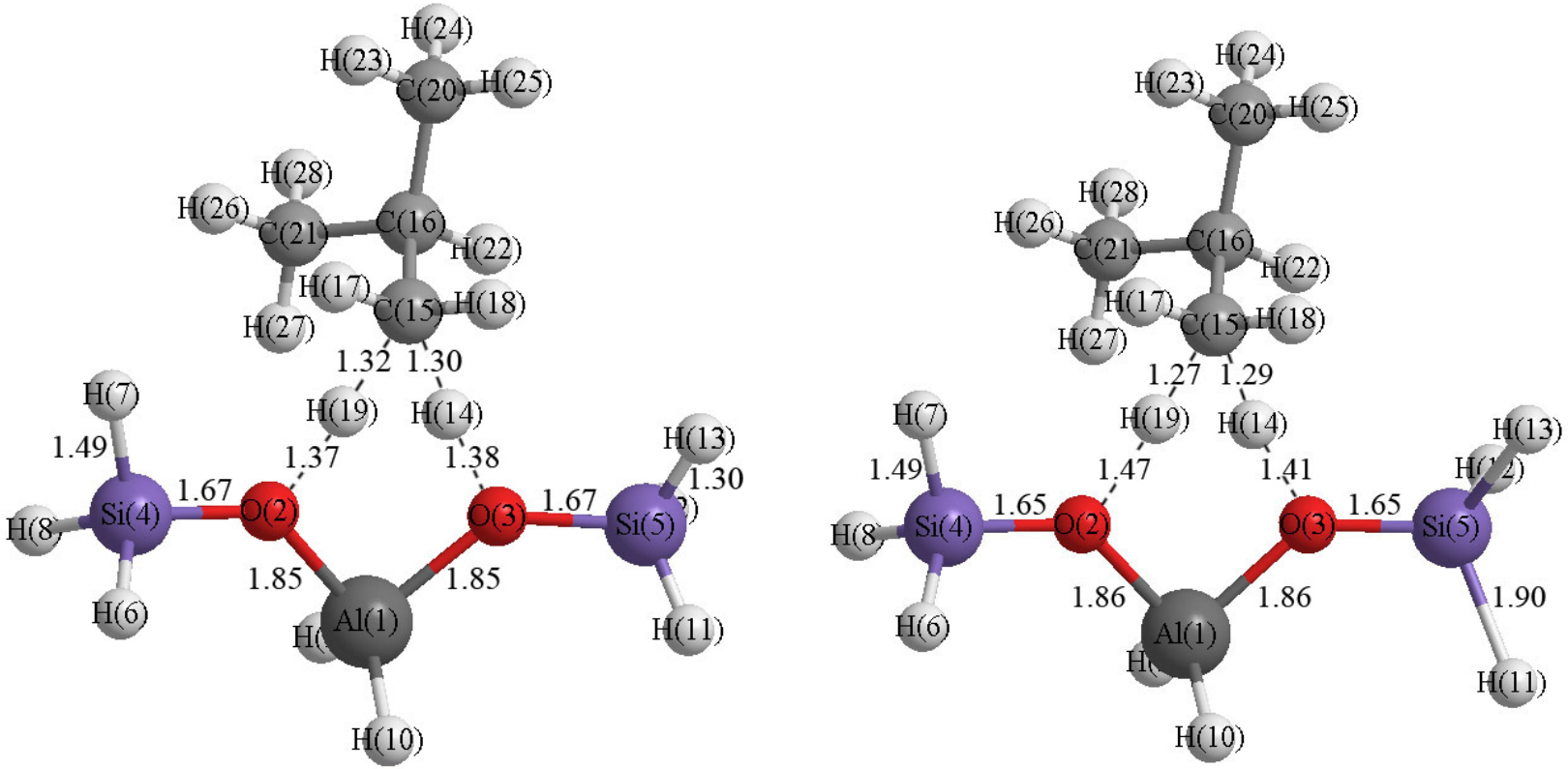

(a) R_{Si-H} = 1.3 Å (less acidic)

(b) R_{Si-H} = 1.9 Å (more acidic)

Figure 6-20. Transition state structures of *iso*-butane primary hydrogen exchange reaction with changing terminal Si-H bond distances (Units in Å)

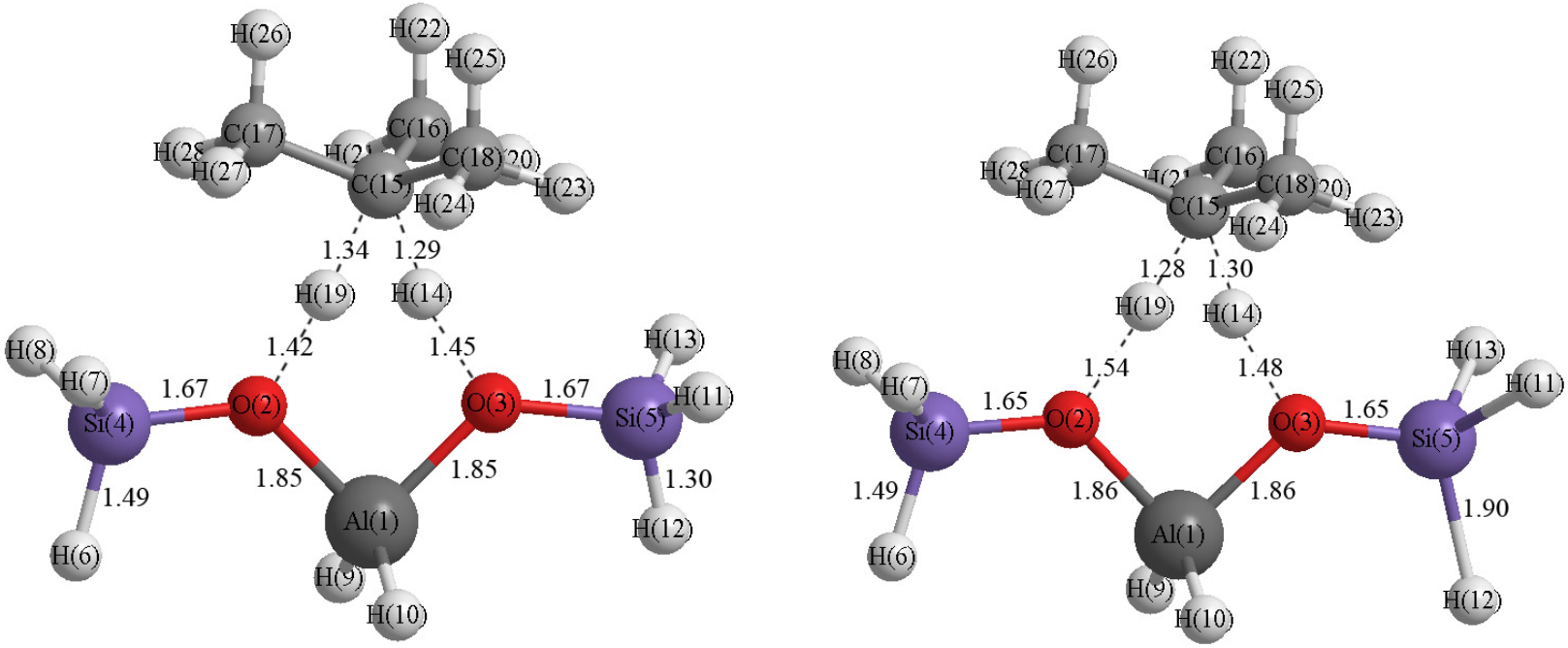

(a) R_{Si-H} = 1.3 Å (less acidic)

(b) R_{Si-H} = 1.9 Å (more acidic)

Figure 6-21. Transition state structures of *iso*-butane tertiary hydrogen exchange reaction with changing terminal Si-H bond distances (Units in Å)

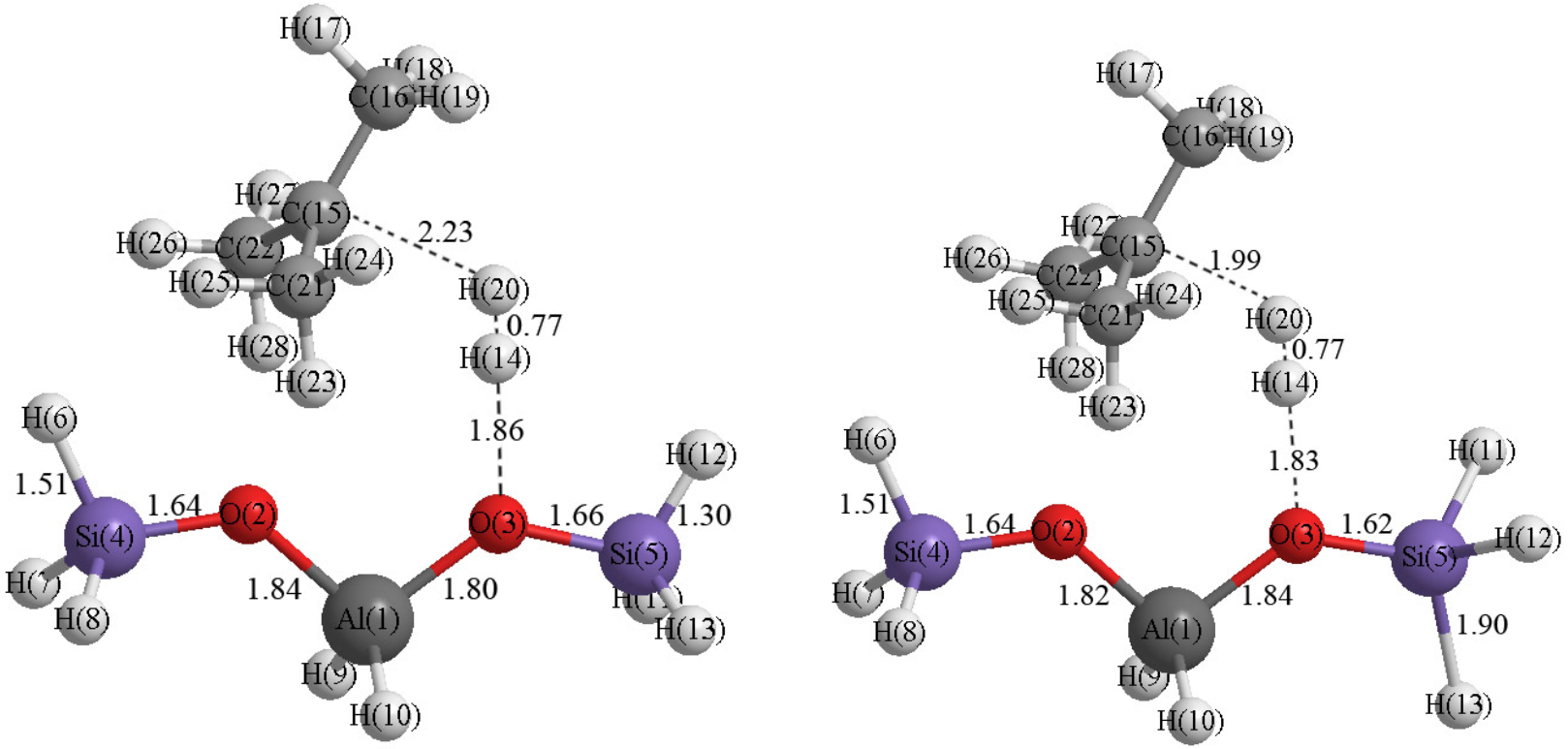

(a) R_{Si-H} = 1.3 Å (less acidic)

(b) R_{Si-H} = 1.9 Å (more acidic)

Figure 6-22. Transition state structures of *iso*-butane dehydrogenation reaction with changing terminal Si-H bond distances (Units in Å)

The change in activation barriers for *iso*-butane cracking, dehydrogenation and hydrogen exchange reactions as the Si-H bond distances varies are listed in Table 6-12. With the increase of the Si-H distance, the activation barriers decrease for all four reactions because of the increased acidity of the zeolite cluster. Applying the Brøsted-Polanyi principle, the following relationship can be used (van Santen and Kramer, 1995):

$$\Delta E_a = c\Delta E_{dep} \quad \text{or} \quad E_a = c\Delta E_{dep} + b$$

As long as the reaction mechanism does not alter, the change in activation energy is linearly correlated to the change in deprotonation energy.

Table 6-12. Effects of Si-H distances on activation barriers (Units in kcal/mol)

	Activation Barrier (E_a)				Deprotonation Energy (E_{dep})
	Cracking	Primary H-Exchange	Tertiary H-Exchange	Dehydrogenation	
R_{Si-H} = 1.30Å	56.7	31.8	32.4	62.9	304.0
R_{Si-H} = 1.47Å	52.3	29.4	29.9	59.4	297.9
R_{Si-H} = 1.70Å	47.3	26.7	26.8	55.5	291.6
R_{Si-H} = 1.90Å	43.4	24.6	24.6	52.5	285.8
HZSM-5	50.3	28.3	28.7	57.9	295.4
Relationship	$E_a = 0.737E_{dep} - 167.3$	$E_a = 0.391E_{dep} - 87.1$	$E_a = 0.435E_{dep} - 99.8$	$E_a = 0.577E_{dep} - 112.4$	

The relationships of the activation barriers with cluster deprotonation energies are illustrated in Figure 6-23. Linear dependence between these two properties is shown, and the analytical expressions are listed in Table 6-12. The slopes of primary and tertiary hydrogen exchange reactions are similar, which are different from those of the cracking and dehydrogenation reactions. This indicates the different dependence of activation barriers on deprotonation energies for cracking, hydrogen exchange, and dehydrogenation reactions.

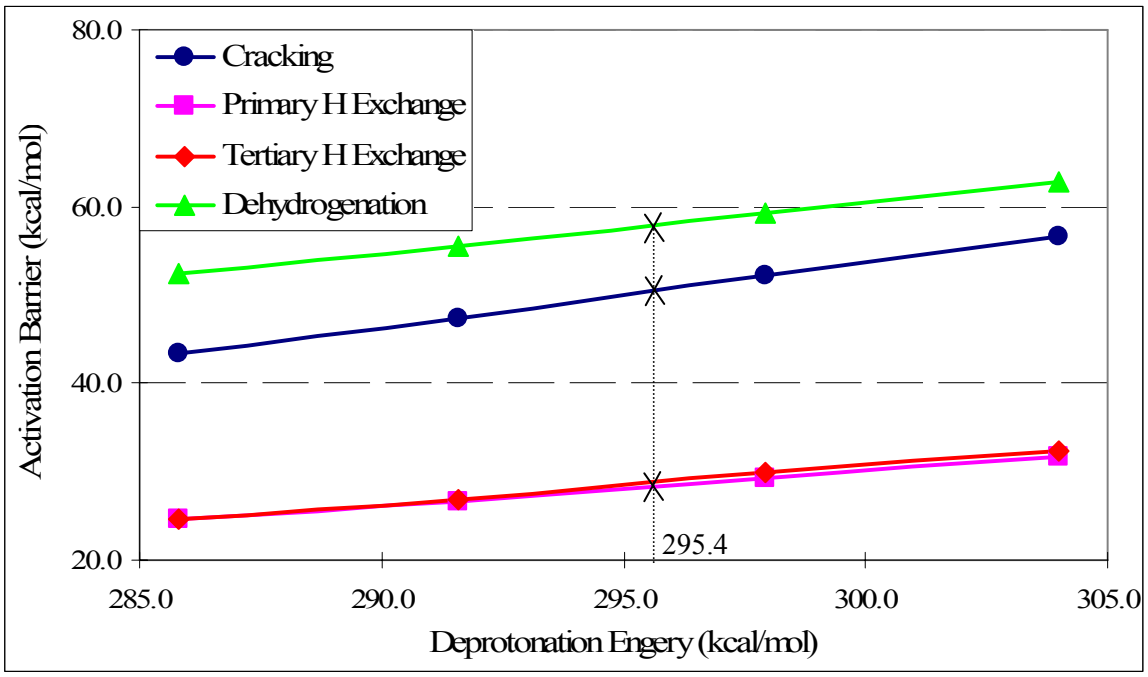

Figure 6-23. Corrections to the calculated *iso*-butane conversion reaction activation barriers for the acidity effects represented by deprotonation energies

For zeolite type H-ZSM-5, the deprotonation energy of 295.4 kcal/mol (Brand et al., 1993; Datka et al., 1988; Eichler et al., 1997; Grau-Crespo et al., 2000; Sauer and Sierka,

2000) has now been widely accepted.(Frash and van Santen, 1999; Zheng and Blowers, 2005a; Zygmunt et al., 2000) Applying this deprotonation energy, the activation barriers are then calculated using the correlations and listed in Table 6-12 as well. With the acidity effects, the activation barriers of the *iso*-butane protolytic cracking, primary hydrogen exchange, tertiary hydrogen exchange, and dehydrogenation reactions are lowered by 2.0, 1.1, 1.2, and 1.5 kcal/mol, which bring our calculated values closer to the experimental results.

With the correlations between the deprotonation energy and activation barrier for *iso*-butane conversion reactions, activation barriers can be obtained for different zeolite catalysts without performing the difficult transition state optimizations as long as the zeolite deprotonation energies are first acquired. Since the calculations to get the deprotonation energy are much easier to conduct, the prediction of activation barriers could become easier for these reactions on other zeolites by using the correlations.

6.5 Conclusions

In this chapter, hydrocarbon conversion reactions on zeolite catalysts were studied using the cluster approach. The zeolite catalysts were represented by a T3 cluster, $H_3SiOAlH_2(OH)SiH_3$ on which methane, ethane, propane, and *iso*-butane reactions were investigated. The reaction energetics were studied using density functional theory and *ab initio* methods. The activation barriers obtained in this chapter are summarized in Table 6-13. From this table, one can find that the reaction barriers decrease as the

carbon chain length increases, and the reactivity sequence for hydrocarbon zeolite catalytic reactions is:

dehydrogenation < protolytic cracking < hydrogen exchange

Moreover, the effects of zeolite acidity on the activation barriers were investigated in this work. The zeolite acidity effects were mimicked by changing the terminating Si-H bond lengths. Linear relationships were found for all hydrocarbon conversion reactions of interest. Analytical expressions between the activation barriers and deprotonation energies were proposed. As a result, accurate reaction barriers can be obtained when using zeolite catalysts with different acidities as long as their deprotonation energies are first acquired.

Table 6-13. Summary of activation barrier calculation results for hydrocarbon conversion reactions of interest in the chapter on zeolites (Units in kcal/mol)

	CH_4	CH_3CH_3	$CH_3CH_2CH_3$	$CH_3CH(CH_3)_2$
Cracking Reaction	N/A	71.4	62.1/62.6	52.3
Primary H-exchange Reaction	33.5	31.4	30.4	29.4
Secondary/Tertiary H-Exchange	N/A	N/A	29.8	29.9
Dehydrogenation Reaction	90.1	76.0	76.7	59.4

REFERENCES:

Abbot, J. and Dunstan, P.R., 1997. Catalytic cracking of linear paraffins: Effects of chain length. *Industrial & Engineering Chemistry Research*, 36(1): 76-82.

Bates, S.P. and Van Santen, R.A., 1998. The molecular basis of zeolite catalysis: a review of theoretical simulations. *Advances in Catalysis*, 42: 1-114.

Bauschlicher, C.W. and Partridge, H., 1995. A Modification of the Gaussian-2 Approach Using Density- Functional Theory. *Journal of Chemical Physics*, 103(5): 1788-1791.

Becke, A.D., 1993. Density-Functional Thermochemistry .3. The Role Of Exact Exchange. *Journal Of Chemical Physics*, 98(7): 5648-5652.

Bhan, A., Joshi, Y.V., Delgass, W.N. and Thomson, K.T., 2003. DFT investigation of alkoxide formation from olefins in H-ZSM-5. *Journal of Physical Chemistry B*, 107(38): 10476-10487.

Blaszkowski, S.R., Jansen, A.P.J., Nascimento, M.A.C. and Vansanten, R.A., 1994. Density-Functional Theory Calculations of the Transition-States for Hydrogen-Exchange and Dehydrogenation of Methane by a Bronsted Zeolitic Proton. *Journal of Physical Chemistry*, 98(49): 12938-12944.

Blaszkowski, S.R., Nascimento, M.A.C. and vanSanten, R.A., 1996. Activation of C-H and C-C bonds by an acidic zeolite: A density functional study. *Journal of Physical Chemistry*, 100(9): 3463-3472.

Blaszkowski, S.R. and Vansanten, R.A., 1995. Density-Functional Theory Calculations of the Activation of Methanol by a Bronsted Zeolitic Proton. *Journal of Physical Chemistry*, 99(30): 11728-11738.

Blowers, P. and Masel, R., 2000. Engineering energies in introduction approximations for

activation hydrogen transfer reactions. *Aiche Journal*, 46(10): 2041-2052.

Bottoni, A., 1996. Theoretical study of the addition of alkyl and halogenoalkyl radicals to the ethylene double bond: A comparison between Hartree-Fock, perturbation theory and density functional theory. *Journal of the Chemical Society-Perkin Transactions 2*(9): 2041-2047.

Brand, H.V., Curtiss, L.A. and Iton, L.E., 1993. Ab-Initio Molecular-Orbital Cluster Studies of the Zeolite ZSM-5 .1. Proton Affinities. *Journal of Physical Chemistry*, 97(49): 12773-12782.

Broclawik, E. et al., 1995. Density-Functional Theory Calculations of the Reaction Pathway for Methane Activation on a Gallium Site in Metal Exchanged Zsm-5. *Journal of Chemical Physics*, 103(6): 2102-2108.

Collins, S.J. and Omalley, P.J., 1994. Density-Functional Studies of the Carbonium-Ion Species Ch5+, C2h7+ and C(3)H(9)(+)E. *Chemical Physics Letters*, 228(1-3): 246-251.

Collins, S.J. and Omalley, P.J., 1995. A Theoretical Description for the Monomolecular Cracking of C-C Bonds over Acidic Zeolites. *Journal of Catalysis*, 153(1): 94-99.

Corma, A., Miguel, P.J. and Orchilles, A.V., 1994. The Role of Reaction Temperature and Cracking Catalyst Characteristics in Determining the Relative Rates of Protolytic Cracking, Chain Propagation, and Hydrogen-Transfer. *Journal of Catalysis*, 145(1): 171-180.

Curtiss, L.A. and Gordon, M.S., 2004. *Computational materials chemistry methods and applications*. Kluwer academic publishers, Dordrecht ; Boston ; London.

Datka, J., Boczar, M. and Rymarowicz, P., 1988. Heterogeneity of Oh Groups in Nah-Zsm-5 Zeolite Studies by Infrared-Spectroscopy. *Journal of Catalysis*, 114(2): 368-376.

Duncan, W.T., Bell, R.L. and Truong, T.N., 1998. TheRate: Program for ab initio direct dynamics calculations of thermal and vibrational-state-selected rate constants. *Journal Of Computational Chemistry*, 19(9): 1039-1052.

Durant, J.L., 1996. Evaluation of transition state properties by density functional theory. *Chemical Physics Letters*, 256(6): 595-602.

Eichler, U., Brandle, M. and Sauer, J., 1997. Predicting absolute and site specific acidities for zeolite catalysts by a combined quantum mechanics interatomic potential function approach. *Journal of Physical Chemistry B*, 101(48): 10035-10050.

Esteves, P.M., Nascimento, M.A.C. and Mota, C.J.A., 1999. Reactivity of alkanes on zeolites: A theoretical ab initio study of the H/H exchange. *Journal Of Physical Chemistry B*, 103(47): 10417-10420.

Evleth, E.M., Kassab, E. and Sierra, L.R., 1994. Calculation of the Exchange Mechanism of D-2 and Cd4 with a Zeolite Model. *Journal of Physical Chemistry*, 98(5): 1421-1426.

Flanigen, E.M., 2001. Zeolites and molecular sieves: An historical perspective. *Studies in Surface Science and Catalysis*, 137(Introduction to Zeolite Science and Practice (2nd Edition)): 11-35.

Frash, M.V., Kazansky, V.B., Rigby, A.M. and van Santen, R.A., 1998. Cracking of hydrocarbons on zeolite catalysts: Density functional and Hartree-Fock calculations on the mechanism of the beta-scission reaction. *Journal of Physical Chemistry B*, 102(12): 2232-2238.

Frash, M.V., Kazansky, V.B., Rigby, A.M. and vanSanten, R.A., 1997. Density functional and Hartree-Fock calculations on the cyclopropane ring intermediates involved in the zeolite-catalyzed skeletal isomerization of hydrocarbons and in the carbon isotope scrambling in 2-propyl cation. *Journal of Physical Chemistry B*, 101(27): 5346-5351.

Frash, M.V. and van Santen, R.A., 1999. Quantum-chemical modeling of the hydrocarbon transformations in acid zeolite catalysts. *Topics in Catalysis*, 9(3-4): 191-205.

Freude, D., Klinowski, J. and Hamdan, H., 1988. Solid-State Nmr-Studies of the Geometry of Bronsted Acid Sites in Zeolitic Catalysts. *Chemical Physics Letters*, 149(4): 355-362.

Frisch, M.J. et al., 1995. *Gaussian 98, Revision A.7*. Gaussian, Inc., Pittsburgh PA.

Frisch, M.J. et al., 1998. *Gaussian 98, Revision A.7*. Gaussian, Inc., Pittsburgh PA.

Furtado, E.A., Milas, I., Lins, J. and Nascimento, M.A.C., 2001. The dehydrogenation reaction of light alkanes catalyzed by zeolites. *Physica Status Solidi a-Applied Research*, 187(1): 275-288.

Gilbert, R.G. and Smith, S.C., 1990. *Theory of unimolecular and recombination reactions*. Blackwell Scientific Publications, Oxford, England.

Goldstein, E., Haught, M. and Tang, Y., 1998. Evaluation of density functional theory in the bond rupture of octane. *Journal of Computational Chemistry*, 19(2): 154-167.

Gonzales, N.O., Chakraborty, A.K. and Bell, A.T., 1998. A density functional theory study of the effects of metal cations on the Bronsted acidity of H-ZSM-5. *Catalysis Letters*, 50(3-4): 135-139.

Gonzalez, C. and Schlegel, H.B., 1989. An Improved Algorithm For Reaction-Path Following. *Journal Of Chemical Physics*, 90(4): 2154-2161.

Grau-Crespo, R., Peralta, A.G., Ruiz-Salvador, A.R., Gomez, A. and Lopez-Cordero, R., 2000. A computer simulation study of distribution, structure and acid strength of active sites in H-ZSM-5 catalyst. *Physical Chemistry Chemical Physics*, 2(24): 5716-5722.

Hay, P.J., Redondo, A. and Guo, Y.J., 1999. Theoretical studies of pentene cracking on zeolites: C-C beta-scission processes. *Catalysis Today*, 50(3-4): 517-523.

Himei, H. et al., 1995. Study of the Activity of Ga-Zsm-5 in the De-Nox Process by a Combination of Quantum-Chemistry, Molecular-Dynamics, and Computer-Graphics Methods. *Journal of Physical Chemistry*, 99(33): 12461-12465.

Holbrook, K.A., Pilling, M.J. and Robertson, S.H., 1996. *Unimolecular Reactions*. John Wiley & Sons, Chichester, New York.

http://www.iza-structure.org/databases/.

Johnson, B.G., Gill, P.M.W. and Pople, J.A., 1993. The Performance Of A Family Of

Density Functional Methods. *Journal Of Chemical Physics*, 98(7): 5612-5626.

Jursic, B.S., 1997. Ab initio and hybrid density functional theory studies of the forward and reverse barriers for the C2H4+H->C2H5 reaction. *Journal of the Chemical Society-Perkin Transactions 2*(3): 637-641.

Kazansky, V.B., 1999. Adsorbed carbocations as transition states in heterogeneous acid catalyzed transformations of hydrocarbons. *Catalysis Today*, 51(3-4): 419-434.

Kazansky, V.B., Frash, M.V. and van Santen, R.A., 1996a. Quantumchemical study of the isobutane cracking on zeolites. *Applied Catalysis, A: General*, 146(1): 225-247.

Kazansky, V.B., Frash, M.V. and van Santen, R.A., 1997. A quantum-chemical study of hydride transfer in catalytic transformations of paraffins on zeolites. Pathways through adsorbed nonclassical carbonium ions. *Catalysis Letters*, 48(1-2): 61-67.

Kazansky, V.B., Frash, M.V. and Vansanten, R.A., 1994a. A Quantum-Chemical Study of Adsorbed Nonclassical Carbonium-Ions as Active Intermediates in Catalytic Transformations of Paraffins .2. Protolytic Dehydrogenation and Hydrogen-Deuterium Hetero-Isotope Exchange of Paraffins on High-Silica Zeolites. *Catalysis Letters*, 28(2-4): 211-222.

Kazansky, V.B., Frash, M.V. and vanSanten, R.A., 1996b. *Quantum-chemical study of the nonclassical carbonium ion-like transition states in isobutane cracking on zeolites*, 11th International Congress on Catalysis - 40th Anniversary, Pts a and B. Studies in Surface Science and Catalysis, pp. 1233-1242.

Kazansky, V.B., Frash, M.V. and vanSanten, R.A., 1996c. Quantumchemical study of the isobutane cracking on zeolites. *Applied Catalysis, A: General*, 146(1): 225-247.

Kazansky, V.B., Senchenya, I.N., Frash, M. and Vansanten, R.A., 1994b. A Quantum-Chemical Study of Adsorbed Nonclassical Carbonium-Ions as Active Intermediates in Catalytic Transformations of Paraffins .1. Protolytic Cracking of Ethane on High-Silica Zeolites. *Catalysis Letters*, 27(3-4): 345-354.

Kenaston, N.P., Bell, A.T. and Reimer, J.A., 1994. Determination of the Al-H and H-H Internuclear Distances in Zsm-5 Using Nmr-Spectroscopy. *Journal of Physical Chemistry*,

98(3): 894-896.

Klier, K., 2002. The transition state in heterogeneous catalysis. *Topics in Catalysis*, 18(3-4): 141-156.

Kramer, G.J., Vansanten, R.A., Emeis, C.A. and Nowak, A.K., 1993. Understanding the Acid Behavior of Zeolites from Theory and Experiment. *Nature*, 363(6429): 529-531.

Kustov, L.M., Kazansky, V.B., Beran, S., Kubelkova, L. and Jiru, P., 1987. Adsorption of Carbon-Monoxide on Zsm-5 Zeolites - Infrared Spectroscopic Study and Quantum-Chemical Calculations. *Journal of Physical Chemistry*, 91(20): 5247-5251.

Larson, J.G. and Hall, W.K., 1965. Studies Of Hydrogen Held By Solids .7. Exchange Of Hydroxyl Groups Of Alumina And Silica-Alumina Catalysts With Deuterated Methane. *Journal Of Physical Chemistry*, 69(9): 3080-&.

Lee, C.T., Yang, W.T. and Parr, R.G., 1988. Development Of The Colle-Salvetti Correlation-Energy Formula Into A Functional Of The Electron-Density. *Physical Review B*, 37(2): 785-789.

Lee, W.T. and Masel, R.I., 1995. Intrinsic Activation Barriers for a Prototype Hydrogenolysis Reaction D+C2h6- Dch3+Ch3 in C-3-Nu Symmetry. *Journal of Physical Chemistry*, 99(23): 9363-9367.

Lee, W.T. and Masel, R.I., 1996. Ab initio calculations of the transition state energy and position for the reaction H+C(2)H(5)R->HH+C(2)H(4)R, with R=H, CH3, NH2, CN, CF3, C5H6: Comparison to Marcus' theory, Miller's theory, and Bockris' model. *Journal of Physical Chemistry*, 100(26): 10945-10951.

Lins, J. and Nascimento, M.A.C., 1996. Theoretical investigation of the methane activation reaction on protonated zeolite from generalized valence-bond plus configuration interaction calculations. *Theochem-Journal Of Molecular Structure*, 371: 237-243.

Lynch, B.J. and Truhlar, D.G., 2001. How well can hybrid density functional methods predict transition state geometries and barrier heights? *Journal of Physical Chemistry A*, 105(13): 2936-2941.

Maesen, T. and Marcus, B., 2001. The zeolite scene - an overview. *Studies in Surface Science and Catalysis*, 137(Introduction to Zeolite Science and Practice (2nd Edition)): 1-9.

Makarova, M.A., Ojo, A.F., Karim, K., Hunger, M. and Dwyer, J., 1994. Ftir Study of Weak Hydrogen-Bonding of Bronsted Hydroxyls in Zeolites and Aluminophosphates. *Journal of Physical Chemistry*, 98(14): 3619-3623.

Martin, J.M.L., Sundermann, A., Fast, P.L. and Truhlar, D.G., 2000. Thermochemical analysis of core correlation and scalar relativistic effects on molecular atomization energies. *Journal of Chemical Physics*, 113(4): 1348-1358.

Masel, R.I., 1996. *Principles of adsorption and reaction on solid surfaces*. Wiley, New York.

Masel, R.I., 2001. *Chemical kinetics and catalysis*. Wiley-Interscience, New York.

McCusker, L.B. and Baerlocher, C., 2001. Zeolite structures. *Studies in Surface Science and Catalysis*, 137(Introduction to Zeolite Science and Practice (2nd Edition)): 37-67.

Milas, I. and Nascimento, M.A.C., 2001. A density-functional study of the dehydrogenation reaction of isobutane over zeolites. *Chemical Physics Letters*, 338(1): 67-73.

Montgomery, J.A., Frisch, M.J., Ochterski, J.W. and Petersson, G.A., 1999. A complete basis set model chemistry. VI. Use of density functional geometries and frequencies. *Journal of Chemical Physics*, 110(6): 2822-2827.

Narbeshuber, T.F., Brait, A., Seshan, K. and Lercher, J.A., 1997. Dehydrogenation of light alkanes over zeolites. *Journal Of Catalysis*, 172(1): 127-136.

Narbeshuber, T.F., Vinek, H. and Lercher, J.A., 1995. Monomolecular conversion of light alkanes over H-ZSM-5. *Journal of Catalysis*, 157(2): 388-395.

Nicholas, J.B., 1997. Density functional theory studies of zeolite structure, acidity, and reactivity. *Topics in Catalysis*, 4(1-2): 157-171.

Okulik, N.B., Diez, R.P. and Jubert, A.H., 2004. A topological study of the transition states of the hydrogen exchange and dehydrogenation reactions of ethane on a zeolite cluster. *Journal Of Physical Chemistry A*, 108(13): 2469-2474.

Okulik, N.B., Diez, R.P., Jubert, A.H., Esteves, P.M. and Mota, C.J.A., 2001. A topological study of the transition states of the hydrogen exchange and dehydrogenation reactions of methane on a zeolite cluster. *Journal Of Physical Chemistry A*, 105(29): 7079-7084.

Porezag, D. and Pederson, M.R., 1995. Density-Functional Based Studies of Transition-States and Barriers for Hydrogen-Exchange and Abstraction Reactions. *Journal of Chemical Physics*, 102(23): 9345-9349.

Rigby, A.M. and Frash, M.V., 1997. Ab initio calculations on the mechanisms of hydrocarbon conversion in zeolites: Skeletal isomerisation and olefin chemisorption. *Journal of Molecular Catalysis a-Chemical*, 126(1): 61-72.

Rigby, A.M., Kramer, G.J. and vanSanten, R.A., 1997. Mechanisms of hydrocarbon conversion in zeolites: A quantum mechanical study. *Journal of Catalysis*, 170(1): 1-10.

Rozanska, X., van Santen, R.A., Demuth, T., Hutschka, F. and Hafner, J., 2003. A periodic DFT study of isobutene chemisorption in proton-exchanged zeolites: Dependence of reactivity on the zeolite framework structure. *Journal of Physical Chemistry B*, 107(6): 1309-1315.

Ryder, J.A., Chakraborty, A.K. and Bell, A.T., 2000. Density functional theory study of proton mobility in zeolites: Proton migration and hydrogen exchange in ZSM-5. *Journal Of Physical Chemistry B*, 104(30): 6998-7011.

Saeys, M., Reyniers, M.F. and Marin, G.B., 2003. Ab initio calculations for hydrocarbons: Enthalpy of formation, transition state geometry, and activation energy for radical reactions. *Journal of Physical Chemistry A*, 107(43): 9147-9159.

Sauer, J. and Sierka, M., 2000. Combining quantum mechanics and interatomic potential functions in ab initio studies of extended systems. *Journal of Computational Chemistry*, 21(16): 1470-1493.

Scott, A.P. and Radom, L., 1996. Harmonic vibrational frequencies: An evaluation of Hartree-Fock, Moller-Plesset, quadratic configuration interaction, density functional theory, and semiempirical scale factors. *Journal of Physical Chemistry*, 100(41): 16502-16513.

Stefanadis, C., Gates, B.C. and Haag, W.O., 1991. Rates of Isobutane Cracking Catalyzed by Hzsm-5 - the Carbonium-Ion Route. *Journal of Molecular Catalysis*, 67(3): 363-367.

Stepanov, A.G., Ernst, H. and Freude, D., 1998. In situ H-1 MAS NMR studies of the H/D exchange of deuterated propane adsorbed on zeolite H-ZSM-5. *Catalysis Letters*, 54(1-2): 1-4.

Torrent, M., Duran, M. and Sola, M., 1996. An assessment of density functional theory on evaluating activation barriers for small organic gas-phase rearrangement reactions. *Theochem-Journal of Molecular Structure*, 362(2): 163-173.

Trombetta, M., Armaroli, T., Alejandre, A.G., Solis, J.R. and Busca, G., 2000. An FT-IR study of the internal and external surfaces of HZSM5 zeolite. *Applied Catalysis a-General*, 192(1): 125-136.

Truong, T.N., 2000. Reaction class transition state theory: Hydrogen abstraction reactions by hydrogen atoms as test cases. *Journal of Chemical Physics*, 113(12): 4957-4964.

Truong, T.N. and Truong, T.T.T., 1999. A reaction class approach with the integrated molecular orbital plus molecular orbital methodology. *Chemical Physics Letters*, 314(5-6): 529-533.

van Santen, R.A., 1997. Quantum-chemistry of zeolite acidity. *Catalysis Today*, 38(3): 377-390.

van Santen, R.A., De Bruyn, D.P., Den Ouden, C.J.J. and Smit, B., 1991. Introduction to zeolite theory and modeling. *Studies in Surface Science and Catalysis*, 58(Introd. Zeolite Sci. Pract.): 317-58.

van Santen, R.A. and Kramer, G.J., 1995. Reactivity Theory of Zeolitic Bronsted Acidic Sites. *Chemical Reviews*, 95(3): 637-660.

van Santen, R.A., van de Graaf, B. and Smit, B., 2001. Introduction to zeolite theory and modelling. *Studies in Surface Science and Catalysis*, 137(Introduction to Zeolite Science and Practice (2nd Edition)): 419-466.

Viruelamartin, P., Zicovichwilson, C.M. and Corma, A., 1993. Ab-Initio Molecular-Orbital Calculations of the Protonation Reaction of Propylene and Isobutene by Acidic Oh Groups of Isomorphously Substituted Zeolites. *Journal of Physical Chemistry*, 97(51): 13713-13719.

Vollmer, J.M. and Truong, T.N., 2000. Mechanisms of hydrogen exchange of methane with H-zeolite Y: An ab initio embedded cluster study. *Journal Of Physical Chemistry B*, 104(26): 6308-6312.

Willis, B.G. and Jensen, K.F., 1998. An evaluation of density functional theory and ab initio predictions for bridge-bonded aluminum compounds. *Journal of Physical Chemistry A*, 102(15): 2613-2623.

Wong, M.W., Pross, A. and Radom, L., 1994. Comparison of the Addition of Ch3-Center-Dot, Ch2oh-Center-Dot, and Ch2cn-Center-Dot Radicals to Substituted Alkenes - a Theoretical-Study of the Reaction-Mechanism. *Journal of the American Chemical Society*, 116(14): 6284-6292.

Wong, M.W. and Radom, L., 1995. Radical-Addition to Alkenes - an Assessment of Theoretical Procedures. *Journal of Physical Chemistry*, 99(21): 8582-8588.

Wong, M.W. and Radom, L., 1998. Radical addition to alkenes: Further assessment of theoretical procedures. *Journal of Physical Chemistry A*, 102(12): 2237-2245.

Xiao, Y.T., Longo, J.M., Hieshima, G.B. and Hill, R.J., 1997. Understanding the kinetics and mechanisms of hydrocarbon thermal cracking: An ab initio approach. *Industrial & Engineering Chemistry Research*, 36(10): 4033-4040.

Yamataka, H., Nagase, S., Ando, T. and Hanafusa, T., 1986. Theoretical-Studies of Substituent Effects on the Additions of Amines to Carbonyl-Compounds - a Relation among Energetics, Structures, and Isotope Effects. *Journal of the American Chemical Society*, 108(4): 601-606.

Zhang, Q., Bell, R. and Truong, T.N., 1995. Ab-Initio And Density-Functional Theory Studies Of Proton-Transfer Reactions In Multiple Hydrogen-Bond Systems. *Journal Of Physical Chemistry*, 99(2): 592-599.

Zheng, X. and Blowers, P., 2005a. An ab initio study of ethane conversion reactions on zeolites using cluster approach. *Journal of Molecular Catalysis A*, 229: 77-85.

Zheng, X. and Blowers, P., 2005b. Reactivity of alkanes on zeolites: a computational study of propane conversion reactions. *Journal of Physical Chemistry A*, (in press).

Zygmunt, S.A., Curtiss, L.A., Zapol, P. and Iton, L.E., 2000. Ab initio and density functional study of the activation barrier for ethane cracking in cluster models of zeolite H-ZSM-5. *Journal of Physical Chemistry B*, 104(9): 1944-1949.

CHAPTER 7
HYDROGEN EXCHANGE REACTIONS OF LIGHT ALKANES ON ZEOLITES

The alkane hydrogen exchange reaction seems to be trivial to study at a first look. However, the reaction is important because these relatively simple reaction pathways and activation barriers can be studied experimentally rather easily, which can then in turn be used to evaluate the choice of computational methods. The zeolite catalytic hydrogen exchanges of methane and ethane have been investigated by several groups using different computational approaches (Blaszkowski et al., 1996; Kazansky et al., 1994a; Kazansky et al., 1994b; Okulik et al., 2004; Okulik et al., 2001; Ryder et al., 2000; Vollmer and Truong, 2000; Zygmunt et al., 2000). But the activation energies obtained are always off by at least 3 kcal/mol from the experiments, depending on the different choice of zeolite cluster models and computational methods. Other researchers have studied the propane hydrogen exchange reaction (Esteves et al., 1999; Ryder et al., 2000) while there have been no reported results for the butane reaction. The hydrogen exchange of propane and butane are included in this chapter

because they are the simplest alkanes where hydrogen exchange on secondary atoms can be observed. In this chapter, quantum chemical methods were applied to study hydrogen exchange reactions of methane, ethane, propane, and butane with a T3 zeolite cluster.

7.1 Computational Methods

The well-known B3LYP method uses Becke's three-parameter density functional (Becke, 1993) and the Lee, Yang, and Parr functional (Lee et al., 1988) to describe gradient-corrected correlation effects. It has been validated to give results similar to that of the more expensive MP2 theory for molecular geometry and frequency calculations (Bauschlicher and Partridge, 1995; Johnson et al., 1993). In this work, the geometry optimizations of the reactants, products and transition state structures were carried out using the B3LYP method combined with a moderate basis set, 6-31g*. The calculations were performed with the GAUSSIAN98 software package (Frisch et al., 1998). All the structures were fully optimized without geometry constraints. The products and reactants were verified with frequency calculations to be stable structures, and the transition states were tested to ensure they were first order saddle points with only one negative eigenvalue. Additionally, intrinsic reaction coordinate (IRC) calculations proved that each reaction linked the correct products with reactants. Zero point vibrational energies (ZPVE) were obtained from

harmonic vibrational frequencies calculated at the B3LYP/6-31g* level with a scaling factor of 0.9806 and the frequencies were scaled by 0.9945 (Scott and Radom, 1996).

7.2 Methane Hydrogen Exchange Reaction

$CH_3Hz + H_3SiOAlH_2(OH')SiH_3 \rightarrow CH_3H' + H_3Si(OHz)AlH_2OSiH_3$

In the reaction schematic above, Hz represents the hydrogen exchanged from the CH_4 reactant, and H' represents the protonic hydrogen from the zeolite cluster. The methane hydrogen exchange reaction was described in the previous chapter, section 6.1.2, and is briefly discussed here to set up the analyses in this work. Figure 7-1 shows the transition state structure for the methane hydrogen exchange reaction calculated at the B3LYP/6-31g* level. The structure clearly has C_s symmetry obtained without any symmetry constraints applied for the optimization step. The protonated carbon atom stays in the main plane of the zeolite cluster and becomes a penta-coordinated structure. The two hydrogen atoms—H', the acidic proton from the zeolite cluster and Hz, the exchange hydrogen from the methane molecule, stay in the middle of the carbon and two zeolite oxygen atoms, which indicates the formation of one C-H bond and breaking of the other. In the reaction process, the right oxygen of the cluster acts as a Brønsted acid which donates a proton. The left oxygen acts as a Lewis base which receives the hydrogen atom from methane molecule.

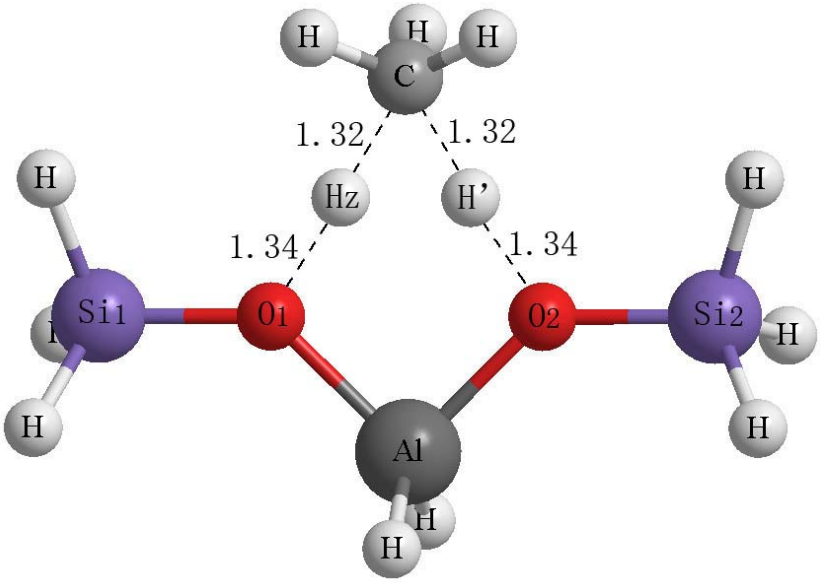

Figure 7-1. Calculated transition state structure for the methane hydrogen exchange reaction on a T3 zeolite cluster (Units in Å)

Selected bond lengths and angles for the transition state structure are reported in Table 7-1 along with a comparison to previous computational results from Esteves *et al.* (Esteves et al., 1999) and Ryder *et al.* (Ryder et al., 2000).

Table 7-1. Selected bond lengths and angles of the methane hydrogen exchange reaction transition state structure

	this work	Esteves *et al.*	Ryder *et al.*
Geom. Optimization	B3LYP/6-31g*	B3LYP/6-31g**	BH&HLYP/6-31++g**
Energy Calculation	CBS-QB3	B3LYP/6-31g**	BH&HLYP/6-31++g**
Cluster Size	T3	T3	T5
R(H'O_2) (Å)	1.34	1.31	1.41
R(HzO_1) (Å)	1.34	1.31	1.41
R(C'H') (Å)	1.32	1.34	1.28
R(C'Hz) (Å)	1.32	1.34	1.28
R(AlO_1) (Å)	1.86	1.82	1.75
R(AlO_2) (Å)	1.86	1.73	1.75
A(O_1AlO_2) (degree)	90.27	91.40	95.70
ν_{TST} (cm^{-1})	1700i	-	1435i
E_a (kcal/mol)	33.5	32.3	40.0

The negative frequency corresponding to the hydrogen exchange mode is 1700 cm^{-1}. The activation energy obtained using the CBS-QB3 composite energy method is 33.5 kcal/mol.

Other researchers have studied this reaction using computational methods and the calculated activation energies range from 30 kcal/mol to 40 kcal/mol depending on the computational methods and the size of the zeolite cluster as shown in Table 6-1 in previous chapter (Blaszkowski et al., 1994; Esteves et al., 1999; Evleth et al., 1994;

Kazansky et al., 1994a; Kramer et al., 1993; Ryder et al., 2000). The experimental study from Larson *et al.* reported the activation energy for methane H/D exchange to be 33.4 kcal/mol (Larson and Hall, 1965). Our calculated activation energy has an absolute error of only 0.1 kcal/mol compared with the experimental data. This agreement proves our choice of zeolite cluster and computational method is valid.

In 1999, Schoofs *et al.* reported an experimental activation energy of 29.2-35.9 kcal/mol (122-150 kJ/mol) for methane H/D exchange reaction (Schoofs et al., 1999). Our calculation result agrees with this experimental data as well.

7.3 Ethane Hydrogen Exchange Reaction

$$CH_3CH_2Hz + H_3SiOAlH_2(OH')SiH_3 \rightarrow CH_3CH_2H' + H_3Si(OHz)AlH_2OSiH_3$$

The ethane hydrogen exchange reaction was described in the previous chapter section 6.2.3. Figure 7-2 depicts the calculated transition state structure for the hydrogen exchange reaction of ethane using the B3LYP method. Similar to the transition state of the methane reaction, the structure keeps its symmetry along the C'-C-Al plane. The protonated carbon atom, C', stays in the main plane of the zeolite cluster and becomes a penta-coordinated structure while the other carbon atom keeps its tetrahedral structure. The proton from the zeolite cluster, H', and the exchange hydrogen from the ethane molecule, Hz, stay between the C' carbon atom and the two zeolite oxygen atoms, indicating the formation of a C'-H' bond and breaking of the C'-Hz bond.

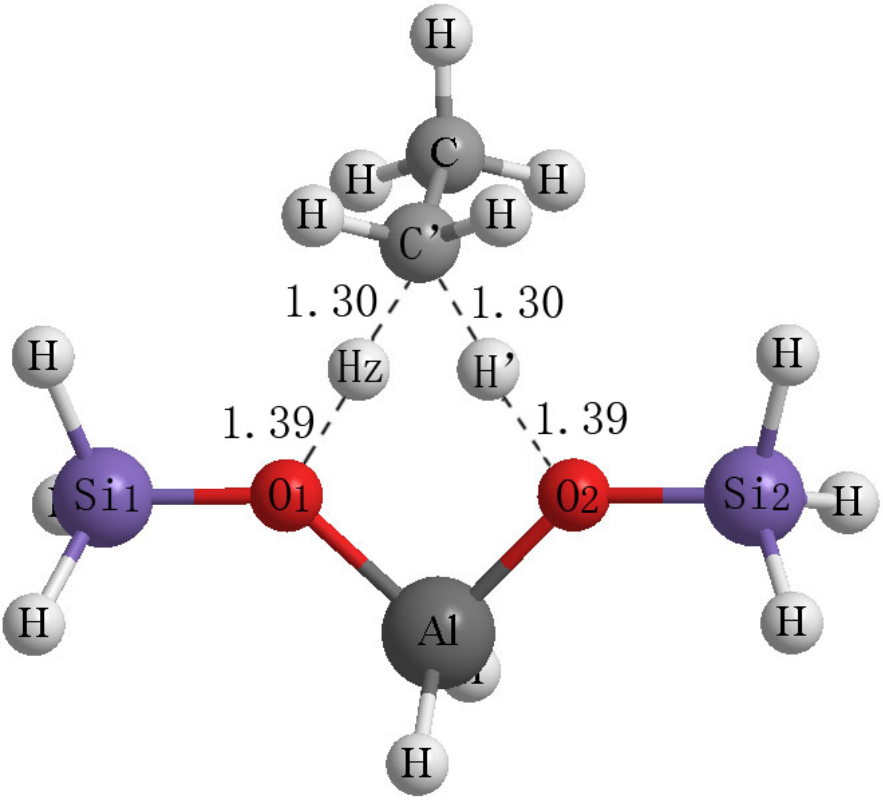

Figure 7-2. Calculated transition state structure for the ethane hydrogen exchange reaction on a T3 zeolite cluster (Units in Å)

Selected bond lengths and angles for the transition state structure are reported in Table 7-2 along with a comparison with previous computational results from Esteves (Esteves et al., 1999) and Ryder (Ryder et al., 2000). The negative frequency corresponding to the hydrogen exchange mode is 1561 cm^{-1}. The activation energy obtained using the CBS energy is 31.0 kcal/mol. The barrier is relatively lower than that of methane, indicating ethane hydrogen exchange is more favorable than methane. Unfortunately, there is no experimental activation energy available for direct comparison.

Table 7-2. Selected bond lengths and angles of the ethane hydrogen exchange reaction transition state structure

	this work	Esteves *et al.*	Ryder *et al.*
Geom. Optimization	B3LYP/6-31g*	B3LYP/6-31g**	BH&HLYP/6-31++g**
Energy Calculation	CBS-QB3	B3LYP/6-31g**	BH&HLYP/6-31++g**
Cluster Size	T3	T3	T5
R(H'O_2) (Å)	1.39	1.36	1.47
R(HzO_1) (Å)	1.39	1.36	1.49
R(C'H') (Å)	1.30	1.32	1.26
R(C'Hz) (Å)	1.30	1.32	1.28
R(AlO_1) (Å)	1.85	1.83	1.75
R(AlO_2) (Å)	1.85	1.83	1.75
A(O_1AlO_2) (degree)	90.56	91.60	95.60
ν_{TST} (cm^{-1})	1561i	-	1147i
E_a (kcal/mol)	31.0	32.3	40.7

7.4 Propane Hydrogen Exchange Reactions

$CH_3CH_2\underline{\mathbf{C}}H_2Hz + H_3SiOAlH_2(OH')SiH_3 \rightarrow CH_3CH_2\underline{\mathbf{C}}H_2H' + H_3Si(OHz)AlH_2OSiH_3$

$CH_3\underline{\mathbf{C}}HHzCH_3 + H_3SiOAlH_2(OH')SiH_3 \rightarrow CH_3\underline{\mathbf{C}}HH'CH_3 + H_3Si(OHz)AlH_2OSiH_3$

The propane hydrogen exchange reactions can take place at either the primary carbon or the secondary carbon shown above. The bold underlined carbon atom indicates the place where hydrogen exchange takes place. The propane hydrogen exchange reaction was described in the previous chapter section 6.3.3 and is briefly discussed here to continue the analyses in this work. The calculated transition state structure of primary carbon hydrogen exchange with the B3LYP method is depicted in Figure 7-3. Similar to the transition state structures of methane and ethane reactions, symmetry along C-Al plane is observed.

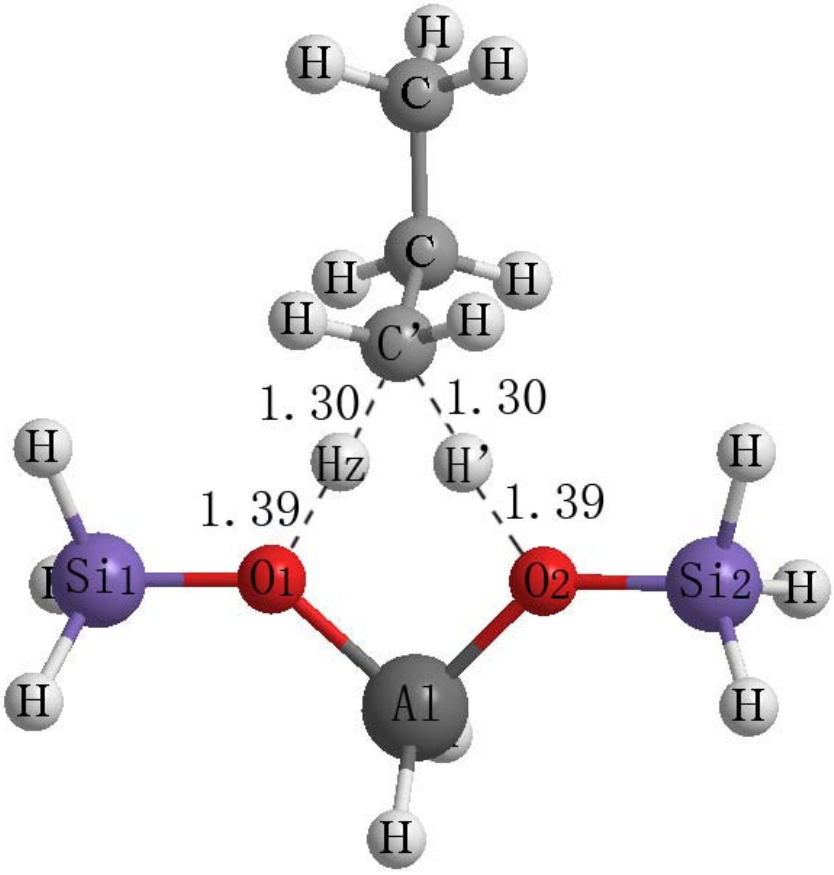

Figure 7-3. Calculated transition state structure for the propane primary carbon hydrogen exchange reaction on a T3 zeolite cluster (Units in Å)

In Table 7-3, selected bond lengths and angles for the transition state structure are reported along with a comparison to previous computational results from Esteves (Esteves et al., 1999) and Ryder (Ryder et al., 2000). The negative frequency corresponding to the hydrogen exchange mode is 1549 cm^{-1}. The activation energy is 30.4 kcal/mol and is relatively lower than the calculated results from Esteves and Ryder, which are 32.2 kcal/mol and 40.5 kcal/mol respectively. The experimental activation energy reported by Stepanov *et al.* is 25.8 ± 1.7 kcal/mol (Stepanov et al.,

1998). Our calculation is only 2.9 kcal/mol higher than the maximum experimental data and much closer to experiment than those from Esteves or Ryder.

Table 7-3. Selected bond lengths and angles of the propane primary carbon hydrogen exchange reaction transition state structure

	this work	Esteves *et al.*	Ryder *et al.*
Geom. Optimization	B3LYP/6-31g*	B3LYP/6-31g**	BH&HLYP/6-31++g**
Energy Calculation	CBS-QB3	B3LYP/6-31g**	BH&HLYP/6-31++g**
Cluster Size	T3	T3	T5
R(H'O_2) (Å)	1.39	1.36	1.50
R(HzO_1) (Å)	1.39	1.36	1.46
R(C'H') (Å)	1.30	1.32	1.24
R(C'Hz) (Å)	1.30	1.32	1.29
R(AlO_1) (Å)	1.85	1.83	1.75
R(AlO_2) (Å)	1.85	1.83	1.75
A(O_1AlO_2) (degree)	90.62	91.70	95.60
ν_{TST} (cm^{-1})	1549i	-	1142i
E_a (kcal/mol)	30.4	32.2	40.5

The calculated transition state structure of secondary carbon hydrogen exchange with the B3LYP method is shown in Figure 7-4. For the first time, the transition state structure does not keep the symmetry seen for the methane, ethane, and propane primary carbon hydrogen exchange reactions. The propane structure tilts to the left side of the zeolite cluster and pushes the Hz atom further away from the C' atom. As a result, the C'Hz distance is slightly larger than the C'H' distance, while the distance of HzO_1 is slightly less than the distance of H'O_2.

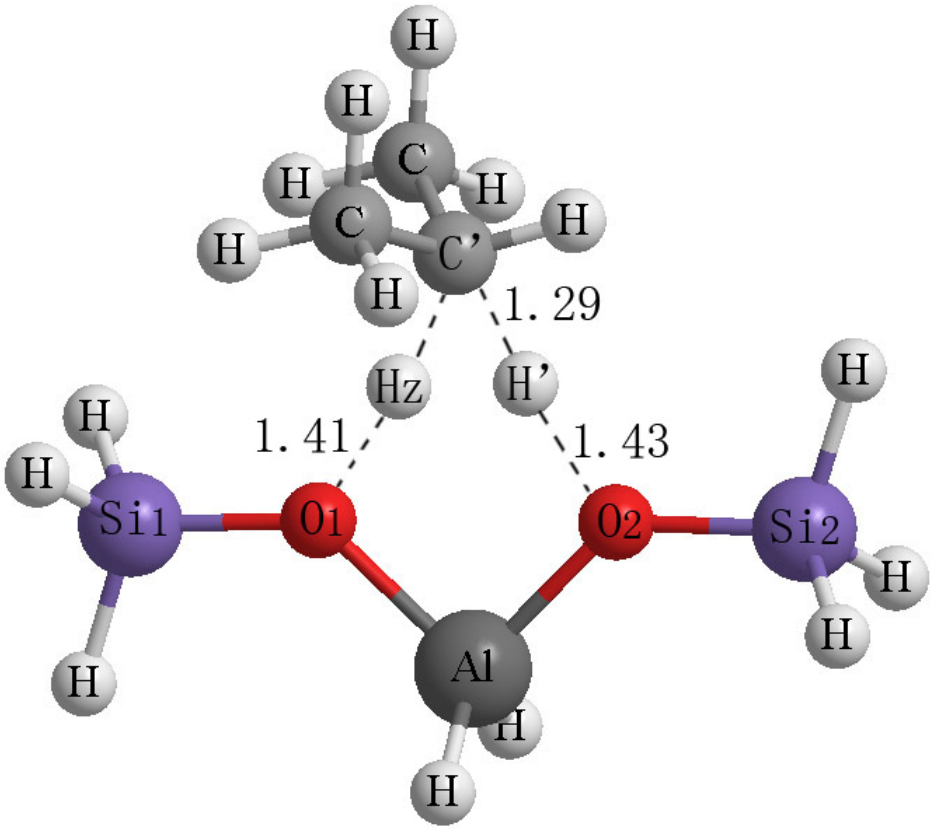

Figure 7-4. Calculated transition state structure for the propane secondary carbon hydrogen exchange reaction on a T3 zeolite cluster (Units in Å)

In Table 7-4, selected bond lengths and angles for the transition state structure are reported with a comparison to previous computational results from Esteves (Esteves et al., 1999) and Ryder (Ryder et al., 2000). The negative frequency corresponding to the hydrogen exchange mode is 1459 cm^{-1}. The activation energy is 29.8 kcal/mol, and is again much lower than the calculated results from Esteves and Ryder which are 33.3 kcal/mol and 39.2 kcal/mol. Compared with the experimental activation energy of 28.0 ± 1.7 kcal/mol (Stepanov et al., 1998), our calculated result is only 0.1 kcal/mol higher. Our calculated results show that the activation energy of secondary

carbon hydrogen exchange reaction is close to, but relatively lower than, that of primary carbon. Even though our calculated trend seems opposite to the experimental results of Stepanov (Stepanov et al., 1998), the experimental trend could be reversed considering the activation energy difference of primary and secondary exchange reactions is only 2.2 kcal/mol, and the relatively large error range ±1.7 kcal/mol for each reaction. Accounting for the errors, the experimental trend could be reversed and become the same as our calculated results. Also, this trend is the same as that obtained by Ryder (Ryder et al., 2000).

Table 7-4. Selected bond lengths and angles of the propane secondary carbon hydrogen exchange reaction transition state structure

	this work	Esteves *et al.*	Ryder *et al.*
Geom. Optimization	B3LYP/6-31g*	B3LYP/6-31g**	BH&HLYP/6-31++g**
Energy Calculation	CBS-QB3	B3LYP/6-31g**	BH&HLYP/6-31++g**
Cluster Size	T3	T3	T5
R(H'O_2) (Å)	1.43	1.41	1.55
R(HzO_1) (Å)	1.41	1.38	1.47
R(C'H') (Å)	1.29	1.30	1.24
R(C'Hz) (Å)	1.30	1.31	1.30
R(AlO_1) (Å)	1.85	1.83	1.76
R(AlO_2) (Å)	1.85	1.83	1.74
A(O1AlO_2) (degree)	90.66	91.70	96.10
ν_{TST} (cm^{-1})	1459i	-	1029i
E_a (kcal/mol)	29.8	33.3	39.2

7.5 Butane Hydrogen Exchange Reactions

$CH_3CH_2CH_2\underline{\mathbf{C}}H_2Hz + H_3SiOAlH_2(OH')SiH_3 \rightarrow CH_3CH_2CH_2\underline{\mathbf{C}}H_2H' + H_3Si(OHz)AlH_2OSiH_3$

$CH_3CH_2\underline{\mathbf{C}}HHzCH_3 + H_3SiOAlH_2(OH')SiH_3 \rightarrow CH_3CH_2\underline{\mathbf{C}}HH'CH_3 + H_3Si(OHz)AlH_2OSiH_3$

Similar to propane, the butane hydrogen exchange reaction can take place at the primary carbon or the secondary carbon shown above. The calculated transition state structure of primary carbon hydrogen exchange with the B3LYP method is depicted in Figure 7-5. Similar to the transition state structures of methane and ethane reactions, symmetry along C-Al plane is observed.

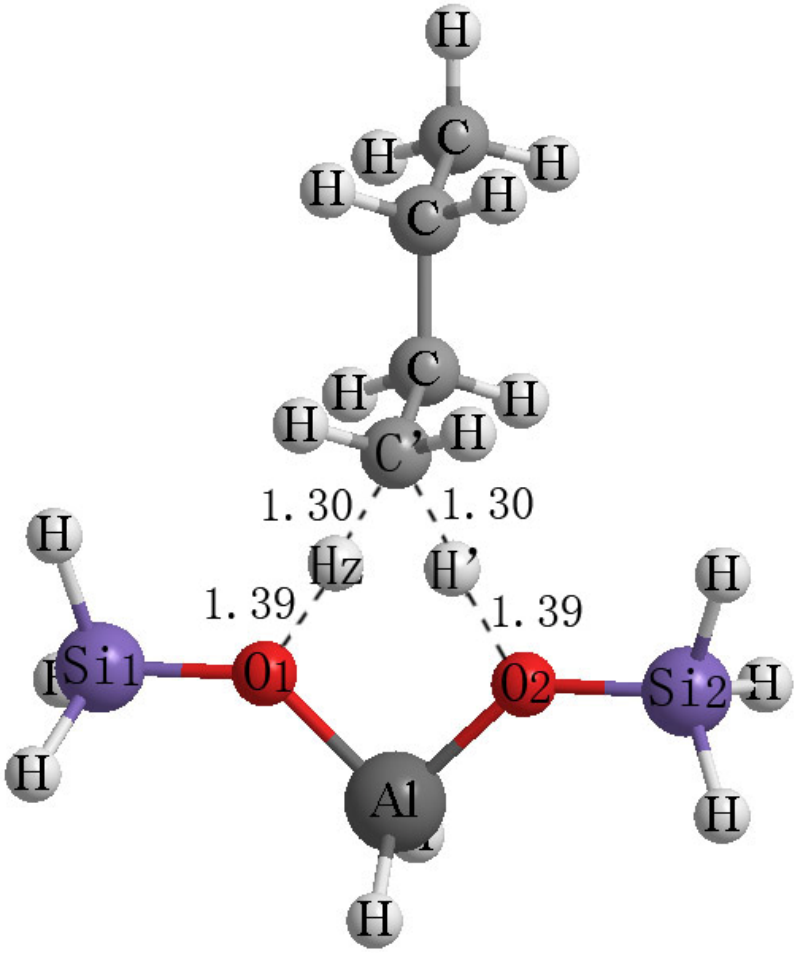

Figure 7-5. Calculated transition state structure for the butane primary carbon hydrogen exchange reaction on a T3 zeolite cluster (Units in Å)

In Table 7-5, selected bond lengths and angles for the transition state structure are reported. The negative frequency corresponding to the hydrogen exchange mode is 1549 cm^{-1}. The activation energy obtained using the CBS-QB3 method is 30.0 kcal/mol.

Table 7-5. Selected bond lengths and angles of the butane primary and secondary carbon hydrogen exchange reaction transition state structures

	$\underline{C}H_3CH_2CH_2CH_3$	$CH_3\underline{C}H_2CH_2CH_3$
Geom. Optimization	B3LYP/6-31g*	B3LYP/6-31g*
Energy Calculation	CBS-QB3	CBS-QB3
Cluster Size	T3	T3
R(H'O_2) (Å)	1.39	1.45
R(HzO_1) (Å)	1.39	1.42
R(C'H') (Å)	1.30	1.29
R(C'Hz) (Å)	1.30	1.30
R(AlO_1) (Å)	1.85	1.85
R(AlO_2) (Å)	1.85	1.85
A(O_1AlO_2) (degree)	90.63	90.90
ν_{TST} (cm^{-1})	1549i	1418i
E_a (kcal/mol)	30.0	28.3

The calculated transition state structure of the secondary carbon hydrogen exchange with the B3LYP method is shown in Figure 7-6. Similar to the propane secondary carbon hydrogen exchange reaction, the transition state structure does not keep the symmetry seen for the methane and ethane hydrogen exchange reactions. As a result, the distances of the acidic proton and secondary carbon, R(C'H'), and exchanging hydrogen and secondary carbon, R(C'Hz), are not identical. In Table 5, selected bond lengths and angles for the transition state structure are reported. The negative frequency corresponding to the hydrogen exchange mode is 1418 cm^{-1}. The activation energy obtained using the CBS-QB3 method is 28.3 kcal/mol. It is close to, but lower than that of the primary carbon hydrogen exchange reaction,

indicating the butane secondary carbon hydrogen exchange reaction is relatively easier to take place. This trend is the same as we found for the propane reactions.

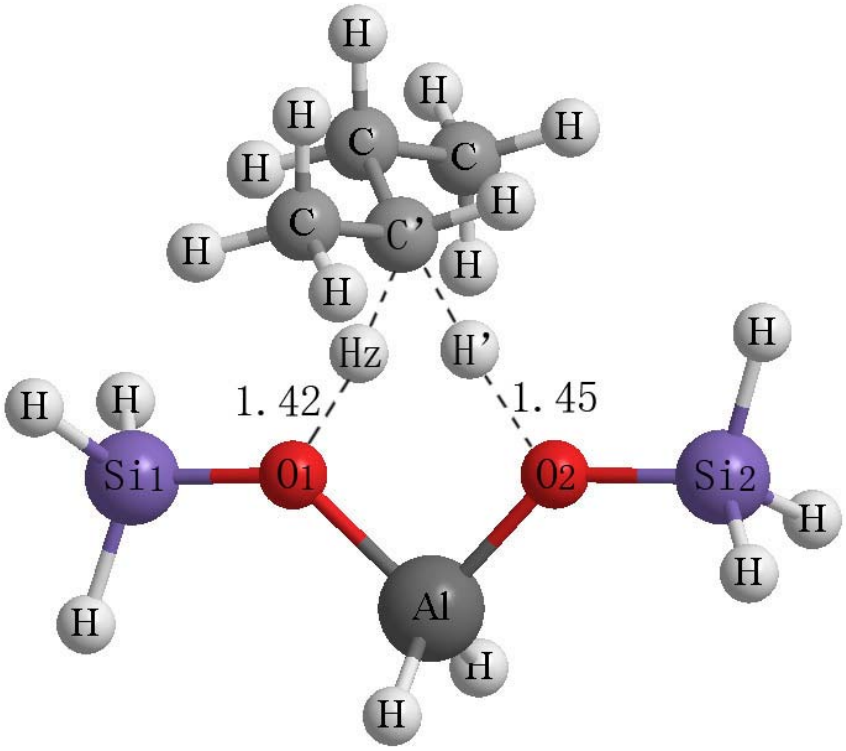

Figure 7-6. Calculated transition state structure for the butane secondary carbon hydrogen exchange reaction on a T3 zeolite cluster (Units in Å)

For the methane, ethane and propane hydrogen exchange reactions from Ryder *et al.*, the application of a large T5 cluster containing one Al and four Si atoms to simulate the long-range interactions of a real zeolite catalyst should help increase the accuracy of their calculated results. However, the prohibitive computational cost of introducing five heavy atoms restricts the computational method to a low to medium level, which on the other hand decreases the accuracy. For methane and propane

reactions, Ryder's calculated activation energies are 7 to 11 kcal/mol higher than the experimental values. In this work, we used a relatively smaller T3 cluster, which is still large enough to describe the vicinity of the Brønsted acid site. Also, the system including the T3 cluster and the alkane reactant is small enough to investigate using high-level computational treatment using the CBS-QB3 composite energy method in this work. As a result, our methane and propane activation energy results are within 3 kcal/mol of the experimental values. The results of Esteves *et al.*, are somewhat unexpected in that the activation energies for primary carbon hydrogen exchange of methane, ethane, and propane are 32.3 kcal/mol, 32.3 kcal/mol, and 32.2 kcal/mol, almost all identical. The increase of the carbon chain should affect the reaction activation energies, which is not found from their work. Also, the activation energies obtained by Esteves show up to a 7 kcal/mol deviation from experiment because of the relatively lower level B3LYP/6-31++g** energy calculation method compared with the CBS-QB3 composite energy method used in this work. This agreement of our results with experimental values again validates our choice of cluster model and computational method. The BH&HLP/6-31++g**//BH&HLP/6-31++g** (energy calculation method//geometry optimization method) method from Ryder, B3LYP/6-31++g**//B3LYP/6-31++g** method from Esteves and CBS-QB3//B3LYP/6-31g* from this work also show how the dependence of the calculated activation energies is strongly determined by the

level of the final energy calculations and much less on the level of the geometry optimization.

For ethane and butane reactions, even though there is no experimental information available, it is still credible to conclude that our calculated activation energies should be close to the real values considering the accuracy of the results for the methane and propane reactions, and the similarity of alkane hydrogen exchange reactions.

7.6 Deprotonation Energy and Activation Energy Relationship

The energy required to deprotonate one proton from RH species is the deprotonation energy (E_{dep}).

$$RH \rightarrow R^- + H^+$$

It is defined as the energy difference between the protonated (RH) and unprotonated (R^-) form (Brand et al., 1993).

$$E_{dep} = E(R^-) - E(RH)$$

Since the activation barrier for the hydrogen exchange reaction is directly related to the strength of the R-H bond, we proposed a relationship between the activation energy and the deprotonation energy for light alkanes, R-H. Figure 7-7 is a plot of the activation energy versus deprotonation energy for methane, ethane, propane, and butane. The deprotonation energies are also obtained at the CBS-QB3//B3LYP/6-31g* level, the same method used to calculate the activation

energies. Since the zeolite acidic OH bond strength stays the same for all of the reactions investigated in this work, the exchange reactions are dominated by the strength of the R-H bonds, which can be described by their deprotonation energies. Therefore, as the deprotonation energy increases, the reaction becomes more difficult to take place and has a higher activation barrier. As long as the reaction mechanism does not alter, the activation energy is linearly correlated to the deprotonation energy. The relationship can be described as:

$$E_a = 0.994E_{dep} - 384.3$$

While E_a and E_{dep} are in the units of kcal/mol.

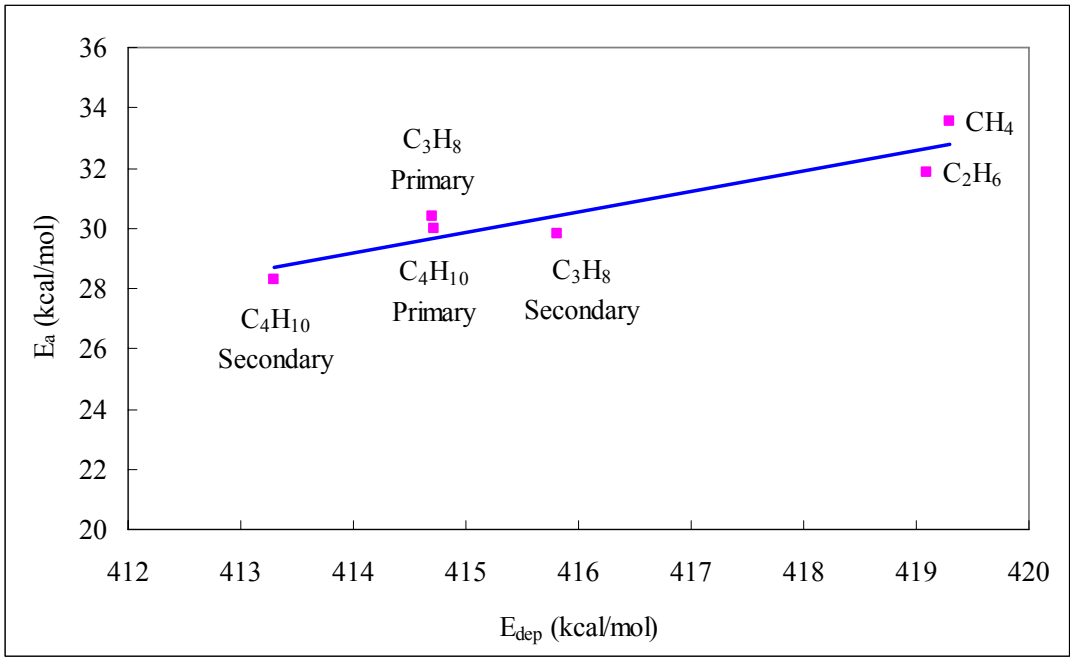

Figure 7-7. Light alkane hydrogen exchange reaction activation energy and deprotonation energy relationship

7.7 Conclusions

In this work, the zeolite catalyzed hydrogen exchange reactions of light alkanes, including methane, ethane, propane, and butane were studied using quantum chemical methods. The transition state structures for each reaction were optimized at the B3LYP/6-31g* level, and the energies were obtained using CBS-QB3, a complete basis set composite energy method. The calculated activation energies for methane, ethane, propane primary carbon, and butane primary carbon are 33.53 kcal/mol, 31.01 kcal/mol, 30.40 kcal/mol, and 29.97 kcal/mol. The calculated activation energies for propane and butane secondary carbon hydrogen exchange reactions were 29.83 kcal/mol and 28.32 kcal/mol, which were relatively lower than that of the primary carbon hydrogen exchange reactions. Furthermore, a linear relationship was found between alkane deprotonation energy and its hydrogen exchange reaction activation barrier. This work has been accepted for publication in the Journal of Molecular Catalysis (Zheng and Blowers, 2005).

References:

Bauschlicher, C.W. and Partridge, H., 1995. A Modification of the Gaussian-2 Approach Using Density- Functional Theory. *Journal of Chemical Physics*, 103(5): 1788-1791.

Becke, A.D., 1993. Density-Functional Thermochemistry .3. The Role Of Exact Exchange. *Journal Of Chemical Physics*, 98(7): 5648-5652.

Blaszkowski, S.R., Jansen, A.P.J., Nascimento, M.A.C. and Vansanten, R.A., 1994. Density-Functional Theory Calculations of the Transition-States for Hydrogen-Exchange and Dehydrogenation of Methane by a Bronsted Zeolitic Proton. *Journal of Physical Chemistry*, 98(49): 12938-12944.

Blaszkowski, S.R., Nascimento, M.A.C. and vanSanten, R.A., 1996. Activation of C-H and C-C bonds by an acidic zeolite: A density functional study. *Journal of Physical Chemistry*, 100(9): 3463-3472.

Brand, H.V., Curtiss, L.A. and Iton, L.E., 1993. Ab-Initio Molecular-Orbital Cluster Studies of the Zeolite ZSM-5 .1. Proton Affinities. *Journal of Physical Chemistry*, 97(49): 12773-12782.

Esteves, P.M., Nascimento, M.A.C. and Mota, C.J.A., 1999. Reactivity of alkanes on zeolites: A theoretical ab initio study of the H/H exchange. *Journal Of Physical Chemistry B*, 103(47): 10417-10420.

Evleth, E.M., Kassab, E. and Sierra, L.R., 1994. Calculation of the Exchange Mechanism of D-2 and Cd4 with a Zeolite Model. *Journal of Physical Chemistry*, 98(5): 1421-1426.

Frisch, M.J. et al., 1998. *Gaussian 98, Revision A.7*. Gaussian, Inc., Pittsburgh PA.

Johnson, B.G., Gill, P.M.W. and Pople, J.A., 1993. The Performance Of A Family Of Density Functional Methods. *Journal Of Chemical Physics*, 98(7): 5612-5626.

Kazansky, V.B., Frash, M.V. and Vansanten, R.A., 1994a. A Quantum-Chemical Study of Adsorbed Nonclassical Carbonium-Ions as Active Intermediates in Catalytic Transformations of Paraffins .2. Protolytic Dehydrogenation and Hydrogen-Deuterium Hetero-Isotope Exchange of Paraffins on High-Silica Zeolites. *Catalysis Letters*, 28(2-4): 211-222.

Kazansky, V.B., Senchenya, I.N., Frash, M. and Vansanten, R.A., 1994b. A Quantum-Chemical Study of Adsorbed Nonclassical Carbonium-Ions as Active Intermediates in Catalytic Transformations of Paraffins .1. Protolytic Cracking of Ethane on High-Silica Zeolites. *Catalysis Letters*, 27(3-4): 345-354.

Kramer, G.J., Vansanten, R.A., Emeis, C.A. and Nowak, A.K., 1993. Understanding the Acid Behavior of Zeolites from Theory and Experiment. *Nature*, 363(6429): 529-531.

Larson, J.G. and Hall, W.K., 1965. Studies Of Hydrogen Held By Solids .7. Exchange Of Hydroxyl Groups Of Alumina And Silica-Alumina Catalysts With Deuterated Methane. *Journal Of Physical Chemistry*, 69(9): 3080-&.

Lee, C.T., Yang, W.T. and Parr, R.G., 1988. Development Of The Colle-Salvetti Correlation-Energy Formula Into A Functional Of The Electron-Density. *Physical Review B*, 37(2): 785-789.

Okulik, N.B., Diez, R.P. and Jubert, A.H., 2004. A topological study of the transition states of the hydrogen exchange and dehydrogenation reactions of ethane on a zeolite cluster. *Journal Of Physical Chemistry A*, 108(13): 2469-2474.

Okulik, N.B., Diez, R.P., Jubert, A.H., Esteves, P.M. and Mota, C.J.A., 2001. A topological study of the transition states of the hydrogen exchange and dehydrogenation reactions of methane on a zeolite cluster. *Journal Of Physical Chemistry A*, 105(29): 7079-7084.

Ryder, J.A., Chakraborty, A.K. and Bell, A.T., 2000. Density functional theory study of proton mobility in zeolites: Proton migration and hydrogen exchange in ZSM-5. *Journal Of Physical Chemistry B*, 104(30): 6998-7011.

Schoofs, B., Martens, J.A., Jacobs, P.A. and Schoonheydt, R.A., 1999. Kinetics of hydrogen-deuterium exchange reactions of methane and deuterated acid FAU- and

MFI-type zeolites. *Journal Of Catalysis*, 183(2): 355-367.

Scott, A.P. and Radom, L., 1996. Harmonic vibrational frequencies: An evaluation of Hartree-Fock, Moller-Plesset, quadratic configuration interaction, density functional theory, and semiempirical scale factors. *Journal of Physical Chemistry*, 100(41): 16502-16513.

Stepanov, A.G., Ernst, H. and Freude, D., 1998. In situ H-1 MAS NMR studies of the H/D exchange of deuterated propane adsorbed on zeolite H-ZSM-5. *Catalysis Letters*, 54(1-2): 1-4.

Vollmer, J.M. and Truong, T.N., 2000. Mechanisms of hydrogen exchange of methane with H-zeolite Y: An ab initio embedded cluster study. *Journal Of Physical Chemistry B*, 104(26): 6308-6312.

Zheng, X.B. and Blowers, P., 2005. A computational study of alkane hydrogen exchange reactions on zeolites. *Journal Of Molecular Catalysis A-Chemical*, 242(1-2): 18-25.

Zygmunt, S.A., Curtiss, L.A., Zapol, P. and Iton, L.E., 2000. Ab initio and density functional study of the activation barrier for ethane cracking in cluster models of zeolite H-ZSM-5. *Journal of Physical Chemistry B*, 104(9): 1944-1949.

CHAPTER 8
CONCLUSIONS

In this research, hydrocarbon cracking reactions were investigated using quantum chemical methods. Two major types of hydrocarbon cracking reactions were considered, namely, thermal cracking and catalytic cracking.

The mechanisms for hydrocarbon thermal cracking is generally accepted as free-radical chain reactions. In this research, propyl (Zheng and Blowers, 2005e), n-butyl (Zheng and Blowers, 2005b), sec-butyl and neo-pentyl (Zheng et al., 2005) carbon-carbon bond cracking and 1-chloroethyl (Zheng and Blowers, 2005h) and tert-butyl carbon-hydrogen bond cracking reactions were investigated. Based on previous research (Blowers et al., 2003) of the CBS-RAD method, a new composite energy method, CBS-RAD(MP2) (Zheng and Blowers, 2005f), was developed before performing reaction kinetic modeling. The CBS-RAD(MP2) energy method replaces the time consuming QCISD(fc)/6-31G* geometry and frequency calculation method in the CBS-RAD method with the MP2(full)/6-31G* method. Compared with the extensively applied G2, G3 and CBS-QB3 composite energy methods in

hydrocarbon cracking reaction heats of reaction predictions, the new CBS-RAD(MP2) method has the second least RMS error of 1.22 kcal/mol, very close to the CBS-QB3 method which has the least RMS error of 1.06 kcal/mol. For the cracking reaction activation energy calculation results, the new CBS-RAD(MP2) method again has the least RMS error of 1.37 kcal/mol. More importantly, the computational cost of the CBS-RAD(MP2) method is 81% of CBS-QB3, 32% of the G3 composite energy methods, and only 15% of G2 composite energy method. The computational expense will become much more important as the reactant species of interest becomes larger. Because of the excellent trade-off of accuracy and computational cost, the CBS-RAD(MP2) composite energy method was applied to investigate hydrocarbon thermal cracking reactions.

For the six hydrocarbon radical thermal cracking reactions investigated in this work, the heats of reaction and activation barriers from calculated results using the CBS-RAD(MP2) method agree well with the available experimental data. RRKM and CTST expressions were then applied to estimate the reaction kinetics. Compared with the experimental data, the CBS-RAD(MP2) method successfully predicted the reaction rate constants in almost all cases. In order to facilitate predictions by engineers who would like to use the kinetic data without going through the complicated theoretical details, analytical formulas of the kinetic model were proposed for each reaction using the statistical software, SAS (SAS Institute, 1999). A summary of the kinetic models obtained for the hydrocarbon radical cracking

reactions studied in this work is shown in Table 8-1. The advantage of the models is that they include pressure as an independent variable, which is important since most of the pyrolysis reactors in the petroleum industry operate at low pressures to increase olefin production and reduce coke formation, and the reaction rate is directly related to pressure. Experimental data is often not available at these conditions.

Table 8-1. Summary of kinetic models of the hydrocarbon radical cracking reactions studied in this work

Reaction	**Kinetic Model ($P \leq P_0$)**	**Kinetic Model ($P > P_0$)**	**Switching Pressure P_0**
$*CH_2CH_2CH_3 \rightarrow CH_2CH_2 + *CH_3$	$k\ [s^{-1}] = 2.59\times10^{11}\times P^{0.40} e^{(-13618.16/T)}$	$k\ [s^{-1}] = 2.70\times10^{13}\times e^{(-15117.33/T)}$	$P_0 = 1.10\times10^{5}\times e^{(-3747.92/T)}$
$*CH_2CH_2CH_2CH_3 \rightarrow CH_2CH_2 + *CH_2CH_3$	$k\ [s^{-1}] = 2.04\times10^{9}\times P^{0.51}\times e^{(-9745.70/T)}$	$k\ [s^{-1}] = 9.43\times10^{13}\times e^{(-15135.70/T)}$	$P_0 = 1.53\times10^{9}\times e^{(-10610.24/T)}$
$CH_3*CHCH_2CH_3 \rightarrow CH_2CHCH_3 + *CH_3$	$k\ [s^{-1}] = 1.82\times10^{11}\times P^{0.51}\times e^{(-13023.70/T)}$	$k\ [s^{-1}] = 7.18\times10^{13}\times e^{(-15916.50/T)}$	$P_0 = 1.23\times10^{5}\times e^{(-5672.16/T)}$
$*CH_2C(CH_3)_3 \rightarrow CH_2C(CH_3)_2 + *CH_3$	$k\ [s^{-1}] = 1.44\times10^{12}\times P^{0.29}\times e^{(-13890.20/T)}$	$k\ [s^{-1}] = 1.04\times10^{14}\times e^{(-16075.80/T)}$	$P_0 = 2.54\times10^{6}\times e^{(-7536.55/T)}$
$*CHClCH_3 \rightarrow CHClCH_2 + *H$	$k\ [s^{-1}] = 7.32\times10^{10}\times P^{0.69}\times e^{(-18727.10/T)}$	$k\ [s^{-1}] = 3.74\times10^{13}\times e^{(-20648.10/T)}$	$P_0 = 8.42\times10^{3}\times e^{(-2782.61/T)}$
$CH_3*C(CH_3)_2 \rightarrow CH_2C(CH_3)_2 + *H$	$k\ [s^{-1}] = 3.93\times10^{12}\times P^{0.35}\times e^{(-17878.5/T)}$	$k\ [s^{-1}] = 2.0\times10^{13}\times e^{(-18096.0/T)}$	$P_0 = 1.04\times10^{2}\times e^{(-621.43/T)}$

In the hydrocarbon catalytic cracking research, methane (Zheng and Blowers, 2005g), ethane (Zheng and Blowers, 2005a), propane (Zheng and Blowers, 2005i), and iso-butane (Zheng and Blowers, 2005d) catalytic reactions on zeolite catalysts were studied using the cluster approach. The zeolite catalysts were represented by a T3 cluster, $H_3SiOAlH_2(OH)SiH_3$, on which methane, ethane, propane, and *iso*-butane reactions were investigated. The reaction energetics were studied using density functional theory and *ab initio* methods. The reactivity sequence for hydrocarbon zeolite catalytic reactions is: dehydrogenation < protolytic cracking < hydrogen exchange.

Moreover, the effects of zeolite acidity on the activation barriers were investigated in this work by changing the terminal Si-H bond lengths. Linear relationships were found for all hydrocarbon conversion reactions of interest. Analytical expressions between the activation barriers and deprotonation energies were proposed and are summarized in Table 8-2. As a result, accurate reaction barriers can be obtained when using zeolite catalysts with different acidities as long as their deprotonation energies are first acquired.

The zeolite catalyzed hydrogen exchange reactions of light alkanes including methane, ethane, propane, and butane were also studied using quantum chemical methods (Zheng and Blowers, 2005c). A linear relationship was found between the alkane deprotonation energy and it's the hydrogen exchange reaction activation barrier with the analytical expression: $E_a = 0.994E_{dep} - 384.3$.

Table 8-2. Summary of analytical expressions for acidity effects of hydrocarbon conversion reactions on zeolites studied in this work (E_a and E_{dep} in the units of kcal/mol)

	CH_4	CH_3CH_3	$CH_3CH_2CH_3$	$CH_3CH(CH_3)_2$
Cracking Reaction	N/A	$E_a = 0.780E_{dep} - 163.9$	$E_a = 0.708E_{dep} - 148.9$	$Ea = 0.737E_{dep} - 167.3$
Primary H-exchange Reaction	$E_a = 0.353E_{dep} - 71.6$	$E_a = 0.403E_{dep} - 88.8$	$E_a = 0.396E_{dep} - 87.6$	$Ea = 0.391E_{dep} - 87.1$
Secondary/Tertiary H-Exchange	N/A	N/A	$E_a = 0.405E_{dep} - 90.8$	$Ea = 0.435E_{dep} - 99.8$
Dehydrogenation Reaction	$E_a = 0.645E_{dep} - 102.6$	$E_a = 0.651E_{dep} - 118.2$	$E_a = 0.686E_{dep} - 127.9$	$Ea = 0.577E_{dep} - 112.4$

References:

Blowers, P., Zheng, X. and Homan, K., 2003. Assessment of the suitability of using the composite G2, G3, and CBS-RAD methods for predicting activation energies. *Chemical Engineering Communications*, 190(9): 1233-1248.

SAS Institute, I., version 8, 1999.

Zheng, X. and Blowers, P., 2005a. An ab initio study of ethane conversion reactions on zeolites using the complete basis set composite energy method. *Journal Of Molecular Catalysis A-Chemical*, 229(1-2): 77-85.

Zheng, X. and Blowers, P., 2005b. The application of composite energy methods to n-butyl radical β-scission reaction kinetic estimations. *Theoretical Chemistry Accounts*, (in press).

Zheng, X. and Blowers, P., 2005c. A computational study of alkane hydrogen exchange reactions on zeolites. *Journal of Molecular Catalysis A-Chemical*, 242(1-2): 18-25.

Zheng, X. and Blowers, P., 2005d. A computational study of iso-butane reactivity on zeolites. *Journal of Physical Chemistry A*, (in review).

Zheng, X. and Blowers, P., 2005e. Evaluate of compound models for estimating rate constants of hydrocarbon thermal cracking reactions: Propyl radical β-scission reaction. *Industrial Engineering Chemistry & Research*, (in review).

Zheng, X. and Blowers, P., 2005f. The investigation of hydrocarbon cracking reaction energetics using composite energy method. *Molecular Simulation*: (in press).

Zheng, X. and Blowers, P., 2005g. An investigation of methane conversion reactions with composite energy method. *Journal of Molecular Catalysis*, (in press).

Zheng, X. and Blowers, P., 2005h. Kinetic modeling of 1-chloroethtyl unimolecular decomposition reaction with composite energy methods. *Industrial Engineering Chemistry & Research*, (in review).

Zheng, X. and Blowers, P., 2005i. Reactivity of Alkanes on Zeolites: a Computational Study of Propane Conversion Reactions. *Journal of Physical Chemistry A*, (in press).

Zheng, X., Blowers, P. and Zhang, N., 2005. Application of compound models for estimating rate constants of hydrocarbon thermal cracking reactions: The neopentyl radical beta-scission reaction. *Molecular Simulation*, 31(9): 615-621.

CHAPTER 9
FUTURE WORK

9.1 Hydrocarbon Thermal Cracking Research

As shown in Chapters 4 and 5, by comparison with the available experimental data, the new composite energy method is capable of estimating energetics and kinetics of hydrocarbon radical cracking reactions. Since the experimental measurement of hydrocarbon cracking reactions is very difficult and not many species have been studied experimentally so far, future work will extrapolate the methodology presented in this work to investigate those reactions where experimental information is not available. The small C2-C5 hydrocarbons studied in this work just serve as benchmarks to test the accuracy of the method choices. Large hydrocarbons, like C_5+, have more important applications in the petroleum industry. Therefore, the prediction of large hydrocarbon cracking reactions will be the next step of future research.

The kinetic information of hydrocarbon reactions, like the NIST chemical kinetics database, is available for reactions under the high pressure region only. On the

contrary, in most petroleum industry situations, the crude oil cracker is operated under low pressure to increase olefin production and reduce coke formation. The reaction rates of hydrocarbon reactions whose number of molecules change before and after reaction highly depend on pressure except in the high pressure region. In order to completely understand reactions under these conditions, a hydrocarbon reaction kinetic database with pressure as an independent variable is highly desired.

Because the new CBS method proposed in this work has shown a good compromise between accuracy and computational cost, the method and reaction rate prediction theories used in here can be applied to kinetic modeling of hydrocarbon reactions which are of great importance for the petroleum industry. Some of these reactions are currently beyond the capabilities of experimental investigation. Therefore, the computational approach becomes the only feasible method for reaction kinetic modeling.

Due to the complexity of the reaction schemes, a large number of hydrocarbon elementary reactions including cracking, dehydrogenation, dehydrocyclization, isomerization, alkylation, metathesis, oxidation, oligomerization, and polymerization, etc., need to be explored. The goal of this future research will be to build up a hydrocarbon reaction kinetics database which can be easily utilized by other researchers.

Moreover, microkinetic modeling is an ideal framework for assembling the microscopic information provided by electronic structure calculations and atomistic

simulations to obtain macroscopic predictions of physical and chemical phenomena in systems involving chemical transformations (Broadbelt and Snurr, 2000). With the availability of the hydrocarbon elementary reaction kinetic information, microkinetic modeling tools, like CHEMKIN, can be applied to obtain macroscopic predictions of overall reaction rates, product selectivity, and concentration profile for hydrocarbon reactors. The simulated results can be then in turn be used to direct the design of hydrocarbon reactors.

9.2 Hydrocarbon Catalytic Cracking Research

While studying the hydrocarbon catalytic reactions, a T3 cluster, $H_3SiOAlH_2(OH)SiH_3$, was used to represent the zeolite catalysts. Despite the fact that this moderate cluster worked well when combined with the high level complete basis set composite energy methods for the four species investigated in this work, discrepancies with the experimental activation energies were found, particularly for propane and iso-butane cracking and dehydrogenation reactions. In order to reach better agreement with the experimental data, several improvements could be made in the future research.

The premise of this cluster approach is that chemisoprtion and reactivity are local phenomena, primarily affected only by the nearby surface structure.(Neurock, 2003) The cluster size becomes important since larger clusters are able to include more long-range interactions as real zeolite catalysts. As a result, the cluster size could be

increased to a T5 cluster, $H_3Si(OH)Al(OSiH_3)_3$. The increase of cluster size should be able to increase the accuracy of calculational results, at the cost of the greatly increasing difficulties in transition state location, however. Another direction of future research is to apply the periodic slab method to represent zeolite catalysts. In this method, one defines a unit cell which comprises a large enough surface ensemble. Periodic boundary conditions are then used to expand the cell in the x, y, and/or z directions, thus providing the electronic structure for linear, slab (surface), and bulk materials, respectively.(Neurock, 2003) Applying the periodic slab method, the long-range interactions of the zeolite structure can be included, and preferably more accurate results should be obtained compared with the cluster approach.

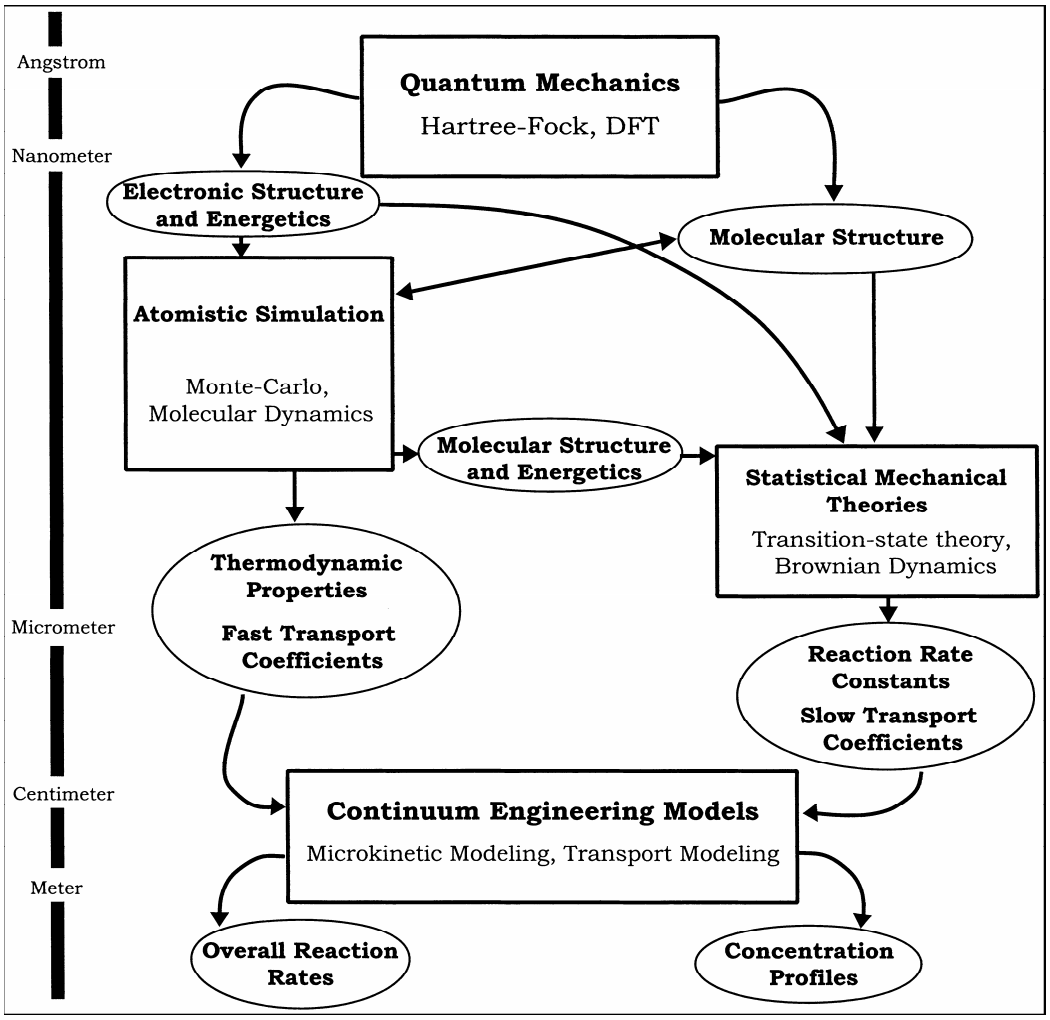

Figure 9-1. Hierarchical approach to catalytic systems modeling

Source: Adapted from L. J. Broadbelt and R. Q. Snurr, 2000, Application of molecular modeling in heterogeneous catalysis research, *Applied Catalysis A*, 200(1-2): 23-46 (Broadbelt and Snurr, 2000)

Figure 9-1 is an illustration of the hierarchical approach to catalytic system modeling. From this figure, one can easily tell that the research of this work using quantum mechanics is just the beginning of the hierarchy, which is at the smallest length scale--angstroms. Another direction of future research is to apply atomistic simulations to investigate hydrocarbon physisorption and diffusion on zeolite catalysts. These phenomena occur on longer time-and length-scales than those accessible to quantum chemical methods. Monte-Carlo and molecular dynamics are the major methods of application, which may require software packages like Vienna Ab-initio Simulation Package (VASP) from Kress and Hafner (Kresse and Furthmuller, 1996a; Kresse and Furthmuller, 1996b; Kresse and Hafner, 1993; Kresse and Hafner, 1994).

The next step beyond this is the application of microkinetic modeling shown in Figure 9-1. Microkinetic modeling is an ideal framework for assembling the microscopic information provided by quantum mechanics calculations and atomistic simulations to obtain macroscopic predictions of physical and chemical phenomena.(Dumesic et al., 1993) Applying the thermodynamic and kinetic parameters obtained from quantum mechanics, atomistic simulations, and statistical mechanics, overall reaction rates and reactant/product concentration profiles can be successfully predicted.

References:

Broadbelt, L.J. and Snurr, R.Q., 2000. Applications of molecular modeling in heterogeneous catalysis research. *Applied Catalysis A-General*, 200(1-2): 23-46.

Dumesic, J.A., Rudd, D.F., Aparicio, L.M., Rekoske, J.E. and Trevino, A.A., 1993. *The microkientics of heterogeneous catalysis*. American Chemical Society, Washington, DC.

Kresse, G. and Furthmuller, J., 1996a. Efficiency of ab-initio total energy calculations for metals and semiconductors using a plane-wave basis set. *Computational Materials Science*, 6(1): 15-50.

Kresse, G. and Furthmuller, J., 1996b. Efficient iterative schemes for ab initio total-energy calculations using a plane-wave basis set. *Physical Review B*, 54(16): 11169-11186.

Kresse, G. and Hafner, J., 1993. Ab initio Molecular-Dynamics for Liquid-Metals. *Physical Review B*, 47(1): 558-561.

Kresse, G. and Hafner, J., 1994. Ab-Initio Molecular-Dynamics Simulation of the Liquid-Metal Amorphous-Semiconductor Transition in Germanium. *Physical Review B*, 49(20): 14251-14269.

Neurock, M., 2003. Perspectives on the first principles elucidation and the design of active sites. *Journal Of Catalysis*, 216(1-2): 73-88.